Luciano Magno Frágola Barbosa

DEVELOPMENT OF A CONCEPTUAL DESIGN METHODOLOGY FOCUSED ON SOLAR AIRCRAFTS

Dissertação apresentada ao Programa de Pós-Graduação em Engenharia Mecânica da Universidade Federal de Minas Gerais, como requisito parcial à obtenção do título de Mestre em Engenharia Mecânica.

Área de concentração: Projeto Mecânico.

Orientador: Prof. Dr. Paulo Henriques Iscold Andrade de Oliveira.

DEMEC UFMG

Belo Horizonte
Escola de Engenharia da UFMG
2014

(Colocar folha de aprovação aqui)

DEDICATÓRIA

Muito aprendi na UFMG sobre engenharia aeronáutica, o que tem sido muito importante. Este trabalho é dedicado a quatro senhores que foram fundamentais para o meu aprendizado, além da UFMG, sobre o que é um avião. Estas são

José Barbosa Filho, meu pai,

Joseph Kovács,

José Renato Melo, e

Yoshihiro Hamada.

Este trabalho é dedicado a estas pessoas que, além de terem me tornado um melhor engenheiro, fundamentalmente me tornaram um melhor ser humano.

AGRADECIMENTOS

A Maria Raimunda de Jesus, uma das pessoas mais maravilhosas que tive e tenho a honra de conhecer, à querida Vó Quinha, à Dona Eny, um anjo em nossas vidas, ao apoio e cumplicidade constante de Celminha Parreiras, meu maior agradecimento. Ao irmão Domingos, ao primo Flavio Coutinho, ao tio Walter Bergo Coutinho, minha gratidão pelos apoios, incentivo, confiança e companhia. Ao pessoal de Santana - Dri, Mirella, Dora, Luciana, Kiko, Clau...-, em São José; aos amigos do centro vivências Nazaré - Cristóvão, Neide, Sônia ...-, à Dona Renate Bell, a Elza Barcala, a Mariza de Senna e ao Sr. José Pedro, pelo companheirismo e acolhimento; à Lu e ao Vitinho pelo grande apoio; ao meu orientador, aos colegas e professores da UFMG; ao Rinaldo Gontigli, ao Eng. José Ilton Gomes, a Antônio Basílio, aos colegas de São José, Franco Olmi, Renato Mazza, Jorge Marino, e tantos outros que foram tão especiais, meu muito obrigado. Este trabalho é de vocês também.

"Oh, I have slipped the surly bonds of earth
And danced the skies on laughter –silvered wings;
Sunward I've climbed, and joined the tumbling mirth
Of sun-split clouds-and done a hundred things
You have not dreamed of-wheeled and soared and swung
High in sunlit silence. Hovering there,
I've chased the shouting wind alone, and flung
My eager craft though footless halls of air.
Up, up the long, delirious, burning blue
I've topped the windswept heights with easy grace
Where never lark, or even eagle flew.
And, while with silent, lifting mind I've trod
The high untrespassed sanctity of space,
Put out my hand, and touched the face of God."

John Gillespie Magee, Jr., "High Flight" *in* McCormick, 1979

INDEX

LIST OF FIGURES

FIGURE **Description** **Page**

LIST OF TABLES

LIST OF SYMBOLS

International System of units has been used unless otherwise indicated.

Symbol or Abbreviation	Value and Unit	Description
MPPT		Maximum power point tracker
VS		Stall speed
VNE		Never exceed speed
Kft		Thousand feet
Ppm		Parts per million
R*	8.31446 J/(K.mol)	Ideal gas constant
MM	kg/kmol	Molecular Mass
K		Kelvin degrees
Km		kilometer
H		Hour
s		Second
W		Watt
ρ, rho	Kg/m^3	Atmosphere local specific mass
T	^oC, ^oK	Temperature
Tr	N	Thrust
TAS, V	m/s, km/h	True Airspeed
EAS	m/s, km/h	Equivalent Airspeed
P	N/m^2	Pressure
Pw	W, hp	Power
ν		Atmosphere local kinematic viscosity
μ		Friction coefficient, atmosphere local dynamic viscosity
NAA		National Aeronautical Association
MDDO		Multi-disciplinary design and optimization

Symbol or Abbreviation	Value and Unit	Description
NASA		National Aeronautics and Space Agency
NASA CR		NASA Contractor Report
NASA TM		NASA Technical Memorandum
NASA TN		NASA Technical Note
AIAA		American Institute of Aeronautics and Astronautics
NOAA		National Oceanic and Atmospheric Administration
USAF		United States Air Force
HPA, MPA		Human-powered aircraft , Man-powered aircraft
L	Newton	Lift force
D	Newton	Drag force
CL		Lift coefficient
CD		Drag coefficient
CDo		Drag coefficient for zero lift
CDmin		Minimum drag coefficient
CLmax		Maximum lift coefficient
CLo		Lift coefficient for $\alpha=0$
2D		Index for two-dimensional
Re, R.N.		Reynolds Number
A		Aspect Ratio
e		Oswald efficiency factor
$CL\alpha$	1/rad, rad^{-1}	Derivative of lift coefficient related to angle of attack
α, alpha	degree or radian	Angle of attack
T/C, t/c		Airfoil thickness ratio
Z/C, z/c		Airfoil camber ratio ratio
z	meter	Max. vertical distance of airfoil camber line from chord line
t	meter	Maximum vertical thickness of airfoil
C, c	meter	Airfoil chord length
CMG		Mean Geometric Chord
S, Sw	m^2	Reference area, wing area

Symbol or Abbreviation	Value and Unit	Description
Alt, H	km, m, feet	Altitude
X, Y, Z	meters	Aircraft coordinates
E		L/D, lift-to-drag ratio
E_*		Maximum lift-to-drag ratio
CL_*		CL for maximum lift-to-drag ratio
CL_{**}		CL for minimum horizontal flight power
E_{**}		E for minimum horizontal flight power
APw	W	power available to be delivered to the air
RPw	W	Required Power to perform horizontal flight; D x TAS
DAE	W.h	Daily Available Energy
DRE	W.h	Daily Req Energy
MOLA		Mars Orbiter Laser Altimeter
Re		Reynolds Number
MDSI	$kW.h/m^2$	Mean Daily Solar Intensity
SAR		Solar array to wing area ratio
ILSPI	W./m	Instantaneous and local Sun power intensity
SLDEI	W.h/m	Solar Local Daily Energy intensity
CL_{saf}		Limitation of high CL for safety in terms of stall avoidance
G		Gravity acceleration
η_{eng}		Engine efficiency
η_{prop}		Propeller efficiency
η_{sist}		System efficiency, aircraft with batteries
η_{sisb}		System efficiency, aircraft with batteries
SHP	hp	Propeller shaft power
δ		Additional induced drag factor for non-elliptical wing
γ	degrees	Local wind angle over propeller blade section
Fax_i	Newton	Axial force at each strip
Ftn_i	Newton	Tangential force at each propeller strip

Symbol or Abbreviation	Value and Unit	Description
β, beta,	degrees	Propeller blade local pitch angle
beta75	degrees	Propeller blade pitch angle at 75% of radius
Nb		Number of blades
Ns		Number of strips
R_i	meters	Distance from propeller strip to rotation axis
ΔV	m/s	Final Incremental speed due to propeller thrust
CT, Ct		Propeller Thrust Coefficient
CP, Cp		Propeller Power Coefficient
J		Propeller Advance Ratio
Sref	m^2	Reference area for Drag coefficients
k	meters	Induced drag coefficient factor
Sdisk	m^2	Propeller Disk Area
D	m	Propeller Diameter
Vdisk	m/s	Air speed at Propeller Disk
Sstm	m^2	Local Area of the propeller stream tube
Vstm	m/s	Local incremental speed at the propeller stream tube
Dstm	meters	Local Diameter of the propeller stream tube
fv		Multiplying factor for take-off speed related to minimum speed
ax	m/s^2	Acceleration in X direction
Dg	Newton	Drag due to wheels and skid contact with ground
N	Newton	Ground normal upward force
θ_{TO}	degrees	Aircraft attitude angle during Take-off run
$Tmax\ (TAS)$	Newton	Maximum Thrust for the specific speed
Vo_i, Vf_i	m/s	Initial and final speeds at the time interval
df_i, df_i	meters	Initial and final distances at the time interval
to_i, tf_i	seconds	Initial and final times at the time interval

Symbol or Abbreviation	Value and Unit	Description
P1	Seconds	Initial time of the time interval; in the Mission Analysis
P2	Seconds	The final time of the time interval, in the Mission Analysis
PM	Seconds	The average time of the time interval, in the Mission Analysis
a-p angle	degrees	Angle between planet's revolution axis, and the normal to the plane of planet's orbital translation around the Sun.
SEL		Sun-Earth Line
M_{Eng}	kg	Engine Mass
Pw_{Eng}	W	Engine Power
M_{Bat}	kg	Mass of Batteries
M_{Cell}	kg	Mass of Solar Panels
S_{Cell}	m^2	Area of Solar Panels
M_{Str} , Mstr	kg	Mass of aircraft Structure, airframe mass
M_{Contrl}	kg	Mass of the Control Systems, including electrical transmission controls
WSM	kg	Wing Structural Mass
N, S		North and South Latitudes
Msys	kg	Mass of Aircraft Systems
Mpayl	kg	Payload Mass
UIUC		University of Illinois at Urbana-Champaign
GRASS		Geographic Resources Analysis Support System
GIS		Geographic Information System

RESUMO

Este trabalho apresenta estudos associados ao projeto de aeronaves solares. Foram pesquisadas características de aeronaves solares existentes, sua história e os desenvolvimentos e desafios técnicos associados, assim como suas limitações e campos de uso potencial. Para fins de análise das aeronaves solares existentes, e projeto de novas aeronaves solares, procurou-se inicialmente entender em que estas aeronaves diferem de aeronaves convencionais. Foi possível observar-se alguma semelhança das aeronaves solares, em termos da carga alar, com aeronaves pioneiras da aviação, dos anos 1890 a 1910. Foram desenvolvidos procedimentos e métodos dedicados à estimativa de arrasto, tração e desempenho de aeronaves de baixa velocidade propelidas por hélices. E utilizaram-se veículos aéreos – solares ou não - com características conhecidas de desempenho para validar estes processos. A partir disto, processos específicos para a análise da propulsão solar foram desenvolvidos: definição de modelo de irradiação solar; definição da cadeia propulsiva, das células solares à hélice, e com uso ou não de baterias. Outras metodologias específicas a aeronaves solares foram investigadas e definidas: uma formulação geral para obtenção de carga alar máxima para viabilidade de uma aeronave solar; características aerodinâmicas de números de Reynolds abaixo de 150000; e métricas para estimativa de massa de aeronaves deste tipo. Com este conjunto de ferramentas, foi possível desenvolver-se dois métodos complementares para definição de uma configuração de aeronave solar, a partir dos requisitos de missão: o Solar Aircraft Design Method e o Mission Analysis Method. O segundo só se faz necessário em missões que envolvem grandes variações de altitude. Com as ferramentas desenvolvidas, três conceitos de aeronaves solares são calculados e apresentados, cada um com utilizações específicas. Em resumo, com este trabalho um cenário geral sobre aeronaves solares é desenvolvido visando o projeto deste tipo de aeronaves, e o trabalho apresentado aponta várias perspectivas e possibilidades de continuidade e aprofundamento.

ABSTRACT

This work presents the studies to associated solar aircraft project. Characteristics of existing solar aircraft, their history and developments and associated technical challenges, as well as their limitations and potential use fields have been surveyed. Development related to solar aircraft and low-speed aircraft have been researched and existing aircraft has been investigated, in order to allow an understanding of these aircraft in a comparative and evolutionary perspective. Studies of low-speed aircraft have been performed, in order to check and validate these tools. Examples of new sun-powered designs are also presented. It was possible to observe some semblance of the solar aircraft, in terms of wing loading, with pioneering aviation aircraft from about the years 1890 to 1910. For purposes of analyzing the already-flown solar aircraft, and designing new solar aircraft, the initial study focused in identifying and understanding the differences from these aircraft to conventional aircraft. Several dedicated tools have been developed to, at first, analyze the existing aircraft, and after that, to support the new aircraft designs. Procedures and methods devoted to the estimation of drag, thrust and performance of low-speed, propeller-driven aircraft have been developed. And air vehicles - solar or not - with known performance characteristics have been considered to validate these processes. From this, specific methods for the analysis of solar propulsion processes were developed: Definition of solar irradiation model; definition of propulsive chain, from solar cells to the propeller, and with or without use of batteries. Other methodologies specific to solar aircraft were investigated and defined: a general formulation for obtaining the maximum feasible wing loading for a solar aircraft; aerodynamic characteristics of Reynolds numbers below 150,000; and metrics for estimating the mass of a solar aircraft. With this group of tools, it has been possible to develop two complementary methods for defining a configuration of the solar aircraft from the mission requirements: the Solar Aircraft Design and the Mission Analysis Method. The second one is only required on missions involving large variations in altitude. With the tools developed three concepts of solar aircraft are calculated and presented each one for a specific use. In summary, through this work a general scenario on solar aircraft is developed, aiming the project of solar aircraft; and several perspectives and possibilities for continuation or next steps are pointed out.

1) INTRODUCTION

A solar aircraft, or Sun-powered aircraft can be defined as an atmospheric vehicle that can move horizontally due to the power extracted from sunlight through photovoltaic cells dispersed in its external surfaces. A power chain inside the vehicle transforms the light energy received from the sun in electrical energy, which is transformed into the mechanical energy by a electrical motor, and is delivered to the surrounding gaseous mean through a rotating propeller. The resulting forward thrust balances the drag related to two main sources, the forward movement, and the aerodynamic lift that balances the vehicle weight. Successful solar aircraft - manned or unmanned - are something new in aviation. The first successful attempts have occurred by 1970 and 1980 decades.

The low power which can be extracted from the sun by aircraft surfaces is very low when compared to the power of conventional internal combustion aircraft. As a result of this fact, a solar aircraft must be, in terms of mass, wing loading, speeds, structures, and other design criteria, remarkably different from the conventional, internal combustion aircraft. The ways to think, design and operate a solar aircraft shall be different – at least in some aspects – than a internal combustion aircraft.

Related to this aspect, several questions can be made. For example: In which aspects solar aircraft can be though by the same viewpoint than a conventional aircraft? Which aspects, from the ones that solar aircraft differ from conventional aircraft, are the most relevant for design and operation studies? Which are the missions that solar aircraft could be useful or advantageous in the present and near future scenario? Can the solar aircraft be used in only one type of operation, or there are different potential fields of use? Is it possible to obtain a methodology for the initial definition of solar aircraft? In which point the nowadays technologies are mature to design a solar aircraft? What should be the critical technologies to take into account in specific the design of a solar aircraft?

The aim of this work is to answer to some of these questions; and to provide an initial step for solar research, based on the available information and technology.

2) MOTIVATION

This chapter presents three main aspects that stimulated this work, and shaped the way it has been developed.

2.1) Reasons to perform solar research in Brazil

A simplified study has been performed by the author in order to obtain an overall picture of solar power distribution on the Earth's Countries. The main results of this study are presented in the following figures.

The solar most relevant information in author's viewpoint is presented in figure 2.1 in which the Mean Daily Solar Intensity MDSI is compared for several countries. This parameter represents the energy received during a day per square meter, and can be expressed in $kW.h/m^2$.

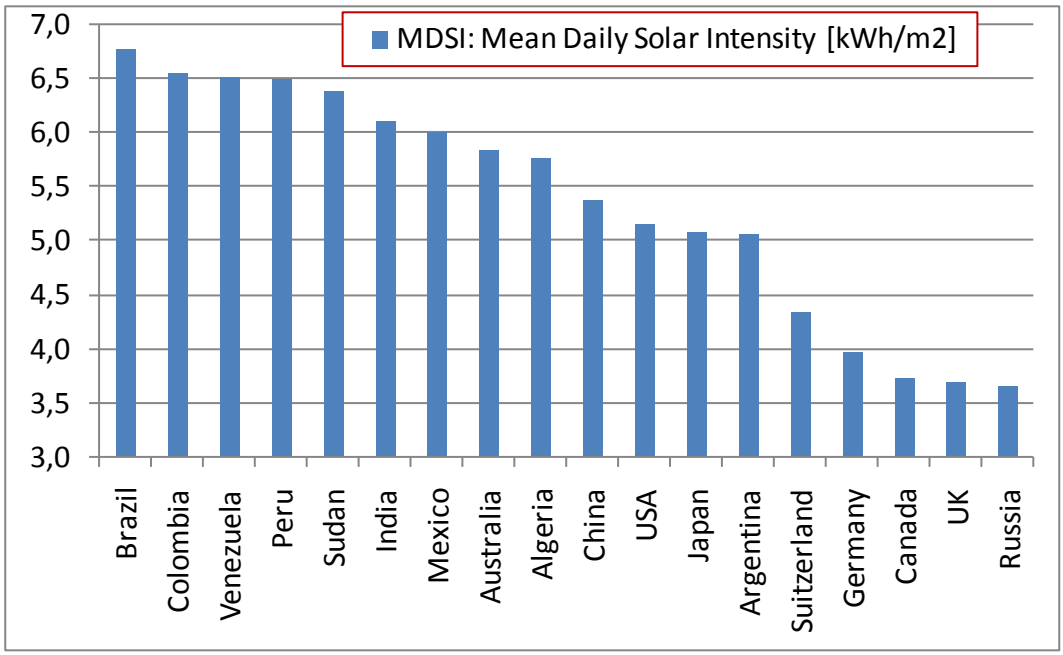

Figure 2.1: Mean Daily Solar Energy Intensity 'MDSI' in some of Earth's countries.

One can see by the figure 2.1 that Brazil presents a high level of daily solar energy intensity when compared to other countries. By this figure it can be observed that Brazil receives per square meter roughly 31% more energy from the Sun than USA, 56% more than Switzerland, 70% more than Germany , 79% more than Canada, United Kingdom (UK) and Russia.

This scenario turns to be even more dramatic if the total energy that sun provides to a country is calculated, i.e. taking into account the country's area. Although this parameter can be questionable for some, even only as a reference, it is interesting to be accounted for. The Mean Daily Solar Energy, which corresponds to the product MDSI x Area is presented, in terms of GW.h, in figure 2.2, for the same countries selected for presentation in figure 2.2. By observing figure 2.2, one can obtain that Brazil presents about 29 times the value of Japan, 39 times the value of Germany, 60 times the value of UK and more than 300 times the value of Switzerland.

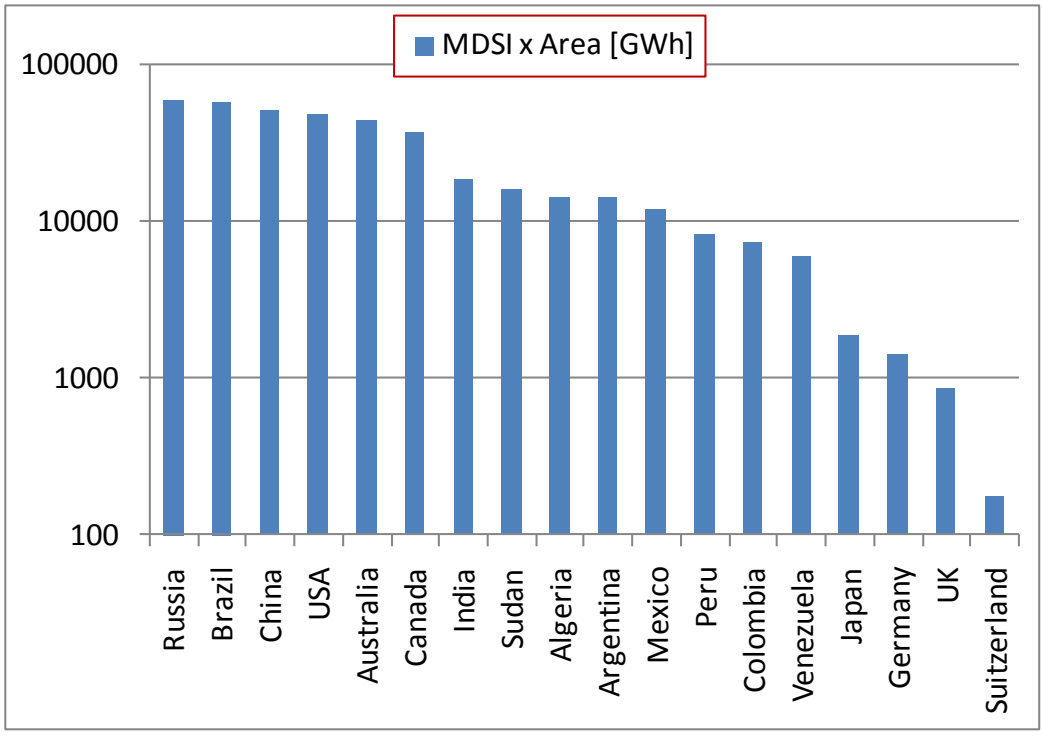

Figure 2.2: Mean Daily Solar Energy, MDSI x Area in some of Earth's countries.

Avoiding discussion of which metrics are the most applicable, the one from figure 2.1 or figure 2.2, it can be said that it is possible to use any of the two to achieve the same conclusion:

- Countries, as remarkably Germany and Switzerland, that have obtained several important results in terms of Solar power research, are less favored by Sun than Brazil; and

- Brazil, which such large solar potential, should also increase efforts in this direction of solar power research.

2.2) Reasons to study solar aircraft

The figures 2.3 to 2.5 present the evolution of the values of altitude, flight time and flight distance achieved by solar aircraft, from the first attempts (circa 1974) up to the present. In order to provide comparison, values for aircraft with combustion engines are also presented in the altitude and flight time figures. The figures show how fast the solar aircraft have progressed in terms of flight performance.

In figure 2.3 the advancement of Solar Aircraft in terms of altitude is presented and compared to typical altitudes of General Aviation and Commercial Aircraft, and the maximum altitude record for a combustion engine aircraft, the SR-71. In figure 2.3 only rocket-propelled or rocket-assisted aircraft are not considered. As can be seen in this figure, the highest altitude level achieved is from a solar aircraft.

In figure 2.4 the advancement of Solar Aircraft in terms of non-refueling flight time is presented, and compared to typical endurance levels of General Aviation and Commercial Aircraft; and the level of the maximum endurance for a combustion engine aircraft, the Rutan Voyager, is also presented. In this figure, only the aircraft which are heavier than air and intended for atmospheric flight are represented. It is possible to observe in this figure the point of about 330 hours, occurred in 2010, significantly above the endurance level achieved by Rutan Voyager; so one can note that the maximum endurance flight for an atmospheric, heavier than air aircraft has been performed by a solar aircraft.

The advancement in terms of range, performed by solar aircraft, is presented in figure 2.5. It can be noticed that the distance values are yet low when compared to combustion propulsion aircraft; due to this fact, no comparison with combustion propulsion aircraft is presented in this figure. From figure 2.5 it can be also noticed that, although the distances obtained are still modest when compared to the records of combustion engines, the values present the tendency of increasing.

In order to avoid the interpretation of the figures 2.3 and 2.4 in an overoptimistic bias, and to provide a better understanding about the limitations of sun-powered aircraft, in the section 4.3 some performance figures related to aircraft payloads are additionally presents.

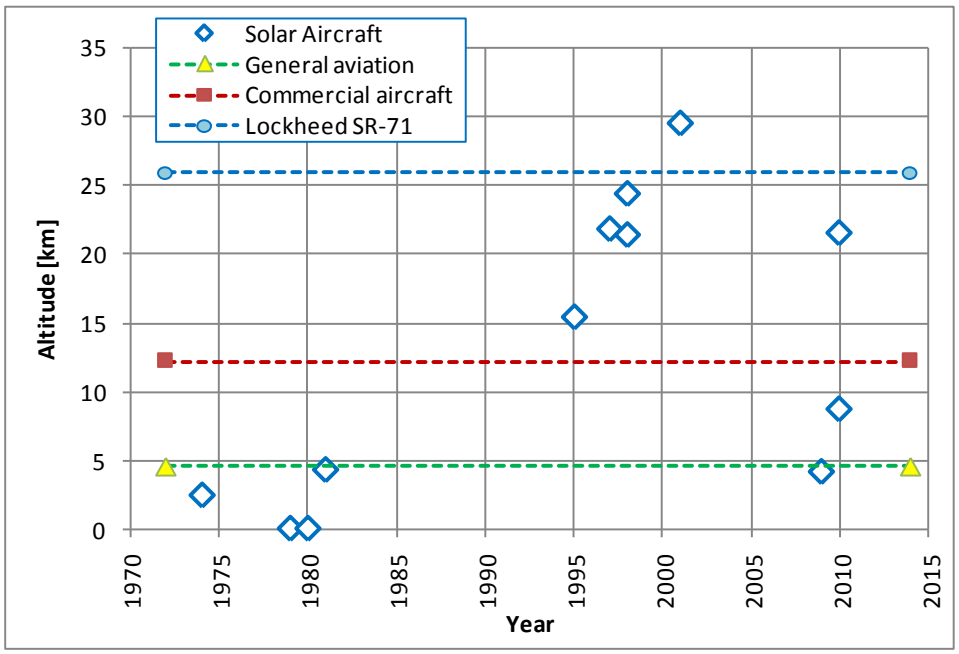

Figure 2.3: Advancement of solar aircraft in terms of altitude over time.

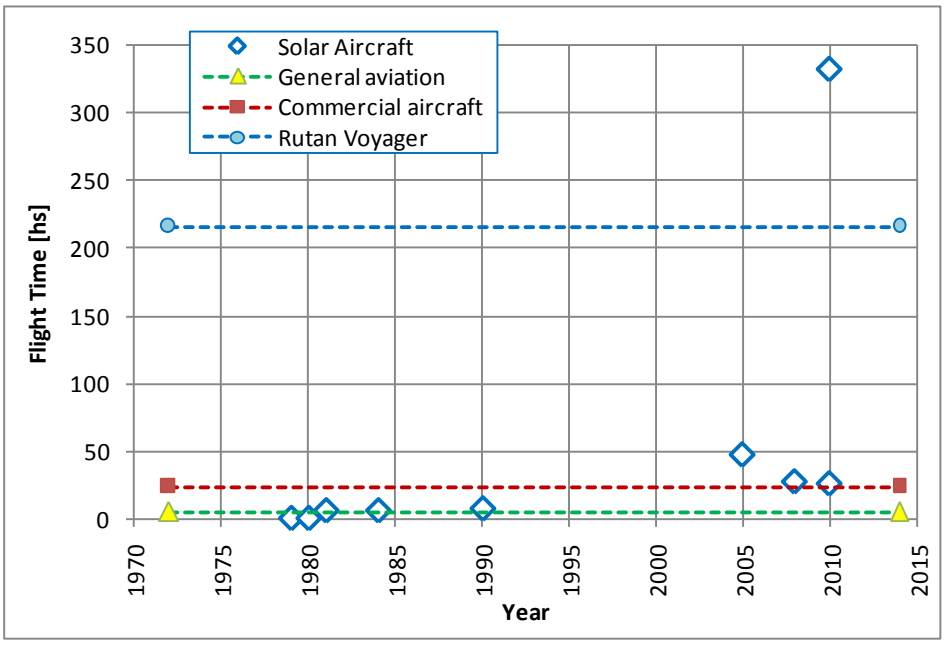

Figure 2.4: Advancement of solar aircraft in terms of endurance over time.

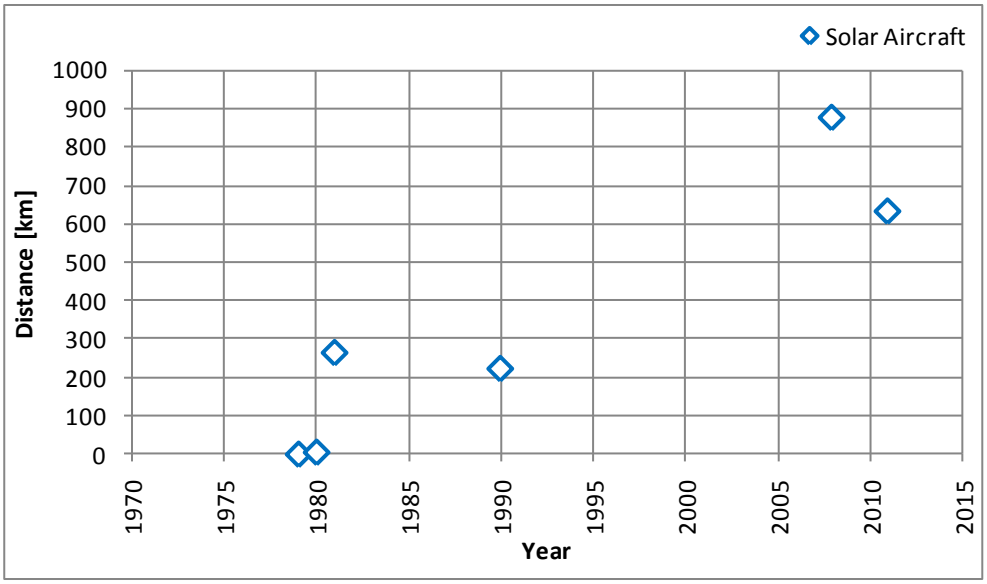

Figure 2.5: Advancement of solar aircraft in terms of range over time

It can be seen from figures 2.3 and 2.4 that, either in terms of altitude and flight time, solar aircraft evolved in a fast way along few decades, and recently surpassed the maximum values hold by the aircraft with combustion engines. These two aspects - tendency of fast growing, and achievement of values beyond the ones of combustion propulsion aircraft - for the solar aircraft in terms of altitude and flight time, are high incentives for solar aircraft researches. Despite this, the - still modest - flight distances achieved by solar aircraft, whose evolution is presented in figure 2.5, can indicate a growth potential, and can be understood as one additional incentive and opportunity for solar aircraft research. So, there is also a great potential and opportunity for solar aircraft researches focusing range.

2.3) Reasons to consider solar aircraft in a historical perspective

The evolution of some parameters from the early days of well-succeeded manned glide flights, circa 1885, up to the present is shown in the figures 2.6 to 2.9. In the figures three types of aircraft, early gliders, combustion propulsion aircraft and solar aircraft, are represented.

The variation along time of values of aircraft maximum mass along and wing loading are presented in figures 2.6 and 2.7 respectively.

From the figure 2.6 it can be noticed that solar aircraft show some tendency of mass increasing, but definitively not as high as the one that occurred with the combustion-powered aircraft; additionally it can be noticed from the same figure that the present mass values are close to the ones developed up to 1915.

From the figure 2.7 it can be noticed a very interesting feature, mainly if one compares this aspect with the one observed for figure 2.6: In a different way from the aircraft mass (figure 2.6), the maximum values of solar aircraft wing loading (figure 2.7) apparently have not increased with time, after 1980. Additionally from figure 2.7 one can note that the steady wing loading values from Solar aircraft are significantly lower compared to nowadays combustion aircraft, and – as also occurs with mass values - the solar wing loading values are in the same magnitude than the wing loading values from early aviation (up to 1915) aircraft.

The figure 2.8 presents the variation of power loading with time of solar aircraft, compared to the power loading of combustion engine aircraft. From this figure one can note the same feature than the one observed from 'wing loading' tendencies of figure 2.7: The power loading of solar aircraft seems to be steady, with a very low value if compared to nowadays combustion-powered aircraft. But one interesting new feature can observed in figure 2.8 which is different from the characteristics observed in figure 2.7 and 2.6: The steady power loading level for solar aircraft is one order of magnitude below the minimum values of combustion-powered aircraft. This can indicate how different this type of aircraft can be from the conventional, combustion-powered aircraft.

The Solar aircraft power loading levels presented in figure 2.8, significantly lower than conventional combustion-powered aircraft (even considering the earliest days of aviation) are one expression of the new and challenging aspects related to solar aircraft. And this can represent the needs of new ways of thinking, and new solutions in terms of arrangement, configuration, aerodynamics, structures and systems, compared to the existing combustion-powered aircraft.

There is one additional aspect is indicated by the 'steadiness' in the tendency of solar aircraft's power loading and wing loading, of keeping constant and presenting very low values, as shown in figures 2.7 and 2.8. This aspect tends to be obvious, but it may be valid to be explicitly written: The wing load values and power load values are very low compared to the existing combustion-powered aircraft, and do not present a significant tendency of increasing, which indicates solar aircraft probably will never be used for functions such as a heavy cargo lifter, or a dozen-passenger commercial aircraft.

The figure 2.9 presents the variation with time of solar aircraft wing aspect ratio, compared to the variation of the same parameter of combustion engine aircraft. From this figure one can note that solar aircraft present a tendency of increasing the wing aspect ratio to values notably higher than the typical ones from combustion-powered aircraft. These last ones presented the tendency of keeping this parameter steady along the last 70 decades. The high-aspect ratio tendency is one of the solutions associated to the very low power levels of solar aircraft compared to combustion-powered aircraft.

Solar aircraft are, among other features, in terms of power loading and aspect ratio, something new in aviation. But in terms of wing load and mass, they can be considered close to the aircraft of early days of aviation. Due to this aspect, it may be important to understand the solar aircraft not only in the new, technological aspects, but also in their similarities with early aviation representatives. In addition, tools intended for analysis of sun-powered aircraft can be also used for - and initially checked through - analysis of well known, early aviation representatives.

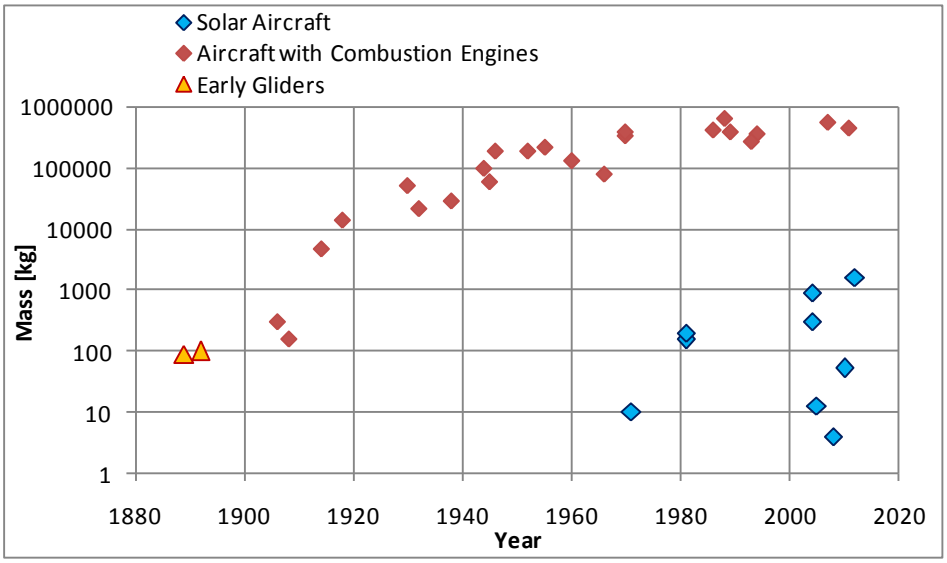

Figure 2.6: Values of aircraft maximum mass along time; solar aircraft are included for comparison.

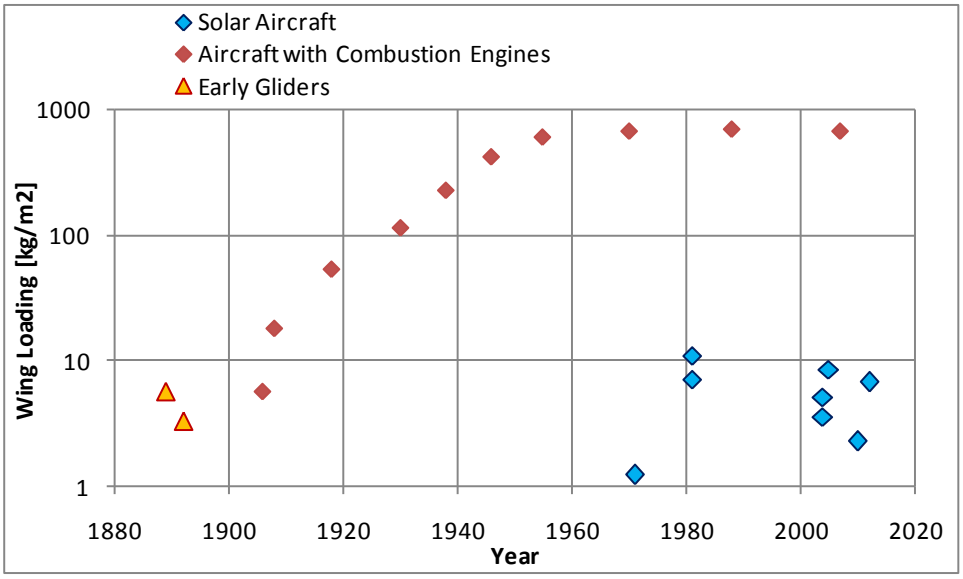

Figure 2.7: Aircraft wing loading growth along time. Solar aircraft are included for comparison.

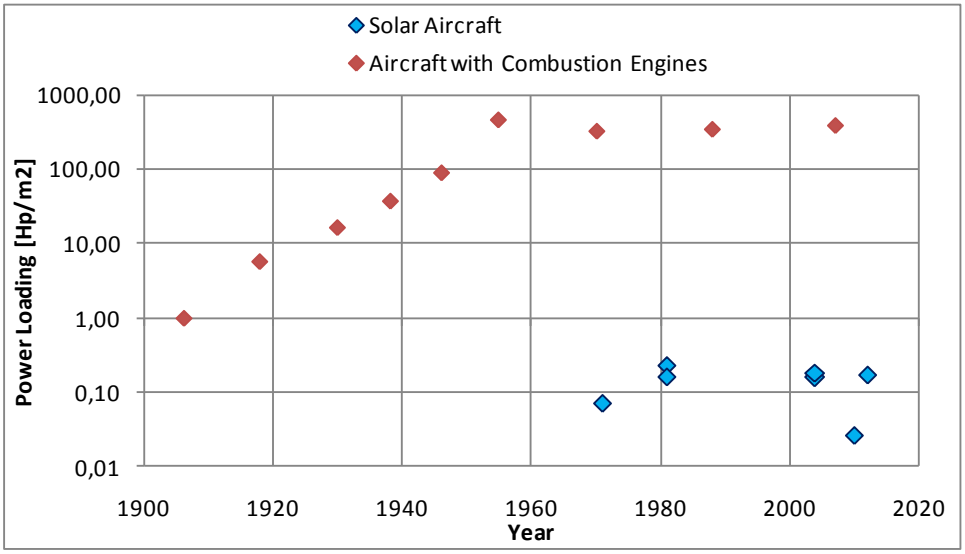

Figure 2.8: Power loading of the aircraft presented in the previous pictures along time.

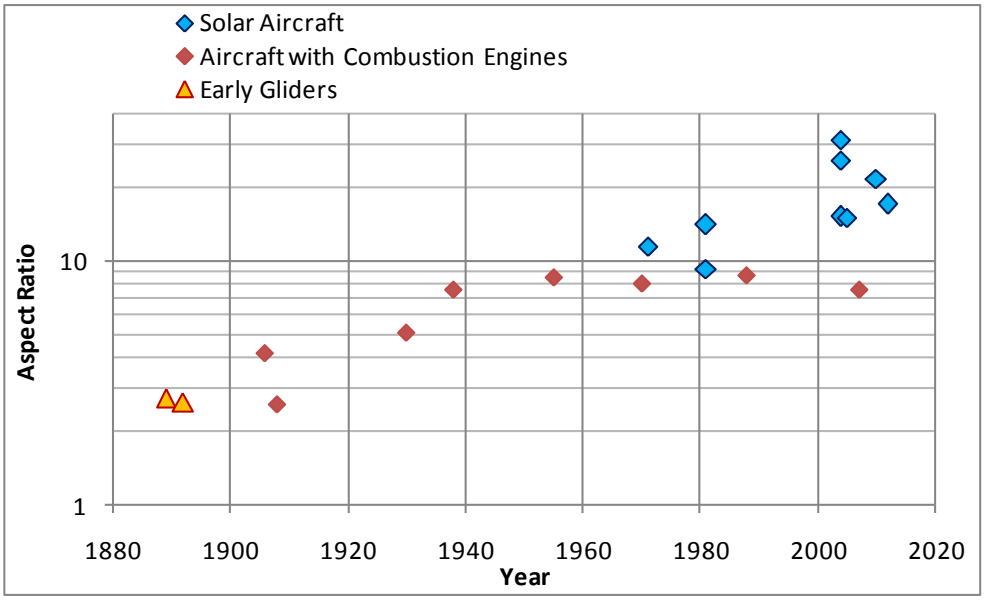

Figure 2.9: Aspect Ratio of the aircraft presented in the previous pictures along time.

3) LITERATURE REVIEW

In this chapter the most important sources to this work are identified and briefly commented. Since several areas of knowledge are involved in the researches performed, the contributions are presented as grouped by main areas, as follows.

3.1) Literature Review of Low Speed, Pioneer Aircraft

The pioneer aircraft considered in this work are some remarkable examples of well succeeded early aircraft from 1890 to 1910. Studies related to these aircraft have been included in this work - even considering that these aircraft are not Sun-powered - due to some similarities of these aircraft to solar aircraft, e.g. the very low speed and very low wing loading, as presented in the section 2.3. From the several publications studied, the ones which have been the most valuable ones are mentioned in this section. Some of the most valuable publications found in this area are from decades ago, as Lilienthal (1889), Baden-Powel (1903), Ferris (1910), Karlson (1940) and Villares (1957).

Lilienthal (1889) presents the airfoil shape and tests for evaluation of the aerodynamic forces at low Reynolds numbers, probably the first scientific research about cambered airfoils. Karlson (1940) also presents reliable information regarding Lilienthal aircraft. The site Otto Lilienthal Museum (2011) presents a vast and consistent data compilation of most of the Lilienthal aircraft, and articles written by Lilienthal for a nineteen-century magazine, explaining the concepts associated to the hang-gliding sport activities.

Villares (1957) presents the history of Santos-Dumont aircraft development, with several data and pictures that are not easily found in other sources. Ferris (1910) presents a detailed description of Demoiselle aircraft, together with other important technical achievements of the 1905-1910 aviation period. Baden (1903) presents a detailed and consistent report of Santos Dumont N.9 airship. Other very useful information for Santos Dumont aircraft is presented in Costa (1971). The electronic sites Flying machines (2014) and Cabangu (2012), from Russia and Brazil respectively, contain rare pictures of Santos-Dumont aircraft, in which valuable information can be extracted.

3.2) Literature Review of Solar Aircraft

As several valuable sources of this group have been considered in this work, in a number significantly higher than the sources related to the other areas, the most important ones are listed in the table 3.1, with the identification of the main point of relevance for this work. In this section the sources related to human powered flight are also included. The level of relevance of the information for the present work is also identified in table 3.1, in the priority order: high and important.

Specific comments about some of the sources are presented as follows.

The Site of Fédération Aéronautique Internationale (2014) presents the officially recognizable records, including the ones for Sun-powered aircraft.

Several highly valuable sources of information have been released by NASA. NASA sites (2010, 2014) present reliable and consistent information regarding the solar aircraft family from Pathfinder to Helios; NASA publications from Phillips (1980), Hall et al (1983, 1985), Hall and Hall (1984), Landis et al (2002), Colozza (1994), Bailey and Bower (1992), Penner (1983) address different aspects related to solar aircraft; in general focusing high-altitude flights. Besides NASA publications, additional information on Pathfinder systems can be found in Colella and Wenneker (1994).

In Noth (2007, 2008a) the most important aspects related to Solar aircraft design are described, together with a reliable design methodology. Based on this procedure, the aircraft sky-sailor has been designed, built and flown continuously 27 hs without the need of thermals (Noth, 2008a). Among several important and useful concepts presented in these sources, it is important to highlight some: The perceived absence of clear design methodologies related to some already-flown solar planes, the absence of prototypes to validate some of the published design methodologies, the drawbacks related to very small and very large solar aircraft, the limits of solar aircraft in terms of wing loading, the structural weight in function of wing area, the issues related to increase flight endurance by using altitude gain or thermal soaring.

On the group of the highest relevant information, it is important also to cite the information presented by Ross (2009) about the main design aspects for a high endurance, low altitude, manned solar powered aircraft, the publication of Roland Boucher (2003) about Sunrise I and the basic principles of directly sun-powered high altitude flight, the work presented by Rappinet (2009) with the

story of Zephyr, the information presented by Cocconi (2008), Murray (2005), Dornheim (2005) about Solong aircraft; among other highly valuable ones.

Table 3.1: List of some of the references about solar and HPA aircraft consulted

Author	Year of Publication	Type of Publication	Relevance for this Work	Main Points for Relevance
Noth, Sigwart, Engel	1.1, 2007	Lecture material	High	concepts for solar aircraft design aimed to 24+ flights, used for Sky-Sailor
André Noth	2008 (a)	Doctoral exam presentation	High	General concepts for solar aircraft design
André Noth	2008 (b)	Report	High	Sky-Sailor characteristics
André Noth	2008 (c)	Report	Important	List with characteristics of 90+ solar powered aircraft
André Noth	Jun2008 (d)	Report	Important	Sky-Sailor Solar proved Continuous Flight
André Noth	2008 (e)	www. sky-sailor.ethz.ch	High	Initial description of work; Important considerations of the solar flight on Mars; Access topublications related to Sky-Sailor.
Alan Cocconi	2008 (a)	Informal Report:	High	Solong: Characteristics, and strategies for the 48hs flight
Alan Cocconi	2008 (b)	Presentation	High	Concepts for solar aircraft engines
Hannes Ross	2009 (a)	Presentation	High	Design concepts related to Solar Impulse
Hannes Ross	2009 (b)	Paper	High	Design concepts related to Solar Impulse
Roland Boucher	2003,	www.project sunrise.info	High	Data, history, mission and description of Sunrise I
NASA	Accessed 2013	Fact Sheets (2)	High	Description of Helios family
Charles Murray	2005	Design News Magazine (1)	High	Description of Cocconi Solong
Michael Dornheim	26 Jun 2005	Aviation Week Magazine (3)	High	Description of Cocconi Solong

Table 3.1 (continuation): List of some of the references about solar and HPA aircraft consulted

Author	Year of Publication	Type of Publication	Relevance for this Work	Main Points for Relevance
Piccard, Borschberg	2009 to present	www.solar impulse.com	High	Data and facts of solar Impulse aircraft
Robert Boucher	1984	Paper : History of Solar Flight	High	Data of SunriseII, Solar Riser, Solar One, Gossamer Penguin, Solair I, S.Challenger
Robert Boucher	1985	Paper	High	History and Data of Sunrise I and Sunrise II
McCready, Lissaman, Morgan	1983	Paper	High	Solar Challenger: Design and test results
Annabel Rapinett	2009	M Sc dissertation	High	Zephyr: History, systems, launching
Colella, Wenneker	1994	Magazine R&TR	Important	Technical solutions for Pathfinder
NASA	1998	NASA Facts PDF	Important	Solar Research at Dryden Center, Helios Family
Manish Bhatt	2012	M Sc research	Important	Design of a long endurance, high altitude solar aircraft
Benedet	1985	NASA TM, M Sc Thesis	Important	Description of solar cells, main principles of solar aircraft and examples of solar aircraft, report made in Argentina
Montgomery Mourtos	2013	Paper	Important	Design example: Photon aircraft
Héctor Vidales	2013	M Sc thesis	Important	Basic concepts and examples aircraft systems definition
Yaser Najafi	2011	M Sc research	Important	Design of a long endurance solar aircraft
Jabbas, Leutenegger	*2010*	paper	Important	Design techniques, flyable envelope; Solar aircraft data
Eric Raymond	Accessed 2013	www. solar-flight.com	Important	Description and missions of Sunseeker aircraft; description of Edelweiss sailplane
Martin Cowley	1981	Aeromodeler Magazine	Important	History of Solar Challenger, following Solar Penguin and Sunrise

Table 3.1 (concluded): List of some of the references about solar and HPA aircraft consulted

Author	Year of Publication	Type of Publication	Relevance for this Work	Main Points for Relevance
Moulton, Lloyd,Cowley	Sept. 1979	Aeromodeler Magazine	Important	Description of the Gossamer Albatross
Shiau, Ma, Chiu, Shie	2010	Paper	Important	Optimization of Solar aircraft for a 9hs mission; presents consistent diagrams
Brian Utley	Jun 2013	NAA Report	Important	Solar Impulse characteristics
Landis, LaMarre, Colozza	2002	NASA TM-/AIAA 2002-0819	Important	Conceptual definition of a solar aircraft for Venus atmosphere
Robert Boucher	1985	AIAA paper	Important	Proposal of a solar airplane to flight up to 200,000 feet, possibly in continuation from Roland Boucher works
Anthony Colozza	1990	NASA CR 185243 AIAA -90-2000	Important	Proposal of a conceptual design of a long-endurance Aircraft for Mars atmosphere

From the several publications referred in this section, one important point to highlight is the general propulsive chain of a sun-powered aircraft. The figure 3.22 at section 3.8 presents a simplified view of the propulsive chain; and this figure can be understood as a synthesis between the several sources studied.

In order to exemplify the type information obtained from the sources, some characteristics of Sunrise aircraft are presented and commented as follows. Sunrise I is the aircraft that performed the first well succeeded solar flight, in 1974, as shown in Roland Boucher (2003). The drag polars from flight tests of Sunrise I and Sunrise II, taken from Robert Boucher (1985), are shown in figure 3.1: Sunrise I with and without the solar array, which is useful to quantify the solar array drag on the aircraft; and from Sunrise II with the solar array only. Apparently no flights of Sunrise II have been performed without solar panels. As a result of the experience with Sunrise I, Sunrise II has flown with an improved solution of cells arrangement - not detachable from the aircraft, and aimed to present lower drag than the solar cells of Sunrise I. The lower drag of Sunrise II compared to Sunrise I is

evident from the difference of the curves ‘Sunrise II, with Cells, CD’ and ‘Sunrise I, with Cells, CD’ from figure 3.1.

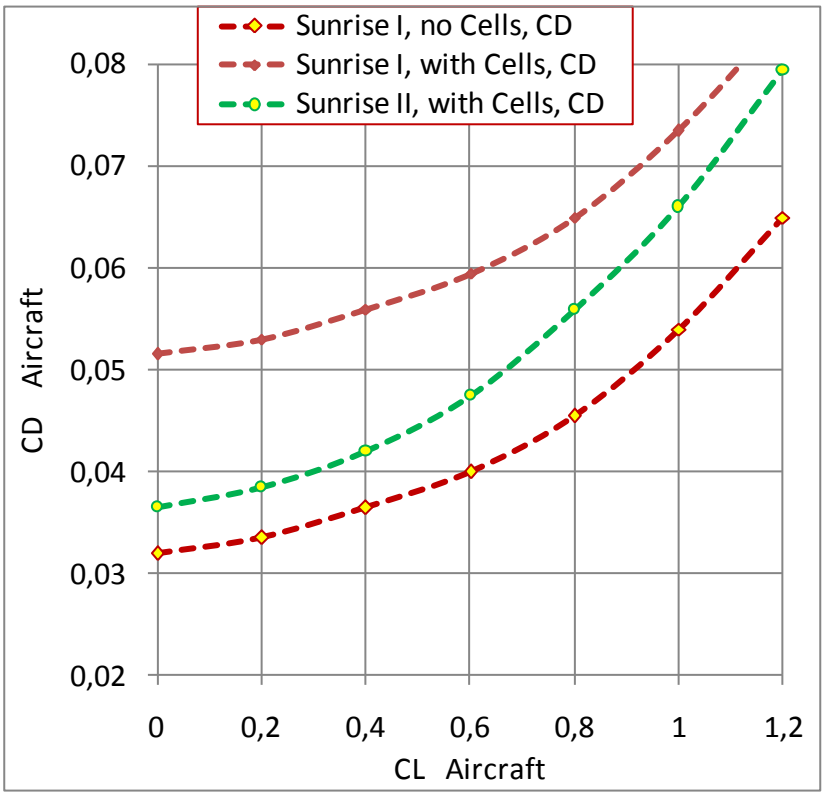

Figure 3.1 Sunrise drag polars reduced from flight trials

Other important information related to Sunrise I is the intended flight profile, also taken from Robert Boucher (1985) and presented in figure 3.2. There are some important aspects to point out, related to this figure, that are specific for sun-powered aircraft and require a different culture from the one commonly considered for combustion-powered aircraft. This figure is related to California, USA, at 21 June; this is a feature specific for solar aircraft that must be taken into account. Differently from combustion aircraft, sun-powered aircraft performance figures should be always related to specific position on the planet, and a specific time on year, even in rough terms, as Country or state, and month. Other aspect is that the mission success is related to the departure time, due to Sun positioning related to ground. The third aspect is that the feasibility of a successful flight starting from the ground is linked to meteorological clearance, not only in terms of turbulence avoidance, but also, the

existence of a clear part of the sky, i.e. without clouds, to allow the suitable connection from the energy source to the aircraft.

As reported in Boucher (2003) and Boucher (1985) both aircraft Sunrise I and II have flown in 1974 and 1975 to altitudes below twenty thousand feet; and as presented in figure 2.3, the altitudes intended for Sunrise have been finally achieved about twenty years later. The concept of a solar aircraft achieving high altitudes, even concerning a large amount of constraints and compromises, was right.

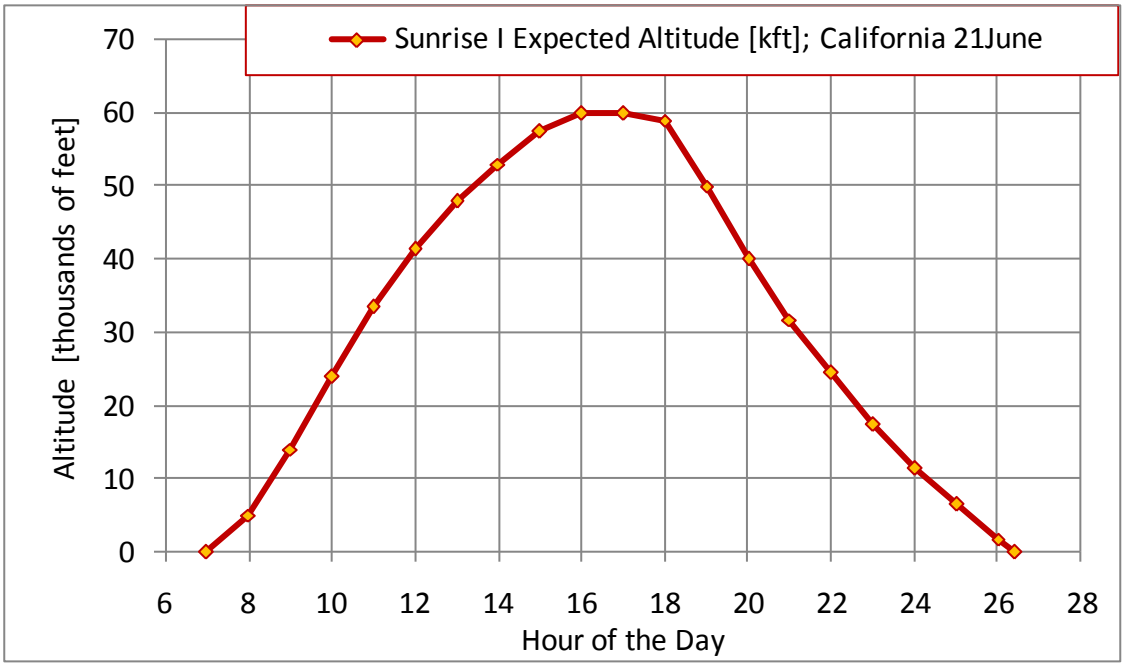

Figure 3.2: Sunrise I expected altitude profile

3.3) Literature Review of Propellers

Biermann and Hartman (1937, 1939) presented in a group of NACA reports, an extensive and very useful series of experimental results of propellers, possibly in a – well succeeded - attempt of providing reliable references for the ongoing efforts to better understanding the propeller behavior.

Ernest Weick (1930) presented, among several other works related to propeller evaluation, the very useful Cs approach for definition of one propeller, a practical procedure, given the desired rpm, power, and reference airspeed.

In McCormick (1980), the information originally produced by Weick, and by Biermann and Hartman, are presented in a summarized way; additionally, the two basic theories for propeller

theoretical and simplified analysis, which are the Blade Element Theory and Momentum Theory', are presented in this source.

Valuable information about analysis and design of low rpm, high effectiveness propeller, can be found in the work from Larrabee (1979), who has became notorious for the re-designing the Gossamer Condor propeller.

Schmitz (1942) also presents some suggestions for basic design of low-Reynolds propellers.

3.4) Literature Review of Lift, Drag, Performance

The starting point for drag and lift studies of this work are Hoerner (1958) and Hoerner (1985). These two masterpieces, besides presenting large amount of consistent information, also furnish indication for other research material covering specific subjects. Several valuable publications could be identified and read by the author as a consequence of the references indicated in these two books. As one example, it is possible to cite the publications of Prandtl et al (1920) in which, among voluminous important information, lift and drag results of airfoils tested from 0 to 360^{o} are presented.

Important summaries on drag and lift data are also presented in McCormick (1980); this source also contains a simplified and useful formulation for performance and atmosphere. To perform the evaluations of aircraft drag polars, besides Hoerner (1958) and McCormick (1980), one important source considered is Pinto et al (1999). One of the important considerations in this publication is the declared relevance of considering the Reynolds number on the drag polar evaluation.

For low-speed airfoil data several NACA reports have been studied, being the most important the NACA Reports 93, 124, 182, 244, and 286 (1928); Louden (1929); Abott, Doenhoff and Stivers (1945). They represent very important compilations of tests results, being a good starting point for understanding the basic characteristics of several low-speed airfoils. Lissaman, Jex and MacCready (1979) also presented, in a summarized way, their efforts to obtain a flyable machine with very low wing loading and power loading, and low-Reynolds airfoil.

For studies of the special aerodynamic characteristics related to low-Reynolds conditions, besides the sources presented above, other specific publications have been considered; they are identified in section 3.5.

Crowley (1925) provides concise and practical information in terms of aircraft drag due to propeller slipstream effects.

3.5) Literature Review of Reynolds Number effects

During the researches and analyses performed during this work, the strong influence of the Reynolds number on the low-speed aircraft aerodynamic performance has been observed. One can say that for low speed aircraft, and high altitude flight aircraft (and some of the analyzed aircraft in this work possess the both characteristics) the Reynolds number is as important as the Mach number is for high-speed aircraft, or jet aircraft. It has been also noticed during the development of this work that some robust, reliable, traceable, and fast-to-use definitions of dependence of coefficients due to Reynolds number in the region of interest are not so well-established as desired; so a specific research in this field has been established, as part of this work, to provide at least the minimum amount information of needed for the 'not-so-conventional aircraft and missions' analyzed herein.

3.5.1) Overview of Reynolds number related to low-wing loading aircraft.

Possibly the first person to recognize the main elements and characteristics of a suitable airfoil for low Reynolds number has been Otto Lilienthal (1889). A remarkable study in terms of lift and drag for low Reynolds is presented in Schmitz (1942, 1967); for the time of that research the interest was much more destined for scale gliders, but from nowadays perspective it can be considered as the basis of the low-Reynolds aerodynamic researches, not only for study of flying animals, but also for small, autonomous artificial flying machines, of small size, very low speed or very high altitude. Other good information on low-Reynolds airfoils can be found in Selig et al (1989), Selig et al (1995), Williamson et al (2012), and at UIUC (2014a, 2014b).

The Reynolds number is defined as:

$$Re = TAS.C/\nu \qquad (3.1)$$

Where:

- TAS [m/s] is the aircraft true airspeed, in meters per second;
- C [m] is the reference dimension of the body or surface in study, which is generally in this study the cord of the surface, or the length of the body;

- ν [m^2/S] is the kinematic viscosity of the air, which is function of the aircraft altitude.

The main point to justify this section is that it has been found that, in a different way from the conventional manned aircraft, sun-powered aircraft can be aimed to flight at Reynolds numbers below Re 2 10^5, due to the low speeds and high altitudes; and the aerodynamic characteristics of objects flying below Reynolds numbers 2 10^5 cannot be accurately predicted by extrapolation of higher Re tendencies.

According to Hoerner (1958), and Schmitz (1942), below Reynolds numbers $2x10^5$ there are two important regions with different characteristics. The first one is the transition region, with Reynolds number between $1.5x10^5$ and $8x10^4$, in which an intense hysteresis of lift and drag due to incidence variation occurs; and the second one is related to Reynolds number below $8x10^4$, in which the hysteresis disappear but, for conventional airfoils with camber and thickness, the lift is significantly lower and the drag significantly higher, when compared to the same characteristics for these airfoils at Reynolds numbers higher than $2x10^5$.

Also from the same sources, in a very interesting way, extremely thin (t/c~3%) cambered airfoils, which are not competitive with common airfoils for Reynolds numbers above $2x10^5$, are the ones which present better characteristics at Reynolds numbers below $8x10^4$.

The transition zone is illustrated by figures 3.3 to 3.5, with values obtained from Hoerner (1958). In these figures the aerodynamic characteristics of two airfoils, presented in figure 3.6, are compared:

- Cambered Plate 417a: T/C = 3.0%, Z/C =5.8% ; taken from chapter 6 of Hoerner (1958)
- Airfoil N60: T/C = 12.4%, Z/C =3.8% ; according to Hoerner (1958), NACA Report 628 (1932), and NACA TN 388 (1931)

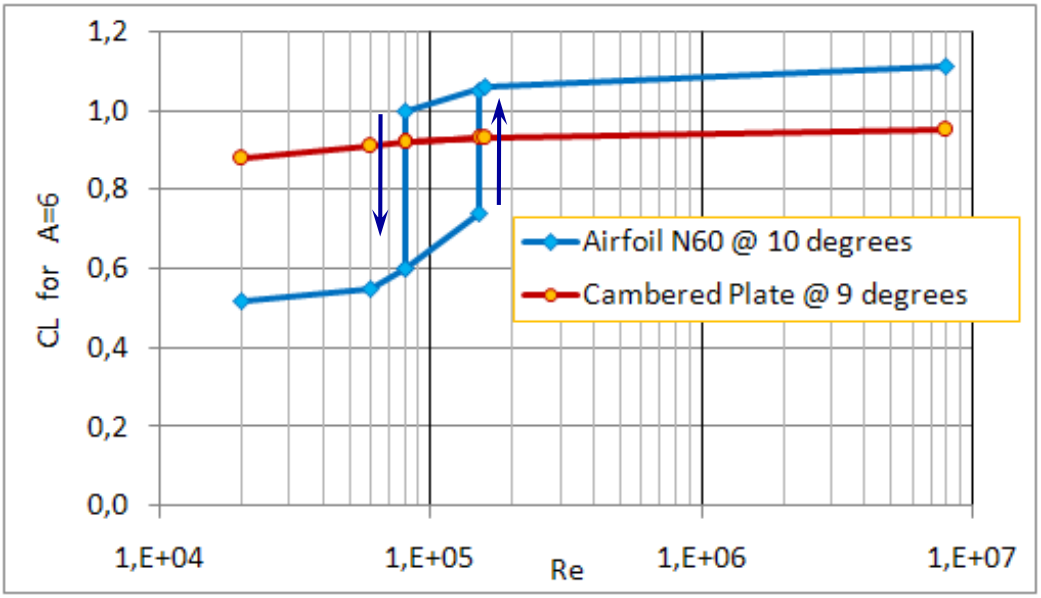

Figure 3.3: Variation of CL with Re for Cambered Plate and a Conventional Airfoil

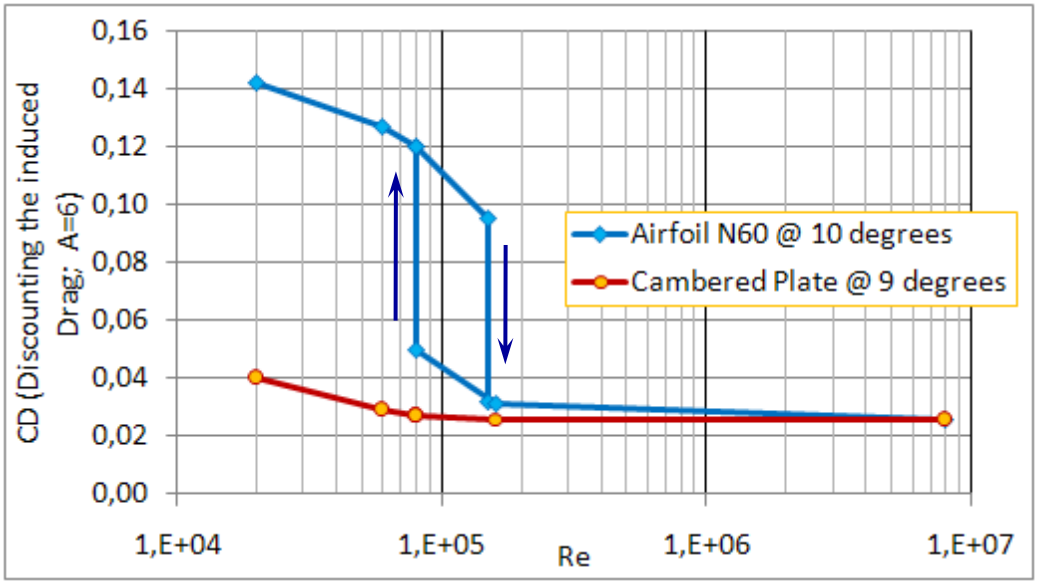

Figure 3.4: Variation of CD with Re for Cambered Plate and a Conventional Airfoil

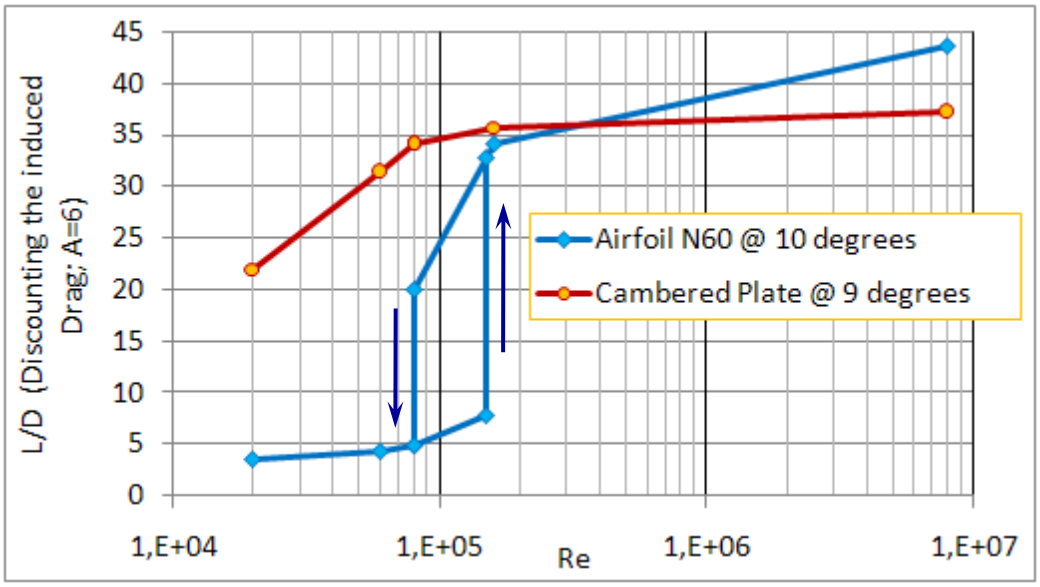

Figure 3.5: Variation of L/D with Re for Cambered Plate and a Conventional Airfoil; values are consistent with the ones presented in figures 3.3 and 3.4

Figure 3.6: Cambered plate '417a' and airfoil N-60, from Schmitz (1942)

The reason for thin cambered surfaces being better at Reynolds numbers lower than 1.5×10^5 according to Schmitz (1942) is that, at these low Reynolds numbers there is a tendency of occurrence of laminar leading edge stall on the airfoils at very low angles of attack. In thin airfoils the transition laminar-to-turbulent flow is forced to occur at leading edge; and apparently this carries energized air closer to the surface, avoiding the laminar leading edge stall to occur.

The very light aircraft Gossamer Condor and Solar Challenger of Paul MacCready, from about 70 to 80 years after, used airfoils with thickness about 12 to 14%, as can be seen in figure 3.7. According to Kroo and Alonso (2012) the Reynolds Number for airfoil 'Lissaman 7769' of Gossamer Condor is about 500,000, and airfoil 'Lissaman-Hibbs 8025' for Solar Challenger, is about 700,000 to 2000,000. Although special care was needed on the design of these 2 airfoils, they are above the Reynolds region of the abrupt reduction of L/D, presented in figure 3.5.

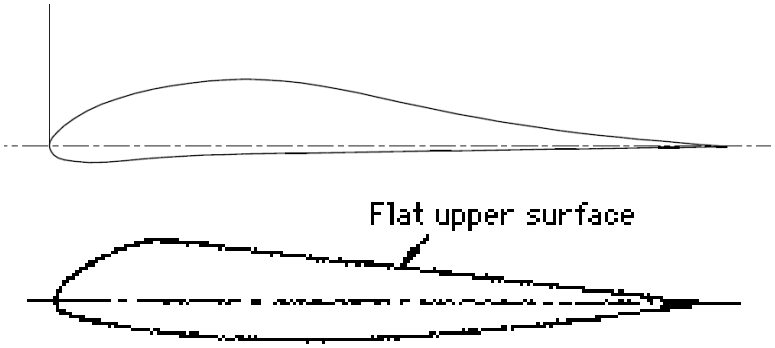

Figure 3.7: Airfoils from two aircraft designed by Paul MacCready; 'Lissaman 7769' (above) for Gossamer Condor, and 'Lissaman-Hibbs 8025' for Solar Challenger.

One interesting aspect related to low Reynolds number characteristics is that, according to Schmitz (1942) and Hoerner (1985), the strong reduction of the Lift-to-Drag ratio of conventional airfoils below $1.5x10^5$ presented in figure 3.5 was not commonly known; some tests performed at low Reynolds number ($2x10^4$ to $2x10^5$) do not reproduce the effects of figure 3.5. The reason for this is that only tunnels of very low turbulence could be able to obtain these results. This effect of Lift-to-Drag ratio reduction occur due to laminar flow conditions; and the normal tunnels present a turbulence level in the test section that does not allow the flow to be laminar, as is the real free-stream flow condition during flight. Due to this, in some tests at these low Reynolds number levels, unrealistic and overoptimistic conclusions of airfoil behavior apparently occurred.

3.5.2) Variation of airfoil lift and drag coefficients with Reynolds number

This sub-section presents the definition and synthesis of aerodynamic characteristics low Reynolds of two airfoils, from different sources. The first airfoil is the N-60, which is introduced in

the previous sub-section. It is an airfoil for airplane models in Germany by 1930. Besides its aerodynamic characteristics presented in NACA Report 628 (1938), its low-Reynolds characteristics have been obtained from the excellent work of Schmitz (1942). The second airfoil is the Eppler 387, which is an airfoil designed for low Reynolds Number, as presented in Selig et al (1989). According to Roland Boucher (2003) and Robert Boucher (1985), this airfoil is used on both aircraft Sunrise I and Sunrise II.

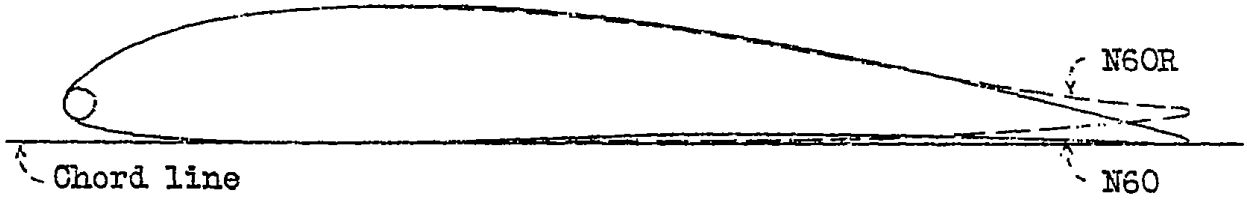

Figure 3.8: Airfoil N-60, T/C=12.4%; Z/C=3.8%, from NACA TN 388 (1931)

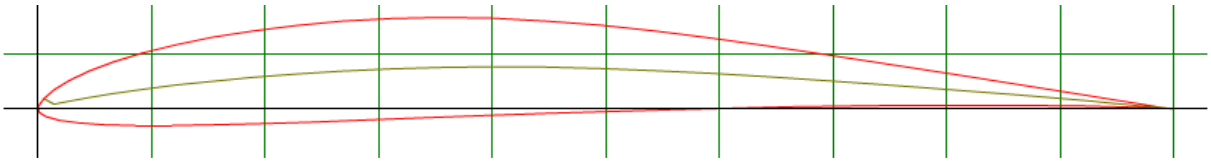

Figure 3.9: Airfoil Eppler 387, T/C~9%; Z/C~3.8%, from UIUC Airfoil Database.

a) Conventional airfoil 'N-60' Lift and Drag Characteristics

The aerodynamic lift and drag characteristics of airfoil N-60 for different Reynolds numbers are summarized in figures 3.10 and 3.11. These figures represent the compilation of values from Hoerner (1985) and Schmitz (1942) for Reynolds number below 150,000; and NACA Report 628 and NACA TN 388 for Reynolds number 3.1×10^6.

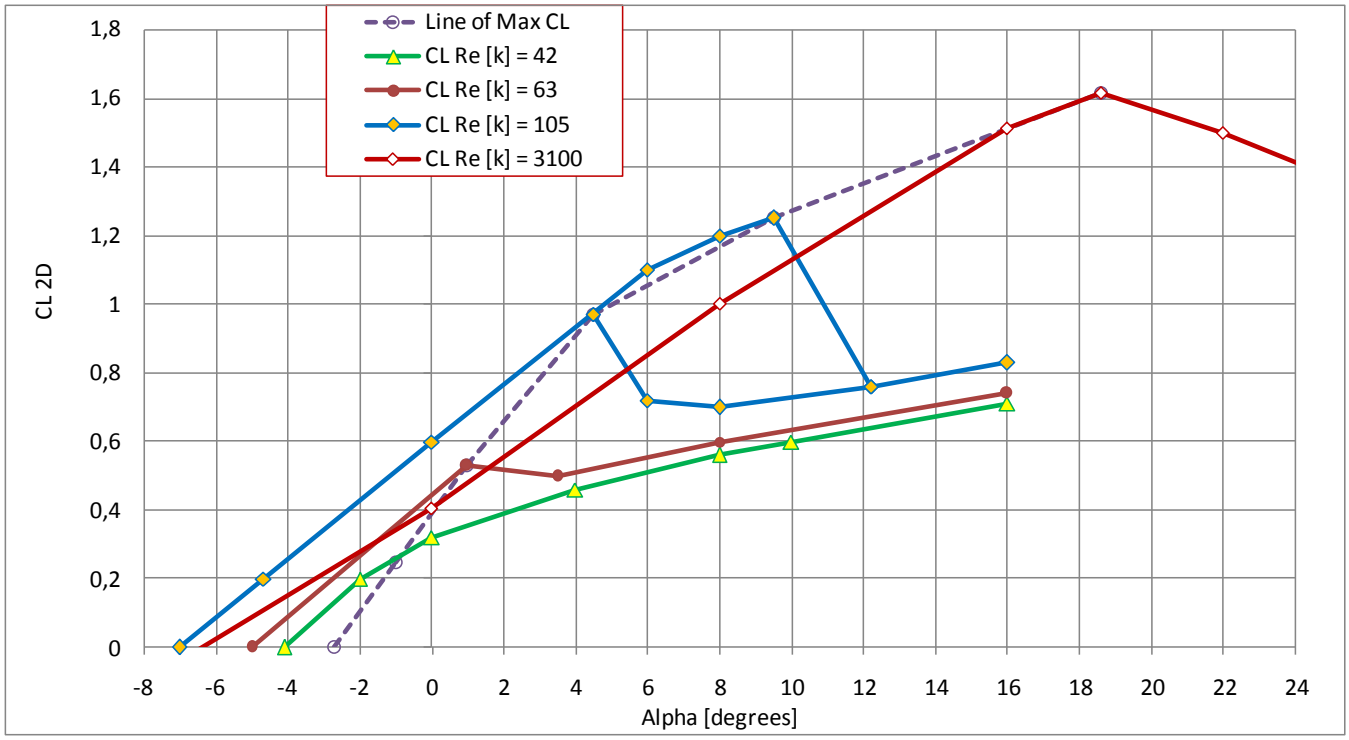

Figure 3.10: 2-dimensional CL versus alpha for different Reynolds numbers, airfoil N-60

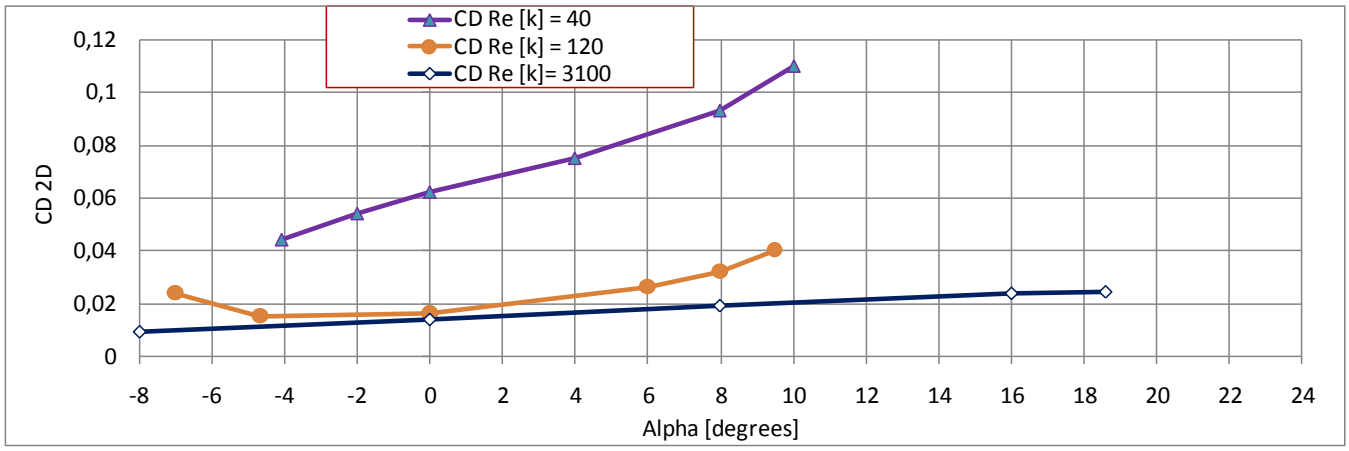

Figure 3.11: 2-dimensional CD versus alpha for different Reynolds numbers, airfoil N-60

An estimation of parameters Alph CLo, CLmax, CDo and K for the available Reynolds numbers have been performed based on the values and curves presented in figures 3.10 and 3-11. The values obtained for the coefficients are presented in figure 3.12, in function of Reynolds number.

One can note that the factor K in this case represents the coefficient of the equation of the parabolic curve:

$$CD = CDo + K.CL^2 \quad (3.2)$$

Being all the values CD, CDo, CL, referred to the curves of the (2-dimensional) airfoil drag and lift coefficients presented in figures 3.10 and 3.11.

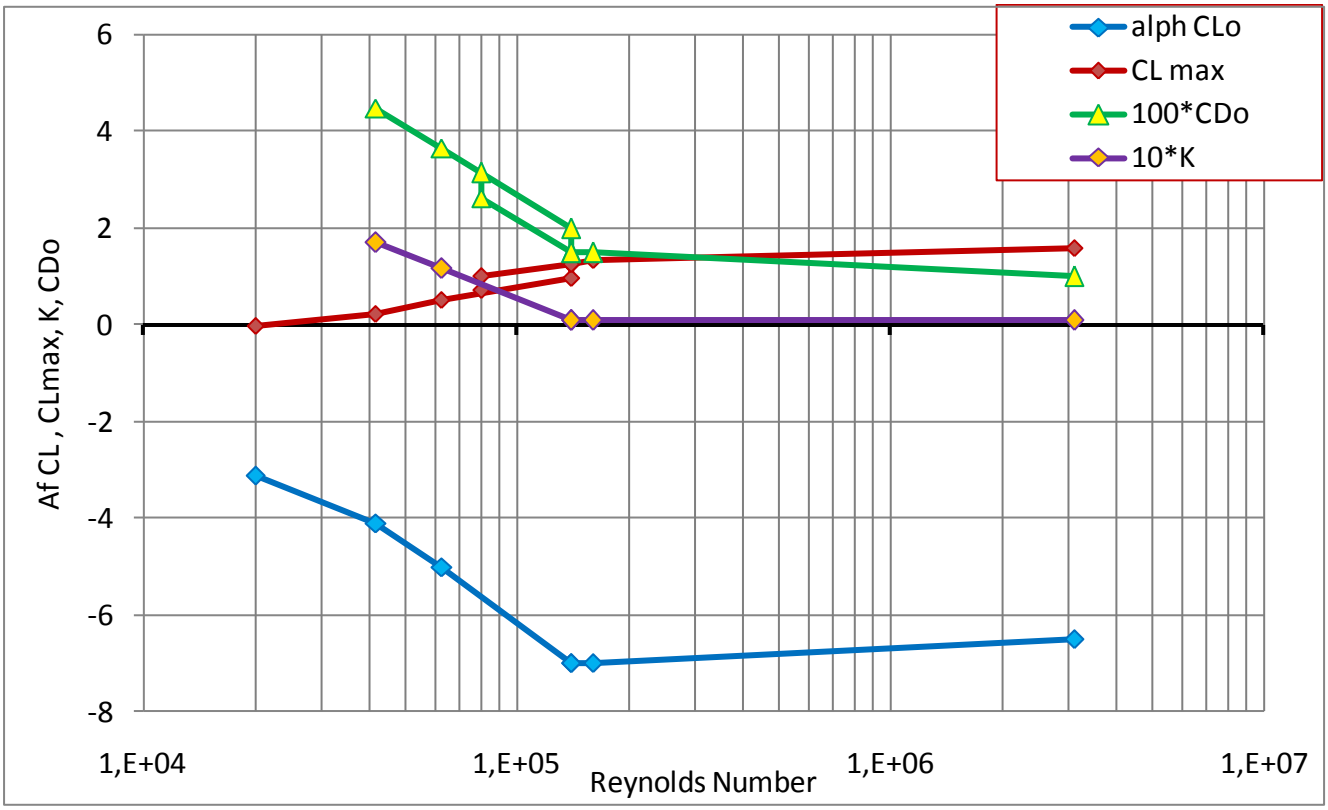

Figure 3.12: Variation of N-60 airfoil 2-dimensional coefficients with Reynolds number

b) Eppler 387 Airfoil Lift and Drag Characteristics

In order to define a variation of the drag with Reynolds Number for a good low-Reynolds number airfoil, the Eppler 387 characteristics are analyzed in this work, as presented in this sub-section. The airfoil main data, which is CD versus CL for several Reynolds Numbers are obtained from UIUC (2014), and presented in figure 3.13.

As performed for N-60 airfoil in previous sub-section, parabolic curves of the type of equation 3.2 are chosen to represent the airfoil CD versus CL curves presented in figure 3.13. The parabolic curves adopted are presented in figure 3.14. The coefficients CDo2D and K2D which define these curves are tabulated, in function of Reynolds number, for interpolation. The suffix 2D in the coefficients is to identify that they are related to the airfoil. The airfoil coefficients CDo2D and K2D obtained are presented as function of Reynolds number in figure 3.15.

The information of figure 3.15 is considered in this work, for the analysis of the aircraft drag, considering Reynolds effects. The values of airfoil lift, CLmax and αCLo, have been also obtained by the same procedure as the one performed for N-60 airfoil; and these values are shown as function of Reynolds number in figure 3.17, compared with the values of the same parameters for N-60 airfoil.

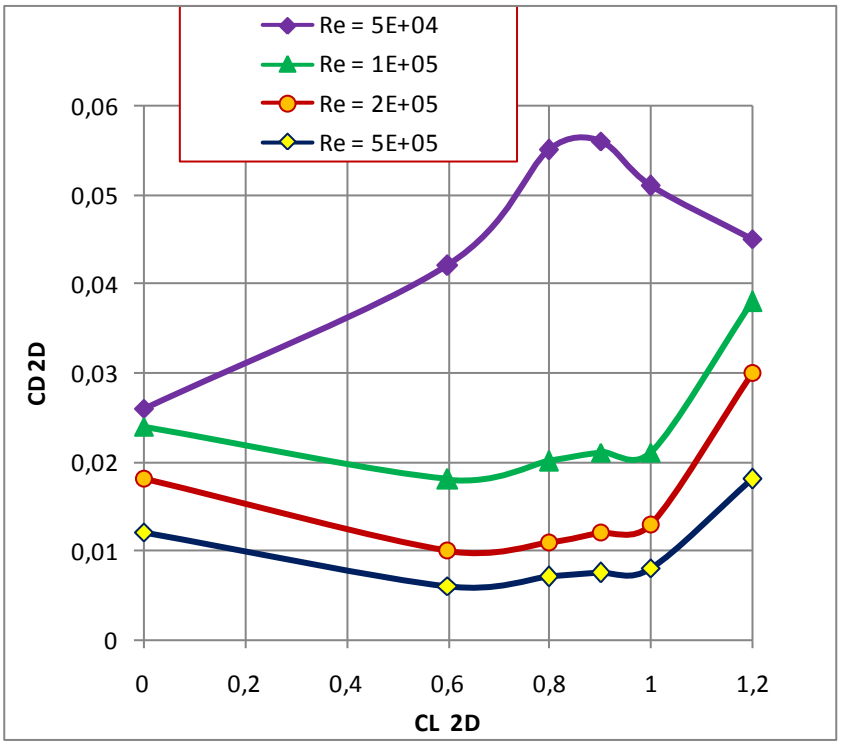

Figure 3.13: CD vs CL of Eppler 387 airfoil, for several Reynolds Numbers

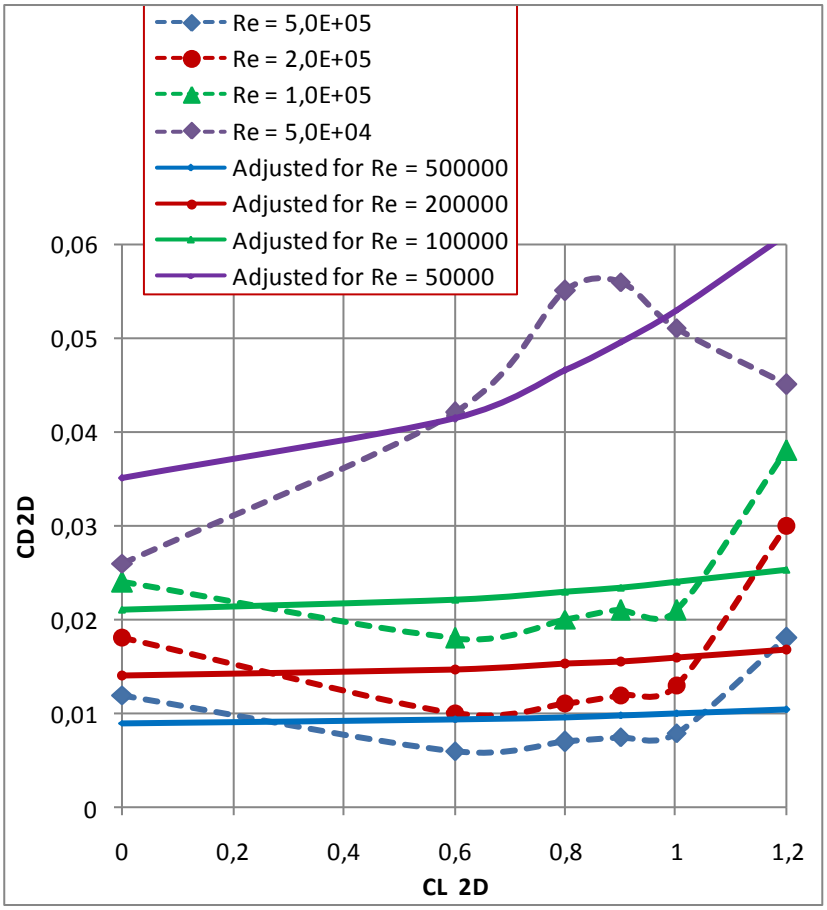

Figure 3.14: Adjustment of Airfoil CD versus CL curves, for several Reynolds numbers

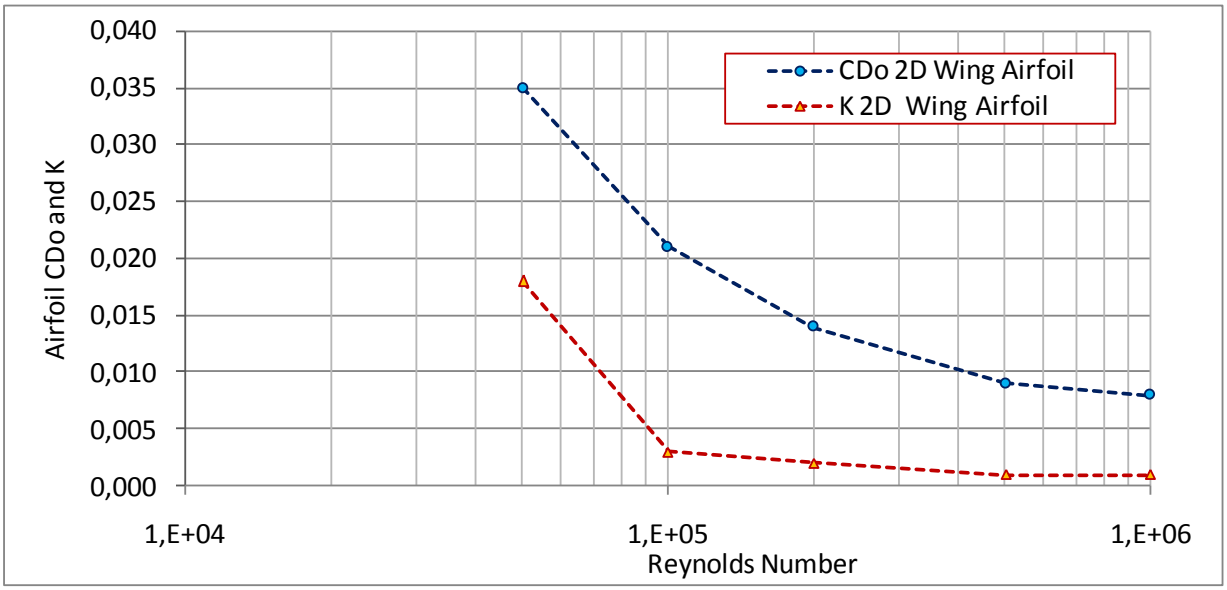

Figure 3.15: Coefficients CDo2D and K2D in function of Reynolds number

c) On comparing results of two airfoils

The values of CDo, K, αCLo and CLmax obtained for N-60 and Epller 387 airfoils are presented together in figures 3.16 and 3.17. In figure 3.16 the values of CDo and K for both airfoils are presented in function of Re, and in figure 3.17 the values of αCLo and CLmax for the two airfoils are presented, also as function of Reynolds number.

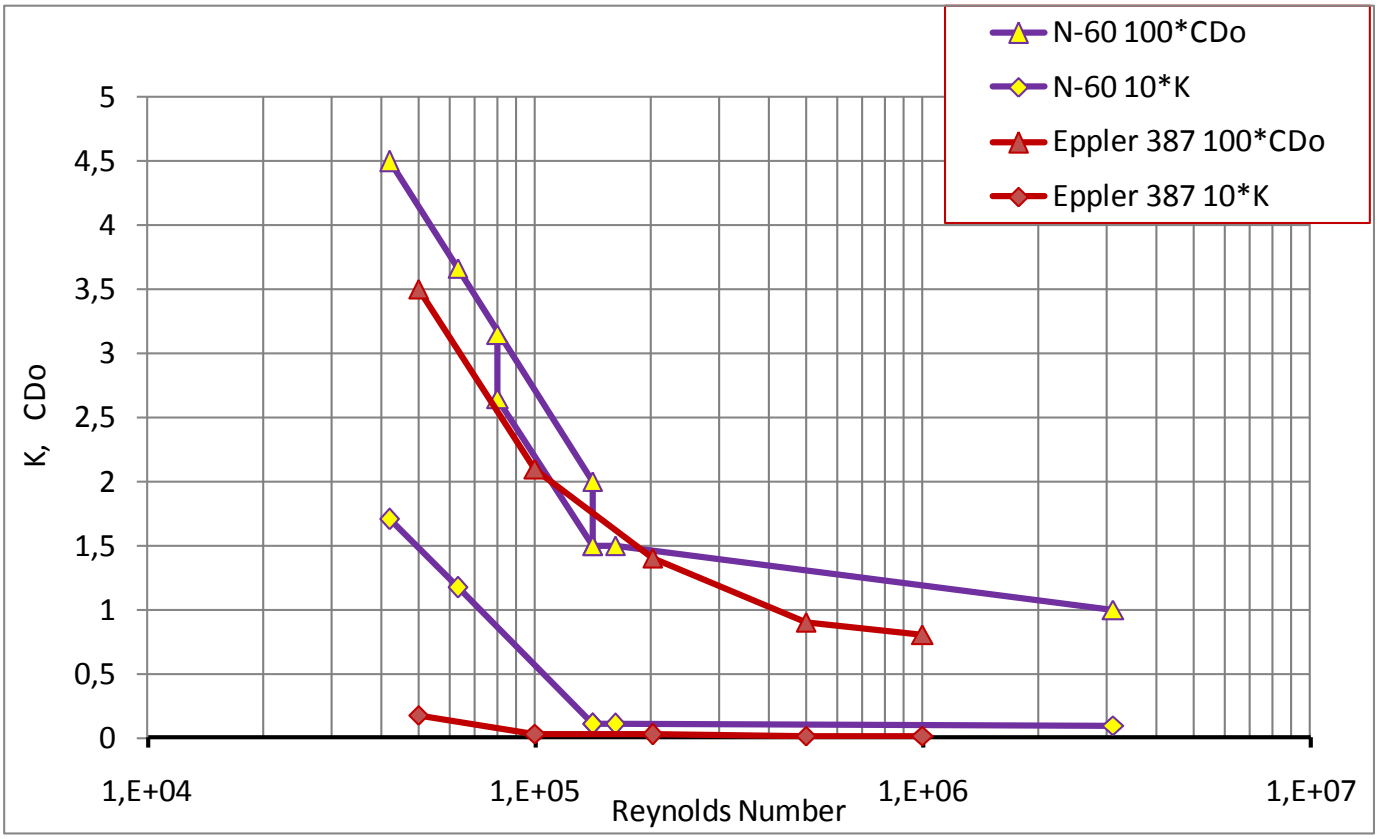

Figure 3.16: CDo and K versus Reynolds number for N-60 and Eppler 387 airfoils.

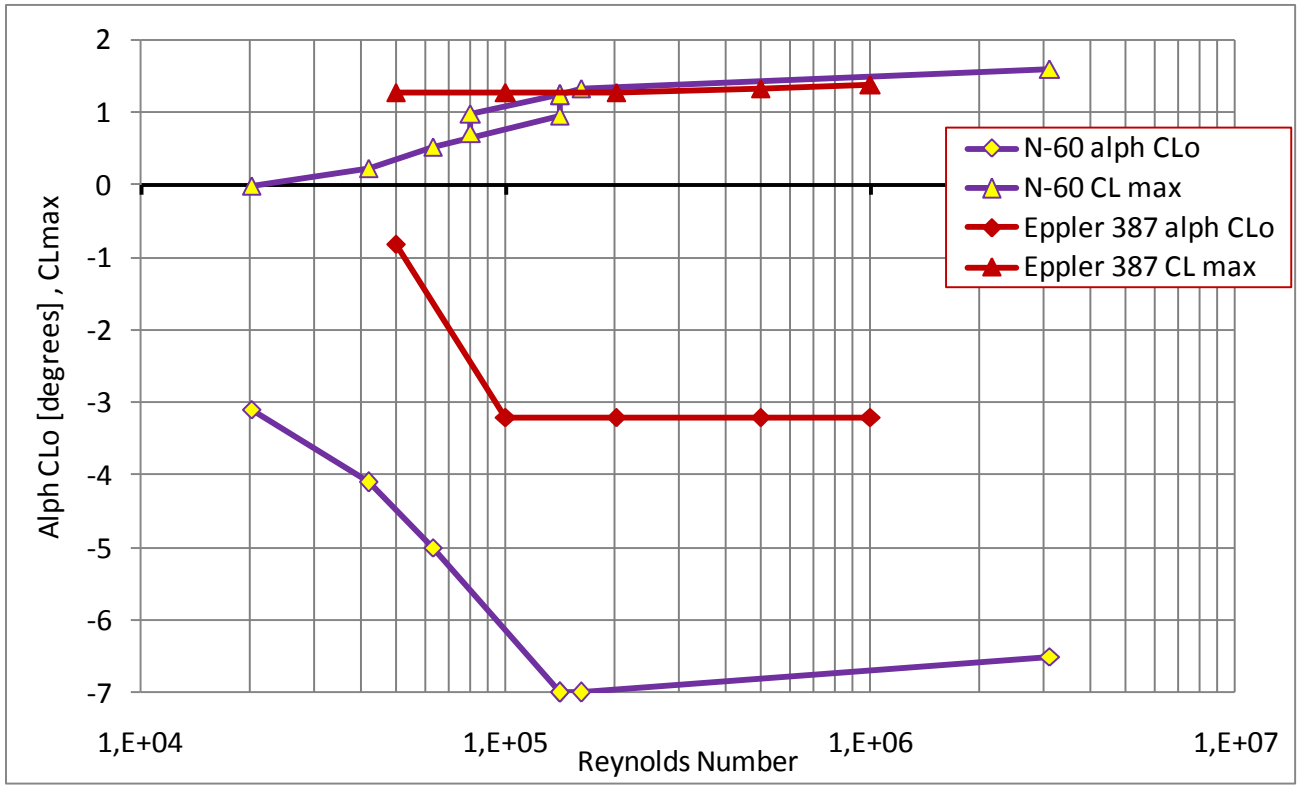

Figure 3.17: αCLo and CLmax versus Reynolds number, for N-60 and Eppler 387 airfoils.

One can note that the hysteresis in the coefficients CDo and CLmax of N-60 airfoil are represented in figures 3.16 and 3.17. It is also evident from these two figures that both airfoil have their drag coefficient increased (by CDo comparison in figure 3.16) and the αCLo reduced (as shown in figure 3.16). Additionally it can be observed in these same figures that the Eppler 387 airfoil presents, for Re lower than 1.5E5, lower value of CDo and higher value of CLmax than the conventional airfoil N-60.

Through these comparisons it is possible to qualitatively show, how better is the Eppler 387 – or airfoils with similar shape – from more conventional airfoils of same camber, in the region of Reynolds number from 40,000 up to 150,000.

3.5.3) General Chart for Drag coefficients variation with Reynolds for non-cambered airfoils

One very useful tool for this research is the diagram of airfoil Drag coefficient versus airfoil Thickness ratio t/c and Reynolds number. This Diagram is presented in the figure 2, chapter 6, of Hoerner (1958). It is important to note that all airfoils of that figure are symmetrical.

It is possible to superimpose the CDo values of Eppler 387 and N-60, presented in figure 3.5-11, to the above mentioned figure from Hoerner (1958). From this comparison, the most important points to observe is that the cambered airfoils Eppler 387 and N-60 presented an increasing in CDo roughly at the same Reynolds number range than the one presented for symmetrical airfoils; and that even in the regions with Re lower than $8x10^4$ as in regions with Re above $4x10^5$, the cambered airfoils presented a CDo significantly higher than the symmetrical airfoils with the same thickness.

Performing a rough analysis in these two regions (Reynolds number lower than 8×10^4 as in regions with Reynolds number above 4×10^5), by comparing the CDo of the two cambered airfoils with the CDo of the non-cambered ones with the same thickness ratio t/c at the same Reynolds number, it is possible to estimate the drag equivalence of delta Cdo due to camber as:

$$CDo\left(z/c\right) \sim 3\ CDo\left(t/c = z/c\right) \tag{3.3}$$

3.6) Literature Review of Solar Incidence Model

Several publications related to solar aircraft design present curves of solar incidence on ground, as Hoss (2009), Noth (2007, 2008), Jabbas and Leutenegger (2010), Najafi (2011), Mattos et al (2013), Vidales (2013), Roland Boucher (2003). The figures presented in these sources provided useful guidelines for the order of magnitude of the solar irradiances considered for study, even some of them being qualitative. Vidales (2013) presents a model for determination of sun irradiance in Portugal. Apparently the software r.sun, related to internet sites of GRASS (2014) and IET (2012) entities, is open source software that allows visualization of sun irradiance on several regions of the Planet, with more focus on Europe. From the researches performed it became apparent that there are several different mathematical models applicable, each one with a specific characteristic as: by being more complex and more reliable, by taking different approaches for considering the atmosphere thickness effects and the diffuse component of the irradiation, or by considering or not the yearly variation of sun-earth distance. In general the mathematical models are for clear sky i.e. their outputs refer to the sky without clouds and excessive dust or aerosols. Reportedly the model from Bird and Halstrom (1981) present results close to other more sophisticated methods, being simpler than those ones. Other more recent method is the ESRA method presented in Riollier et al (2000). Reno et al (2012) present a comparative study of several methods. One beneficial feature of these three sources

is the definition of several terms and concepts related to solar energy. But apparently, these models presented in these sources are destined to activities related to fixed points on Earth – such as satellite information check and solar power stations - in which the daily amount of solar energy is more important than the instantaneous solar power.

During the development of this work, soon it became evident that a self-sufficient model should be at least tried to be defined, for the purposes of solar aircraft research, since the model could be easier linked to the other tools. One additional stimulus to obtain a self-sufficient model is that this model could also be used for investigation of the sun-powered aerial navigation on other planets, as presented in Noth (2007, 2008e), proposing a Mars aerial vehicle and by Landis et al (2002) proposing a Venus aerial vehicle.

According to NASA (2014) the Sunlight power intensity - or irradiance - on the upper layer of atmosphere of Venus, Earth and Mars, are respectively 2613.9, 1367.6 and 589.2 W/m^2 respectively. These values are the average, as the planets' distance to the sun suffers variation along the year. Considering the average distance to the Sun for the three planets, of 108.21, 149.60, and 227.92 all in magnitude of 10^6 km, it can be checked that the power intensity is consistent with the inverse of the square of the distance from the sun, which means that the reduction of the irradiance in the space between Sun and the planets is negligible.

3.7) Literature Review of Atmosphere

3.7.1) Earth's atmosphere

In terms of atmosphere, the most reliable information is the one found in NACA and ICAO (1954); ESDU (1986); and NOAA, NASA and USAF (1976).

The two most important parameters for the altitude flight analysis are air specific mass ρ and air kinematic viscosity ν. The air specific mass ρ can be obtained directly from the formulation presented in ESDU (1986). The kinematic viscosity ν is obtained from the dynamic viscosity μ and the air specific mass ρ, by:

$$\nu = \mu / \rho \qquad (3.4)$$

The values of μ are obtained as function of the temperature, according to the relationship presented in Hoerner (1958). The variation of Temperature, ρ and ν with altitude, considered for this work, is presented in the figures 3.18 and 3.19.

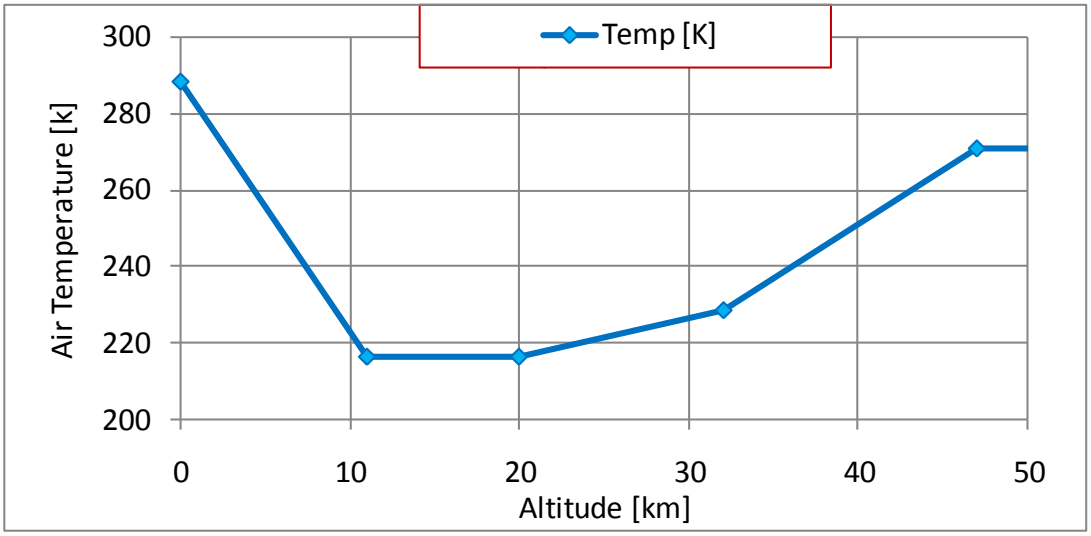

Figure 3.18: Variation with altitude, of air absolute temperature

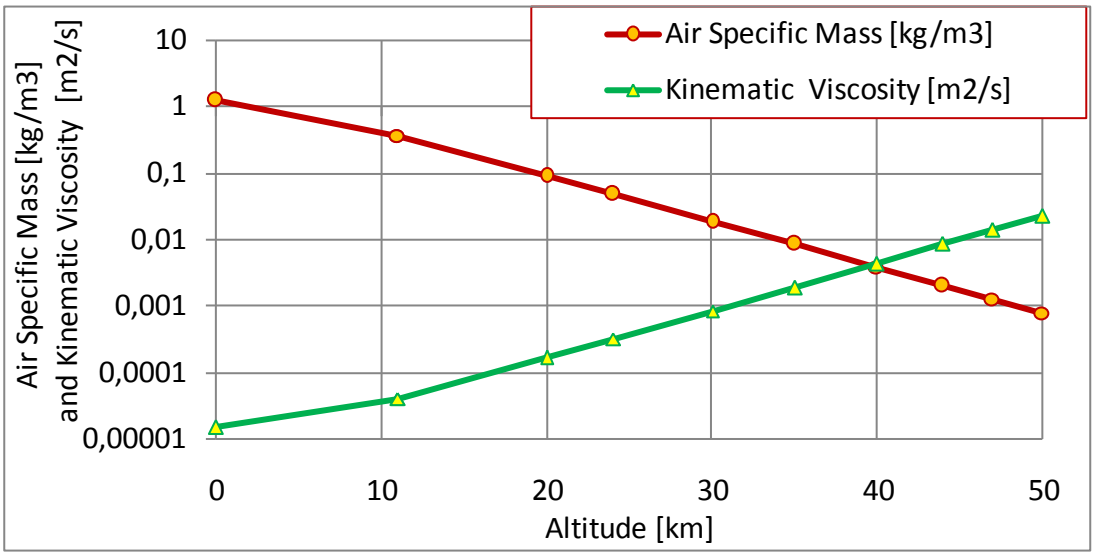

Figure 3.19: Variation with altitude, of air specific mass and kinematic viscosity

3.7.2) Sun irradiation and Earth's atmosphere

One important characteristic of atmosphere for the solar aircraft is the variation with sun power density, or solar irradiance – given in W/m^2 units – with altitude, due to the atmosphere thickness. This parameter, sun irradiance, is often used in this work.

The solar irradiance decreases, from value at the top of the atmosphere down to the value at the ground level. In Stine and Harrigan (2001) is presented, at the chapter 2, the diagram of the parts of solar irradiance that are absorbed or reflected by several layers of the Earth's atmosphere, resulting in a solar irradiance on the ground at sea level that averages 73.2% of the value above the atmosphere. As the average annual irradiance above the atmosphere is defined as 1367 N/m^2, the resulting value of sun irradiance on the ground with the Sun at the zenith is approximately 1000 N/m^2.

The curve of the atmosphere resistance to the Sun light presented in figure 3.20 is elaborated according to the above referred diagram from Stine and Harrigan. The consistence between the values of irradiance on the ground and the total atmosphere resistance to sunlight, in a clear sky and with the sun at zenith, is presented in the equation:

$$\text{Irradiance Reduction} = 1 - 1000/1367 = 1 - 0.732 = 0.268 \text{ or } 26.8\% \qquad (3.5)$$

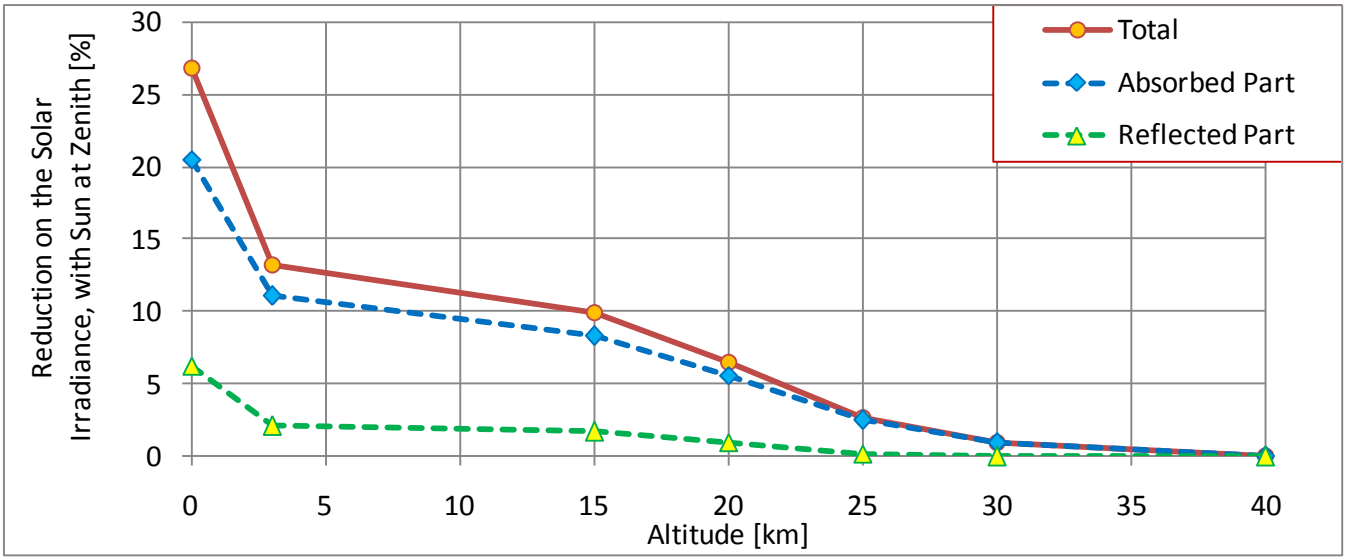

Figure 3.20: Variation with altitude, of sunlight irradiance reduction due to atmosphere; Sun positioned at the zenith, and the sky without clouds.

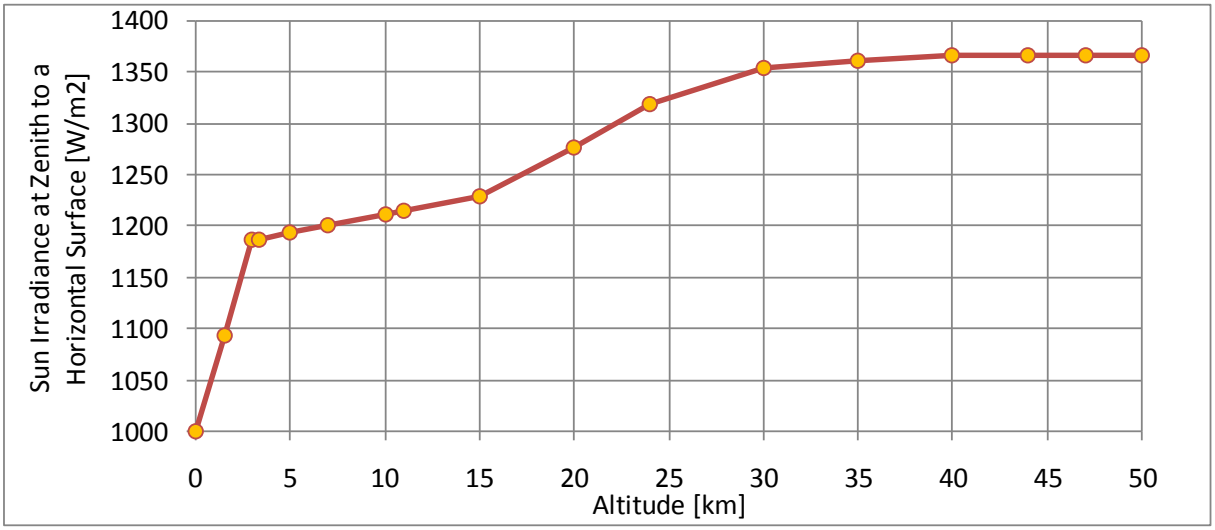

Figure 3.21: Variation with altitude of the Sun irradiance;
Sun positioned at the zenith, and the sky without clouds.

This average value of 1000 W/m^2 on ground at sea level is slightly lower than the one defined for the manufacturer of solar irradiance simulators Newport (2014): *"For a typical cloudless atmosphere in summer and for zero zenith angle, the 1367 W m^{-2} reaching the outer atmosphere is reduced to ca. 1050 W m^{-2} direct beam radiation, and ca. 1120 W m^{-2} global radiation on a horizontal surface at ground level".* This source also presents the concepts of AM0 and AM1.

AM0 corresponds to the sun irradiance on a plate normal to Sun, at the threshold of earth upper atmosphere, and AM1 corresponds to the sun irradiance on the ground, at sea level with the Sun at the zenith in a clear day, with no clouds.

Also other sources as the ones presented in Damon (2013) and E7/PPA (2005) define the value of 1000 W/m^2 as the reference for Sun irradiance on ground at sea level with the Sun at the Zenith in a clear day, with no clouds. The curve of solar intensity in function of altitude presented by Colella and Wenneker (1994), fully dedicated to a solar aircraft design, also points out the value of 1000 W/m^2 at sea level, a value of about 1225 W/m^2 at 10 km and a value of about 1280 W/m^2 at 20 km.

So the adoption of 1000 W/m^2 as the maximum value of sun irradiance on ground at sea level can be considered as a conservative approach for the analyses in this work, and is the one considered in this work for the AM1 condition, as is considered the variation presented in figures 3.20 and 3.21.

3.8) Literature Review of Solar Aircraft Systems

3.8.1) Propulsive Chain

The main focus in terms of aircraft systems in this study is the propulsive chain system, from the solar cell to the propeller. The propulsive chain is schematically presented in the figure 3.22. The figure 3.22 may be understood as a synthesis between the sketches of Noth (2008), Montgomery and Mourtos (2013), Ross (2008), and Colella and Wenneker (1994), among others. In the figure 3.22, the MPPT is the electronic device destined to control the amount of voltage and current from a solar panel, in order to deliver the maximum possible power from the solar panel, to charge the battery or to feed the engine.

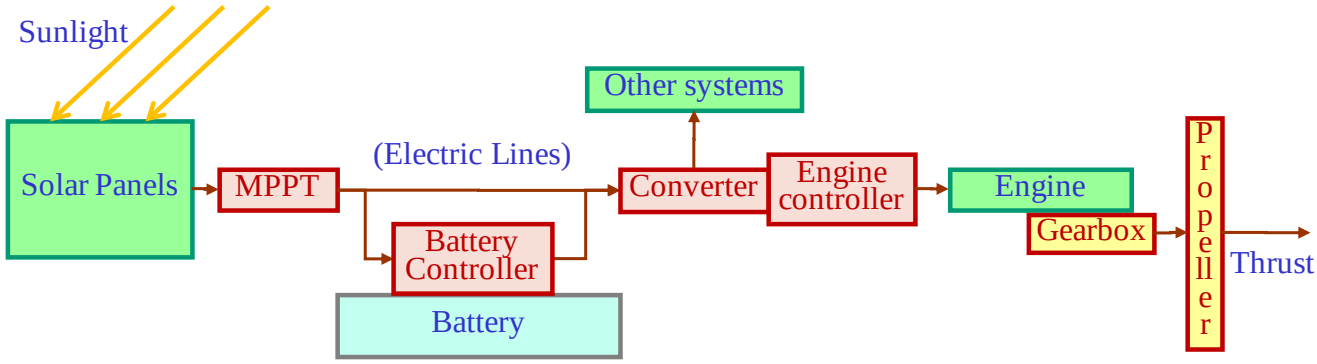

Figure 3.22: Sketch of the general propulsive chain in a sun-powered aircraft.

3.8.2) General characteristics of the system and system components

Several sources, among the ones cited in section 3.2, present useful information about specific solar aircraft systems. The most important information collected is the group of concepts, associated to the propulsive system architecture and to the characteristics of the aircraft system components: manufacturer, limitations, mass, capability and effectiveness. Some relevant sources, among several other valuable ones, are Noth (2008a, 2008b, 2013), Roland Boucher (2003), Robert Boucher (1985), McCready et al (1983), Ross (2009a, 2009b), Cocconi (2008a, 2008b), Montgomery and Mourtos (2013).

Valuable information of system components has been also obtained from manufacturers of batteries, engines, and solar cells. As an example, solar cells characteristics are obtained from released information from manufacturers as Power film (2013), Sion Power (2010), Sun Power (2009) . The publication of Palmisano and Cirimina (2008) also presents very useful basic concepts.

From the information obtained mainly from the sources referred in the two paragraphs above, the table 3.2 and figures 3.23 to 3.26 have been elaborated. The table 3.2 presents a simplified comparison of the propulsive chain obtained from the more detailed information of the three different sources, indicated in the table, each one related to a specific design. The figures 3.23 to 3.26 present in a comparative form, the characteristics of system components of several solar aircraft: in figure 3.23, the batteries specific mass; figure 3.24, the mass-to-area ratio of solar cells; figure 3.25, the power-to-area and power-to-mass ratios of solar cells from different solar aircraft; and figure 3.26, the mass-to-power ratio of engines. The information presented in the tables and the figures referred in this paragraph served as very important guidelines for some assumptions defined along this work.

Table 3.2: Simplified and conceptual values of the propulsive chain for three different aircraft

Source	Noth	Ross	Montgomery and Mourtos
Related Aircraft	Sky-Sailor	Solar Impulse I	Photon
Item	Effectiveness [%]		
Solar Cells	17	20	20
Transmission[1]	92	93	90
Battery and controller	96	96	90
Engine, gearbox	81	93	76
Propeller	85	77	80
Global	**10**	**13**	**10**

Note (1): Transmission includes electric lines, MPPT, converter and engine controller, when applicable.

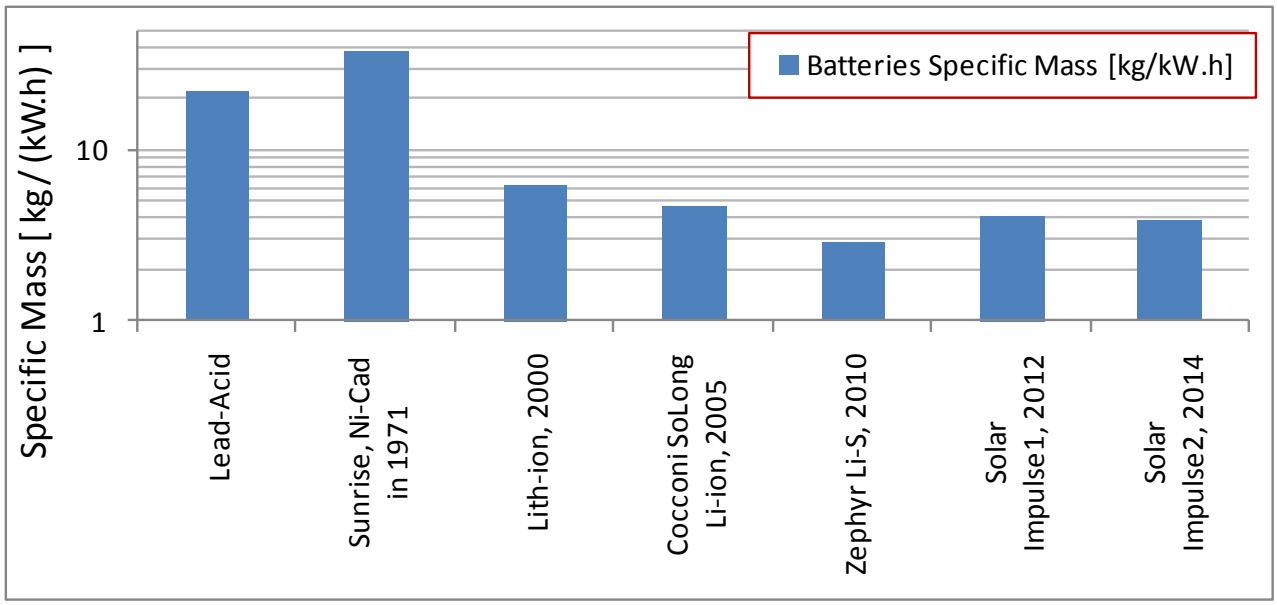

Figure 3.23: Specific mass of different types of batteries for Solar aircraft; lead-acid are presented only for comparison

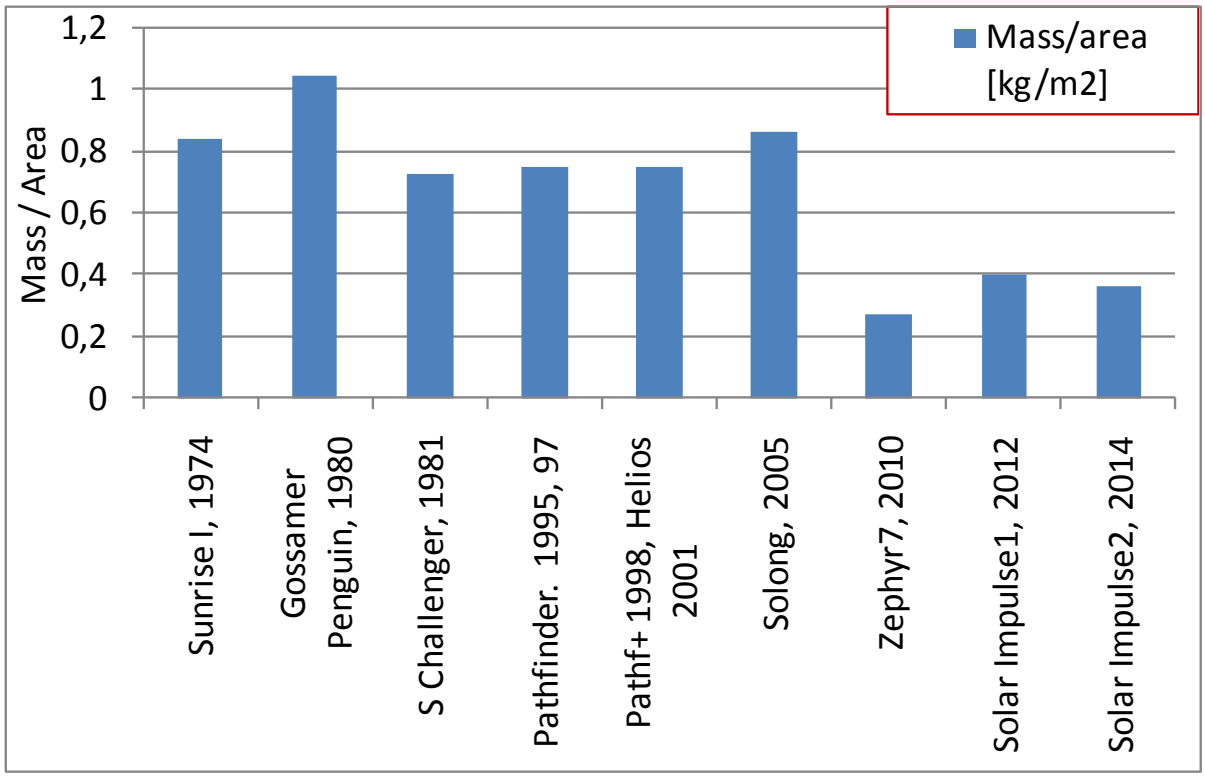

Figure 3.24: Mass/Area ratio of solar cells from different solar aircraft.

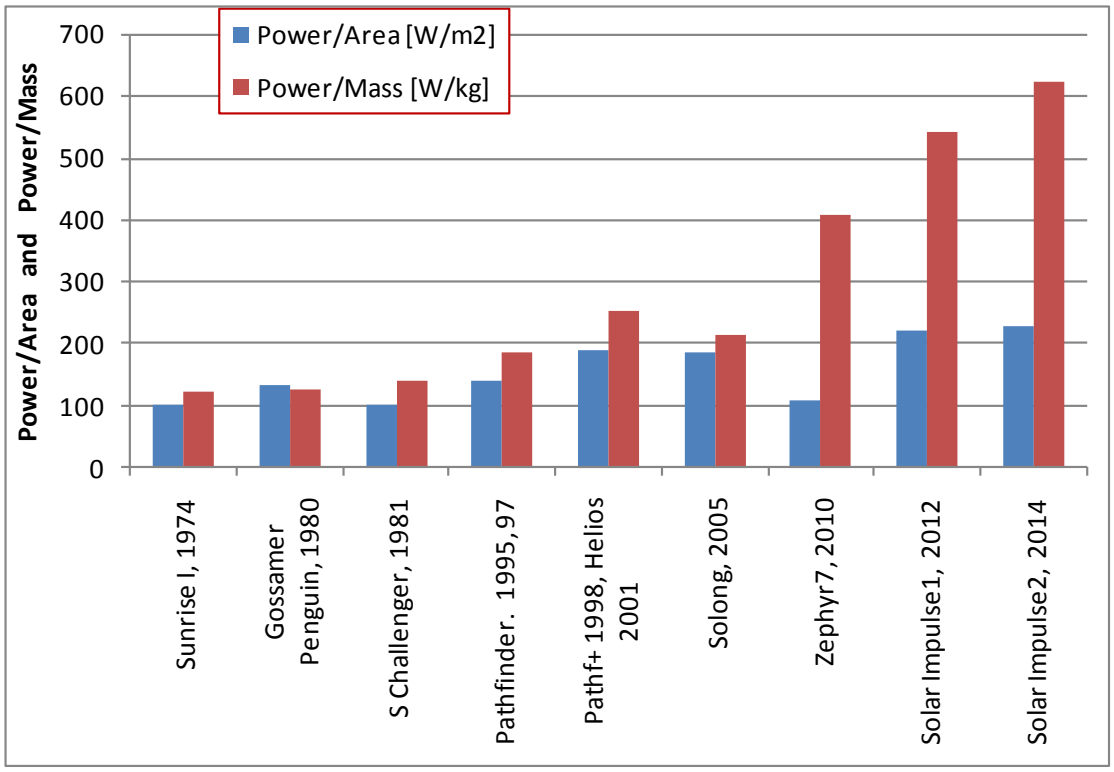

Figure 3.25: Power/Area and Power/Mass ratios of solar cells from different solar aircraft.

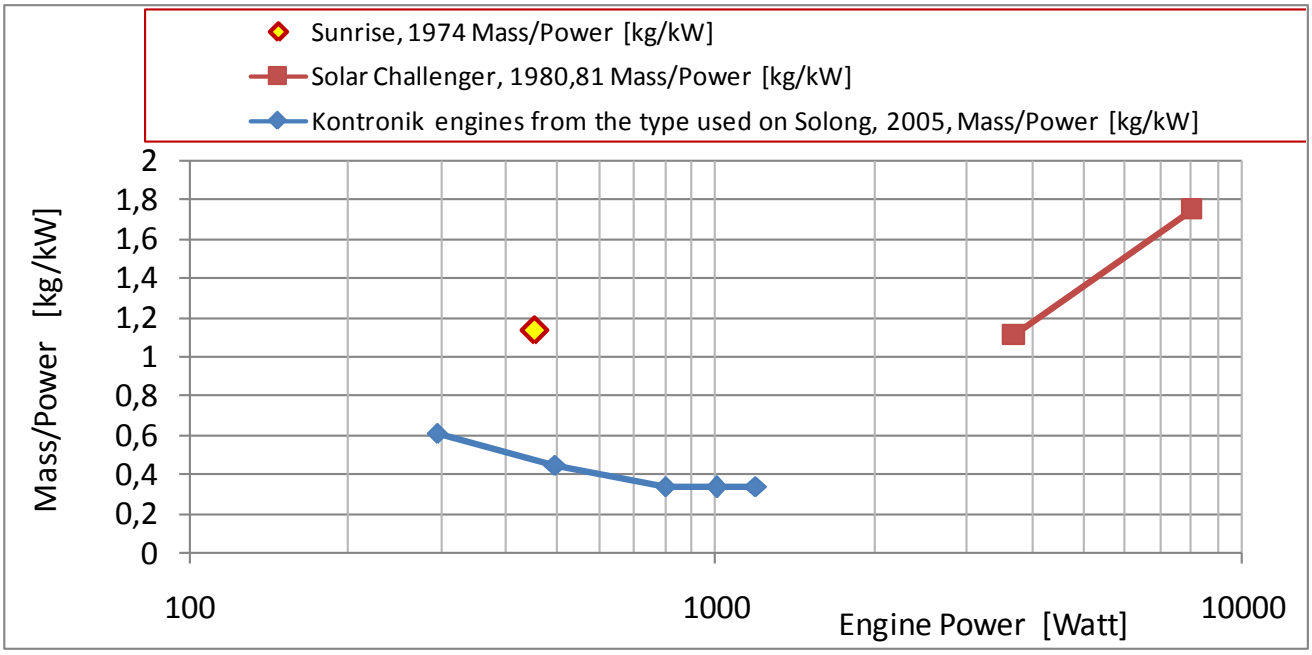

Figure 3.26: Mass/Power ratio of engines from different solar aircraft.

3.8.3) Cells efficiency variation with altitude due to atmospheric effects

A specific research is conducted to examine the altitude effects on the solar Cells. According to McCready (1983) there is an increasing in solar arrays effectiveness with altitude increasing, due to two main factors, the reduction of ambient temperature, and the reduction of the atmosphere thickness above the aircraft. The effectiveness ratio curves of figure 3.27 are elaborated considering these two factors, temperature and air thickness. McCready observed a variation of 0.4 to 0.5% on the solar effectiveness per Celsius degrees. The temperature effect in figure 3.27 is defined considering the variation of temperature with altitude and considering a intermediate value of 0.44%/^{o}C of reduction on the effectiveness. The atmosphere thickness effect is defined from the values of atmospheric resistance to the Sunlight presented in figure 3.7-3 in function of altitude. As presented in figure 3.27, with the both effects together, a solar cell at 25 to 30 km can present its maximum effectiveness, about 70% above the effectiveness obtained at sea level. With 2 values of Solar Challenger cells output power, for sea level and 15 km, reported by McCready et al (1983), it is possible to define the point of effectiveness ratio of 1.607 for altitude of 15 km, also presented in figure 3.27. One can note on the figure 3.27 that this point from McCready et al coincides with the curve for temperature plus thickness effects on the effectiveness ratio, thus increasing the confidence in this curve.

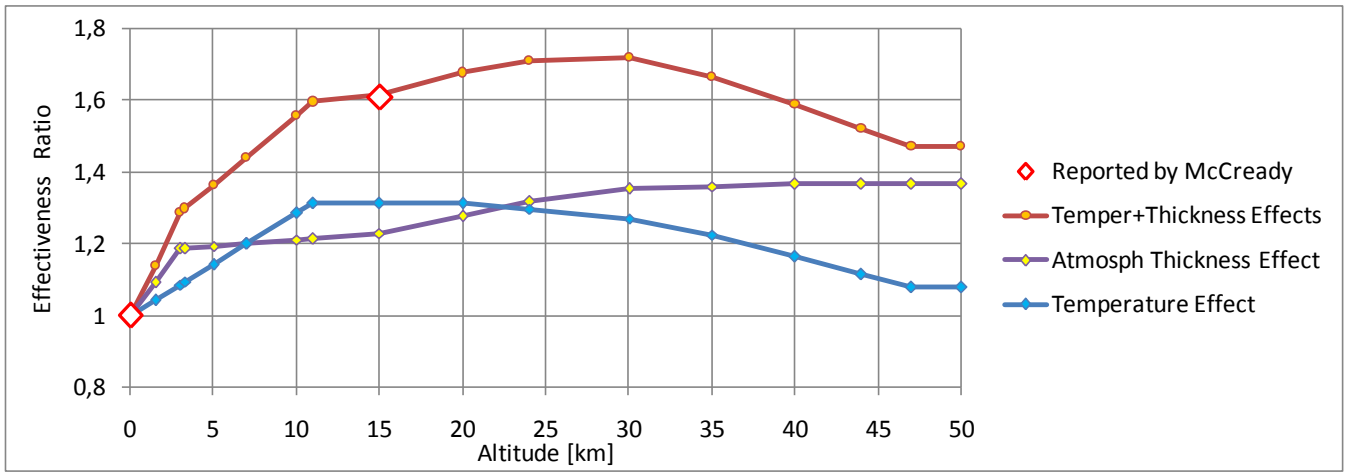

Figure 3.27: Changes in solar cells effectiveness as function of the altitude, due to atmosphere thickness and temperature effect

4) METHODOLOGIES

4.1) Overview

Along this study, in order to allow the aimed analyses, several methodologies, tools and criteria have been developed; these ones are presented in the following sections.

A simplified manner to visualize the way the different methodologies are link to work together is presented in figure 4.1. In this figure the main inputs are presented in yellow rectangles, the main processes are presented in blue rectangles and the main outputs are presented in brown rectangles. In the figure 4.1, the starting point is the rectangle of intended mission and aircraft characteristics, presented at the left side of the figure.

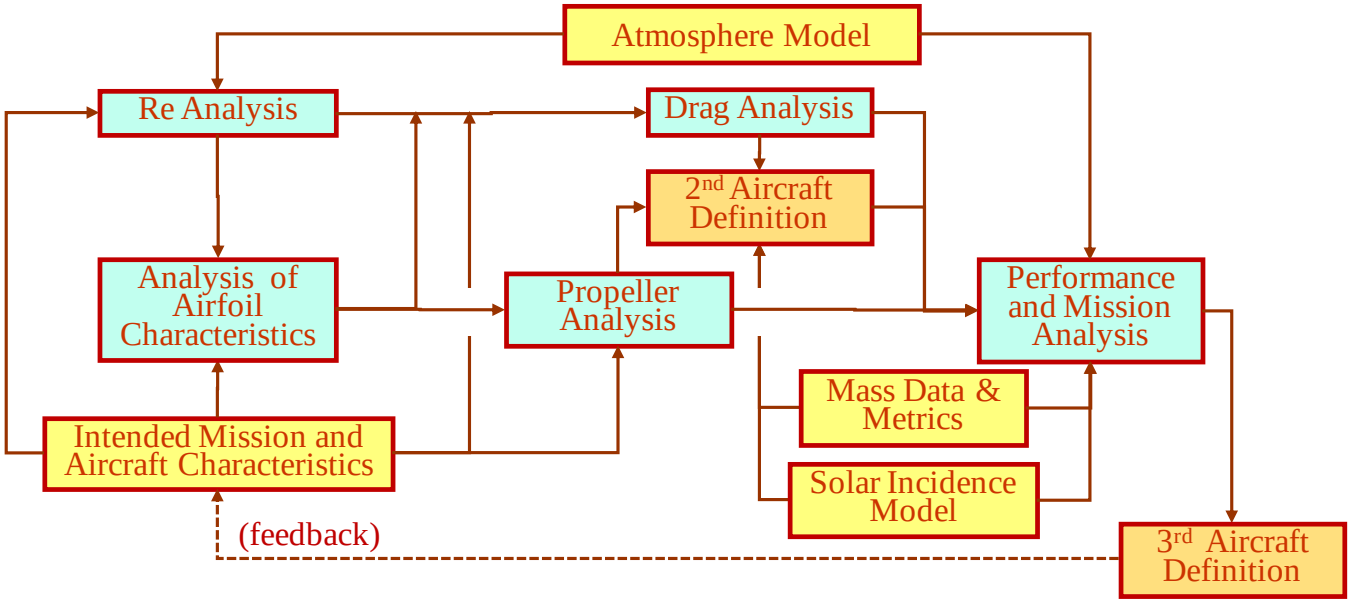

Figure 4.1: Simplified view of the link between the methodologies in the design/analysis process

One can see that in figure 4.1 a feedback is indicated; this may happen if the information at the rectangle named 3rd Aircraft Definition does not match with the information at the initial rectangle named Intended Mission and Aircraft Characteristics; so a re-definition of the mission or of the aircraft should be made and the process should be re-started. This loop should be iteratively

performed up to the defined mission and aircraft obtained meet the intended values of the rectangle at the left side.

4.2) Reference Systems

The main reference systems adopted for the aircraft analyses are the Aircraft Axis System and the Ground Axis System.

The Aircraft Axis System is linked to aircraft, being the X-axis positioned along the aircraft centerline and oriented backwards, the Y-axis oriented to the aircraft left side, and Z-axis oriented upwards. The Ground Axis System, used for flight mission analysis and take-off simulations, is fixed on the ground, and presents the X axis oriented forward and Z axis oriented upwards.

4.3) Characterization of Solar Aircraft

Some comparisons of sun-powered aircraft with internal combustion aircraft, that can be referred in this work as "conventional" aircraft are presented in chapter 2. In general it can be said that the sun-powered aircraft have a wing load significantly lower than the average values of conventional aircraft. The low wing load is consequence of the low power that can be extracted from sun light through photovoltaic cells dispersed in aircraft external surfaces – mainly wing upper surfaces- compared to the energy that can be currently obtained from combustion of liquid fuels, carried in tanks inside the aircraft, and using atmospheric oxygen as the oxidizer.

Due to the lower wing load, the values of sun-powered aircraft mass are significantly lower than the values of conventional aircraft of the same size; and the same can be said in terms of speed. And in consequence of the aircraft mass, the payload mass for a sun-powered aircraft is also much lower than a conventional aircraft of the same size. For comparison, it can be shown that the Solar Impulse aircraft has a wing span value (63.4 m) very close to the Airbus A-380 span value (79.75 m), but the aircraft mass, payload mass and speed (about 1600 kg, 200 kg and 50 km/h respectively) hardly compare with the corresponding A-380 values (about 575,000 kg, 89,200 kg and 900 km/h respectively).

In order to improve the understanding of sun-powered aircraft compared to conventional aircraft, and complementing the comparative figures 2.3, 2.4 and 2.5 presented in chapter 2, the

performance parameters of representative aircraft are presented in figures 4.2 to 4.5. The conventional aircraft are the Airbus A-380, the Northrop-Grumman Global Hawk, the Rutan Voyager and the Lockheed SR-71. The sun powered aircraft are the Qinetiq Zephyr 7 Aerovironment Pathfinder+ and the Aerovironment Helios. The comparison of payload-endurance diagrams from conventional and sun-powered aircraft is shown in figure 4.2. One can note that although the sun-powered Zephyr holds the largest endurance, its payload is extremely small compared to the conventional aircraft. In fact, the differences in payload – heavier payloads for the conventional aircraft - are so strong that the ordinate axis has to be presented in logarithmic scale.

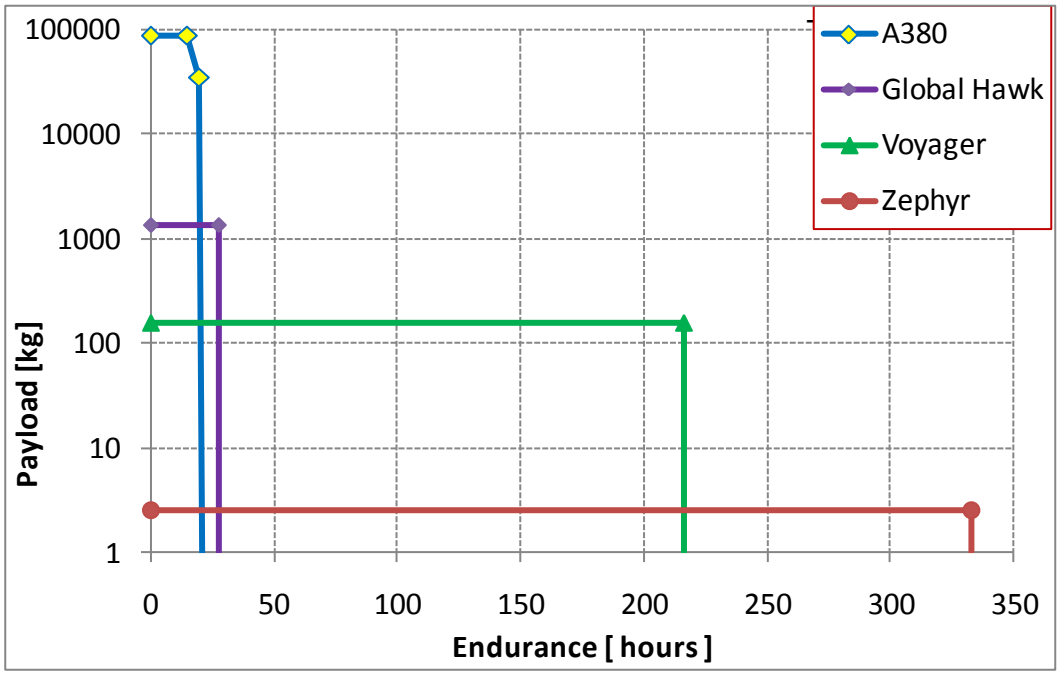

Figure 4.2: Comparison of payload-endurance diagrams from conventional and sun-powered aircraft

The comparison of diagrams of specific payload-endurance from conventional and sun-powered aircraft is shown in figure 4.3. The term specific payload refers to the percentage of payload related to the aircraft maximum take-off weight. One can note that, similarly to figure 4.2, there is a tendency of decreasing of specific payload with the increasing of endurance, but differently from figure 4.2, the differences in terms of specific payload are not so drastic from conventional aircraft to sun-powered aircraft. In figure 4.2 the payload decreases drastically from conventional to sun-powered aircraft, mainly due to drastic difference in MTOW of the two types of aircraft.

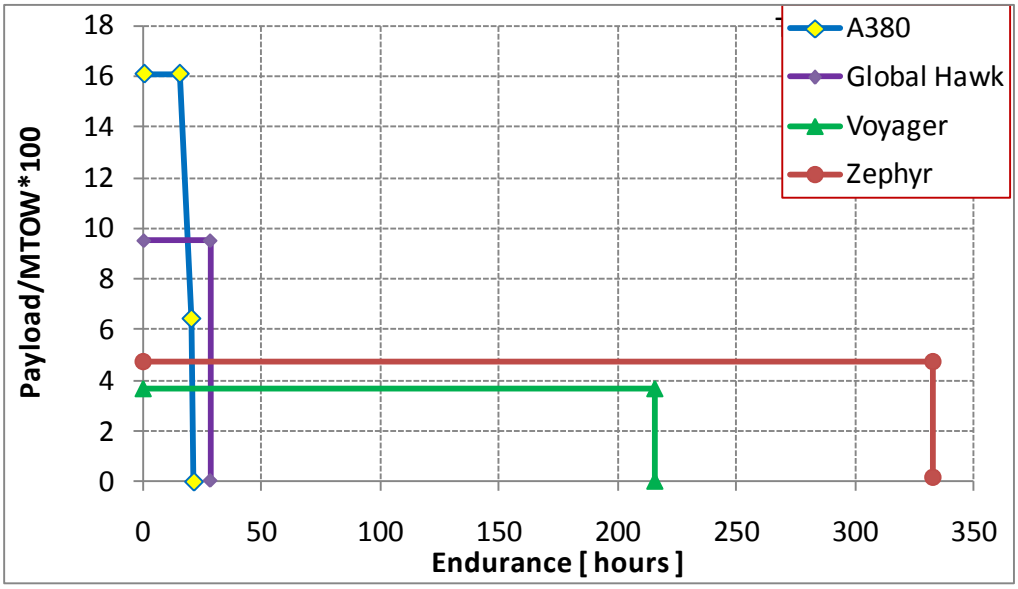

Figure 4.3: Comparison of specific payload - endurance diagrams, conventional and solar aircraft

In Figure 4.4 it is shown the comparison of payload-altitude diagrams from conventional and sun-powered aircraft. The same aspect already presented in figure 4.2 can be noted in this figure. One can note that although the sun-powered Helios holds the largest altitude, its payload is extremely small compared to the one for conventional aircraft. Again, as in figure 4.2, the differences in payload – heavier payloads for the conventional aircraft - are so strong that the ordinate axis of figure 4.4 is presented in logarithmic scale.

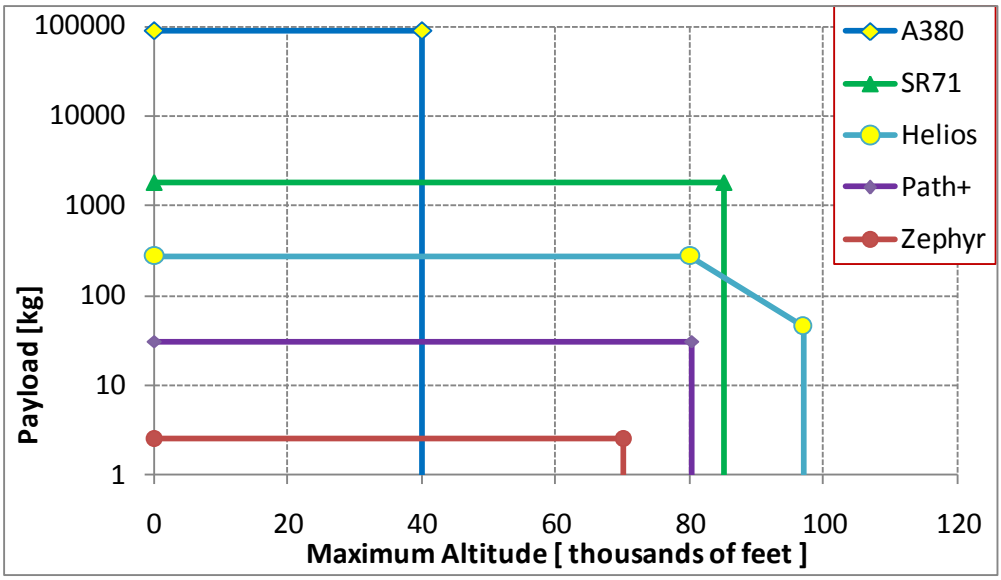

Figure 4.4: Comparison of payload-altitude diagrams of conventional and sun-powered aircraft

The comparison of diagrams of specific payload-altitude from conventional and sun-powered aircraft is shown in figure 4.5. One can note that, also similarly to figure 4.4, there is a tendency of decay of specific payload with the increasing of altitude, but differently from figure 4.4, the differences in terms of specific payload are not so drastic from conventional aircraft to sun-powered aircraft. Again, as shown in figure 4.2, in figure 4.4 the payload also decreases drastically from conventional to sun-powered aircraft, mainly due to drastic difference in MTOW of the two types of aircraft. One additional observation that can be made is that the largest specific payload in figure 4.5 is related to a sun-powered aircraft, the Helios aircraft. Possibly this high value of specific payload for Helios, related to altitudes below 90 km - obtained from NASA site - is overoptimistic and may be related to the aircraft accident occurred in 2003; the accident is reported by Noll et al (2004).

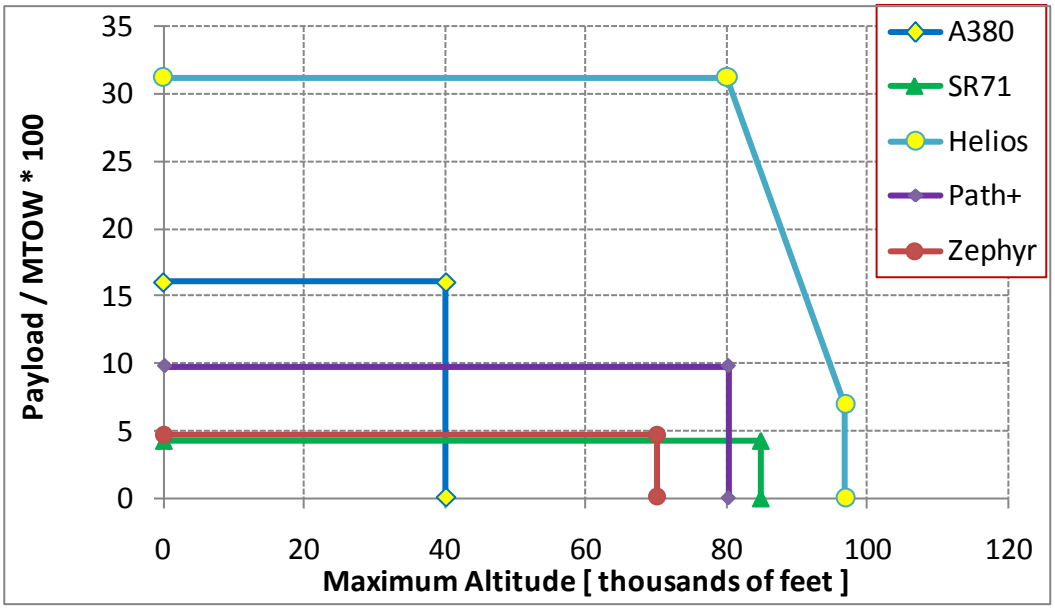

Figure 4.5: Comparison of specific payload - altitude diagrams of conventional and solar aircraft

Regarding the figures 4.2, 4.5, one can conclude that sun-powered aircraft are not competitive with conventional aircraft for the missions already performed by the conventional aircraft. Sun-powered aircraft can be attractive for specific niches, specific flight missions that can be beyond normal limits for conventional aircraft. Such attractive missions for sun-powered aircraft can be high-endurance or high-altitude ones, but one must be aware of the penalties of considering a very low-speed and a very light payload.

Other applications that can keep being into consideration are the flight missions in atmospheres with access to sunlight, and absence of oxygen enough to burn fuel, as Mars or Venus environments.

In the scenario of solar aircraft, mission potential limiting factors are not exactly the same as for the conventional aircraft design characteristics, as fuel capacity or high power-to-mass ratio. Philosophically, it could be said that, if one analyses solar aircraft he is going away from the design determined by the classical Breguet Formula, which is very interesting. Possibly, in a near future it will be possible to discover a new law for determination of range of some types of Solar Aircraft, starting from the Breguet Formula.

Through the studies on Solar Aircraft, it has been possible to define five main mission limiting factors, which are not the classic ones as fuel capacity or power-to-mass ratio:

1. Capability of on-board systems to operate days (or months) continuously;
2. Better knowledge of atmosphere in order to anticipate and avoid adverse conditions, as clouds over the aircraft and strong gusts;
3. Semi-intelligent Systems of automatic control of flight and very low weight
4. Ground crew distributed, in an organized and decentralized way, in groups to provide continuous ground support to the aircraft airworthiness;
5. To possess a better knowledge of the distributed energy from the sun to the several Earth regions, along the several year months.

4.4) General Rules for Maximum Wing Load of Solar Aircraft

In this section, definitions for two formulae are presented, one for aircraft without batteries, and other for aircraft with batteries. Both formulae refer to horizontal flight conditions. Some examples of application are presented in chapter 5.

4.4.1) Formulation for maximum wing load, aircraft without batteries

Considering a sun powered aircraft, the aircraft required level power RPw is given by:

$$RPw = D \,.\, TAS \tag{4.1}$$

$$D = {}^{1}/_{2}\ \rho\ TAS^2\ S\ CD \tag{4.2}$$

So, $$RPw = {}^{1}/_{2}\ \rho\ TAS^2\ S\ CD \tag{4.3}.$$

As $$TAS = \left(2\,M\,\frac{g}{\rho\,S\,CL}\right)^{\frac{1}{2}} \tag{4.4}$$

The required power can be written as:

$$RPw = \frac{1}{2}\,\rho\left(2\,M\,\frac{g}{\rho\ S\ CL}\right)^{\frac{3}{2}}\ S\,CD \tag{4.5}$$

Developing the formula, we have:

$$\mathrm{R}Pw = \left(\frac{1}{4}\ \rho^2\,8\ M^3\ \frac{g^3}{\rho^3\ S^3\ CL^3}\ S^2\ CD^2\right)^{\frac{1}{2}}$$

$$\mathrm{R}Pw = \left(2\ M^3\ \frac{g^3}{\rho\ S\ CL}\ \frac{CD^2}{CL^2}\right)^{\frac{1}{2}} \tag{4.6}$$

$$RPw = \frac{1}{E}\left(2\ M^3\ \frac{g^3}{\rho\ S\ CL}\right)^{\frac{1}{2}} \tag{4.7}$$

Where $$E = CL/CD \tag{4.8}$$

In terms of aerodynamic characteristics, the lowest required power condition is obtained from derivation of equation 4.6 in respect to CL, and considering CD = CDo + K.CL^2, equation 3.2:

From equation 4.6:

$$RPw = \frac{CD}{CL^{3/2}} \left(2\ M^3\ \frac{g^3}{\rho\ S} \right)^{\frac{1}{2}}$$

$$RPw = \frac{CDo + K\ CL^2}{CL^{3/2}} \left(2\ M^3\ \frac{g^3}{\rho\ S} \right)^{\frac{1}{2}} \quad (4.9)$$

Finding CL for Minimum Required Power:

$$\frac{d\ RPW}{d\ CL} = 0 \quad (4.10)$$

$$=> \frac{d\left(\frac{CDo + K\ CL^2}{CL^{3/2}}\right)}{d\ CL} = 0 \quad (4.11)$$

$$\frac{2\ K\ CL\ CL^{3/2} - (CDo + K\ CL^2)\ .\ 3/2\ .\ CL^{1/2}}{CL^3} = 0 \quad (4.12)$$

$$2\ K\ CL^{5/2} - 3/2\ .\ CDo\ .\ CL^{1/2} - 3/2\ .\ K\ CL^{5/2} = 0$$

$$1/2\ K\ CL^{5/2} - 3/2\ .\ CDo\ .\ CL^{1/2} = 0$$

$$1/2\ K\ CL^{5/2} = 3/2\ .\ CDo\ .\ CL^{1/2}$$

$$K = 3\ CDo\ .\ \frac{CL^{1/2}}{CL^{5/2}}$$

$$\mathrm{K} = 3\ \mathrm{CDo}\ .\ \frac{1}{\mathrm{CL}^2}$$

$$CL^2 = \frac{3\ CDo}{K}$$

$$CL = \left(\frac{3\ CDo}{K}\right)^{1/2} \quad (4.13)$$

It is possible to name CL for minimum required power as CL_{**} :

$$CL_{**} = \left(\frac{3\ CDo}{K}\right)^{1/2} \quad (4.14).$$

As $(CDo/K)^{1/2}$ is the CL for the best glide ratio (McCormick, 1980), which is commonly called as CL_{*},

$$CL_{*} = \left(\frac{CDo}{K}\right)^{1/2} \quad (4.15),$$

It is possible to write:

$$CL_{**} = 3^{1/2}\, CL_{*} \quad => \quad CL_{**} \sim 1.63\, CL_{*} \quad (4.16).$$

This value of CL_{**} can be very high for some aircraft, and sometimes it is not achievable.

So, a limit must be observed:

$$\text{If} \quad 1.63\, CL_{*} < CL_{saf} \quad \text{then} \quad CL_{**} = 1.63\, CL_{*} \quad \text{else} \quad CL_{**} = CL_{saf} \quad (4.17),$$

Where CL_{saf} is the maximum safety lift coefficient for the aircraft, i.e. the maximum lift achievable for a safe flight in terms of stability and control. Considering that the aircraft is safe for flight at speeds down to 1.10 Vs, this parameter can be assumed as:

$$CL_{saf} \sim 0.83\ CLmax \quad (4.18).$$

The equations above are applicable for all aircraft. Now, considering a sun-powered aircraft, the following applies. At first let us analyze a sun powered aircraft that does not use batteries. For this type of aircraft, the power available to be delivered to the air APw can be defined as:

$$APw = ILSPI\ \ SAR\ \ S\ \ \eta_{sist} \quad (4.19),$$

Where:

ILSPI = Instantaneous and local Sun power intensity,

SAR = Solar array to wing area ratio,

η_{sist} = System efficiency; this is the product of several efficiencies:

$$\eta_{sist} = \eta_{array} \cdot \eta_{cond} \cdot \eta_{eng} \cdot \eta_{prop} \quad (4.20),$$

η_{array} = solar array efficiency,

η_{cond} = transmission efficiency: electric lines (wiring), MPPT,

converter and engine controller, when applicable,

η_{eng} = engine efficiency ,

η_{prop} = propeller efficiency.

Admitting horizontal flight condition, required power equals available power:

$$RPw = APw \qquad (4.21).$$

From the equations 4.21, 4.6 and 4.19 it is possible to obtain:

$$\frac{1}{E}\left(2\ M^3\ \frac{g^3}{\rho\ S\ CL} \right)^{\frac{1}{2}} = ILSPI\ \ SAR\ \ S\ \ \eta_{sist} \qquad (4.22)$$

$$=> \quad \left(M^3\ \frac{g^3}{\rho} \right)^{\frac{1}{2}} = ILSPI\ \ SAR\ \ S\ \ \eta_{sist}\ \ E\ \left(\frac{CL\ S}{2}\right)^{1/2}$$

$$\left(M^{3/2}\ \frac{g^3}{\rho} \right)^{\frac{1}{2}} = ILSPI\ \ SAR\ \ S^{3/2}\ \ \eta_{sist}\ \ E\ \left(\frac{CL}{2}\right)^{1/2}$$

$$\left(M/S\right)^{3/2} = \left(1/2\right)^{1/2} E\ \ CL^{1/2}\ SAR\ \ \eta_{sist}\ \ ILSPI\ \ \left(\rho/g^3\right)^{1/2} \qquad (4.23).$$

Through the equation 4.23 the upper limit for wing loading can be established, for sustained horizontal flight, in function of aircraft aerodynamic characteristics E and CL, the aircraft energy absorption and transmission characteristics SAR and η_{sist} , and the environment local characteristics ILPSI, ρ, g. This simple equation can be considered as a general rule for an aircraft which is directly powered by the light emission from the strongest available local source, as the main star for a generic planet, or as the Sun on Venus, Earth, Mars; flying in an atmospheric environment, and using its lift to balance the weight force from its mass subjected to the local gravitational field.

4.4.2) Formulation of maximum wing load, aircraft with batteries

Now let us consider a sun-powered aircraft that uses batteries to allow night flights with energy collected during the day and stored. For this type of aircraft, the Daily Available Energy to be delivered to the air (DAE) can be defined as:

$$DAE = SLDEI \cdot SAR \cdot S \cdot \eta_{sisb} \quad (4.24)$$

Where:

SLDEI = Solar Local Daily Energy intensity

SAR = Solar array to wing area ratio

η_{sisb} = System efficiency with batteries; similarly to equation 4.20 this is the product of several efficiencies:

$$\eta_{sist} = \eta_{array} \cdot \eta_{dailybat} \cdot \eta_{cond} \cdot \eta_{eng} \cdot \eta_{prop} \quad (4.25)$$

η_{array} = solar array efficiency

$\eta_{dailybat}$ = battery storage efficiency related to the whole day flight

$\eta_{dailybat} = \eta_{bat} * (\text{bat parcel}) + (1 - \text{bat parcel})$

η_{bat} = battery efficiency related to input and output

bat parcel = parcel from daily energy which is stored in the batteries; 0 to 1

η_{cond} = transmission efficiency: electric lines (wiring), MPPT, converter and engine controller, when applicable

η_{eng} = engine efficiency

η_{prop} = propeller efficiency

And the daily required Energy for horizontal flight DRE, in W.h, is obtained from equation 4.7 as:

$$DRE = 24\, RPw \Rightarrow DRE = \frac{24}{E}\left(2\, M^3 \, \frac{g^3}{\rho\, S\, CL} \right)^{\frac{1}{2}} \quad (4.26).$$

Admitting that the energy absorbed from the Sun over a period of 24 hours is the exact amount to allow horizontal flight during the same 24 hours, the Daily Required Energy equals the Daily Available Energy:

$$DRE = DAE \quad (4.27).$$

From equations 4.26 and 4.24:

$$\frac{24}{E}\left(2\ M^3\ \frac{g^3}{\rho\ S\ CL} \right)^{\frac{1}{2}} = SLDEI\ SAR\ \ S\ \ \eta_{sisb} \tag{4.28}$$

$$=> \quad \left(M^3\ \frac{g^3}{\rho} \right)^{\frac{1}{2}} = \frac{SLDEI}{24}\ SAR\ \ S\ \ \eta_{sisb}\ E\ \ \left(\frac{CL\ S}{2} \right)^{1/2}$$

$$M^{3/2} \left(\frac{g^3}{\rho} \right)^{\frac{1}{2}} = \frac{SLDEI}{24}\ SAR\ \ S^{3/2}\ \ \eta_{sisb}\ E\ \ \left(\frac{CL}{2} \right)^{1/2}$$

$$\boldsymbol{\left(\frac{M}{S}\right)^{3/2} = \frac{1}{24 \cdot 2^{1/2}}\ \ E\ \ CL^{1/2}\ \ SAR\ \ \eta_{sisb}\ \ SLDEI\ \left(\frac{\rho}{g^3} \right)^{1/2}} \tag{4.29}.$$

Analogously to equation 4.23, through the equation 4.29 the upper limit for wing loading can be established, for sustained sun-powered daily horizontal flight, as function of aircraft aerodynamic characteristics E and CL, the aircraft energy absorption and transmission characteristics SAR and η_{sisb} , and the environment local characteristics SLDEI, ρ, g.

It is possible to use the formulae 4.23 and 4.29 to define the maximum wing load for several different purposes. Some examples of application are presented in chapter 5.

4.4.3) Procedure for definition of the required capability of batteries for a multi-days solar flight

For a sun-powered aircraft with batteries, intended for very-long duration time - i.e., to stay flying at night with stored energy collected during the day - besides the check presented in previous sub-section 4.2, a second definition is very important, which is the batteries capability. The definition procedure conceived in this study is presented in figure 4.6.

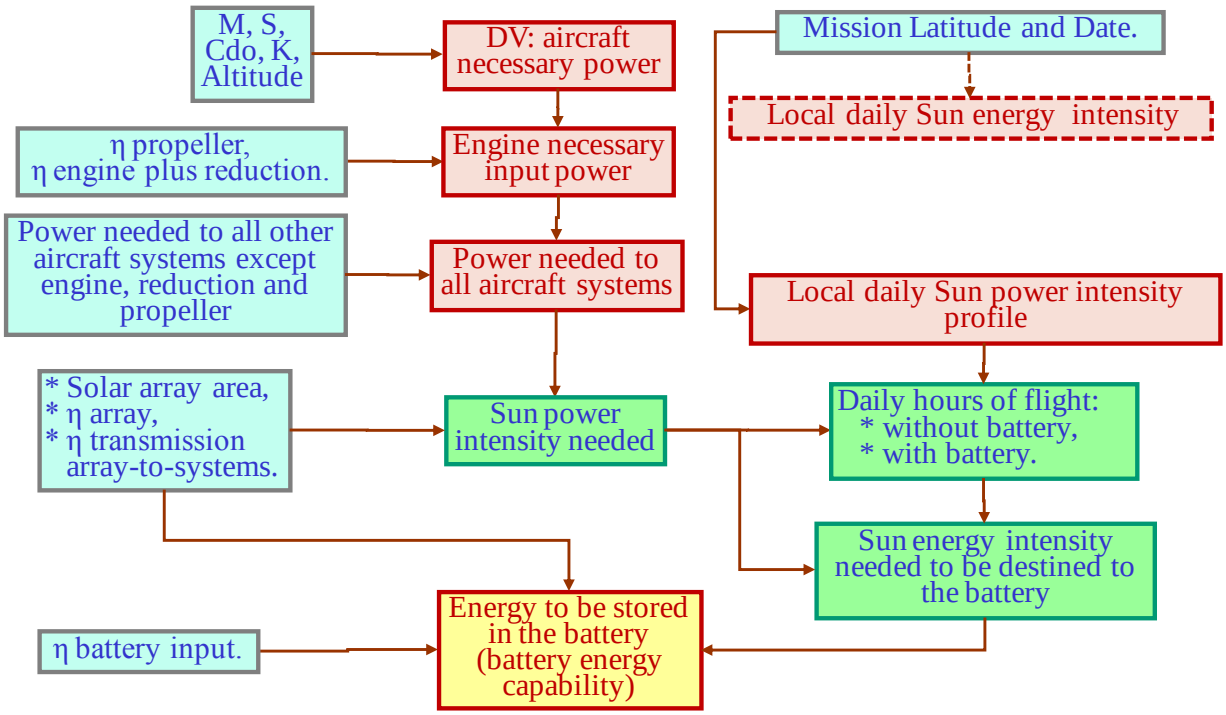

Figure 4.6: Procedure to define and to check batteries capability

4.5) Method for Solar Aircraft Design

The general process is illustrated in the flowchart below. The flowchart can present variations from this general version, depending on the special features on the desired mission or the desired configuration. Such special features can be, for example, large height variations on the typical mission path, solar panels intended to be installed in the fuselage or buoyancy devices intended to be added. Such requirements and constraints can be considered as particular cases from the general flowchart presented as follows. The flowchart is structured based on the concepts and guidelines presented by Gane and Sarson (1984).

In the flowchart presented of figure 4.7, the data are parameters in boxes at left hand side, including the initial values of (1) and (2) presented in the figure. Also referring to the figure 4.7, the main input data are positioned at the column at the left hand side; and the control parameters for convergence are Aircraft Mass and Wing Area.

The process is iteratively run until Aircraft Mass and Wing Area values converge. During the iterations, the data values at left side are kept constant. The values of (1) and (2), presented in figure 4.5-1, change during the iterations. If convergence is not achieved, values of data are changed. If

convergence is achieved, but resulting undesirable values of area and mass, again data values are changed until reasonable results of mass and area are achieved.

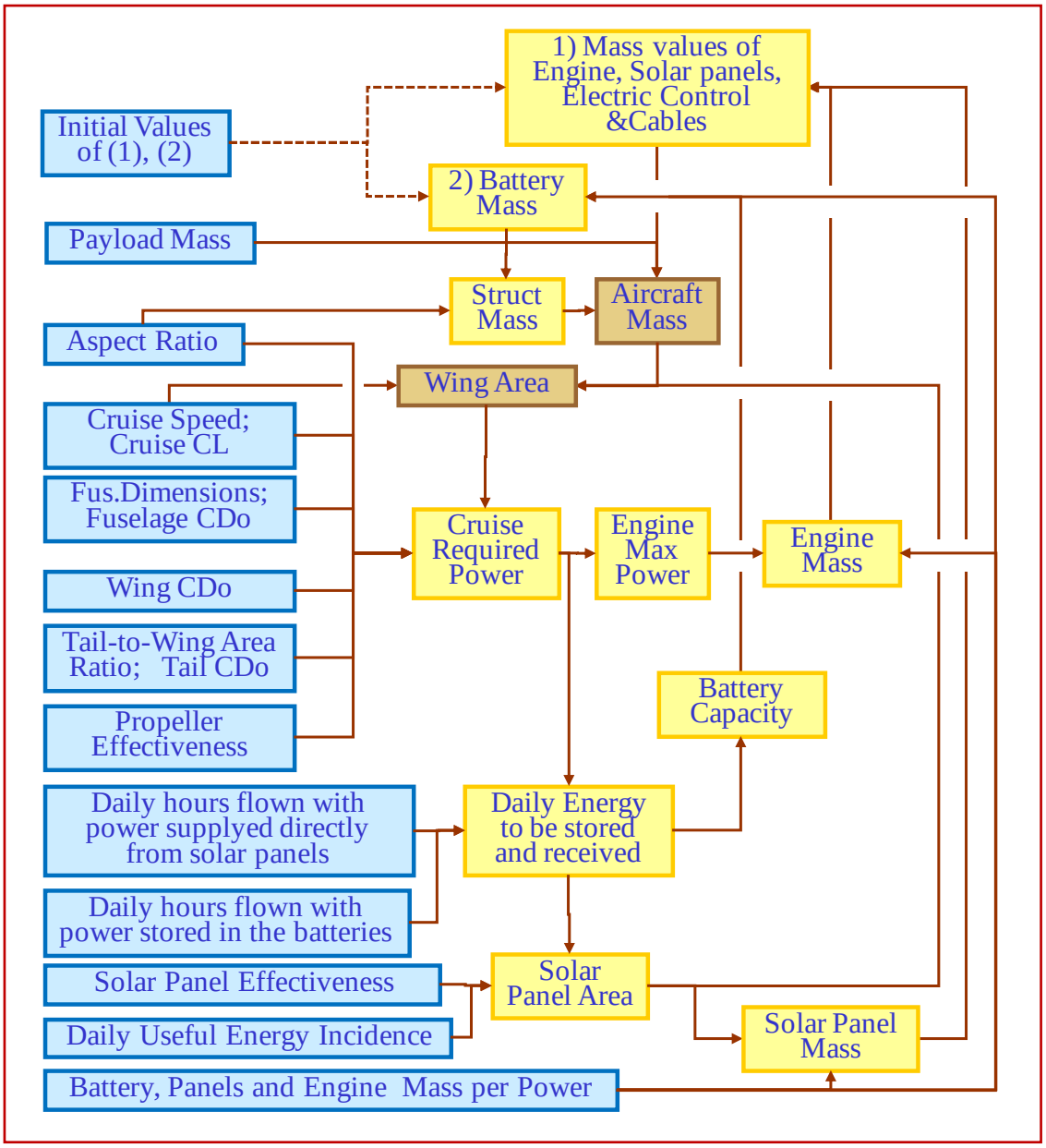

Figure 4.7: General Flowchart Considered for Solar Aircraft Definition and Design.

The flowchart of figure 4.7 can be explained in a summarized way by the following sequence:

- In function of the initial values of masses of payload, batteries, engine, propeller, solar panels, other electrical systems, and the aspect ratio, the structural mass of the wing is obtained, from the curve developed by the author and presented in the previous sections.

- In function of this value, and the adopted wing structure to aircraft structure mass ratio, the value of aircraft structure mass is obtained.

- Adding the structural mass Mstr to the initial values of payload mass Mpayl and systems mass Msys, the aircraft mass value is defined:

$$M = Mstr + Mpayl + Msys \quad (4.30).$$

- With the values of cruise equivalent airspeed EAS and aircraft lift coefficient CL, the Wing Area is defined:

$$Sw = \frac{2\ M\ g}{1.225\ EAS^2\ CL} \quad (4.31).$$

- With wing area, and the defined value of Tail-to-wing area ratio, the tail area St, comprising the sum of horizontal and vertical tail areas, can be defined.

- With the areas of Wing and Tail, the given values of Wing and Tail Drag Coefficients, CDow and CDot respectively, the Fuselage Equivalent Drag Area CDof.Sf, and the interference percentage ip, the total Drag Area CDo.S can be obtained:

$$CDo.S = (Sw.CDow + St.CDot + CDof.Sf)(1 + ip) \quad (4.32).$$

- In function of the Wing Aspect Ratio, the Oswald Coefficient, and the wing airfoil characteristics, the Induced drag factor K is defined.

- With the total Drag Area CDo.S and the induced factor K defined, and with the given values of cruise lift coefficient CL, cruise speed EAS, the intended cruise altitude H, and propeller

efficiency ηprop the necessary cruise engine power SHP can be defined, through the following sub-steps:

The air specific mass at the altitude is obtained in function of the altitude:

$$\rho = f(H) \quad (4.33),$$

i.e., ρ is obtained in function of H by the rules of the ESDU Standard Atmosphere (1986), also presented in section 3.7. The aircraft True Airspeed TAS, and propeller shaft power necessary for cruise SHP, are obtained by:

$$TAS = EAS \left(\frac{1.225}{\rho}\right)^{1/2} \quad (4.34).$$

$$SHP = \frac{1}{2} \rho TAS^3 \frac{CDo.S + Sw.K.CL^2}{\eta prop} \quad (4.35).$$

- The value of engine cruise required power SHP is one of the major parameters in this approach of the Solar Aircraft Design, since several other parameters are direct function from it, as can be seen in the following steps.

- In function of SHP and the intended hours per day to be flown without direct solar power, i. e. flown from the stored power on batteries, the capacity of batteries is determined. And from the given parameter battery mass per capacity, the battery mass can be obtained.

- In function of SHP, the considered hours per day to be flown with power supplied directly from solar panels, the amount of power to be stored in the batteries for flight without direct solar power, the daily amount of energy to be collected is determined.

- Once known the value of daily energy to be collected, and given the values of daily useful solar energy available, (which is function mainly of the solar irradiance model and the aircraft location on earth and the flight date in the year) and the solar panels effectiveness, the solar panel area can be defined.

- The solar panel mass is defined in function of the area defined, and the data of Mass panel per area.

- The Engine Maximum power is defined from the Engine power required for cruise, and from that parameter the engine mass can be defined.

- With the mass values for engine, solar panels and batteries, the assumed mass value of cables, controls, payload are added and a new value of Payload and Systems mass is defined. With this value, a new aircraft value is obtained.

- Once defined this value of aircraft total mass, a new wing structure value is defined, leading to the new aircraft structure value and new values of aircraft total mass and wing area.

The process is iteratively repeated, through values of drag, SHP, energy to be collected and stored, mass of batteries, panels and engine, structural mass, aircraft total mass and wing area, until the values of total mass and wing area converge to constant values throughout the iterations. As commented above, if the values do not converge or lead to undesirable, i. e. higher than expected, values, the input data needed to be changed until a convergence is obtained.

The example of use of this method is presented in the chapter 6, Results.

4.6) Comment on Influence of Reynolds Number on Lift and Drag

4.6.1) General Aspects

In order to illustrate the strong influence of Reynolds number for this study, a comparison of the Reynolds Number related to Wing and Propeller of some of the aircraft analyzed in this work is presented in the figure 4.8. In the figure it also defined three different regions in terms of Reynolds number, according to the effects presented in the section 3.5: The region above $1.5x10^5$, good for conventional airfoils; the transition region between $1.5x10^5$ and $8x10^4$; where hysteresis occurs, and the region below $8x10^4$, good for thin airfoils, and in which the laminar leading edge stall occurs for angles of attack about 5 to 7 degrees for conventional airfoils.

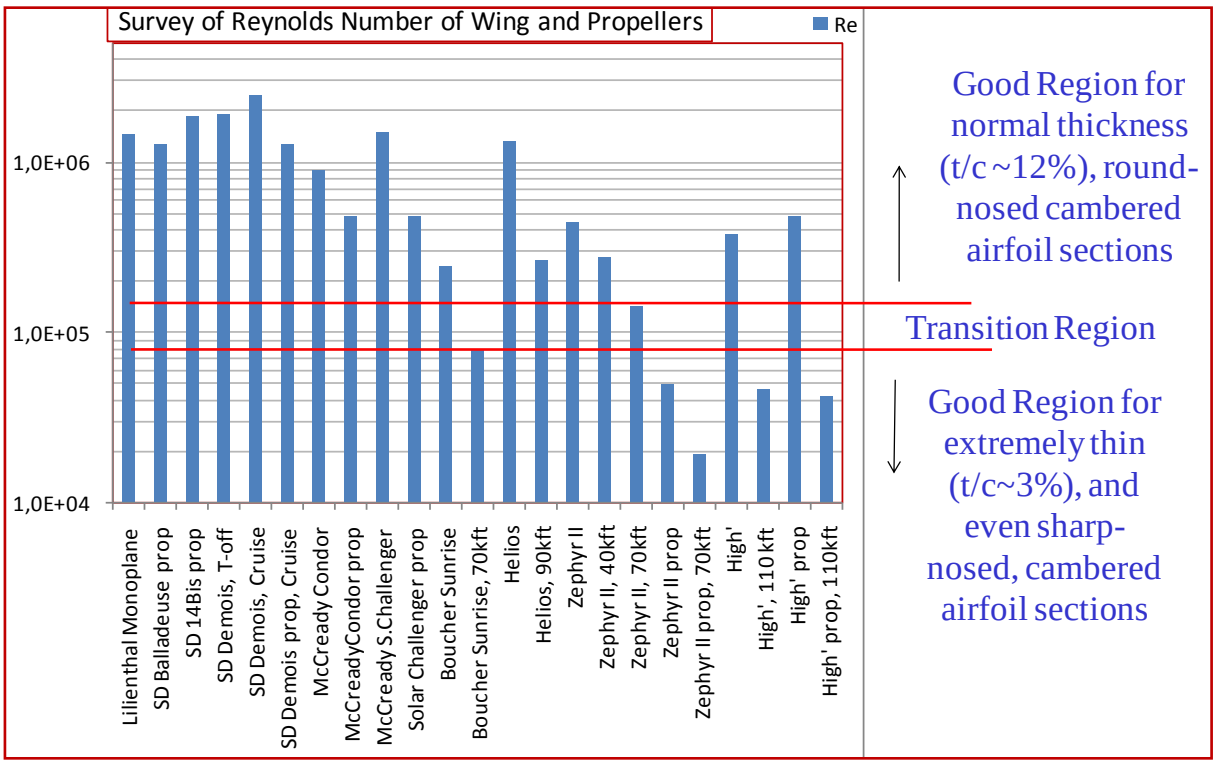

Figure 4.8: Survey of Re of Wing and Propellers, of several aircraft analyzed in this work

In general, the existing aircraft present Reynolds numbers above or well above $2x10^6$; Reynolds numbers above this level correspond to the region airplanes are commonly flown, aeronautic engineers and schools in general focus. But this is not the case of several of the aircraft studied in this research. One can note that the Reynolds numbers for almost all the aircraft and propellers presented in figure 4.8 are below $2x10^6$; and some of them are even below $1.5x10^5$, in the region where, as presented in section 3.5, the Lift-to-Drag ratio of a conventional airfoil decreases considerably.

Through examination of figure 4.8 in can be noticed that the Reynolds numbers for Lilienthal Gliders, 14-Bis, Demoiselle, Gossamer Condor and Solar Challenger are roughly in the same range, above $4x\ 10^5$, and thus, above the transition region. But the new generation of high altitude solar aircraft such as the Zephyr, started entering in the Reynolds Number transition region, in which the extremely thin airfoils are better suitable than the normal thickness airfoils; the Reynolds number related to Zephyr wing are presented in 15^{th} to 17^{th} columns of figure 4.8. If Boucher brothers' Sunrise I and Sunrise II aircraft had been successful in the so-intended altitude flights, these aircraft

would also fly in the transition region in terms of Reynolds Number, as can see by the eleventh and twelfth columns of figure 4.8.

In the figure 4.8 the High aircraft is also presented, as can be seen 20^{th} and 21^{st} columns. This aircraft is one result of the conceptual design performed in this work and is described in chapter 6. From the figure 4.8 one can note that this aircraft, as Zephyr, presents a flight mission in which very low Reynolds numbers are achieved.

In figure 4.8 the Reynolds numbers of the propellers are also presented for some already flown air vehicles, as the Balladeuse, the 14-Bis, the Demoiselle, the Condor, the Solar Challenger, and the Zephyr in two altitudes, which correspond to the 2^{nd}, 3^{rd}, 6^{th}, 8^{th}, 10^{th}, 18^{th} and 19^{th} columns respectively. It can be noticed that most part of the propellers are above the transition region, and could have conventional airfoils. This is not the case of propeller of Zephyr aircraft. The propeller for the High aircraft also should be designed for very low Reynolds number. Although not presented in the figure 4.8, the Helios aircraft propellers have been also calculated and present the same Reynolds number characteristics as the Zephyr aircraft propellers.

4.6.2) Guidelines for considering effects of Low Reynolds number on design

In order to deal with the issue of the abrupt Lift-to-Drag decreasing at Reynolds numbers below $1.5x10^5$ on conventional airfoils, some actions should be taken for design and analysis as:

- From the aircraft mission profile and preliminary characteristics of aircraft and propeller, to correctly define for both, wing and propeller airfoils:
    - The range of Reynolds number corresponding to the aircraft mission;
    - The Reynolds number at the aircraft design point.
- If the Reynolds number for the wing or propeller is in the transition region i.e. between 1.5×10^5 and 8×10^4, to try to increase this Reynolds number, by trying the compromise of decreasing the surface propeller aspect ratio, or increasing the local airspeed, and checking the penalties associated.
- If the Reynolds number in the wing or propeller is still below 1.5×10^5 in important segments of flight:
    - To choose a suitable airfoil for the surface, wing or propeller, considering this low Reynolds number, and

- Considering the aircraft using this new airfoil, to check its performance along the whole mission, regarding the variation of the aerodynamic characteristics of the airfoil with the variation of the Reynolds numbers along the mission.

4.7) Simplified Methodology for Airfoil Preliminary Analysis

Due to the large amount of airfoils to be studied in this work, the definition of a procedure allowing fast evaluation of drag and lift characteristics of a given airfoil shape and Reynolds number became one of the basic requirements for the feasibility of this work, from its first stages. Other important factors that have driven the need of a specific and dedicated method for airfoil studies are: The need of understanding the effects of low Reynolds numbers lower than the ones considered in general aviation, due to the special conditions, related to some of the aircraft studied, of low speed, small chords, and very high altitude; and the – nowadays - uncommon shape of some airfoil shapes studied, as large camber and low thickness. Thus, a dedicated and simplified airfoil analysis procedure has been defined. A research have been performed in order to identify the most relevant influences on CL and CD specific for this study, based on Hoerner (1958), Hoerner (1985) , McCormick (1980), Abbot et al (1945) , NACA (1928, 1927, 1924, 1923, 1921), Prandt et al (1920). The method is explained briefly, and focusing the main steps, since this is analysis is not the main subject of the study.

The procedure can still be improved and transformed in an automatic routine, but for the objectives of this study, it has been already effective.

One important point is that this approximation is not applicable for surfaces subjected to lift at Reynolds numbers below 1.5 x 10^5. The effects of Reynolds numbers below 1.5 x 10^5, if the surface is on lift, are presented in section 3.5.

In terms of CD, the objective is to find a law of the type: $CD=CDo+K.CL^2$. This law is in the 3D domain, i.e. the aspect ratio of the surface must be considered. The value of K is obtained from:

$$k = \frac{1}{\pi . A . e} + Kabr \qquad (4.36)$$

Where A and e are input data, and Kabr is the value for abrupt leading edge, given by the figure 4.9 in function of camber ratio.

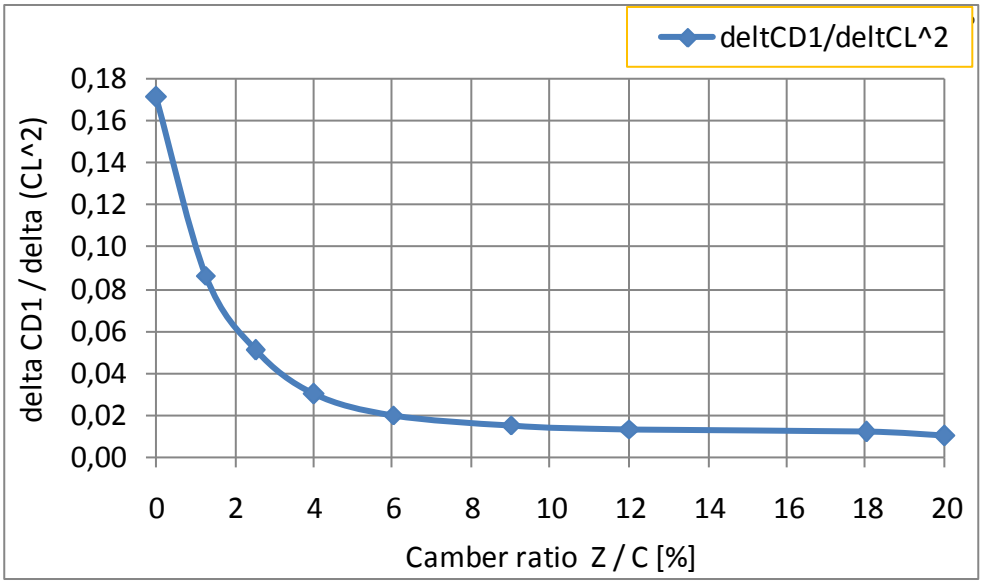

Figure 4.9: Kabr as function of camber ratio Z/C

For the definition of the airfoil three-dimensional CDo, it is assumed that it has the same value of the two-dimensional CDo, which is defined from the ratios T/C, Z/C, and Reynolds number. For Z/C=0 the value of CDo can be obtained directly from the figure 4.10.

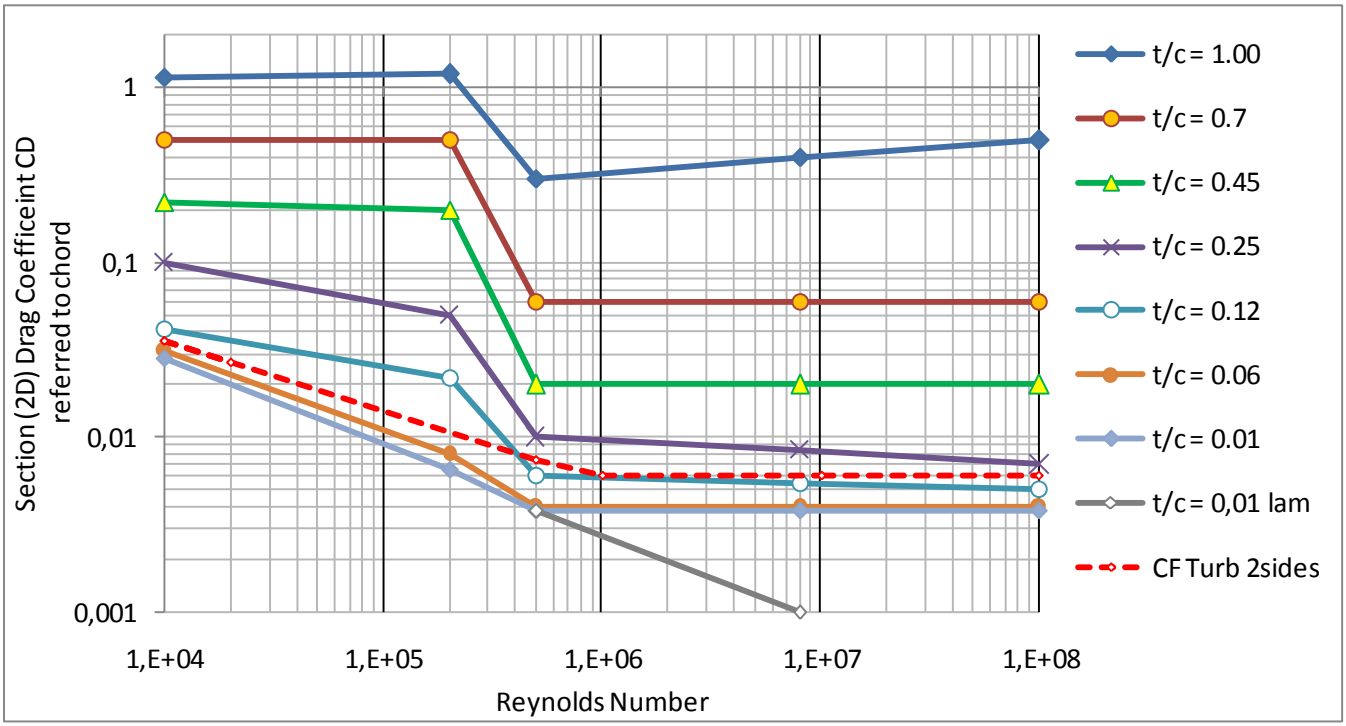

Figure 4.10: CDo 2D as function of thickness ratio T/C and Reynolds Number.

For cambered airfoils, i.e. Z/C higher than zero, the following simplified considerations apply: The CDo is considered as the sum of two parcels, one due to shape other due to Reynolds, Cdo_{shape} and CDo_{Re} respectively.

The value of CDo due to shape is function of camber and thickness is presented by figure 4.11. The value of the parcel of CDo due to Reynolds number is presented by figure 4.12, for two possible conditions: fully turbulent flow, and intermediate flow i.e. partially laminar. The condition is an input definition, in function of the type of airfoil.

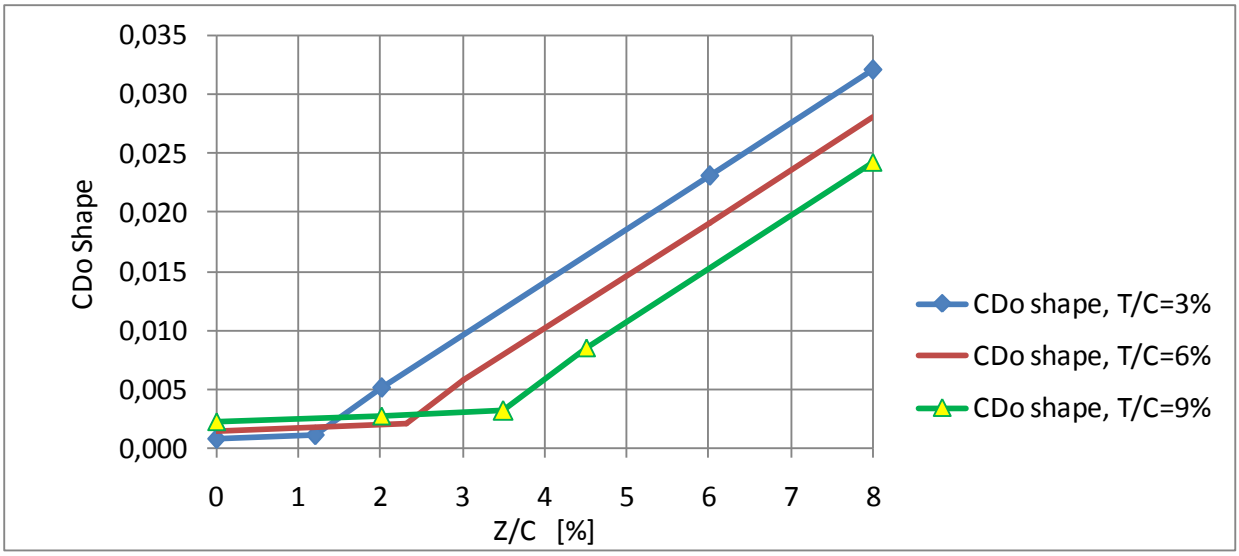

Figure 4.11: CDo_{shape} in function of thickness ratio T/C and camber ratio Z /C.

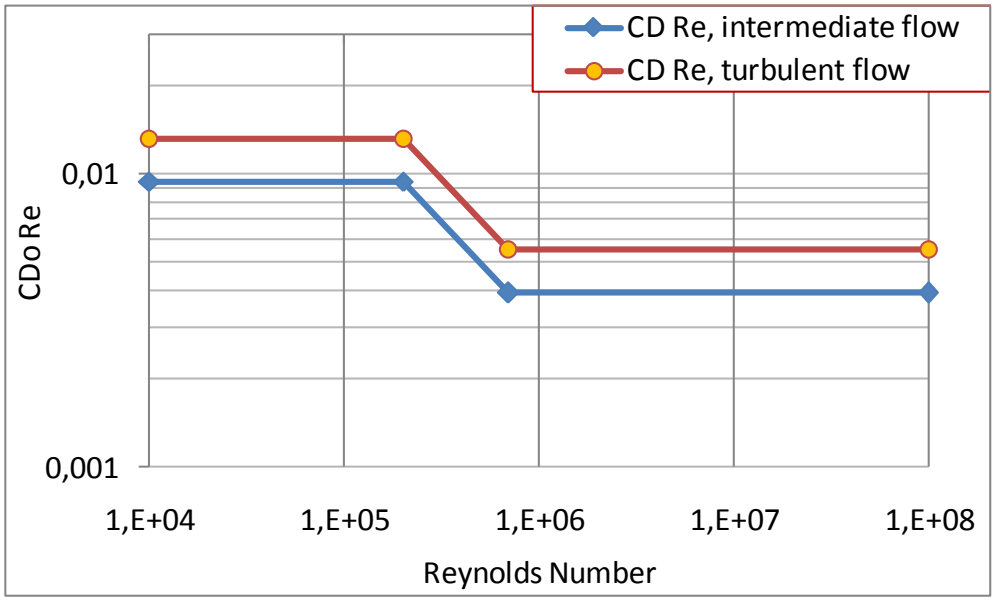

Figure 4.12: CDo_{Re} as function of Reynolds number, for fully turbulent flow and intermediate flow.

In terms of CL, the following equation applies:

$$CL = CLo + CL\alpha . \alpha \quad (4.37)$$

This equation is valid up to the value of CL not higher than a CLmax, also to be defined. These values of CL, CLo, CLα and CLmax are in three-dimensional domain i.e. they refer to lifting surface with a finite aspect ratio. In order to obtain values for these 3-D parameters, the corresponding 2-D ones CL_{2D}, CLo_{2D}, $CL\alpha_{2D}$ and $CLmax_{2D}$ must be defined at first. The CLα2D, which is the slope of the CL2D versus α curve, can be obtained from the figure 4.13 in function of the airfoil thickness; this curve is obtained from analysis of CLα from airfoils with different thicknesses.

The coefficient CLo_{2D} is obtained in function of airfoil camber. In terms of potential flow, according to McCormick (1980) the CLo_{2D} corresponds to:

$$CLo_{2D} = CL\alpha_{2D} \left(2 \frac{Z}{C}\right) \quad (4.38).$$

By comparison of the airfoils test results presented in NACA (1928) a formula with a lower value of the multiplying factor can be considered:

$$CLo_{2D} = CL\alpha_{2D} \left(1.2 \frac{Z}{C}\right) \quad (4.39).$$

The formula (4.7.3) is considered in the procedure.

The $CLmax_{2D}$ of the airfoil can be obtained from sum of two parcels, the $CLmax_{2D}$ due to camber and the $\Delta CLmax_{2D}$ due to Reynolds number and thickness ratio:

$$CLmax_{2D} = CLmax_{camber\ 2D} + \Delta CLmax_{ReT\ 2D} \quad (4.40)$$

The figure 4.14 presents the value of CLmax due to camber, obtained from analysis of several airfoils presented in Hoerner (1985); and figure 4.15 presents the curves of CLmax due to thickness ratio and Reynolds number, which have been derived from the data presented in McCormick (1980).

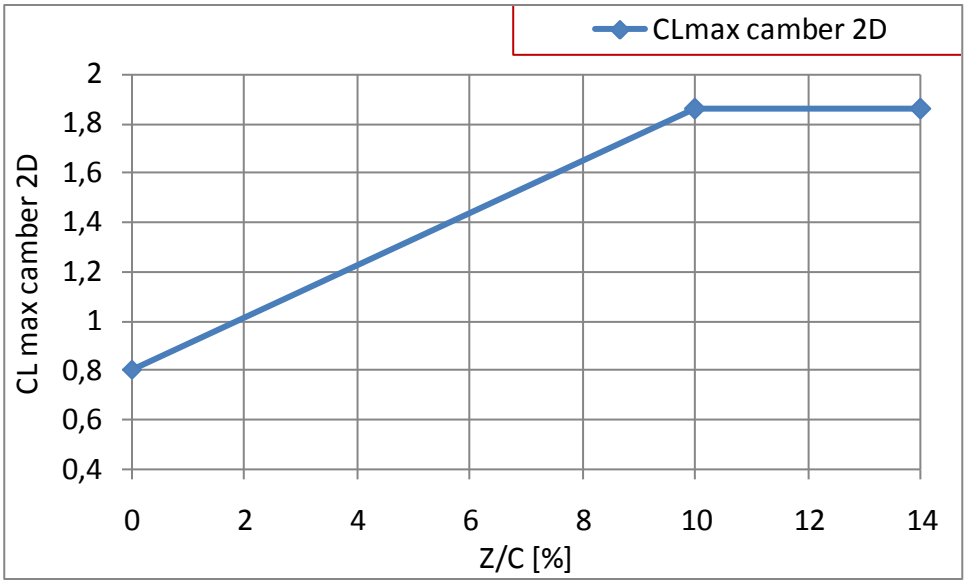

Figure 4.13: $CLmax_{camber\ 2D}$ as function of camber ratio Z/C

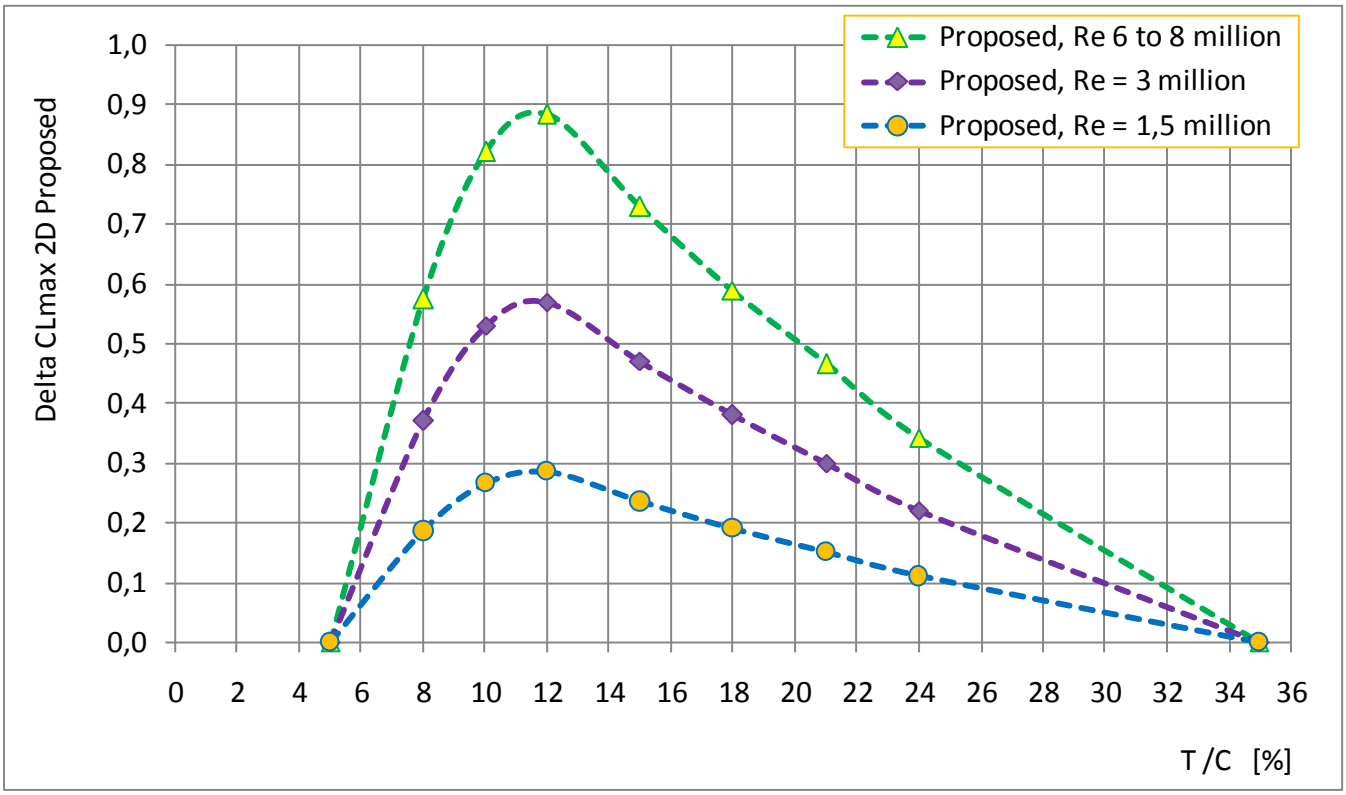

Figure 4.14: $\Delta CLmax_{ReT\ 2D}$ as function of thickness ratio T/C and Reynolds Number

The figure 4.15 presents the value of $CL\alpha_{2D}$ in function of the thickness ratio T/C.

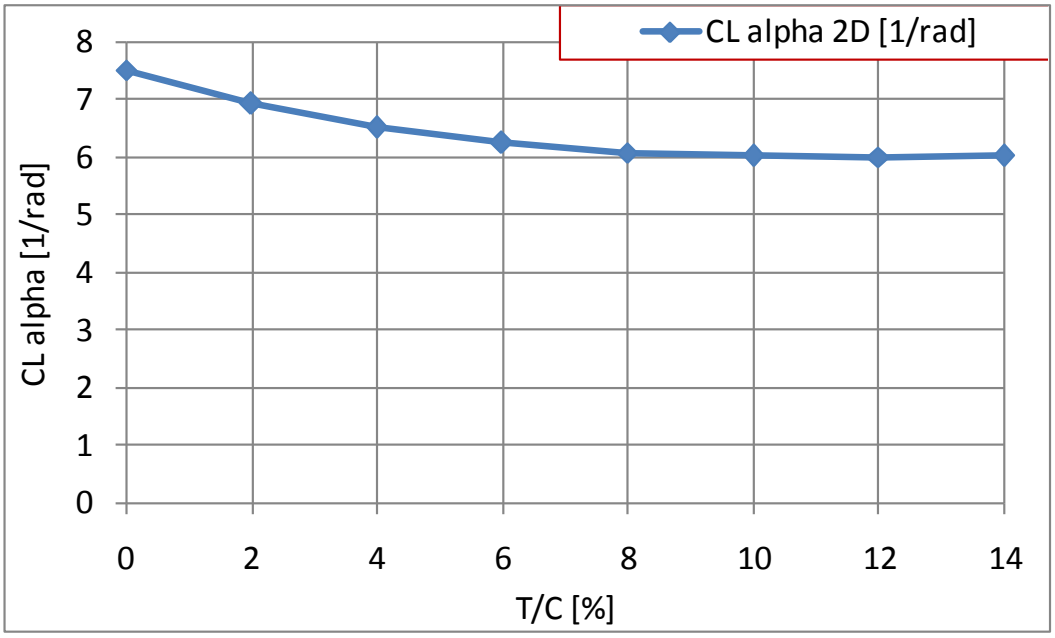

Figure 4.15: $CL\alpha_{2D}$ as function of thickness ratio T/C

Once obtained the values for the 2-dimesional coefficients, the corresponding 3-dimensional ones are obtained as follows. The 3-dimensional CLα derivative is obtained, in function of the surface aspect ratio, as presented by McCormick (1980) by:

$$CL\alpha = CL\alpha_{2D}\left(\frac{A}{A+2}\right) \tag{4.41}$$

The 3-dimensional lift coefficient for zero angle of attack is obtained, based on equation 4.38, by:

$$CLo = CL\alpha\left(1.2\ \frac{Z}{C}\right) \tag{4.42}$$

And the 3-dimensional CLmax coefficient is obtained by:

$$CLmax\ = f\ .CLmax_{\ 2D} \tag{4.43}$$

Where the factor f is defined in function of aspect ratio as presented in figure 4.16.

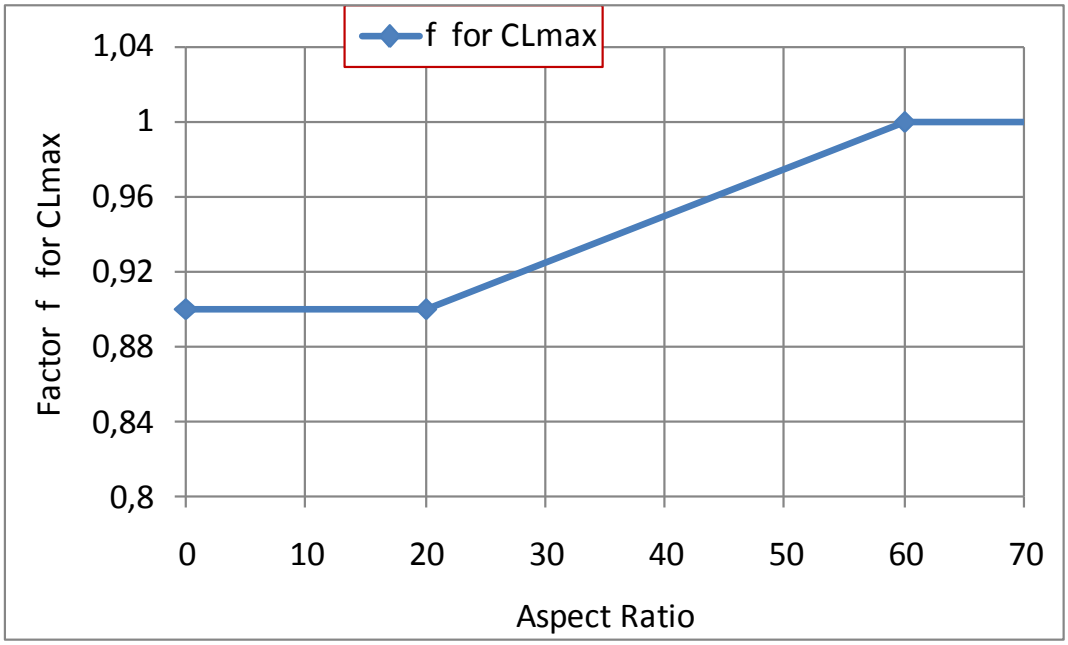

Figure 4.16: Multiplying factor f for CLmax.

The figures 4.17 and 4.18 show comparison between calculated values of CL and CD, and the corresponding experimental results from NACA (1928).

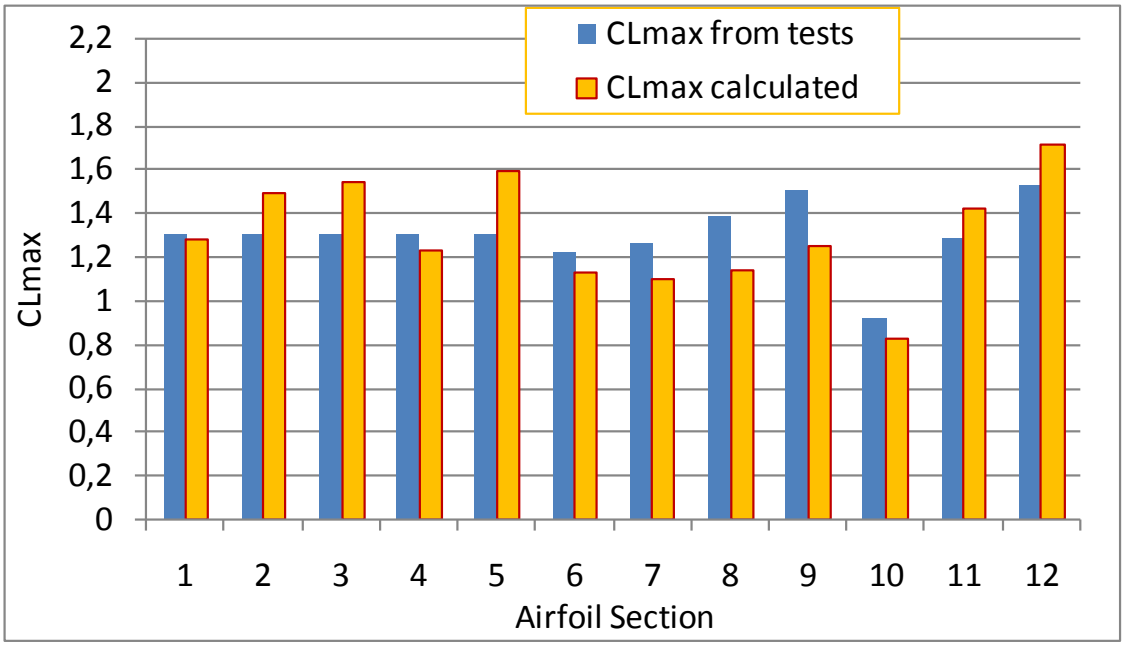

Figure 4.17: Comparison of results from the method, CLmax comparison

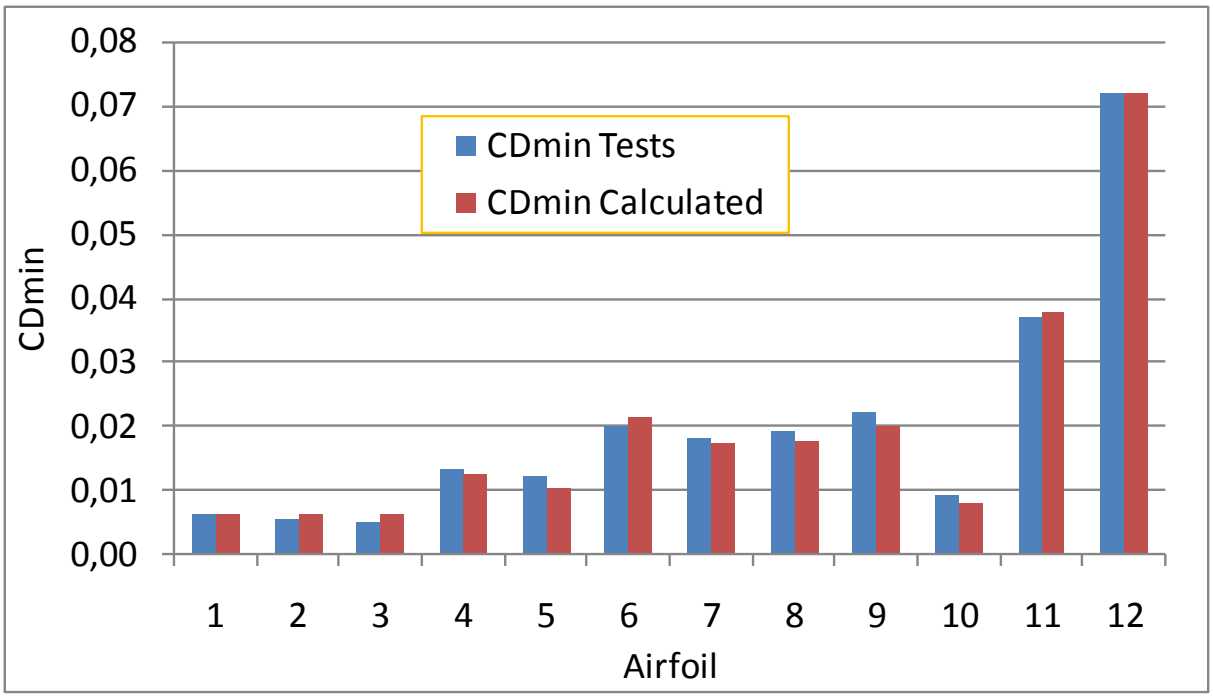

Figure 4.18: Comparison of results from the method, CDmin comparison

4.8) Methodology for Propeller Studies

4.8.1) Formulation

The aim of propeller analysis methodology is to obtain, from a given propeller geometric data and RPM, an estimation of propeller thrust and power versus airspeed. The general process is schematically presented in the flowchart of the figure 4.19.

The two bases for the propeller evaluation process defined in this work are the Blade Element Theory and the Momentum Theory. As can be noted by the orientation of the arrows in the upper right part of figure 4.19, the process is iterative. This is a consequence of using the momentum theory, which improves the process reliability, most remarkably at lower aircraft airspeeds.

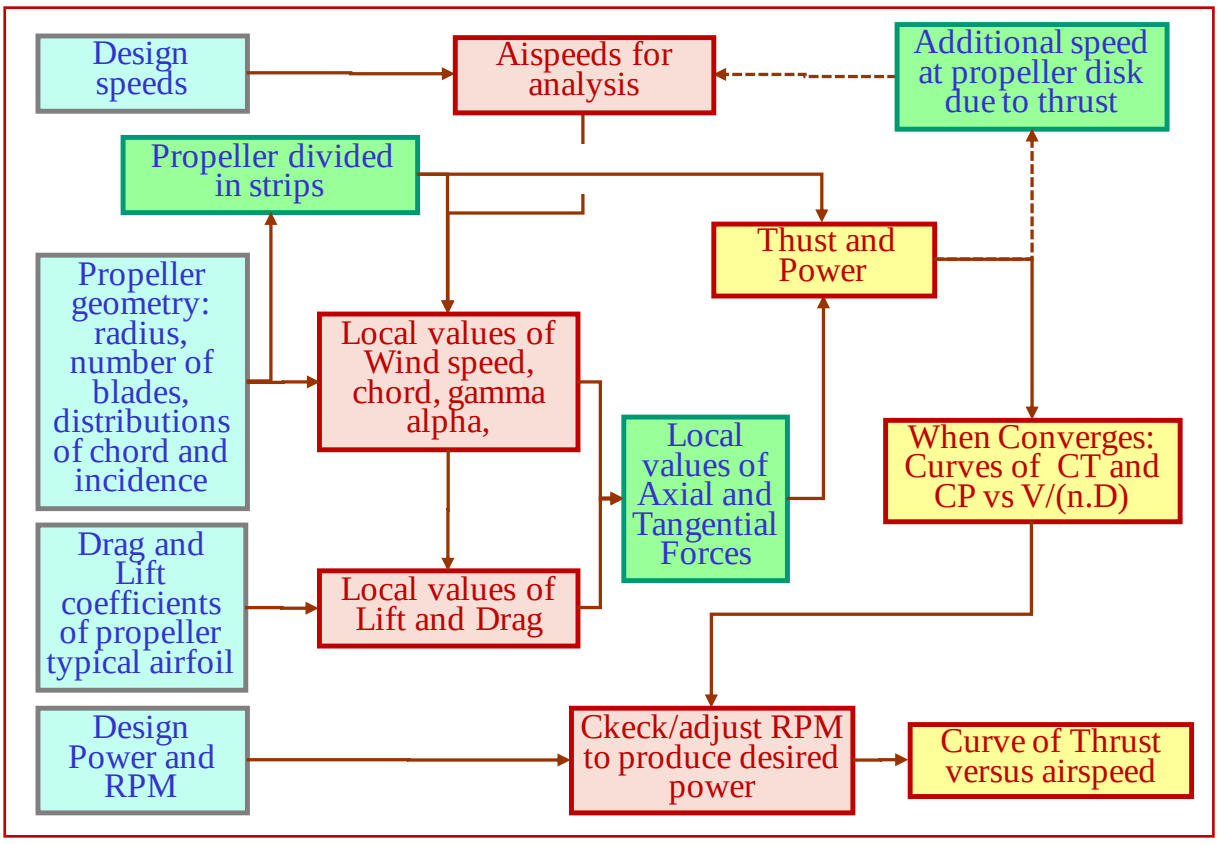

Figure 4.19: Flowchart for propeller evaluation

Adopting the Blade Element Theory, the propeller blade is considered as divided in several strips. Along each strip, the aerodynamic and geometric characteristics are considered as constant. The orthogonal aerodynamic forces Lift and Drag of each strip are given by:

$$L_i = \frac{1}{2} . \rho . {V_i}^2 . S_i . CL_i \tag{4.44}$$

$$D_i = \frac{1}{2} . \rho . {V_i}^2 . S_i . CD_i \tag{4.45}$$

Where CL_i and CD_i are lift and drag coefficients of the blade strip sections, given by:

$$CL_i = CL\alpha . \alpha_i + CLo \tag{4.46}$$

$$CD_i = CDo + CD\,(CL_i) + CD\,(\alpha_i) \qquad (4.47)$$

The coefficient CDo is function of the Reynolds Number at the strip and the shape of the propeller airfoil. The values of CLα, CLo, CD(CL_i), CD(α_i) are function of the propeller airfoil shape and the equivalent aspect ratio of the propeller blade, obtained from the airfoil analysis, presented in the previous section 4.7.

α_i is the angle of attack wind-to-blade at the strip, which is the angle between the resultant local wind and the local pitch angle of the blade, at the strip section.

The initial values of γ_i are obtained in function of the aircraft True airspeed TAS, in meters per second; propeller revolution speed n, in revolutions per second; and by the local radius of the strip R_i , in meters:

$$\gamma_i = arctan\frac{TAS}{2.\pi.n.R_i} \qquad (4.48),$$

being:

$$n = RPM/60 \qquad (4.49).$$

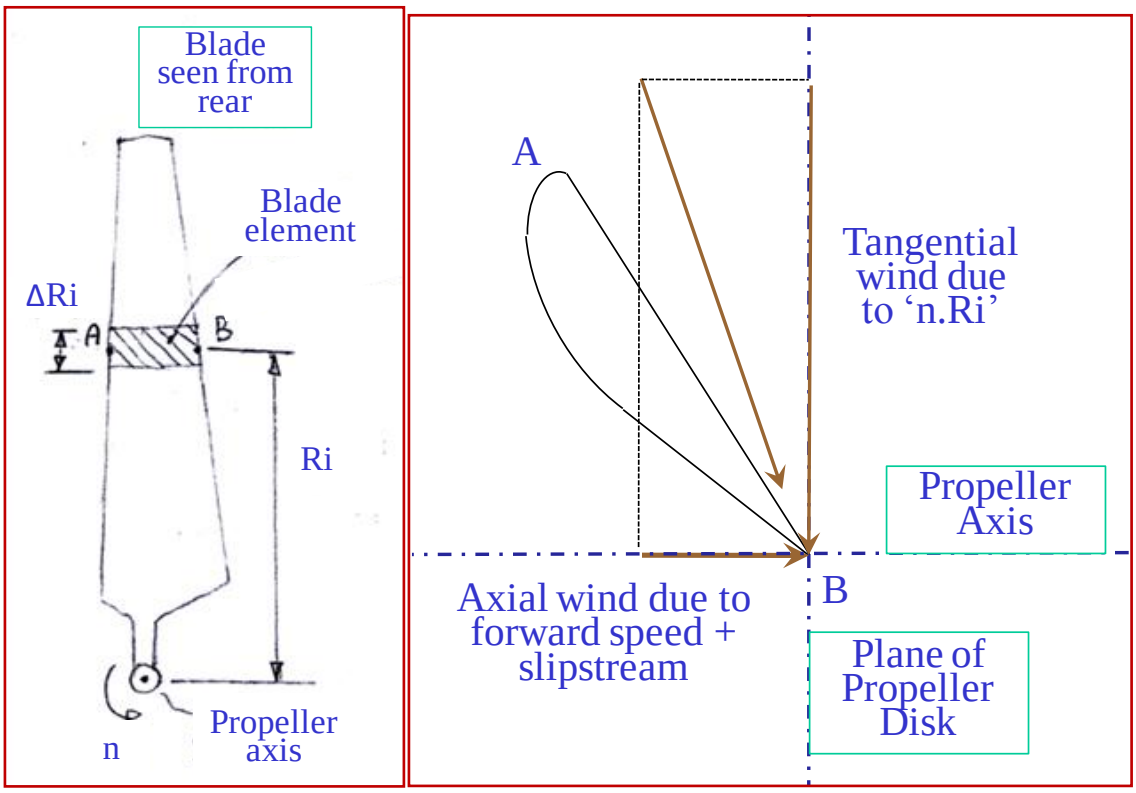

Figure 4.20: Propeller Blade, with a blade element 'AB' (left);
and the local wind speeds at that blade element 'AB' (right)

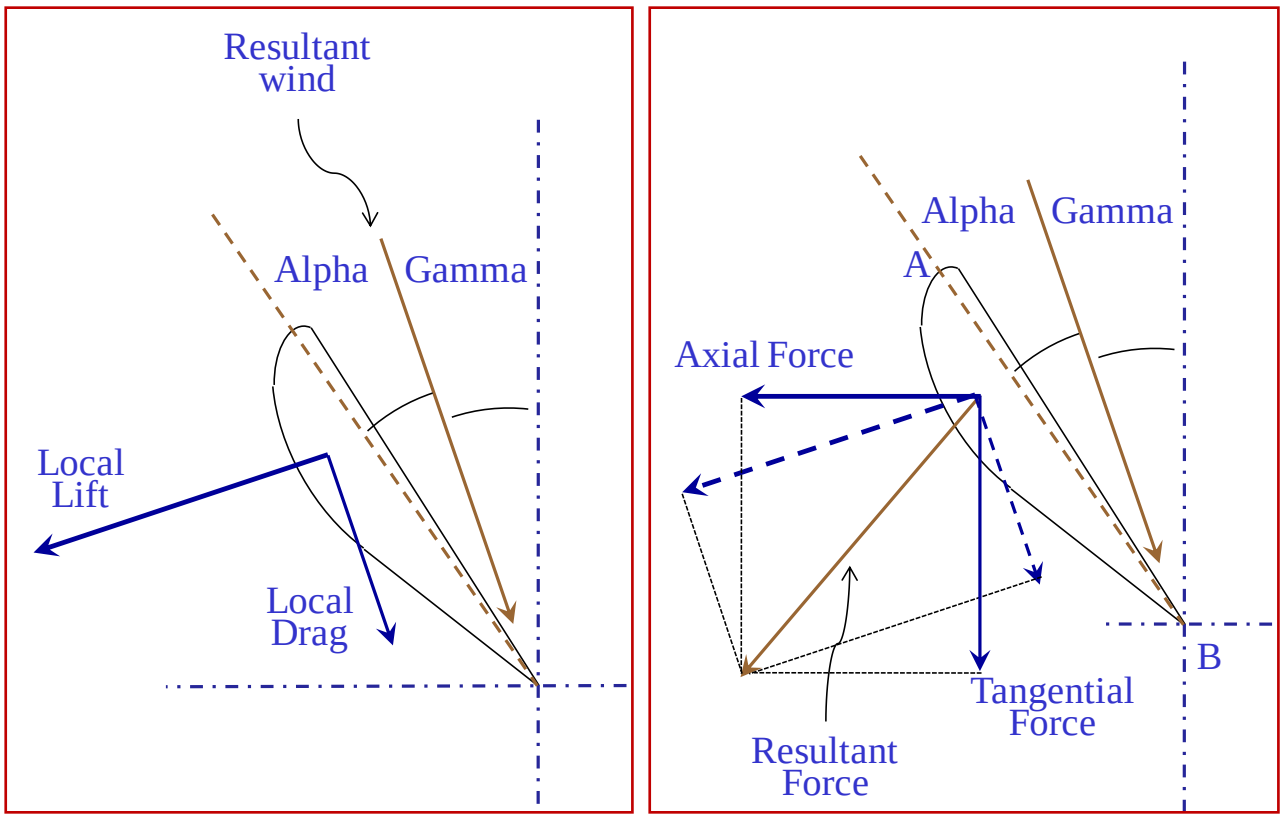

Figure 4.21: Same propeller blade element 'AB' from figure 4.20; but now presenting the local angles γ and α, and the local Lift and drag forces (left); and the components of the local resultant aerodynamic force into tangential and axial forces (right) .

The aerodynamic forces on each strip are expressed in terms of axial force Fax_i and tangential force Ftn_i, by the transformation:

$$Fax_i = L_i . cos(\gamma_i) - D_i \, sin(\gamma_i) \quad (4.50)$$

$$Ftn_i = L_i . sin(\gamma_i) + D_i \, cos(\gamma_i) \quad (4.51)$$

Where γ_i is the strip pitch angle. The forces presented in this axis system, with axial and tangential directions, are more suitable for propeller blade analysis.

The sum of the axial forces of each strip, times the number of blades gives the propeller Thrust Tr:

$$Tr = Nb \sum_{i=1}^{ns} Fax_i \quad (4.52)$$

Where ns is the number of strips per blade and Nb is the number of blades of the propeller.

The Propeller power is given by:

$$Pw = 2.\pi.n.Nb \sum_{i=1}^{ns} Ftn_i . R_i \qquad (4.53)$$

Where n is the number of revolutions per second, and R_i is the distance of the center of the strip to the axis of rotation of the propeller.

The Propeller Thrust increases the air speed not only in the region downstream the propeller disk; but the flow throughout the disk is also partially accelerated. In terms of the additional airstream speed due to the propeller thrust, the common understanding is that the additional speed at the propeller disk is half of total additional speed, which happens far downstream from the propeller, as presented by McCormick (1980). The change in speed and diameter of the flow that passes by propeller is schematically represented in figure 4.22.

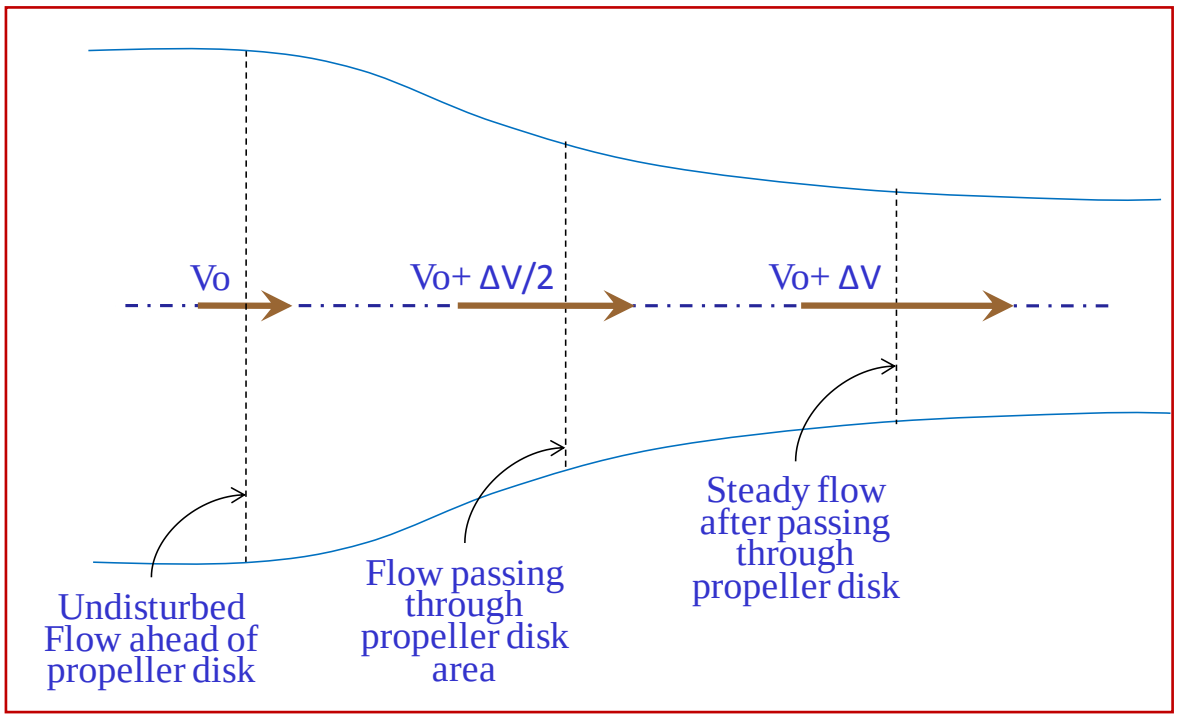

Figure 4.22: Stream tube of air flow passing through propeller disk; aircraft is flying from right side to left side

The consideration of stream due to the propeller thrust is the so-called Momentum Theory; and due to this consideration, the process is forced to be iterative. The way the stream is considered is explained in the continuation of this text.

The starting point is the 2nd Newton's Law:

$$F = m \, . \, a \tag{4.54}$$

Being, in this case:

F the force in X direction due to the propeller;

m the mass of air, accelerated by the propeller;

a the acceleration in X direction occurring to the air due to the force from the propeller .

It is possible to consider the following identities:

$$F = Tr \, ; \qquad m.a = m/\Delta t \, . \, \Delta V \tag{4.55}$$

and

$$m/\Delta t = \rho \, . \, Sdisk \, . \, Vdisk \tag{4.56}.$$

Being Tr the propeller thrust, Δt the time interval for total acceleration of the air, ΔV the total increment of speed of the air accelerated by the propeller, Sdisk the propeller disk area, Vdisk the air speed when passing by the propeller disk. The airspeeds increased by Propeller Thrust are defined as:

- The airspeed at the Propeller disk as:

  $$Vdisk = TAS + \Delta V/2 \tag{4.57}$$

- The final airspeed downstream from the Propeller as:

  $$Vf = TAS + \Delta V \tag{4.58}.$$

Combining equations 4.54, 4.55, 4.56:

$$Tr = \rho \, . \, Sdisk \, . \, Vdisk \, . \, \Delta V \tag{4.59}.$$

Substituting terms of equation 4.8-16 by equation 4.8-14, and developing it:

$$Tr = \rho . Sdisk . (TAS + \frac{\Delta V}{2}) . \Delta V \quad (4.60)$$

$$Tr = \rho . Sdisk . TAS . \Delta V + \frac{\rho . Sdisk}{2} . \Delta V^2$$

$$\frac{\rho . Sdisk}{2} . \Delta V^2 + \rho . Sdisk . TAS . \Delta V - Tr = 0$$

$$\Delta V^2 + 2\ TAS\ \Delta V - \frac{2\ Tr}{\rho\ Sdisk} = 0 \quad (4.61)$$

Equation 4.61 is a quadratic equation having ΔV as the incognita. Solving the equation, the expression for ΔV is:

$$Delta = 4\,TAS^2 + \frac{8\ Tr}{\rho\, Sdisk} \quad (4.62)$$

$$\Delta V = -2\ TAS \pm \left(4\,TAS^2 + \frac{8\ Tr}{\rho\ Sdisk}\right)^{1/2}$$

$$\Delta V = \pm 2\left(TAS^2 + \frac{2\ Tr}{\rho\ Sdisk}\right)^{1/2} - 2\,TAS \quad (4.63).$$

One can check that the negative value of the 1st term of the 2nd member has no physical meaning. So equation 4.63 turns into:

$$\frac{\Delta V}{2} = \left(TAS^2 + \frac{2\ Tr}{\rho\ Sdisk}\right)^{1/2} - TAS \quad (4.64).$$

This value of ΔV/2 is so obtained from propeller thrust, aircraft true speed and air specific mass. It can be added to the aircraft true airspeed according to equation 4.55 thus defining the first value of the airspeed at the Propeller disk Vdisk, the airspeed passing by the disk. For a positive thrust, this airspeed is slightly higher than TAS.

The values of γ_i and V_i should be adjusted with this new value of Vdisk. These new values lead to slightly different values of L_i and D_i, and consequently, new values of Power and Thrust; and new value of Vdisk. An iterative process is needed and after few iterations a consistent global set of values of thrust, power, ΔV_i , γ_i , V_i , L_i and D_i is finally attained.

It is common to present the propeller Thrust Tr and the Propeller power Pw in the non-dimensional form:

$$CT = \frac{Tr}{\rho \ D^3 \ n^2} \quad (4.65)$$

$$CP = \frac{Pw}{\rho \ D^6 \ n^4} \quad (4.66).$$

Additionally the propeller effectiveness Eta or η_{prop} is given by:

$$\eta_{prop} = J \, . \, Ct \, / \, Cp \quad (4.67).$$

The intermediate results of this analysis are the coefficients CT and CP versus J; being the values of η_{prop} versus J auxiliary results for consistency checks.

The calculated values of Power are compared to the defined engine-to-propeller shaft power and propeller RPM, which are also, inputs for the analysis. The value of RPM is slightly adjusted in order to allow the calculated power to be equal to the input Shaft Power value. The main result for the propeller analysis is thus the available thrust in function of aircraft true airspeed.

4.9) Methodology for Drag Analysis

4.9.1) General

Aircraft Drag coefficient can be considered as the sum of the parasite drag coefficient CDo and induced drag coefficient CDi:

$$CD = CDo + CDi \quad (4.68)$$

Where the induced drag coefficient CDi is obtained in function of the lift coefficient CL:

$$CDi = K \cdot CL^2 \qquad (4.69)$$

The equations 4.68 and 4.69 together result in the parabolic equation 4.45. This formula describes what is known as the aircraft Drag Polar, which is a very important concept for this work.

The parasite drag coefficient CDo is obtained from the drag coefficient of each relevant individual item of the aircraft, exposed to wind, including interference, as presented in Pinto et al (1999), Hoerner (1958) and McCormick (1980). CDo is the sum of the product drag coefficient x reference area of each relevant item, divided by the aircraft reference area:

$$CDo = \frac{1}{Sref} \cdot \sum_{i=1}^{n} CDo_i \cdot S_i \qquad (4.70),$$

Where: n is the number of items considered,

Sref is the reference area of the aircraft.

$CDo_i \cdot S_i$ is the drag area of each item considered:

CDo_i is the drag coefficient of each item considered.

S_i is the reference area for the drag coefficient CDo_i of each item considered.

Normally for airplanes the reference area Sref corresponds to the area of the wing horizontal projection. For airships the reference area can be the area of the frontal projection of the hull. The coefficient K for the induced drag is obtained from the wing Aspect Ratio and the wing Oswald efficiency factor ‘e’:

$$K = \frac{1}{\pi \cdot A \cdot e} \qquad (4.71).$$

The factor ‘e’ is a the Oswald factor for induced drag, which is function of the wing geometry, and express, in terms of induced drag, how worse from the ideally elliptical, the analyzed lift distribution is. It is presented in the several good aerodynamics sources, including McCormick (1980).

In order to provide a general law for the different planforms studied in this work, the factor e can be calculated for different geometries, through the data presented in figure 4.23, which have been obtained from lifting line method. The lifting line model considered presents 65 discrete vortices distributed along the wing span, in a co-sinusoidal arrangement, as presented in McCormick (1980). The formulation for the vortices definition and their interaction is according to McCormick (1980). The CLα 2D of the wing airfoil has been considered as constant along span, and with value of 2.π, and the wing is considered as without geometric washout. In figure 4.9-1 it is presented, as an example, the spanwise CL distribution obtained for one of the geometries considered, which is A=24, and rectangular planform (constant chord).

The procedure to obtain the factor e is: From wing aspect ratio A and taper ratio, to obtain through figure 4.24 the value of δ, and to obtain the Oswald factor e, as presented by McCormick (1979), through the formula:

$$e = \frac{1}{1+\delta} \qquad (4.72).$$

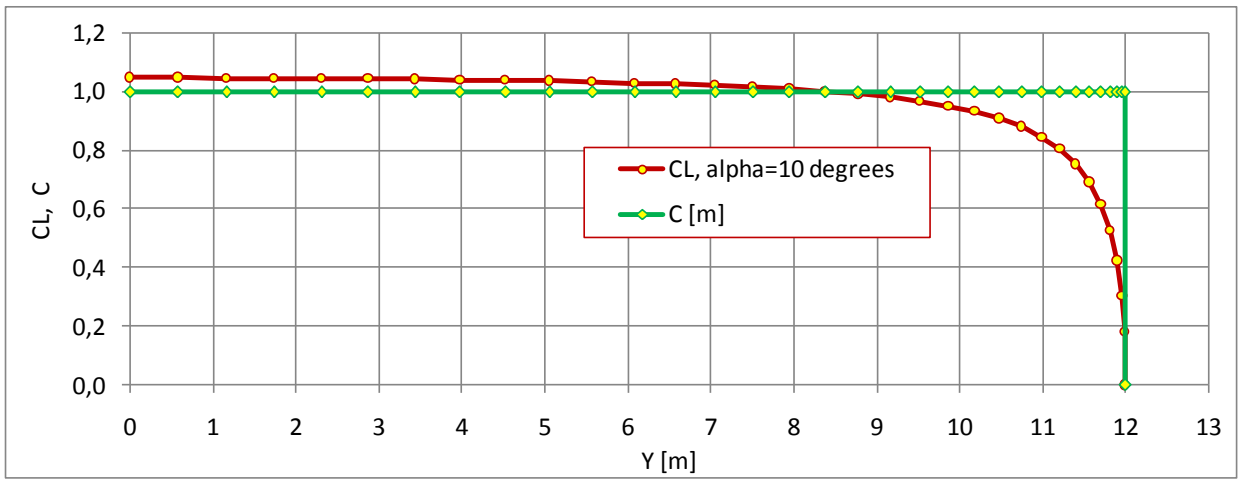

Figure 4.23: Example of CL distribution as output from the lifting line model, for a rectangular wing of aspect ratio 24.

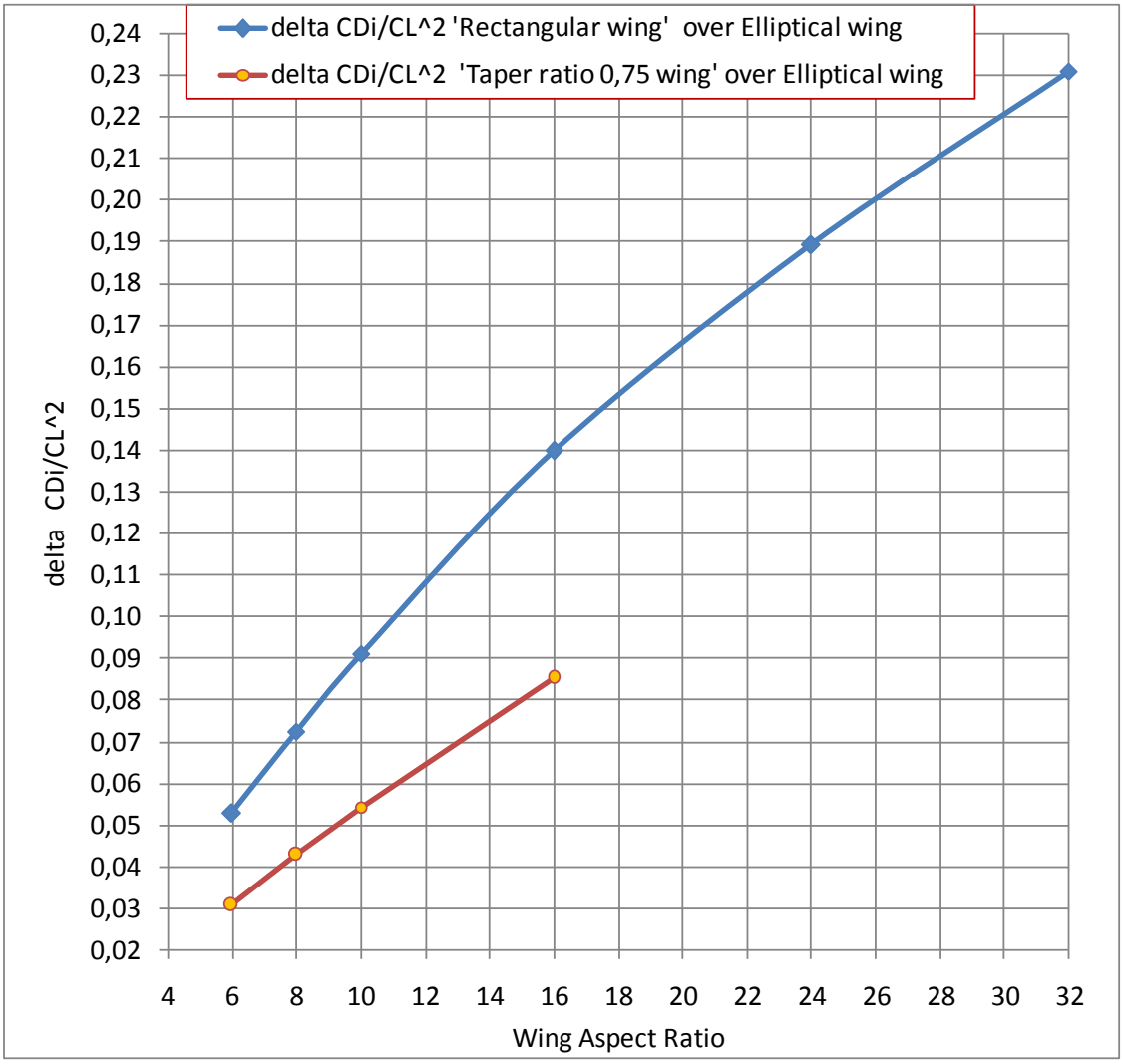

Figure 4.24: Definition of additional induced drag coefficient δ for non-elliptical wings.

The wing Aspect Ratio, for the monoplane aircraft, is calculated as:

$$A = \frac{b^2}{S} \qquad (4.73).$$

For the biplane aircraft, the Aspect Ratio is pondered from upper and lower wing aspect ratios; additionally, for biplanes, the aspect ratio shall be corrected by the factor defined in figure 19, chapter 7, of Hoerner (1958).

4.9.2) Propeller influence on Drag Analysis

The propeller influence on Drag Analysis refers to the increase in the aircraft drag due to the exposition to some parts of the aircraft to the air flow accelerated by the propeller. This is also named in this work as the propeller Stream Effect. According to McCormick (1979), Hepperle (2008) among several others, the air accelerated by the propeller can considered as being fully inside the propeller stream tube, which is presented in figure 4.22; and this approach is also considered in this sub-section.

Initially, the propeller effects have not been considered in the analysis. But after several attempts of matching the theoretical results obtained in this work for some aircraft with the corresponding reported ones, it has been realized that the differences could be explained by the propeller stream effect, in terms of increasing the drag, mainly at lower speeds. This effect has shown to be almost negligible at high-speed cruise, which is in general the design point for most of the aircraft; so possibly it has been transparent for most part of the design processes. Low-wing load aircraft fly at low speeds; if one aircraft of this type presents a low diameter propeller, and is moving at a low speed, the airspeed inside the propeller stream tube due to the propeller thrust can be significantly higher than the free stream airspeed; so the regions of the aircraft in contact with this faster flow will suffer a higher drag than the one produced only by the free stream conditions.

The aim of this subsection is order to provide a simplified model of the propeller stream to be used as an additional tool on drag analyses. The inputs for the model are the propeller diameter, free stream true airspeed, air specific mass to the propeller thrust. The result of this model can be referred as the stream tube; the model outputs are the diameter of the stream tube in function of the longitudinal – i.e. in X direction – distance, ahead from and behind the propeller; and the longitudinal wind speeds along the longitudinal distance, ahead from and behind the propeller.

The starting point for the stream tube model is formulation presented in section 4.8 for the propeller longitudinal flow definition. The equations 4.55, 4.63, 4.64 are based in the assumption of a constant acceleration from unperturbed TAS ahead of the propeller to the final stream speed Vf, behind the propeller. This assumption is considered in McCormick (1979), Hepperle (2008) among other sources. This assumption results in a speed profile of linear increasing from TAS to Vf. From the figure presented in Hepperle (2008) it is possible, for a simplified model, to consider the point in which the air inside the stream starts to accelerate at the distance corresponding to 1 propeller diameter ahead the propeller disk, and the acceleration ends behind the propeller, at the distance

corresponding to 1 propeller diameter. It is also considered that the speed is constant for the all points of each cross-section of the stream tube. One important consideration, as presented in figure 4.22 and equation 4.56, is that the stream tube has the diameter of the propeller, at the propeller position. The stream tube diameter variation along longitudinal axis is defined from continuity law, assuming flow as incompressible, and taking into the speed variation inside the stream tube.

The propeller stream incremental speed so varies linearly along longitudinal axis, from zero to ΔV; and the value of the stream incremental speed at the propeller disk is $\Delta V/2$.

The variation of propeller stream incremental speed along longitudinal axis is presented in figure 4.25. The local stream incremental speeds are presented in non-dimensional form i.e. divided by the final incremental speed ΔV. The speeds are presented in function of the non-dimensional longitudinal distance i.e. the local longitudinal distance divided by the point in which the stream speed starts to increase.

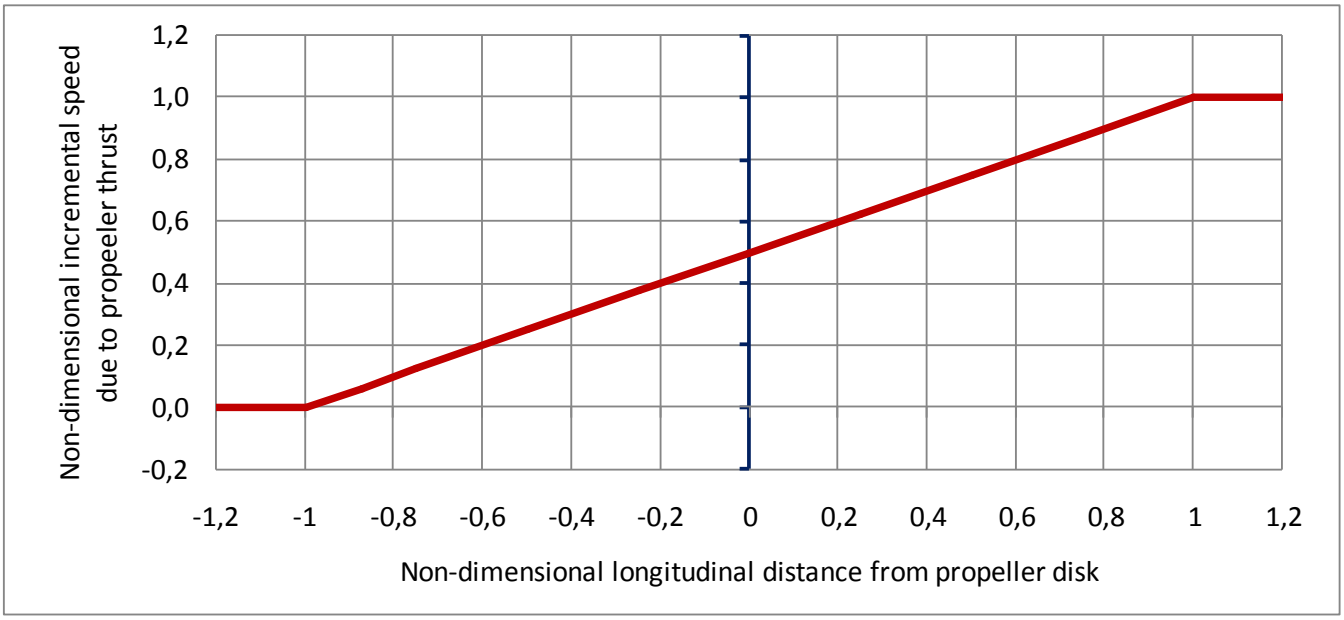

Figure 4.25: Non-dimensional incremental speed due to propeller thrust along longitudinal axis.

With the assumption of stream variation, and considering that the speed variation occurs in the longitudinal interval corresponding to –D to +D as explained above, it is possible to define the variation of local speeds along longitudinal axis knowing the propeller diameter D, and the instantaneous values of propeller thrust Tr, aircraft true speed TAS and air specific mass ρ, by the following procedure:

The disk area S_{disk} is calculated by:

$$S_{disk} = \pi \frac{D^2}{4} \quad (4.74).$$

The value of ΔV is obtained in function of Sdisk, Tr, TAS and ρ from equation 4.64. The values of the local speeds on the stream tube V_{stm} are calculated by the equations 4.75 as follows. For this, it is necessary to consider at first:

- The variation of the speed ΔV presented in figure 4.25,
- The X axis as positive backwards, and
- The longitudinal distance from the desired position to the propeller as X – Xprop.

From these considerations, and knowing TAS and ΔV , the values of V_{stm} are calculated in function of the local position X:

$$\text{At} \quad X - Xprop < -D: \quad Vstm = TAS \quad (4.75a)$$

$$\text{At} \quad X - Xprop > \quad D: \quad Vstm = TAS + \Delta V \quad (4.75b)$$

$$\text{At} \quad -D < X - Xprop < D: \quad Vstm = \frac{\Delta V}{2D}(X - Xprop) + TAS + \frac{\Delta V}{2} \quad (4.75c)$$

The local diameter of the stream tube is calculated considering continuity law:

$$V_{stm} . S_{stm} = V_{disk} . S_{disk} \quad (4.76)$$

Where V_{disk} is defined in equation 4.59 and S_{stm} is given by:

$$S_{stm} = \pi \frac{D_{stm}{}^2}{4} \quad (4.77).$$

So the diameter at a specific longitudinal distance from the desired position to the propeller X – Xprop is given in function of the speed V_{stm}, by:

$$=> D_{stm} = D.\left(\frac{TAS + \frac{\Delta V}{2}}{V_{stm}}\right)^{1/2} \quad (4.78)$$

The Figure 4.26 presents the variation of the diameter of the stream tube of the energized flow which passes by the propeller disk. By superimposition of the shape of the defined stream tube over the aircraft geometry, it is possible to define which regions of aircraft are subjected to additional speeds due to propeller stream.

As an example, of the superimposition of the stream tube with the aircraft, the figures 4.27 and 4.28 show the stream tube at 14-Bis aircraft, 50 HP, at average speed during take-off run.

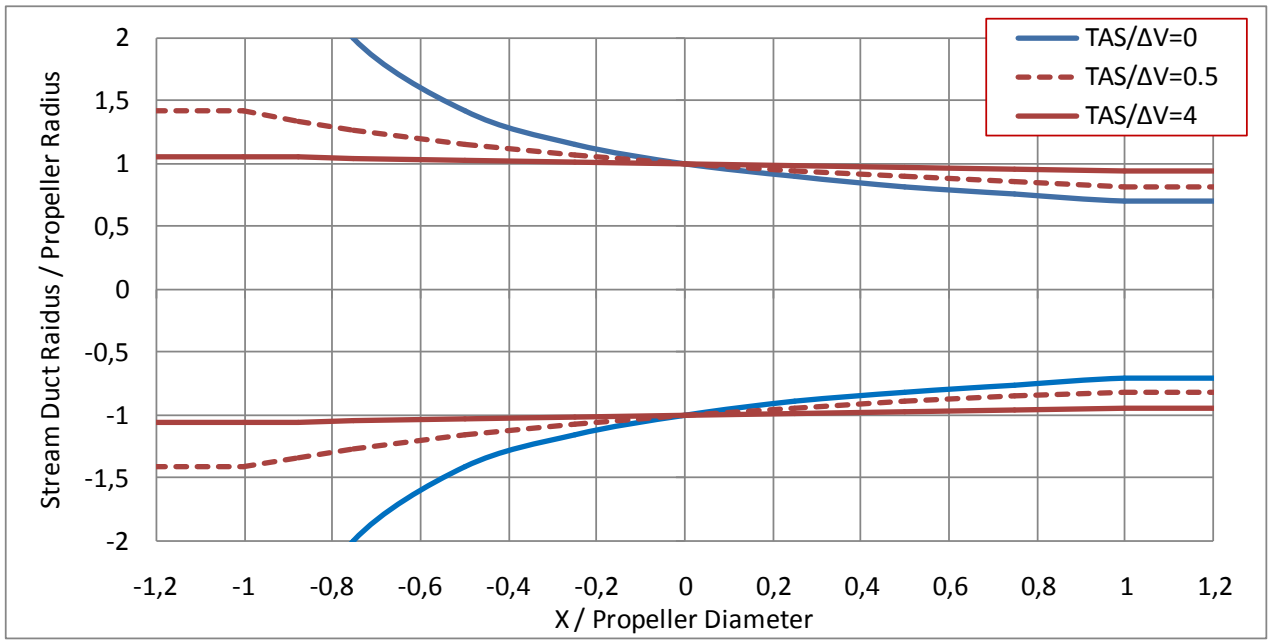

Figure 4.26: Variation of speeds along longitudinal axis for several aircraft speed ratios TAS/ΔV.

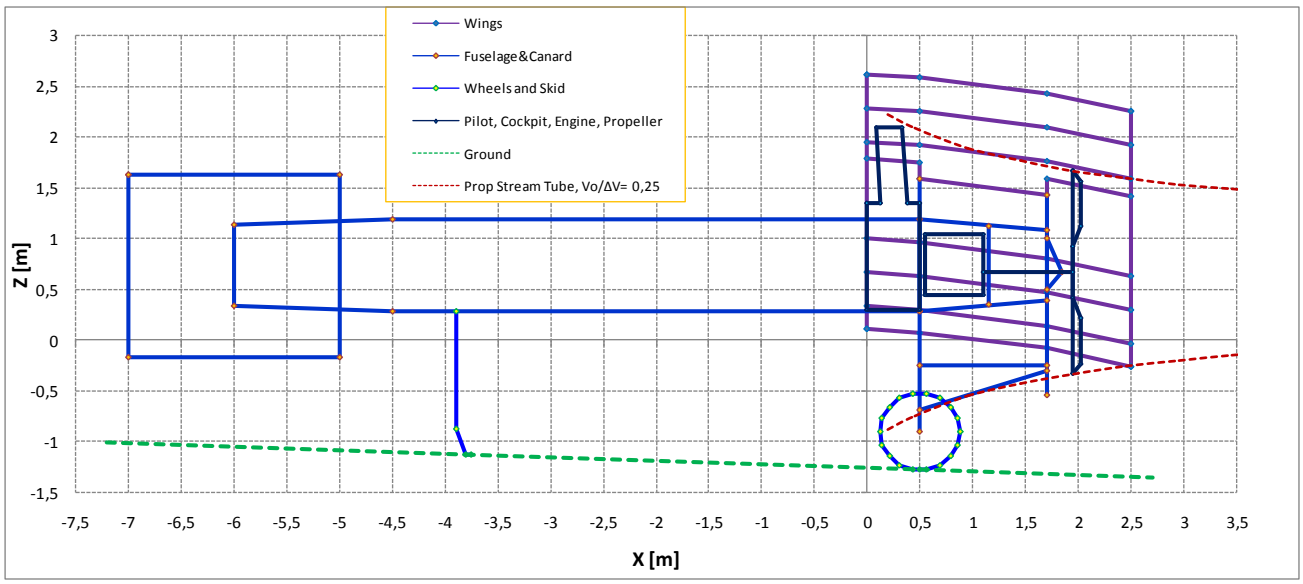

Figure 4.27: Example of Stream Tube of Propeller Stream definition; 14-Bis aircraft.

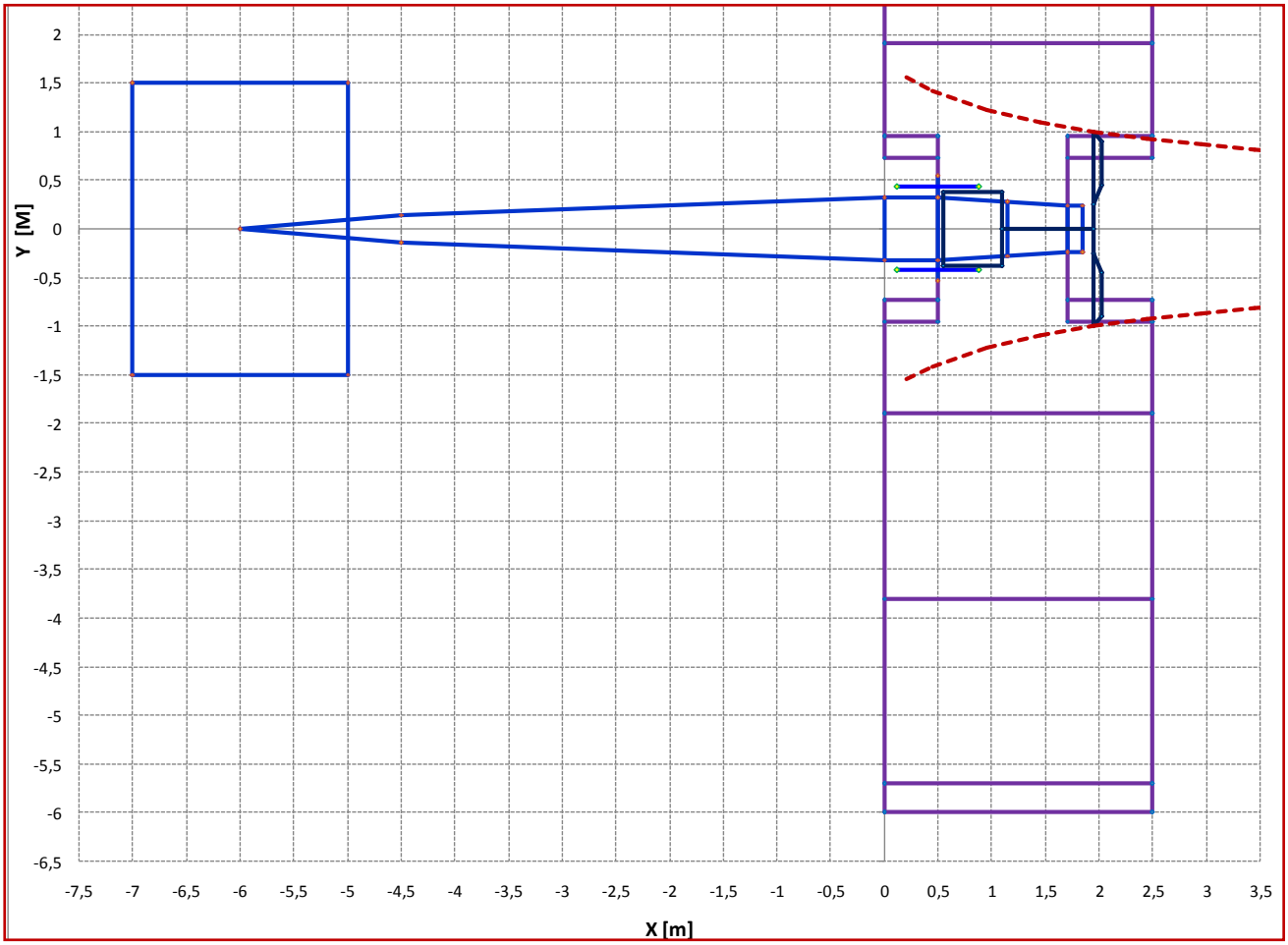

Figure 4.28: Example of Stream Tube of Propeller Stream definition; 14-Bis aircraft.

In order to account for propeller stream effect in drag, an average stream speed ahead and behind the propeller is adopted, and a percentage of wing and fuselage area is adopted as washed by the stream, in function of geometry and arrangement of both aircraft and propeller.

4.10) Low-wing-load Aircraft Performance

The following performance features are investigated herein:

- Gliding Flight: Best glide ratio, and its corresponding speed.
- Horizontal flight: Required Thrust versus airspeed, maximum horizontal speed
- Take-off: Take-off speed, take-off distance

The main formulation and criteria for the above features are presented as follows:

4.10.1) Gliding Flight

The best glide ratio E_* is given by:

$$E* = CL*/CD* \quad (4.79);$$

Where, if CD is given by the parabolic equation 3.2, CL_* is given by equation 4.15 and CD_* is given by:

$$CD* = 2.CDo \quad (4.80).$$

The speed for the best glide ratio TAS_* in meters per second is given by:

$$TAS* = \left(\frac{2\ M\ g}{\rho\ S\ CL*}\right)^{1/2} \quad (4.81).$$

4.10.2) Horizontal flight: Required Thrust versus Speed Curve

In horizontal flight the required Thrust equals the Drag:

$$Tr = D \quad (4.82),$$

Where D is given by equation 4.2: $D = {}^{1}/_{2}\ \rho\ TAS^2\ S\ CD,$

CD is given from equation 3.2: $CD = CDo + K\,.\,CL^2,$

And CL is given by:

$$CL = \frac{2\ M\ g}{\rho\ S\ TAS^2} \quad (4.83).$$

So, with a set of airspeeds TAS, all above the stall speed, the required thrust for each speed can be calculated.

4.10.3) Horizontal flight: Maximum Horizontal Speed

The maximum horizontal speed is defined through the intersection of the curve of required thrust versus speed, obtained from the formulation of sub-section 4.10.2, and the curve of maximum thrust versus speed, obtained from the propeller analysis, section 4.8.

4.10.4) Take-off

The take-off speed is obtained as

$$Vto = fv\,.Vmin \quad (4.84),$$

Where

$$Vmin = \left(\frac{2\ M\ g}{\rho\ S\ CLmax}\right)^{1/2} \quad (4.85).$$

And the multiplying factor fv is, for conventional and tested aircraft, a value generally about 1.15 and 1.25, depending on the temperature and aircraft mass-to-power ratio. As the aircraft studied in this work have been experimental aircraft, probably their pilots tested them in a more cautious way than

the normal flight procedures. For 14-Bis simulation, from which the corresponding real flight should be has been probably performed with caution, the value of 1.20 is considered; and for Demoiselle simulation, from which the corresponding real flight has been a successful record attempt of minimum distance, the value of 1.10 is considered.

The take-off distance is obtained from the take-off simulation technique explained as follows. The total take-off time is considered as the sum of several very small time-intervals in which the forces, and so the acceleration, are considered as constant. The simulation initial conditions are:

$$Vo_1 = 0; \quad do_1 = 0 \tag{4.86}$$

During each time interval, the main calculations performed are the following:
The horizontal acceleration is given by:

$$ax = Fx / M \tag{4.87}$$

Where

$$Fx = Tr - D - Dg \tag{4.88},$$

Being $Dg = \mu . N$ (4.89),

$$N = L - M . g \tag{4.90},$$

$$L = {}^{1}/_{2}\ \rho\ TAS^2\ S\ CL \tag{4.91},$$

D given in function of CD by the equation 4.2, and

CD given in function of CL by the equation 3.2,

$$CL = CL\alpha\ .\ \alpha + CLo \tag{4.92},$$

$$\alpha = \theta_{TO} \tag{4.93},$$

$$T = ft\ .Tmax\ (TAS) \tag{4.94}.$$

θ_{TO} is the aircraft attitude angle during Take-off run; ft is a value equal to or slightly lower than 1, representing the power control from the pilot; Tmax(TAS) is the maximum Thrust for the specific speed, obtained as from the propeller analysis.

With the acceleration ax, the speed, distance and time at the end of that time interval are given by, respectively:

$$Vf_i = Vo_i + ax.\Delta t \quad (4.95),$$

$$df_i = \frac{Vfi^2 - Voi^2}{2\,ax} + do_i \quad (4.96),$$

$$tf_i = to_i + \Delta t \quad (4.97).$$

For the next time interval, the following attribution is made:

$$Vo_{i+1} = Vf_i \qquad do_{i+1} = df_i \qquad to_{i+1} = tf_i \quad (4.98).$$

The calculation is performed up to the time interval that the speed Vf_i overcomes the take-off speed Vto.

4.11) Solar Aircraft Typical Mission Analyses

In order to better understand and analyze the existing solar aircraft, and to check the feasibility of new designs, a specific mission simulation methodology has been developed. For a new design, this simulation methodology shall be applied after the first aircraft definitions are obtained, through the methodologies presented in the previous sections.

Through this routine, the aircraft typical mission (declared, for existing aircraft, or intended, for new designs) can be calculated in order to check, mainly:

- the consistence of the input parameters and
- the feasibility of achievement of the aircraft mission

For the simulation, the 'quasi-static' approach is considered.

The general process of mission evaluation through simulation, developed in this work to obtain an overall picture of the mission and design analysis for the different solar aircraft types is summarized in the next pages.

4.11.1) Overall Views of Mission Evaluation Process

For purposes of introducing the elements and concepts of the process, the general relationship between the main characteristics and data, related to Solar Aircraft Analysis is presented in the figure 4.29.

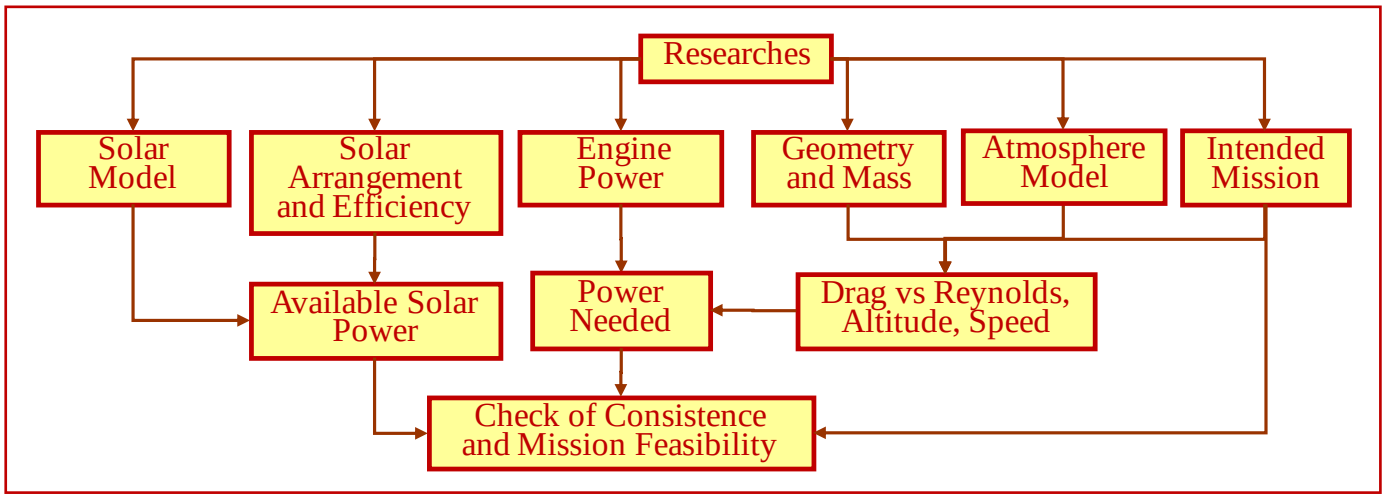

Figure 4.29: General relationship between the main characteristics and data, related to Solar Aircraft Analysis

It has been observed that in order to better analyze the aircraft missions an important definition of solar aircraft is needed prior to the analysis. This definition, although very simple proved to be very useful:

- Solar aircraft type 1: aircraft intended to perform the flight mission with without batteries.
- Solar aircraft type 2: aircraft intended in which a large batteries are needed to complete the flight mission. This type of aircraft is characterized by use of batteries, with time for in-flight recharging.

This distinction of the solar aircraft in the two types has been very useful in section 4.4 and will also be used in chapter 5.

The figures 4.30 and 4.31 present the calculation process in one time interval of the quasi-static mission simulation approach. Two figures are necessary, in order to present the significant difference in terms of analysis complexity, between mission simulation of aircraft type 1 (i.e. without

batteries), from aircraft type 2 (i.e. with batteries). Figures 4.30 and 4.31 are related to aircraft type 1 and type 2 respectively.

One can compare the mission simulation flowcharts of figure 4.30, for aircraft type 1, without batteries, and figure 4.31 for aircraft type 2, with batteries. One can note that the flowchart for aircraft type 1 is a simplified case of flowchart for aircraft type 2. For aircraft type 2, characterized by use of batteries, with time for in-flight recharging, the key point for the aircraft mission analyses performed has been identified as the electrical power management inside the aircraft along the flight period.

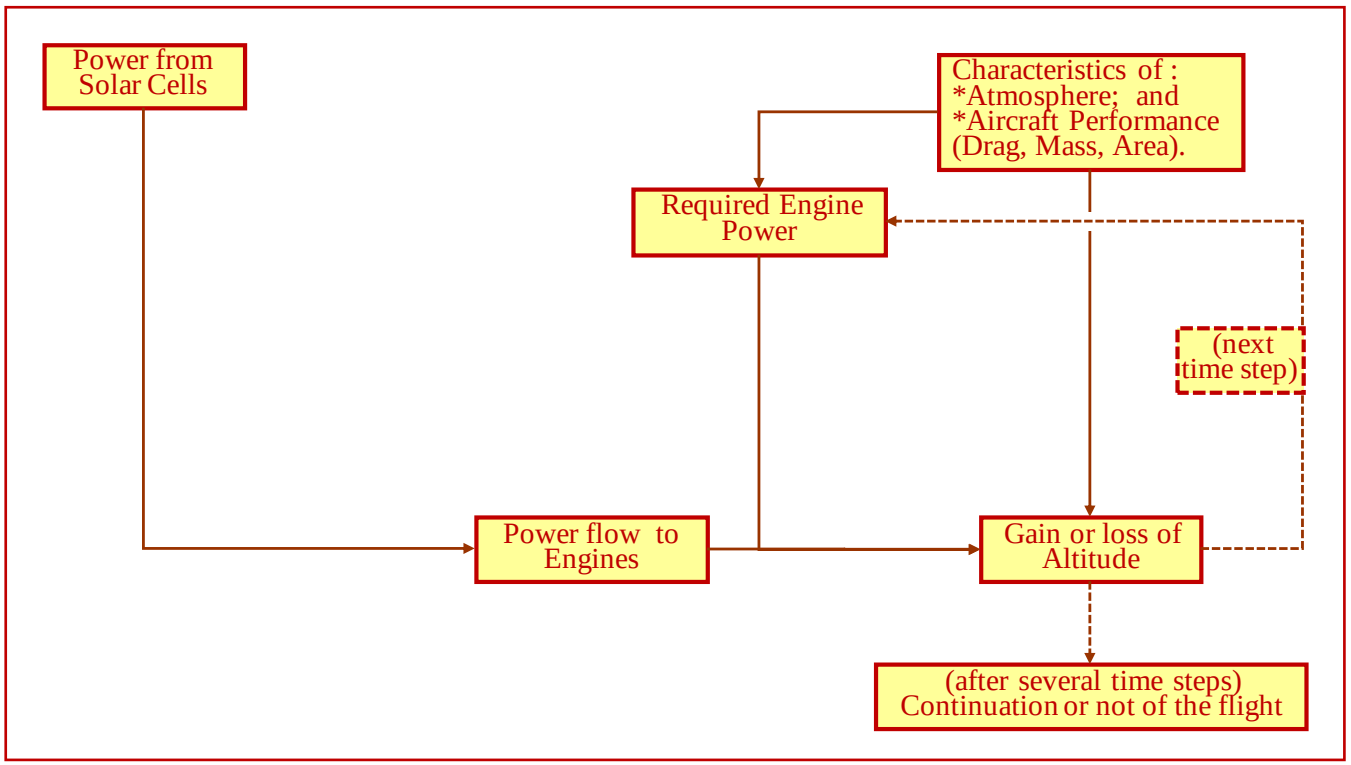

Figure 4.30: Mission Simulation Flowchart, one time interval: Aircraft Type 1, without batteries.

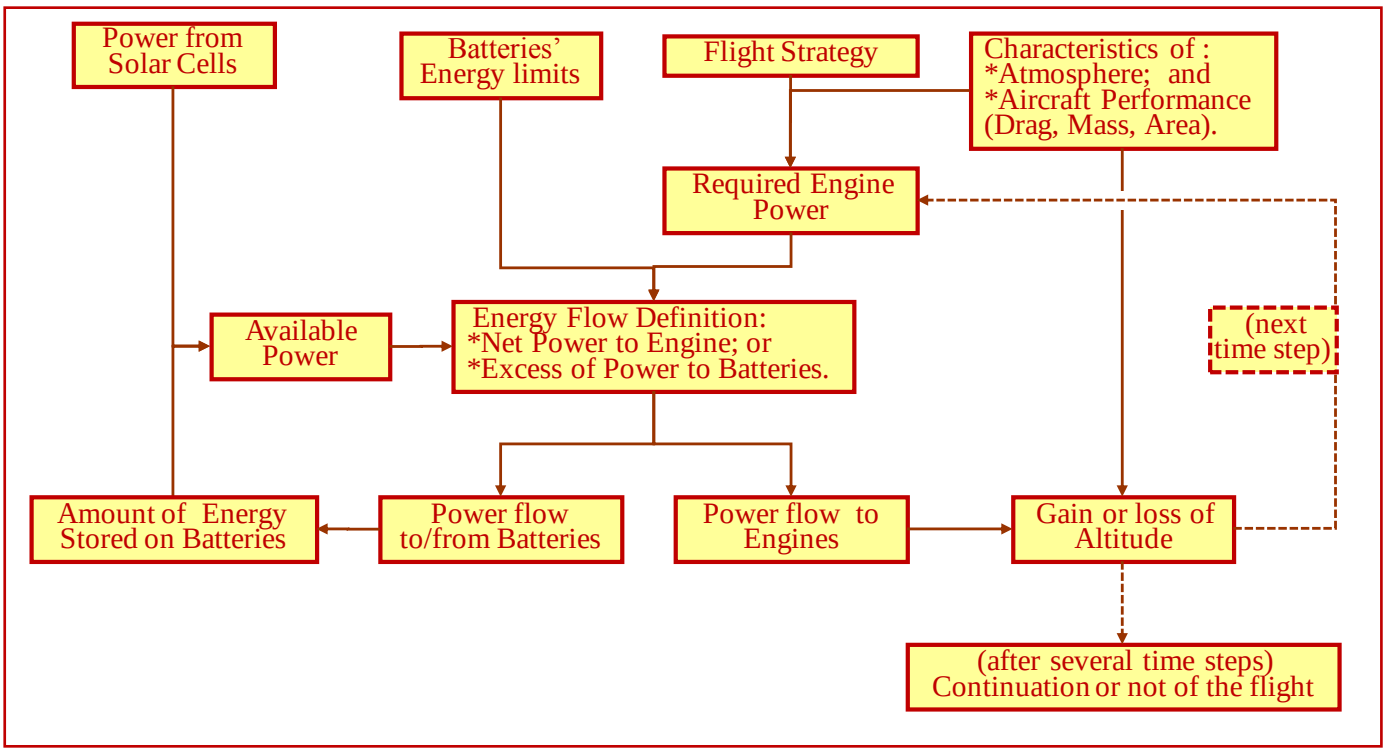

Figure 4.31: Mission Simulation Flowchart, one time interval: Aircraft Type 2, with batteries.

4.12.2) The Issue related to Propeller data for Mission Analysis

In the methodology developed, there are two differed approaches to consider the specific power to be transmitted from engines to air, via propeller:

- 1st approach: To consider a fixed, assumed value of propeller effectiveness;
- 2nd approach: To define a suitable geometry for the propeller; and to calculate the propeller effectiveness from this information.

The 1st approach is obviously simpler and faster and can be useful when one is only interested in the order of magnitude of the aircraft performance. And the 2nd approach should be considered when the other aircraft data are more precise, and it is desired to raise, in the overall model, the level of accuracy of the propeller to the same level of the other parts of the model.

For the reliability and better accuracy of the analysis of the low-speed aircraft (pioneer, human powered and solar) presented before, the dedicated propeller analysis for each aircraft has been one of the key factors.

It has been noticed that the propeller specific analysis (i.e. the 2nd approach), which has been used to analyze already-flown, non-solar aircraft, should be also used in some of the mission analyses for solar aircraft

In terms of use of the 2nd approach (definition of propeller characteristics from the author's propeller analysis method) for Solar Aircraft Mission Analysis, four additional challenges, that are interconnected, must be taken into account:

- The geometry and RPM data for propellers of sun powered aircraft are, for most of them, not available. Due to this, some intense search for information and some reversal engineering are needed.
- As some of the most important data of the propeller geometry are not available, (and a suitable propeller must be defined,) the 'blanks' in the data must be provided through a propeller definition method; from the power, speed and Reynolds number requirements. In other words, it is needed to design the propeller to be analyzed.
- The Typical mission for several sun-powered aircraft involves large variation of height, which results by its hand in a large variation of the Reynolds number; and the Reynolds number at both wing and propeller tends to migrate to very low values, quite unusual ones for aircraft. In order to obtain the propeller requirements (such as power, speed, thrust, air specific mass and Reynolds number) for the typical mission, it is necessary to simulate the mission.
- Since the propeller is not known yet, one strategy the author used in this work has been to use at first the 1st approach, i.e. to simulate the mission considering a specific, adopted, and constant, propeller effectiveness. One very important point: In order to adopt this value, the experience gained analyzing the low-speed aircraft propellers, presented before, has been of crucial value.

So, if one needs to use the 2nd approach for a deeper and more precise understanding of the solar aircraft behavior, he needs to execute the tasks below:

- At first to use the 1st approach, and obtain the 1st definition of the aircraft mission;
- From the 1st definition of the aircraft mission, one or more design points are chosen;
- With the requirements associated to these points, the aircraft propeller is designed;
- This design is adjusted with the known data of the propeller;
- Once defined the propeller, the propeller must be analyzed, to obtain the curves of Ct, Cp and η_{prop} versus J;

- With these curves, the mission simulation, 2nd approach, can be run, and the 2nd definition of the aircraft mission is obtained;
- The output values should be checked with the ones obtained from the 1st approach to check the consistence of the process.

The results of one analysis using the 2nd approach are presented in the mission analysis of a new aircraft design, in the chapter 6, sub-section 6.4.2.

The general procedure considered for the analysis is presented in the steps below. The procedure presented refers to the same time interval, and in general, the steps are presented in the calculation order. The most important nomenclature that must be taken into account is:

- P1 is initial time of the time interval;
- P2 is the final time of the time interval;
- PM is the average time of the time interval: PM = (P1+P2)/2.

The first group of analysis occurs at the known parameters at the starting of the time interval i.e. at P1:

- From the initial altitude of the time interval, and from the standard atmosphere model, the air specific mass is calculated;
- From the initial daily time of the time interval, and from the daily solar insulation variation considered, the instantaneous solar insulation is obtained;
- Considering the area and effectiveness of solar panels, the total instantaneous power output from solar panels is calculated at P1;
- The instantaneous power available from panels to engine is defined from the ratio defined in the input data;
- The corresponding part of this power which is delivered to air is calculated from the engine+propeller+reduction effectiveness defined in the input data;
- Check of needs of liberation of power from batteries to engine is performed (yes or no), in function of aircraft altitude;
- Check of availability of liberation of power from batteries to engine is performed (yes or no), in function of battery available energy;

- The Difference between Power from panels delivered on the air and Power needed for horizontal flight is calculated
- From this difference, the power to eventually be conducted from panels to Battery is defined;
- The Battery energy is checked in order to the maximum value be not surpassed;
- From the checks above, the power to be delivered in the air from both Panels + Battery, at instant P1, is defined;
- And the corresponding power solely delivered from the battery to engine at P1 is obtained;
- Since the aircraft does not change its mass (one of the characteristics of solar aircraft) at least not due to propulsion issues, and the lift coefficient is assumed as constant, the aircraft equivalent airspeed EAS is constant along all flight mission;
- The true airspeed is calculated from EAS and the air specific mass 'rho' already calculated for the aircraft altitude at P1;
- From the altitude at P1, the Temperature is calculated, as well as the local sound speed and the air kinematic viscosity ν;
- and from ν, the aircraft true airspeed TAS, and the wing chord, the Reynolds number related to the wing is obtained;
- With the wing Reynolds number, and the wing drag coefficient data (input data), the values of K and CDo for the wing at the specific flight conditions of P1 are defined;
- Considering the aircraft CL, the Wing drag coefficient is calculated; and considering the incremental and additional drag coefficients of the whole aircraft related to the wing drag coefficient, and the aircraft equivalent airspeed, the total drag of the aircraft is calculated;
- With the of aircraft drag and TAS, the required horizontal flight power is calculated;
- With the required horizontal flight power, the aircraft mass, the true airspeed TAS, the power delivered by the aircraft to the air, and the daily mean upstream wind speed, the aircraft ratio of climb (or descent) and the path angle γ at P1 are obtained.

The following steps are related to parameters calculated for time instants P2 e PM of the time interval:

- With the value of rate of climb at P1 and the value of the time interval, the value of the altitude gain (or loss) in the time interval is obtained, and with this, the final altitude H2 of the time interval;

- The air specific mass related to H2is calculated, and with this value, the aircraft TAS at P2 is obtained;
- With TAS at P1 and P2, the mean TAS, and the corresponding Mach Number for the time interval are obtained;
- With the time interval mean TAS and with the time interval value, the daily time corresponding to the mean time of the time interval is defined;
- With the daily time representative of the time interval and the irradiance model chosen, the solar irradiance representative of the middle of the time interval is obtained;
- With this value, the panels output power, and the power delivered to air due to this instantaneous output power are defined for the middle of the time interval (as presented above for the instant P1);
- The power from Panels plus Battery, delivered to air, related to the middle of the time interval, is calculated;
- With the Drag at P1 and the TAS at PM, the required horizontal flight power for the middle of the time interval is calculated;
- As presented previously for instant P1, the aircraft ratio of climb (or descent) and the path angle γ at PM are obtained;
- With the True airspeed and the angle γ, the Distance achieved in the time interval, and the total distance achieved up to that instant are calculated;
- The values of TAS, distance, altitude, elapsed time, and battery energy are considered for the next time instants.

The mission analysis methodology presented above in this section has been used for evaluation of some solar existing aircraft and for new designs. Some of these evaluations are presented in the following chapters ‘Studies’ and ‘Results’.

4.12) Solar Incidence Model

4.12.1) General

In order to better analyze the feasibility of solar aircraft use in different places of the planet, and in different seasons of the year, a model of solar energy intensity incidence on the ground has

been developed by the author. The main parameters to be considered are the Earth geometry, position of Earth rotation axis related to the plane of the Earth's orbit around the Sun. The effect of luminosity reduction due to atmosphere thickness has been also taken into account.

This study has been motivated by results of preliminary calculations performed by the author, in which some configurations should have potential of operating in very long distance missions, being even possible to them to achieve continental or global ranges.

As presented in the last part of section 4.3, one of the sun-powered aircraft mission limiting factors is a better knowledge of the distributed energy from the sun to the several Earth regions, along the several year months, and daily hours. The method presented in this section is aimed to fill part of the needs related to this issue.

The general flowchart of the method is presented in figure 4.32. At this figure, the main input data are positioned at column at the left hand side. The outputs are the three incidence parameters, also presented in figure 4.32, at bottom of right hand side (in brown color); from these three outputs, the two last ones, in dotted lines, are optional.

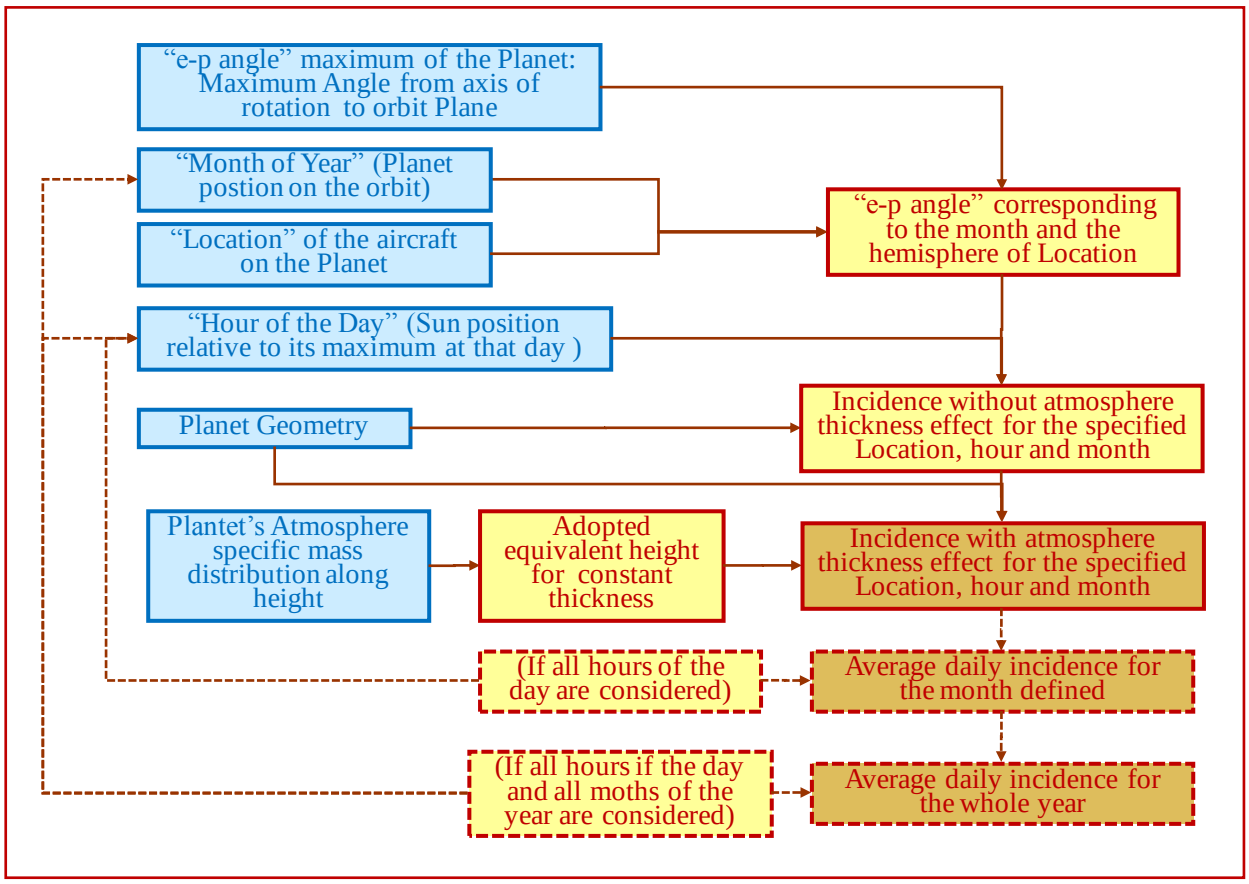

Figure 4.32: General Flowchart Considered for the Solar Incidence Evaluation.

4.12.2) Model of sun incidence without atmosphere effects

The aim of this part of the study is to obtain one general, easy-to-understand, geometric model to describe the sunlight incidence on each part of the planet, along all weeks of the year and all latitudes. The basic rationale for the model is explained as follows. The Earth attitude related to Sun, along its around-sun orbital path is present figure 4.33. For simplicity, and in order to provide a easier understanding of the Earth attitude changes, only five positions are presented for the upper view, at left side of the figure, and three positions are presented in the right side of the figure, corresponding to the side view of the Earth-Sun system. In this figure 4.33, the acronym SEL means Sun-Earth Line. At the right side of the figure, the Sun is represented as a flat vertical surface. One can note by both sketches of left and right side of figure 4.33 that the Earth's north pole, which corresponds to the intersection of the northern hemisphere surface with the Earth rotation axis, is most close to the sun at June, and it is most away to sun in December; at March the axis of rotation is perpendicular to SEL.

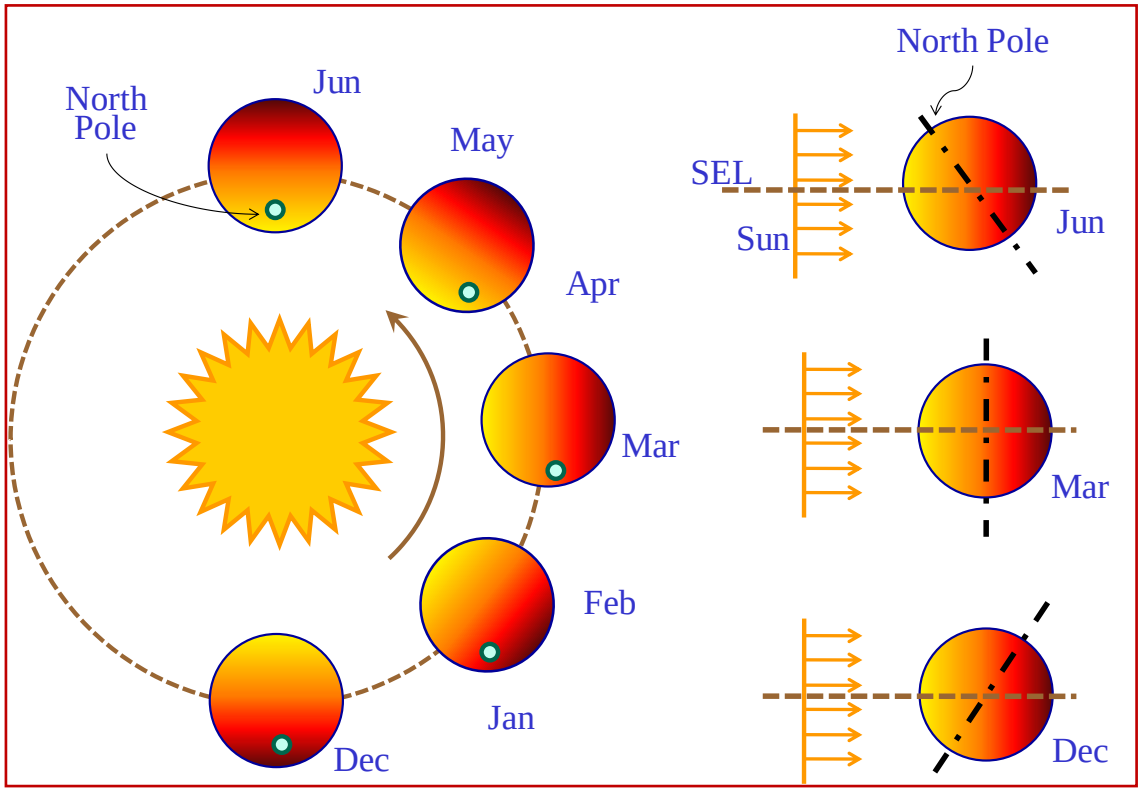

Figure 4.33: Basic elements for Earth attitude related to Sun

Considering one observer in an arbitrary position on earth surface, and considering the Earth axis rotation as vertical, the sun path during the day as perceived by the observer can be interpreted as a cone. This cone changes its shape depending on the Earth's location on the orbit around the sun. Figures 4.34, 4.35, 4.36 present the shape of the cones representing the sun path related to the observer in the southern hemisphere, at June, March and December respectively. The cones are named in this method as solar cones. In the figures 4.34, 4.35, 4.36, the orange lozenges on the solar cones correspond to sun positions at the even hours. The observer is located in the apex of the solar cones. The lines linking the orange lozenges to the observer, at the apex, are the SEL lines.

Based on this model the hour of sunrise and sunset of any day of the year at any latitude can be determined. And most important, the intensity of the sunlight perpendicular to the ground at any hour of the day, at any day of the year and any latitude can be also obtained.

The definition of the Solar Cones as presented in figures 4.34 to 4.36 is the key factor for definition of the Incidence Model. Once obtained this geometrical model of the Solar Cones, the sun intensity can be calculated for each hour of the day, at each week of the year, and latitude of interest, by laws of trigonometry.

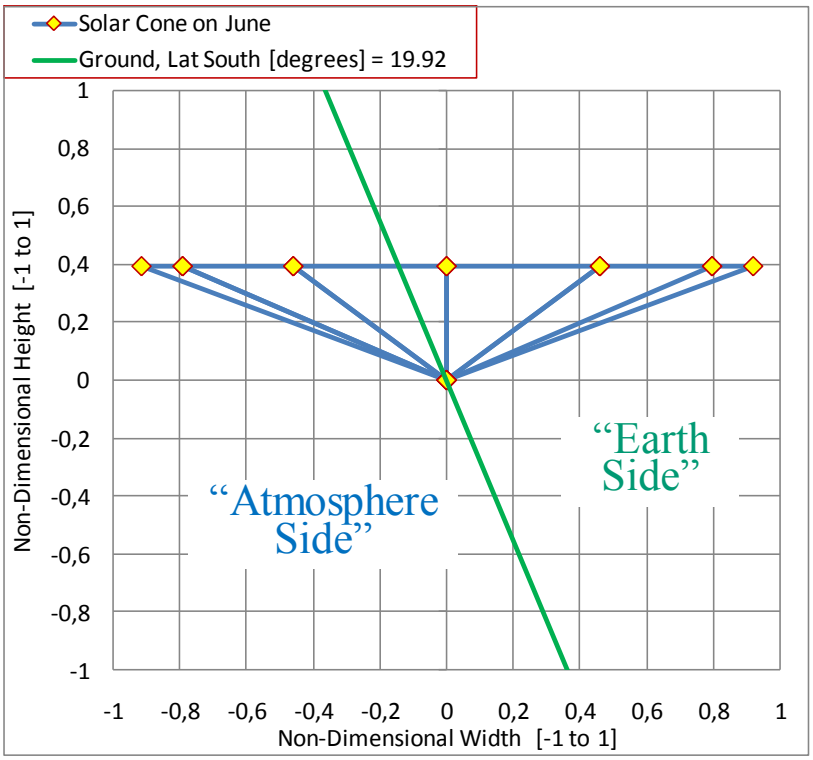

Figure 4.34: Solar Cone for June, and local surface corresponding to Latitude of 19.92 S.

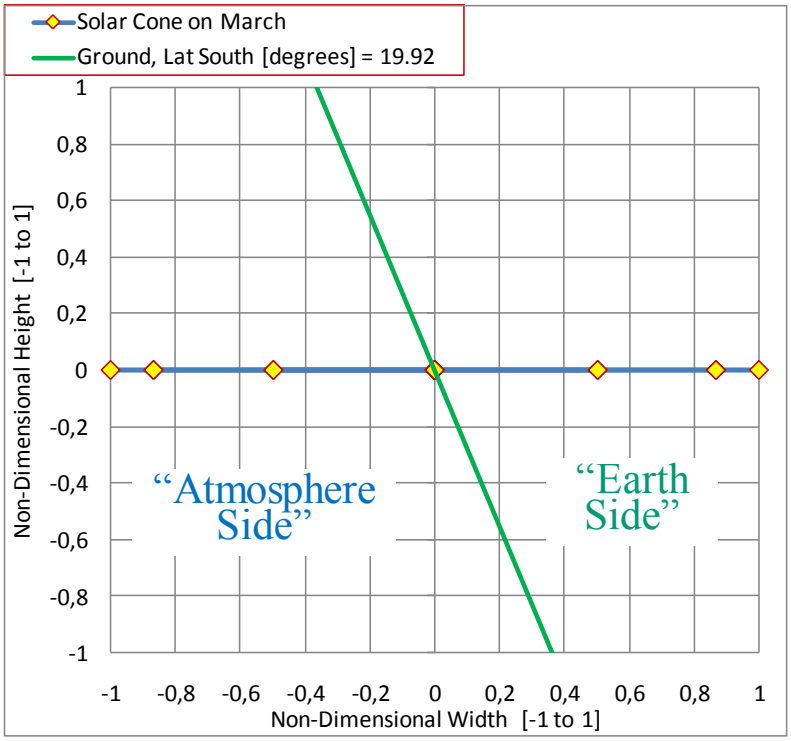

Figure 4.35: Solar Cone for Sept. or March, and local surface corresponding to Latitude of 19.92 S

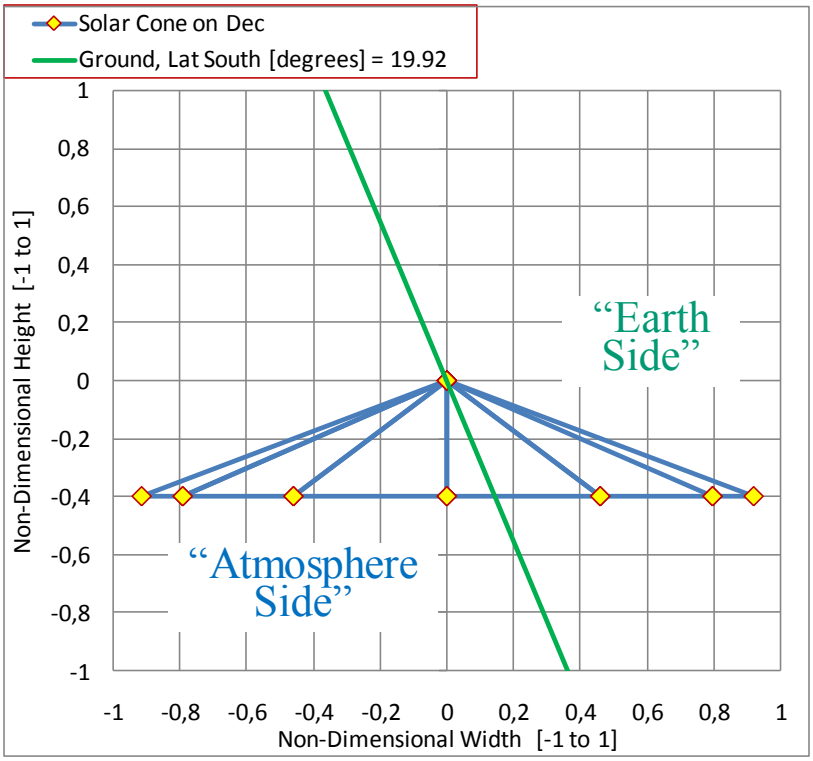

Figure 4.36: Solar Cone for December, and local surface corresponding to Latitude of 19.92 S.

It is possible to observe that this model is not only applicable to Earth, since the geometry considered is applicable at any close-to-spherical planet performing revolution about a steady axis, and performing a steady, close-to-circular orbit around a star. In other words, this model can also be used for determining sunlight incidence on Mars or Venus, which can be useful for conceptual designs of solar aircraft destined to exploration on these worlds.

As one of the results from the model, the Plot with Hour of sunrise for several latitudes on the southern hemisphere in function of the weeks of the year, is shown in the figure 4.37. Other additional results are presented in the sub-section 4.12.3.

In the figure 4.37, at the X axis, the week zero corresponds to week of September 22nd (spring equinox); additionally, the number of sunny hours of a specific day can be obtained from the values of Sunrise Time at the Y axis from figure 4.37, by the formula:

$$TSun\ [hs] = 2\ (12 - \text{'}Sunrise\ Time\text{'}) \qquad (4.100).$$

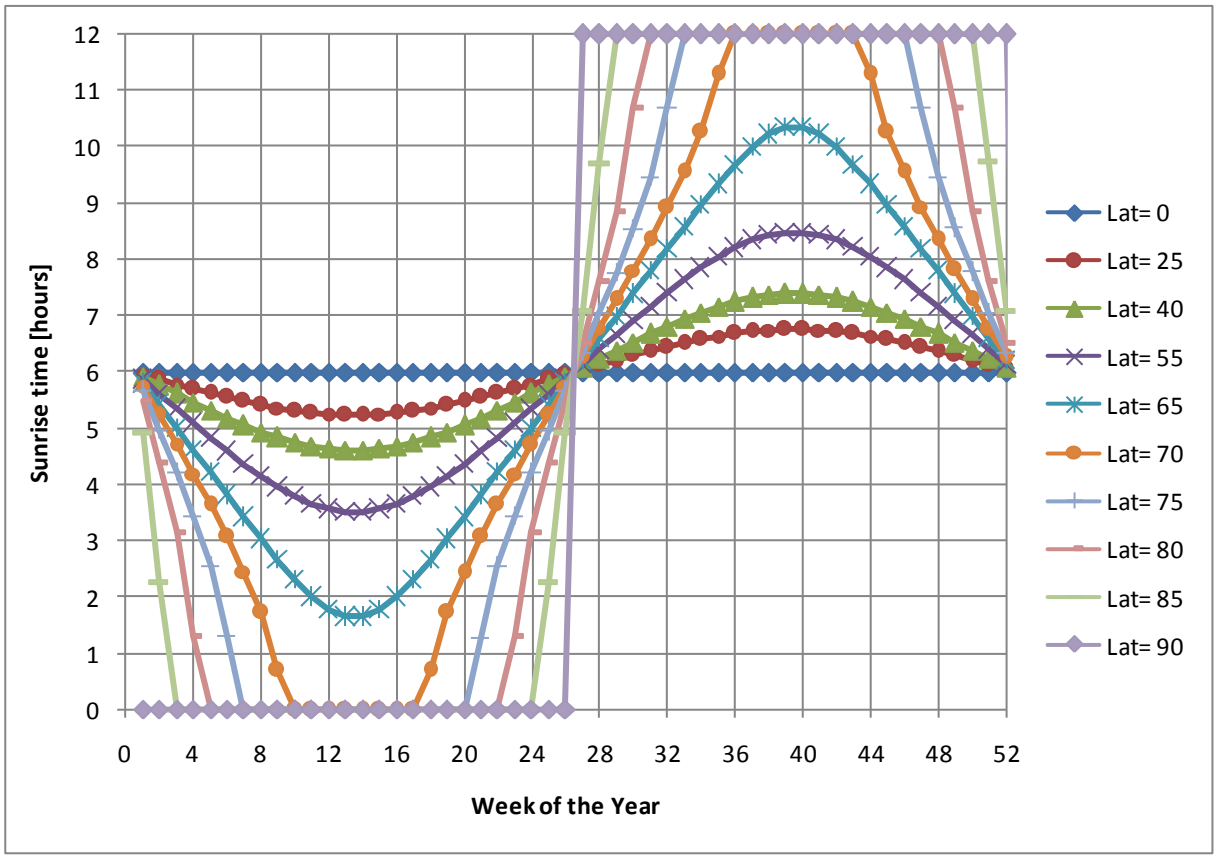

Figure 4.37: Hour of sunrise for several latitudes on the southern hemisphere in function of the weeks of the year

4.12.3) Solar Incidence Model Results: Earth

Some important outputs from the solar incidence model for Earth are presented in the figures 4.38 to 4.41. The description of the figures is shown as follows.

The figure 4.38 presents the plot of Sun daily energy incident in a horizontal surface on the ground, at sea level, for several latitudes of Southern hemisphere, from December to June; the values for months from July to November are the same from the months May to January. The a-p angle shown in the legend refers to the angle between Earth's revolution axis and the normal to the plane of Earth's orbital translation around the Sun.

Plots of distribution of Solar Power in function of hour of the day and Latitude for two months, for the Southern Hemisphere, which are December and June, are presented in Figure 4.39 and 4.40 respectively.

Figure 4.41 presents the solar irradiance in a different way from the previous plots. In this figure the solar irradiance is presented above the Earth's atmosphere, and for a specific latitude, in this case 20 ^{o}, being each curve of the figure representative of one month of the year.

The Comparison of Solar incidence values obtained with the present model, with the corresponding ones from by Roland Boucher (2003) is presented in figure 4.42.

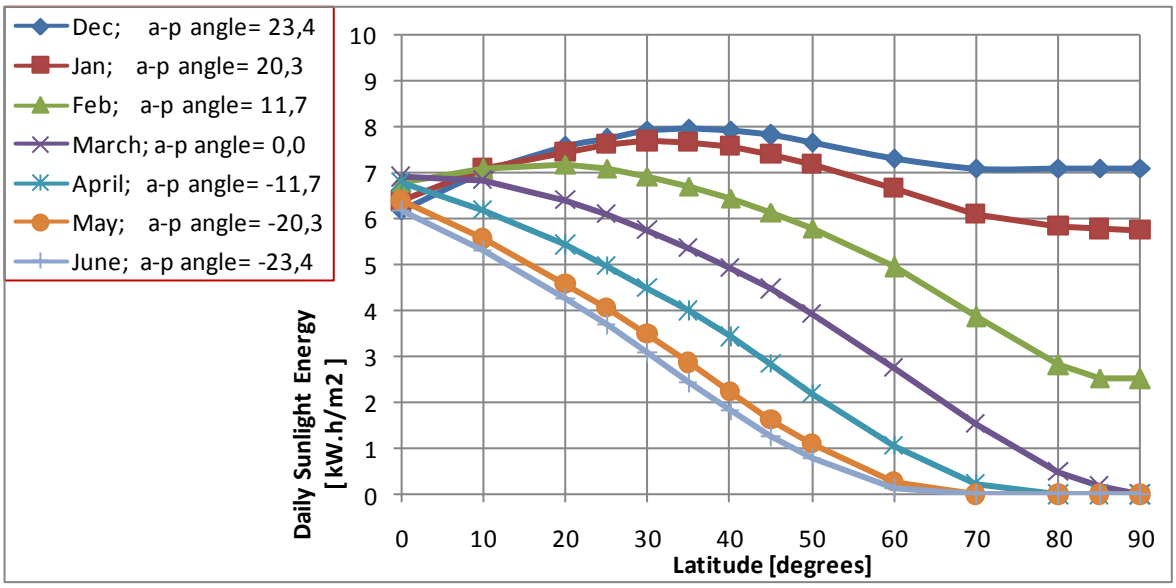

Figure 4.38: Sun daily energy incident in a horizontal surface on the ground, at sea level, for several latitudes of southern hemisphere, from December to June.

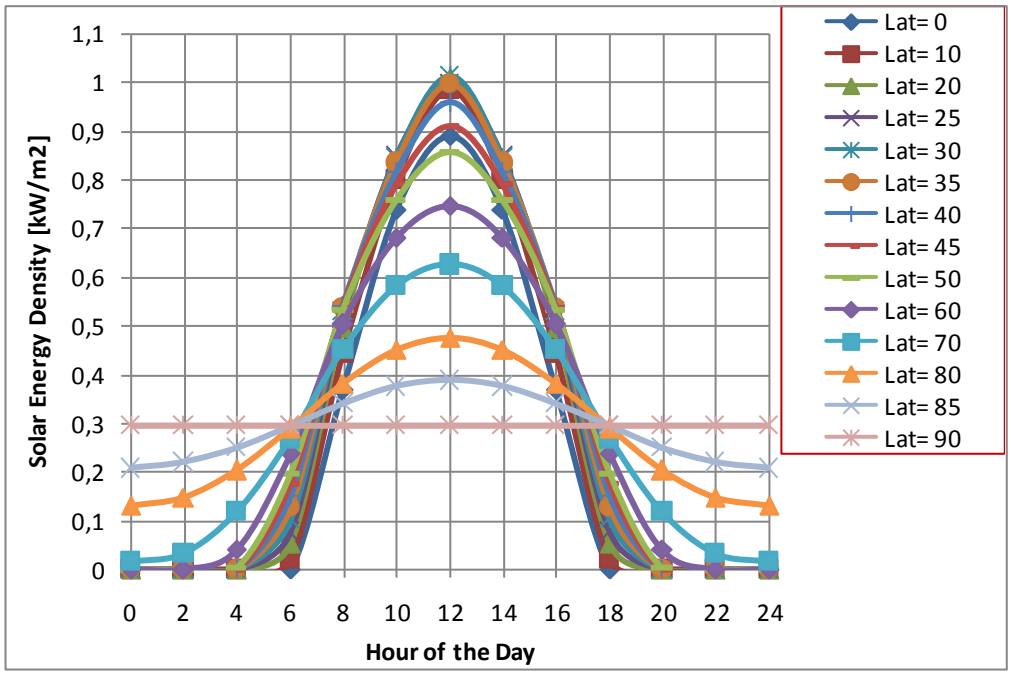

Figure 4.39: Distribution of solar power in function of hour of the day and Latitude, in December, at the southern hemisphere

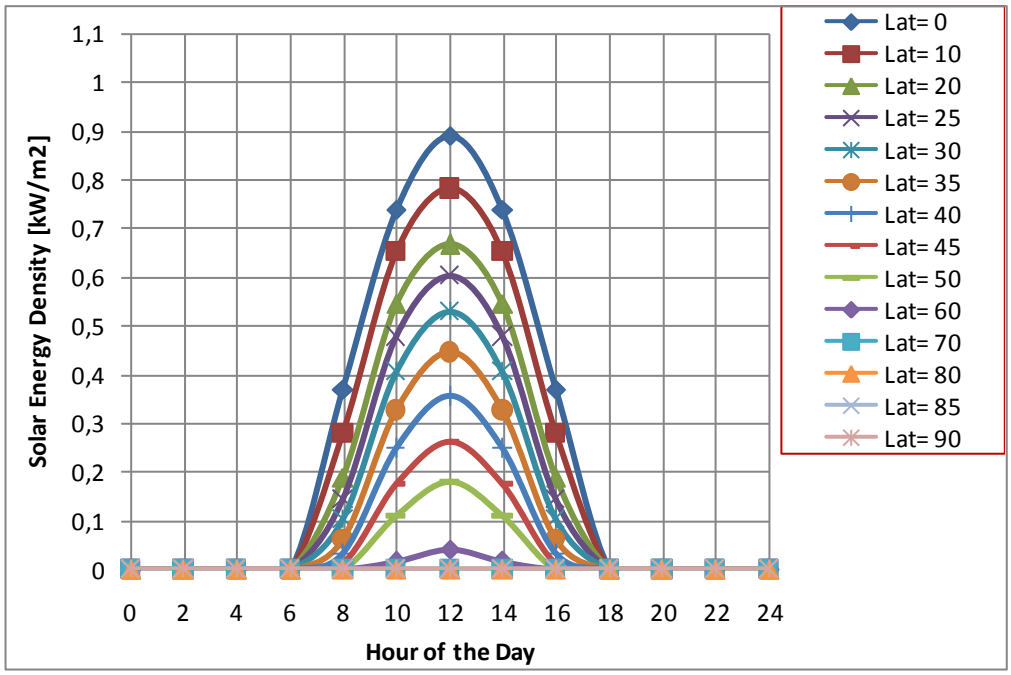

Figure 4.40: Solar power density in function of hour of the day and Latitude, in June, at the southern hemisphere

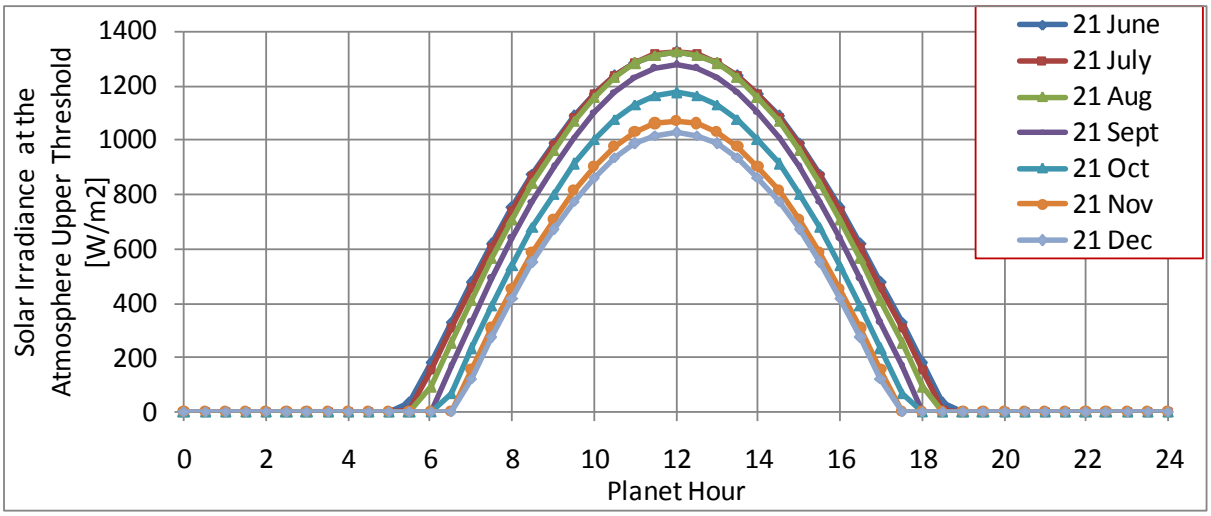

Figure 4.41: Results of solar irradiance above atmosphere, Earth, latitude 20 north.

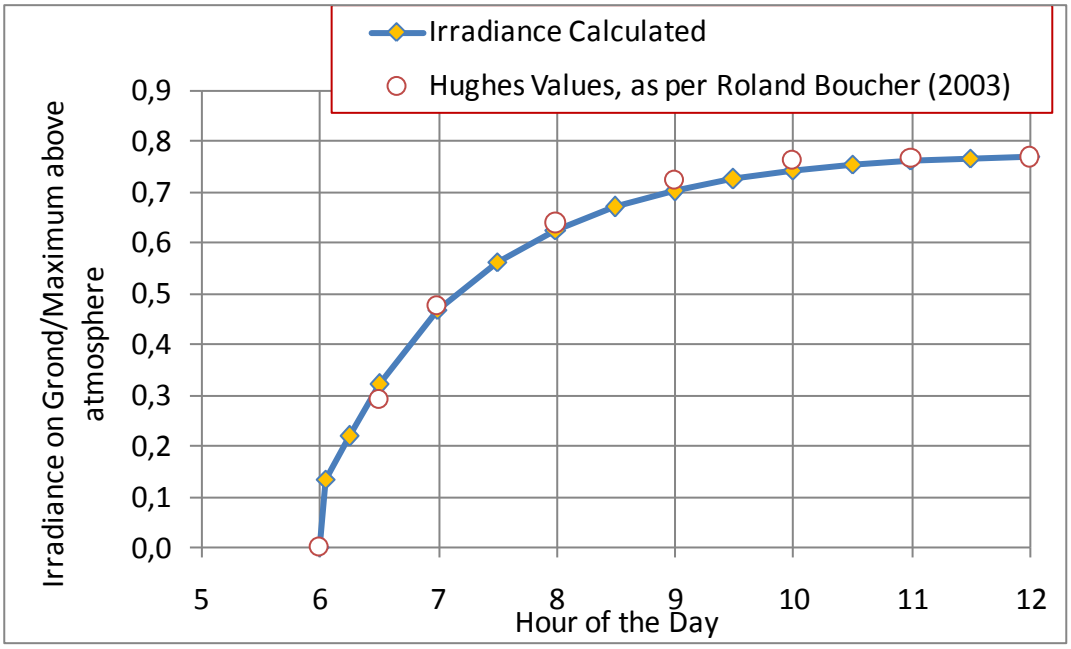

Figure 4.42: Calculated solar power curve for a specific day and latitude: Equator, Equinox; surface perpendicular to sun compared with the one obtained from Roland Boucher (2003)

4.13) Mass Estimation: Method and assumptions

One of the critical tasks of aircraft design is the mass definition of aircraft's main items. Depending on the type of aircraft - e.g. commercial, general aviation, highly-maneuverable - different types of mass distribution data or trend curves are available; and in general these curves are based on the existing aircraft. But some lack of data is noticeable in terms of solar aircraft, i.e. the available information in terms of mass trends does not fulfill the needs of the designers of this type of aircraft as noted by Ross (2009a, 2009b). So, the main motivation of this study is to provide some information, in terms of mass trends, that could fill part of the gap.

Basically, two different lines of research are considered in this study:

- The estimation of the mass breakdown of relevant sun-powered aircraft; and in general each aircraft is itself significantly different from the other ones;
- The definition of a trend curve of the optimum wing structural mass in function of aircraft mass, for very light aircraft, such as solar aircraft.

The mass values have been obtained directly or estimated from the available data of aircraft geometry, systems power and typical mission.

4.13.1) Method

For the analysis presented in this work, MTOW is the maximum aircraft take-off mass, EEW is the aircraft empty mass - i.e., structure plus systems - M/S is the wing loading, A is the wing aspect ratio.

a) Solar Aircraft Mass Distribution:

The total mass of the aircraft and mass values of some components, such as payload, batteries, engines and solar cells have been obtained directly or indirectly from several sources. In the absence of direct information, solar cells are estimated from cells area and the mass/area attainable values by the aircraft construction year. In a similar way, Battery and engine masses are indirectly estimated, when necessary, from the declared power of battery and engine. Airframe mass is taken as the remaining part of the mass value, after discounting the other mass values from aircraft total mass.

So, it is possible to consider the following formulation:

$$M_{Eng} = Pw_{Eng} \cdot kg/kW_{Engine} \quad (4.101)$$

$$M_{Bat} = E_{Bat} \cdot kg/kWh_{Battery} \quad (4.102)$$

$$M_{Cell} = S_{Cell} \cdot M/S_{Cell} \quad (4.103)$$

being: $S_{Cell} = SAR \cdot S$ (4.104);

and

$$M_{str} = MTOW - M_{Payl} - M_{Eng} - M_{Bat} - M_{Cell} - M_{Contrl} \quad (4.105)$$

One point of attention is that the name engine in the mass distributions presented in this work refers to the engine itself, plus propeller and the reduction device, if applicable.

The following aircraft have been analyzed:

1. Roland Boucher Sunrise I, 1971: 1st solar aircraft;
2. Alan Cocconi Solong, 2005: 1st solar aircraft to stay airborne more than 48hs;
3. Qinetiq Zephyr 7, 2010: 1st solar aircraft to stay airborne more than 2 weeks;
4. Paul MacCready Solar Challenger, 1981: 1st manned solar aircraft to fly without batteries;
5. Erick Raymond Sunseeker II, 2009: Most flown solar aircraft, flights beyond 400 km;
6. AeroVironment 'Helios', 2001: 1st solar aircraft to carry payloads of 300kg, and to achieve 96 kft (Helios HP01), also aimed for long endurance missions (Helios HP03);
7. Bertrand Piccard Solar Impulse, 2012: 1st manned solar aircraft to stay airborne more than 24hs, aimed for cross-country missions.

b) Wing Structural Mass Trend:

In order to obtain data for the trend curve, three approaches, related to three different types of aircraft, have been performed:

- **1st Approach, solar aircraft evaluation:** The starting point for this approach is the group of structural mass values, obtained for the seven analyzed solar aircraft listed above in this sub-

section. In function of the aircraft arrangement and geometry, a percentage of this value is assumed to be the wing structure. The percentage value is adopted in function of the projected area the wing related to the projected area of other parts of the aircraft. With this percentage defined, the wing structural mass, abbreviated as WSM, is obtained:

$$WSM = M_{str} . (WSM/M_{str}) \quad (4.106)$$

Where: Mstr is the airframe mass, and
(WSM/Mstr) is the ratio of wing structural mass over airframe mass.

- **2nd Approach, pioneer aircraft:** The values of wing structural mass have been obtained from low-weight, pioneer aircraft in aviation history. Four remarkable aircraft from 1895 to 1909 are considered: Lilienthal Monoplane and Biplane, Santos-Dumont 14-Bis and the 1909 Demoiselle. Since these aircraft present a very low wing loading and have used very lightweight structural solutions - with the penalties of not presenting a clean aerodynamics, due to the stabilization strings – it was expected that their wing mass should be close to a mass trend line, and presenting values of wing mass slightly above the trend line of the sun-powered aircraft wing mass. The wing structural mass of Lilienthal gliders has been obtained from the aircraft EEW, and extracting the mass estimated for the aircraft tail:

$$WSM = EEW - M_{Tail} \quad (4.107),$$

Where M_{Tail} is the tail mass. The wing structural mass of Demoiselle aircraft is taken as a percentage of the aircraft's airframe mass, in a similar way from the first approach, trough equation 4.106. The wing structural mass of 14-Bis, due to its more complex geometry and mass distribution, has been obtained from a more detailed breakdown, based on the volume and specific mass of the aircraft items.

- **3rd Approach ultra-light sailplanes evaluation:** The wing structural mass values of ultra-light, high structurally and aerodynamically efficient sailplanes have been also investigated. Five very light modern sailplanes, which are identified in table 4.3, have been analyzed. In an analogous

way from the solar aircraft, the evaluation of wing structural mass for these aircraft are evaluated from the EEW of the aircraft, and assuming a 'wing structure/EEW' mass ratio:

$$WSM = EEW \,.(WSM/EEW) \tag{4.108}$$

The values obtained of wing structural mass for all the above referred aircraft are presented in the table 4.4. Once defined the data, different attempts have been made in order to obtain a trend curve as simple as possible, but encompassing the most important factors. The best compromise found is to show the values of Structural Mass in function of MTOW x $A^{1/2}$, as shown in the figure 4.43.

4.13.2) Examples of Analysis

The mass distribution evaluation for some of the considered solar aircraft is presented in table 4.1 and table 4.2., according to the procedure presented in the sub-section 4.13-1.
The collected data, and adopted values for input parameters for the analysis are presented in table 4.1. Table 4.2 shows the values calculated for each aircraft from the parameters from table 4.1. Solong aircraft parameters are not presented, but the calculation of its parameters follows the same procedure.

The total mass of the solar aircraft presented in table 4.1 are shown in figure 4.43; and the mass distributions of these aircraft, defined in table 4.2, are presented in figure 4.44.

The wing structural mass parameters for the pioneer aircraft (2nd Approach) is summarized in table 4.3. The mass evaluation of these aircraft is performed through a specific research, based on Villares (1957), Costa (1971), Otto Lilienthal Museum (2011). From the four pioneer aircraft, the more detailed analysis required for mass determination is the one referred to 14-Bis aircraft, due to the aircraft higher complexity in terms of geometry and structure, compared to the other three aircraft.

Table 4.1: Solar Aircraft Mass Distribution Evaluation: Input Data

Parameter and Unit	Solar Challenger	Sunrise I	Helios 03	Path-Finder	Solar Impulse	Sun-Seeker II	Zephyr II
Span [m]	14.2	9.75	75,3	29.5	63.4	17.0	22.5
Wing Area S [m2]	21.8	7.93	183,6	73.1	236.0	12.8	30.0
MTOW [kg]	147.4	11.8	929	254.0	1600	240	53.0
Payload Mass [kg]	59.3	0.68	329	45.0	110	74.9	3.5
Engine Power [kW]	8.0	0.6	20,9	7.5	29.8	6.4	0.9
Batteries Energy [kWh]	0.0	0.0	41,0	10.0	86.0	5.6	3.2
Cells Area / S	1.19	0.67	0,90	0.90	1.02	1.10	0.95
kg/kW Engine	1.75	1.70	0,90	1.00	0.90	1.20	0.45
Cells Mass/Area [kg/m2]	0.73	0.62	0,65	0.65	0.48	0.75	0.30
Kg/kW.h Batteries	0.0	0.0	5,0	5.0	5.0	5.0	4.8
Control System Mass [kg]	0.0	2.0	20	10	120	10	4.0
WSM/ Airframe Mass	0.65	0.53	0.80	0.80	0.63	0.66	0.70

Table 4.2: Solar Aircraft Mass Distribution Evaluation: Calculated Values

Parameter and Unit	Solar Challenger	Sunrise I	Helios 03	Path-Finder	Solar Impulse	Sun-Seeker II	Zephyr II
S Cells [m^2]	26.0	5.29	165	65.8	241	14.1	28.5
Solar Cells Mass [kg]	19.1	3.28	107	42.8	115.5	10.6	8.55
Engines Mass [kg]	14.1	0.95	18.8	7.5	26.8	7.65	0.39
Batteries Mass [kg]	0	0.56	205	50	430	27.9	15.3
Airframe Mass [kg]	54.9	4.28	249	98.7	798	109	21.3
Wing Structural Mass [kg]	35.7	2.27	199	79.0	502	71.9	14.9
Aspect Ratio A	9.2	12.0	30.9	11.9	17.0	22.6	16.9
M/S [kg/m^2]	6.76	1.49	5.06	3.47	6.78	18.8	1.77
WSM / Area [kg/m^2]	1.64	0.29	1.08	1.08	2.13	5.62	0.50

Table 4.3: Pioneer Aircraft Parameters

Aircraft	Lilienthal Monoplane Glider	Lilienthal Biplane Glider	SD Demoiselle 35 hp	SD 14-Bis 50hp
MTOW [kg]	100	114	164	300
EEW [kg]	20	34	110	225
Airframe Mass [kg]			60	149
W S M [kg/100]	16	30	27	62
Wing Area S [m2]	13.6	24.0	10.2	53.0
Wing Span [m]	7.0	6.3	5.5	12.0
WSM / Airframe Mass	0.80	0.88	0.45	0.42
Aspect Ratio A [-]	3.6	3.4	2.9	5.4
M/S [kg/m2]	7.35	4.75	16.08	5.66
Sqrt (A)* M [kg/100]	1.90	2.09	2.80	6.99

The wing structural mass evaluation for the ultra-light sailplane aircraft (3rd Approach) is presented as follows. The data from the analyzed sailplanes are presented in table 4.4, and the parameters calculated and estimated for these aircraft are presented in table 4.5. In the aircraft presented in Table 4.5, the airframe mass can be considered as the same as the EEW.

Table 4.4: Sailplane Mass Distribution Evaluation: Input Data

Aircraft	Moyers Microflight	Gliderspor Lighthawk	Carbon Dragon	Aeromarine Sierra	Sparrow-hawk
MTOW [kg]	181	170	152	206	188,2
EEW [kg]	91	68	66	93	70,3
Wing Area S [m^2]	14	12	14,2	13,2	6,5
Wing Span [m]	13	15	13,4	13	11,0
Max Glide Ratio	23	35	----	25	37,0

Table 4.5: Sailplane Mass Distribution Evaluation: Calculated Values

Aspect Ratio A [-]	12,1	18,8	12,6	12,8	18,5
M/S [kg/m^2]	12,93	14,17	10,70	15,61	28,95
Sqrt (A)* M [kg/100]	6,29	7,36	5,41	7,37	8,10
Structural Mass [kg/100]	0,91	0,68	0,66	0,93	0,70
Wing Structural Mass [kg/100]	0,60	0,45	0,44	0,61	0,49

The values of the wing structural mass from the all the aircraft of tables 4.1 to 4.5 are presented, in function of parameter MTOW. $A^{1/2}$ in the figure 4.45 , of mass trend.

4.13.3) Mass results:

The Results are presented in two parts: Mass distribution for Solar Aircraft, and Wing Structural Mass Trend.

a) Mass Distribution for Solar Aircraft for Solar Aircraft

The comparisons of mass distribution from the selected solar aircraft are presented in crescent order of MTOW, in figures 4.43, for MTOW, and 4.44, for mass breakdown. The figure 4.44 presents agreement with the figure of Presentation from Ross (2009b), in which a generic mass distribution of a solar aircraft is presented.

In figures 4.43 and 4.44, the fifth aircraft is referred as "adjusted", because its mass value has been adjusted from the tendency of the family of the Very Light Modern sailplanes, which possibly present the same building and design techniques.

From the mass distribution comparison of figure 4.44 it is possible to notice that there are large differences in mass distributions from each aircraft to the other ones. Probably the mass distribution depends largely on two main factors:

- The aircraft mission which is very specific for each aircraft; and
- The aircraft total mass, which also presents large variation among the aircraft considered (from 10 kg up to more than 1 Ton, as presented in figure 4.43).

As shown in figure 4.44, the main mass item in general is structure (30 a 50%). For long endurance aircraft, solar cells and batteries masses present also large percentages. With the exception of Helios, all the aircraft larger than the long-endurance Zephyr, present the tendency of a percentage decreasing in payload with the increasing of the total aircraft mass.

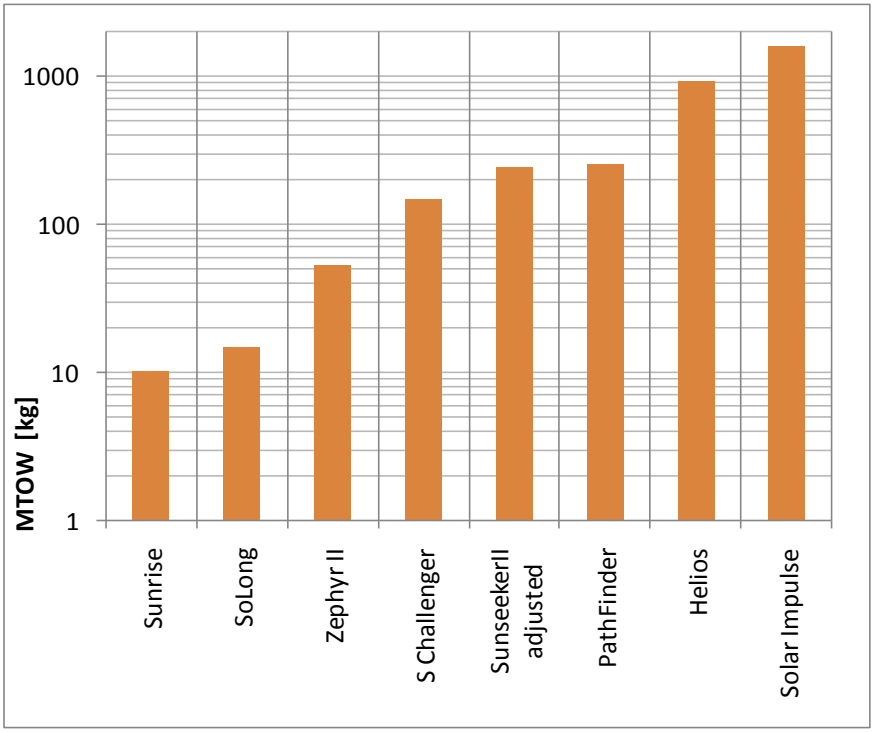

Figure 4.43: Take-off mass comparison of solar aircraft representatives

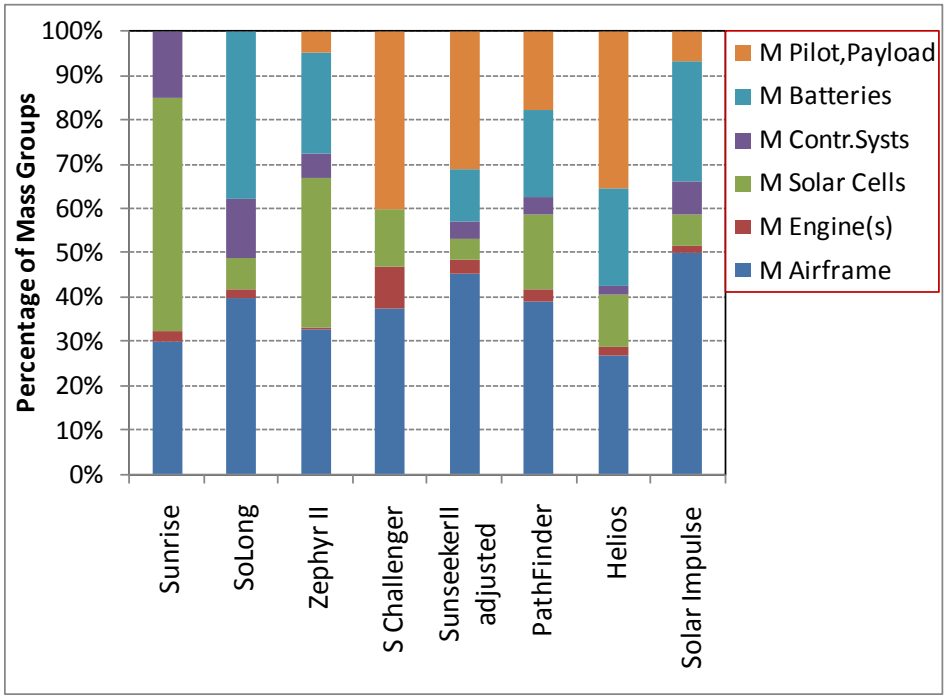

Figure 4.44: Mass breakdown comparison of solar aircraft representatives

b) Mass Results: Wing Structural Mass Trend

The Diagram Wing Structural Mass versus MTOW x $A^{1/2}$ for Solar and non-Solar Aircraft, but with very low-wing loading, is presented in figure 4.45. In the figure, the aircraft are grouped in three families: Solar aircraft, very light modern sailplanes, and early aviation pioneer aircraft. Considering the examples presented in the figure, the trend curve of the Possible Safety Limit, or the Optimized Structure Mass, is defined as also presented in the figure. The equation of the defined curve is:

$$Y = 0.05431\, X^{1.1111} \qquad (4.109).$$

It can be noticed that, almost all of the Very Light Modern Sailplanes, even not being solar, are very close to the trend line. The Sunseeker II mass value needed to be adjusted from the tendency of the family of the Very Light Modern sailplanes. Helios 3 mass value is significantly below the trend line, which may be related with the damage aircraft suffered in flight tests as presented by Noll et al (2004).

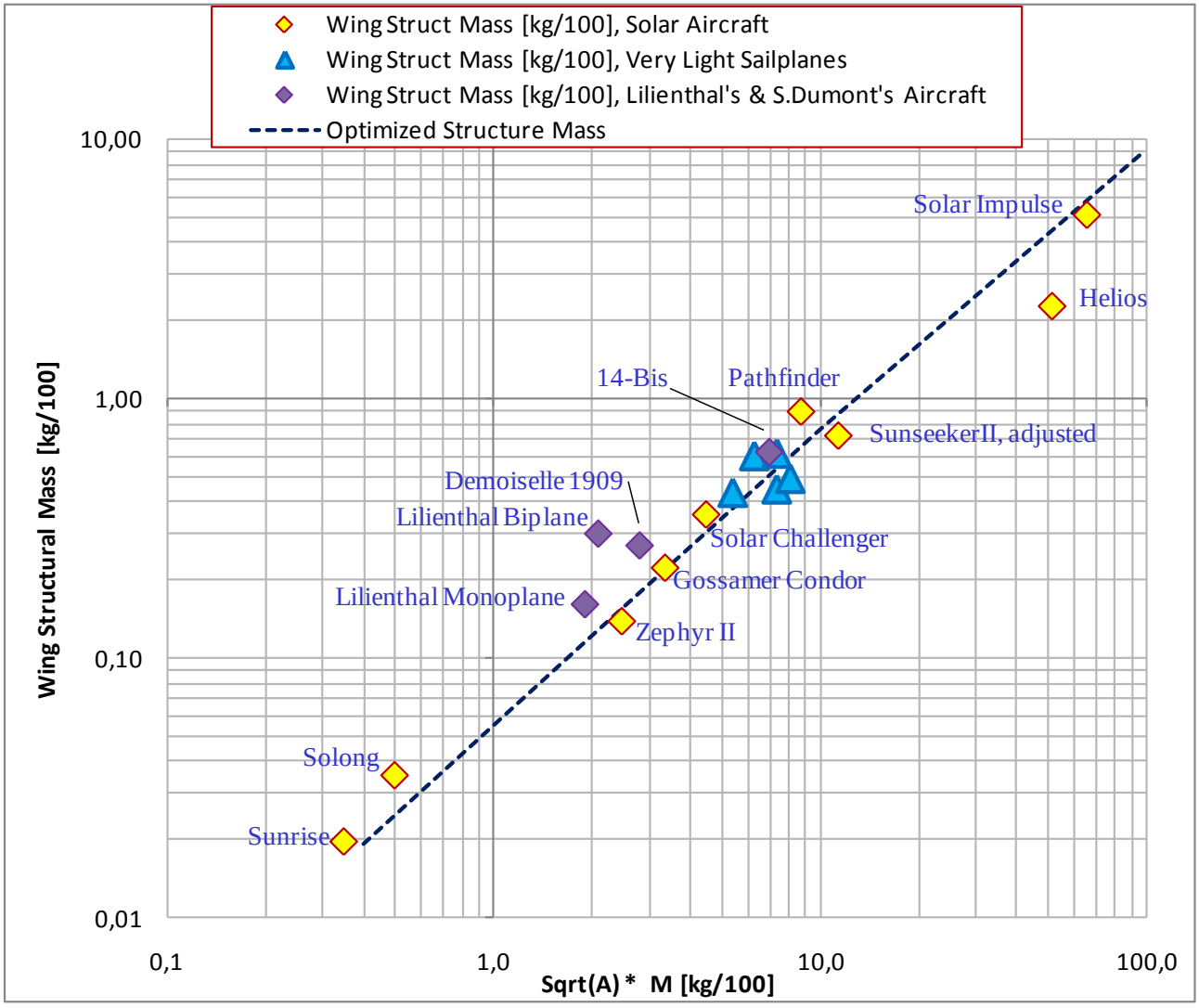

Figure 4.45: Diagram of Wing Structural Mass versus MTOW x $A^{1/2}$

4.13.4) Discussion of Mass Results

As presented in figure 4.44, there is a large variation of percentage mass distributions among the solar aircraft, which is probably dependant on the desired aircraft mission and aircraft total mass.

As presented in figure 4.45, it has been possible to define a trend line for minimum, or optimal, wing structure mass of extremely light aircraft, such as solar aircraft, based on aircraft total mass and its aspect ratio. The trend curve presented in figure 4.45 can be useful for purposes of early design mass estimation related to very light, extremely effective aircraft.

5) STUDIES

In this chapter some specific analysis performed with the methods from the chapter 4 are presented.

5.1) Checking the limits of a Sun-powered aircraft.

In this section some examples of application of the maximum wing load formulae defined in section 4.3 are presented. The first two examples refer to the basic definition of two hypothetic piloted sun-powered aircraft, both with the same wing area and aspect ratio than a current high-speed, long-range, internal combustion large passenger commercial aircraft. The second group of examples refers to the fast check of the limits of some already-flown solar aircraft.

5.1.1) Limits of a large solar aircraft

The aircraft Airbus A-380 can be considered as an example of a large aircraft.

It is possible to perform a study in order to check the order of magnitude of the performance of a solar aircraft with the same wing area and span of an existing aircraft. For a comparative study, the Airbus A-380 has been considered. The two aircraft, the A-380 and a equivalent sun-powered aircraft, with the same area and span, are presented in figure 5.1. The equivalent solar aircraft is conceived as being mostly composed by the wing, in order to minimize the drag coefficient CDo.

The most relevant data from A-380 are taken from the sites Wikipedia and airliners.net. This aircraft is designed for 555 to 853 passengers or 89,200 kg of payload, with a MTOW of 575,000 kg, a span of 79.75 m and wing area of 845 m^2, a maximum cruise speed of Mach 0.89, or 945 km/h, and a normal cruise speed of Mach 0.85.

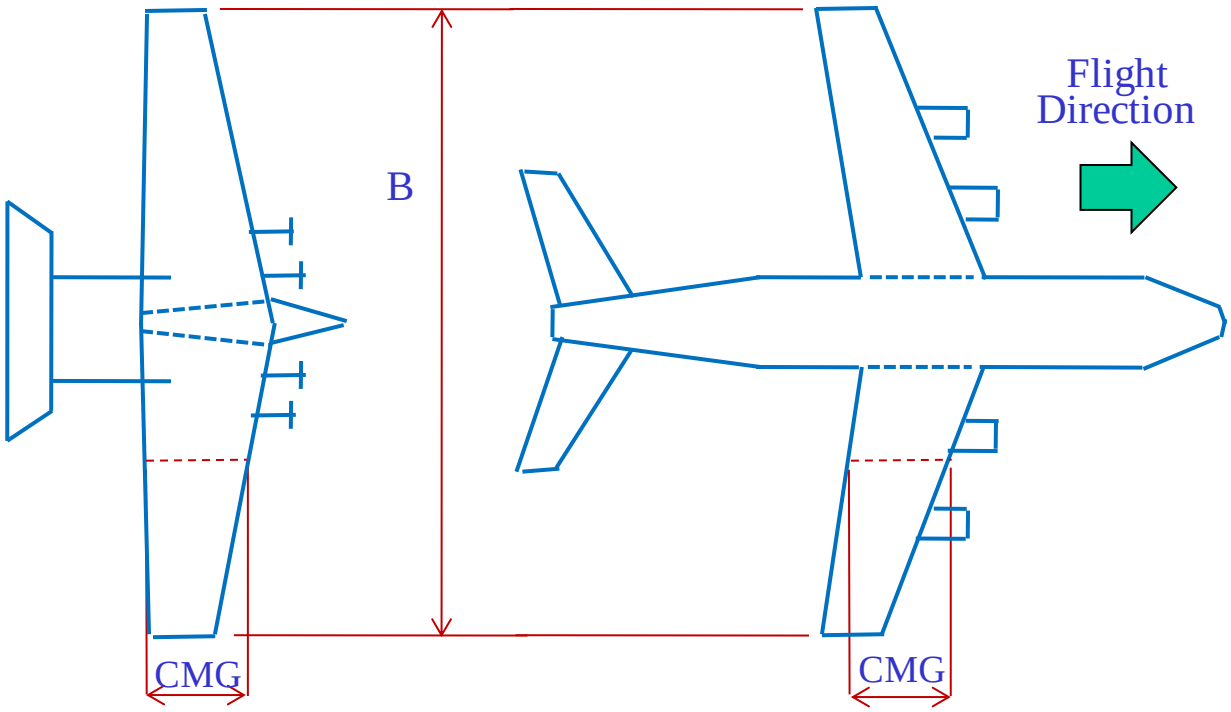

Figure 5.1: A hypothetical Solar Aircraft (left) with the same wing area and aspect ratio of the Airbus A-380 aircraft (right)

For the equivalent aircraft it is adopted a CDo of 0.013, and its induced drag factor k is about 0.044, which roughly corresponds to the aspect ratio of 7.5, the same from the A-380 wing.These values lead to

CL_{*}=0.540; CL_{**} = 0.936; E_{**}=18.0 .

The flight altitude considered is 8,000 feet. The sun local daily energy intensity considered is 7500 W.h/m^2, and the maximum sun local power intensity is 1000 W/m^2; these two values roughly correspond to the sun irradiance values about November 23 to January 23, at the latitudes of 20^o to 50^o south. In order to allow a minimum useful flight time, the minimum Sun Power intensity to provide horizontal flight is determined as 650 W/m^2 which, in latitudes of 20 to 50^o south and from about November 23rd to January 23rd, corresponds to about 6 hours of daily flight.

The considered values of system and mass parameters necessary to perform the aircraft definition:

Solar array effectiveness = 0.2

Effectiveness of transmission systems, wiring plus controllers = 0.85

Engine effectiveness = 0.85

Propeller effectiveness = 0.85

Total mass, of engine plus propeller plus reduction, per power [kg/kW] = 0.7

Solar array mass per area [kg/m^2] = 0.5

Aircraft structural mass over wing structural mass ratio = 1.30

Engine maximum power /maximum deliverable sun power = 1.00

Mass of aircraft movable surfaces actuation systems/aircraft mass = 0.01

Mass of each passenger or crew, including seat and other cabin items per passenger = 120 kg

Number of daily hours in which the flight with sun direct power is possible = 8

Two scenarios are examined: aircraft without batteries and aircraft with batteries. For the aircraft with batteries, the following parameters are considered:

Battery input-to-output effectiveness = 0.81

Battery mass per energy [kg/kW.h]= 3.0

Mass of electric control, per battery mass [kg/kg] =0.02

Number of daily hours in which the flight with sun direct power is possible = 8

a) Aircraft with batteries:

A series of solutions of wing loading can be found, in function of the parameter SAR - the percentage of the wing area is covered by solar arrays - as presented in figure 5.2.

A lower limit for the wing loading of 5.0 kg/m^2 is established, in order to avoid extremely unrealistic solutions. As can be seen through figure 5.2, for the hypothetical aircraft in study, this corresponds to the SAR value of about 0.91.

Considering this SAR value and the wing load of 5.0 kg/m^2, the aircraft maximum mass is 4225 kg. The wing structural mass, obtained from the aspect ratio and the aircraft maximum mass is 1067 kg, and from this value the total aircraft structure mass is found as 1388 kg. The remaining mass items, which are payload plus systems, should totalize not more than 2837 kg. From the engine power, the solar array area, and the battery necessary energy, the masses of engines, solar arrays and batteries are obtained as 100 kg, 386 kg and 1922 kg respectively. This leaves 349 kg to be used by crew or passengers, which resumes to slightly less than three people with the corresponding individual cabin equipment. The aircraft true airspeed is about 37.5 km/h; so the total time for a non-stop, 24hs a day,

travel, corresponding to the 15700 km flyable by the A-380, in this hypothetical equivalent solar aircraft, is 17.4 days.

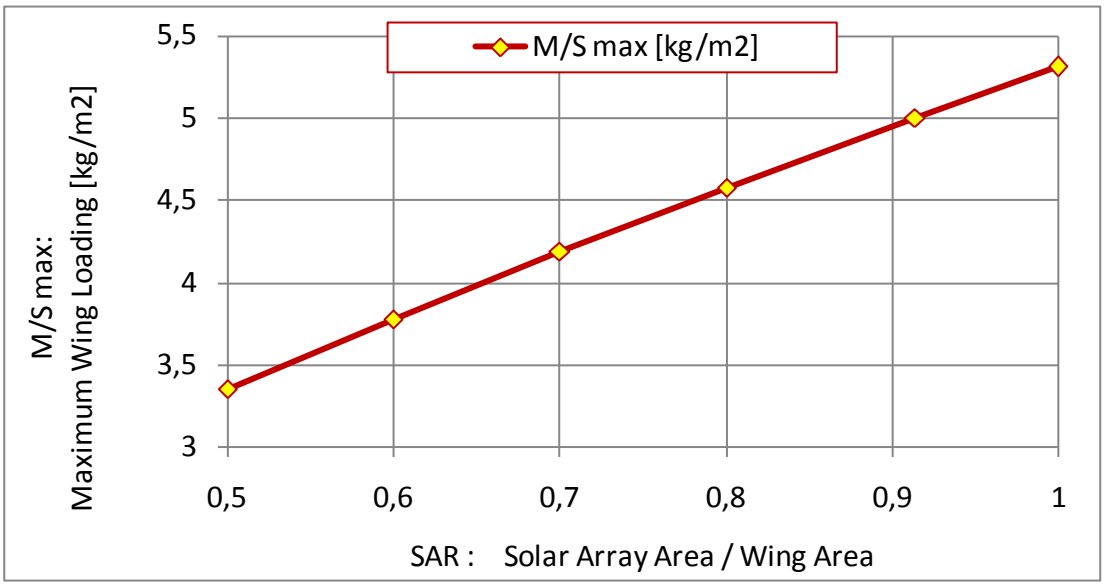

Figure 5.2: Values of M/S max obtained for different SAR values, aircraft with batteries.

b) Aircraft without batteries:

In this second scenario our hypothetical aircraft shall perform a long-distance travel in a series of short sun-light flights. The minimum Sun Power intensity to provide horizontal flight is determined as 650 W/m^2 which, in latitudes of 20 to 50^o south and from about November 23rd to January 23rd, corresponds to about 6 hours of daily flight. Considering the same SAR value than the previous scenario, 91%, the maximum wing load obtained is 8.60 kg/m^2. The maximum aircraft mass is so 7268 kg. Analogously to the scenario of aircraft with batteries, the wing structural mass obtained is 1950 kg, and the total aircraft structure mass is found as 2535 kg. The payload plus systems mass items should thus totalize not more than 4732 kg. The mass of engine and solar arrays are the same from previous scenario, and the mass of control systems is about 101 kg. These values lead to a maximum payload value of 4145 kg, which corresponds to, in terms of crew plus passengers plus individual equipment an appropriate cabin, 34.5 people. The aircraft true airspeed is 49.2 km/h; so these people, flying 6 hours a day could perform 319 km a day, and could finish a trip corresponding

to A-380 range of 15700 km in 53 days, one flight a day, provided there are runways available during the intended path, and cloud conditions are favorable.

5.1.2) Checking the limits of the already-flown Sun-powered aircraft

Besides the example of feasibility study of the 2 hypothetic transport aircraft presented in sub-section 5.1.1, an interesting use for the equations 4.23 and 4.29 is the check for already-flown solar aircraft. The use of the formulae is simple; the more difficult task is obtaining the consistent values for input data. The input data are:

- In terms of aircraft: The estimated aircraft drag, the reported aircraft mass and area, the estimated efficiency of the systems, the reported altitude achieved, or potentially achievable;
- In terms of environment: The latitude and month associated to the altitude data.

The aircraft considered for the analysis are:

- Cocconi Solong;
- Solar Impulse 1;
- Solar Impulse 2;
- Qinetiq Zephyr 7, also known as version II;
- Aerovironment Helios, light version, which achieved 96 000 feet;
- Aerovironment Helios, heavier version, aimed for 80 000 feet;
- Aerovironment Pathfinder+, aimed for 80 000 feet;
- Aerovironment Pathfinder, flown in Dryden, California, USA;
- Aerovironment Pathfinder, flown in Kauai, Hawaii, USA;
- MacCready Solar Challenger;
- Boucher Sunrise II.

From the data gathered and calculated, the results obtained are:

- The maximum horizontal flight altitudes, which have been obtained indirectly via equation 4.23, by isolating the term ρ and calculating the altitude corresponding to the value of ρ obtained. The values of maximum horizontal flight altitudes are presented in figure 5.3, compared to the reported ones as achieved or intended. The achieved or intended value of altitude for Solong is defined in function of the reported range of the telemetry and control system.

- The maximum level, constant altitudes for continuous flight, which have been obtained also indirectly via equation 4.29, by isolating the term ρ and calculating the altitude corresponding to the value of ρ obtained. The term continuous flight in this case refers to flight with more than 24hs, i.e. more than 1 day of sun-night cycle. For this purpose of continuous flight a large amount of batteries inside the aircraft is a must. The values of altitude obtained are shown in figure 5.4.
- The maximum wing loadings for continuous flights, at a constant altitude, in this case chosen as 3Km, have been obtained using equation 4.29 directly. The calculated values are presented in figure 5.5, compared with the wing loading values obtained from reported information.

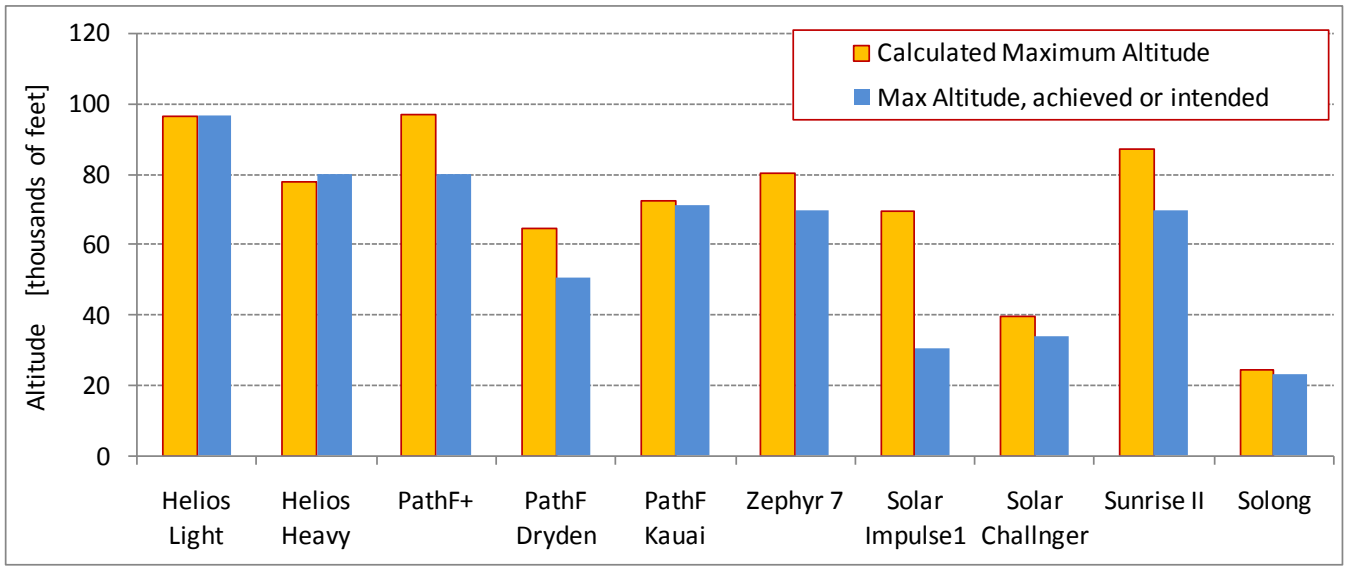

Figure 5.3: Maximum horizontal flight altitudes; comparison between calculated and intended values

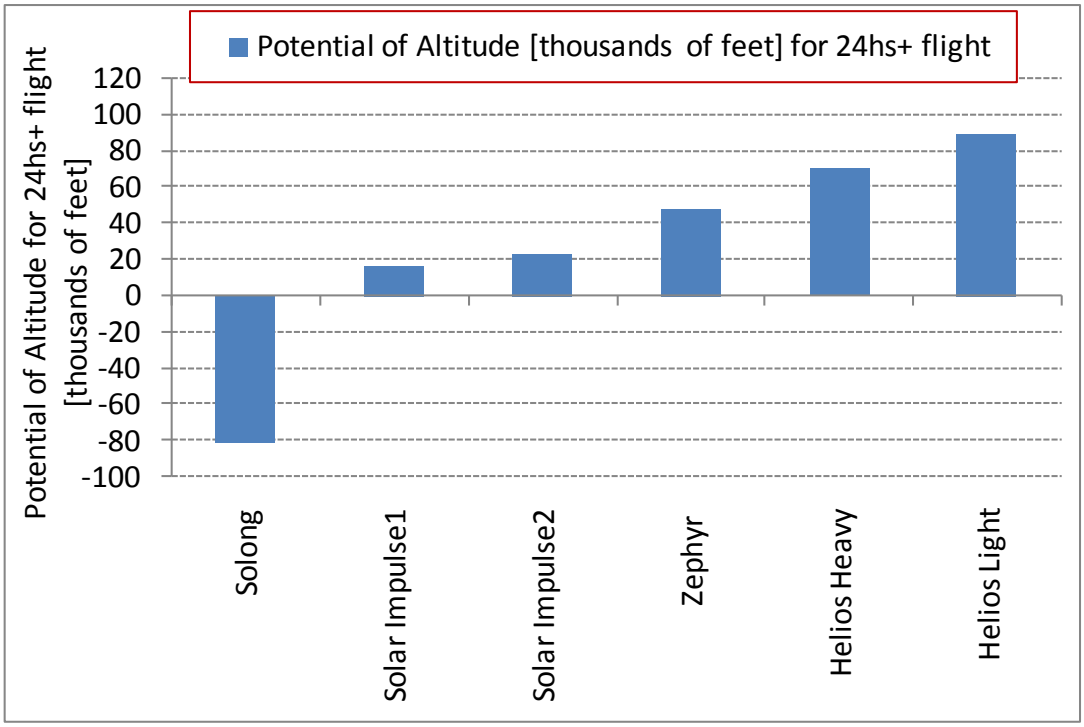

Figure 5.4: Calculated maximum altitudes for continuous flight at constant altitudes

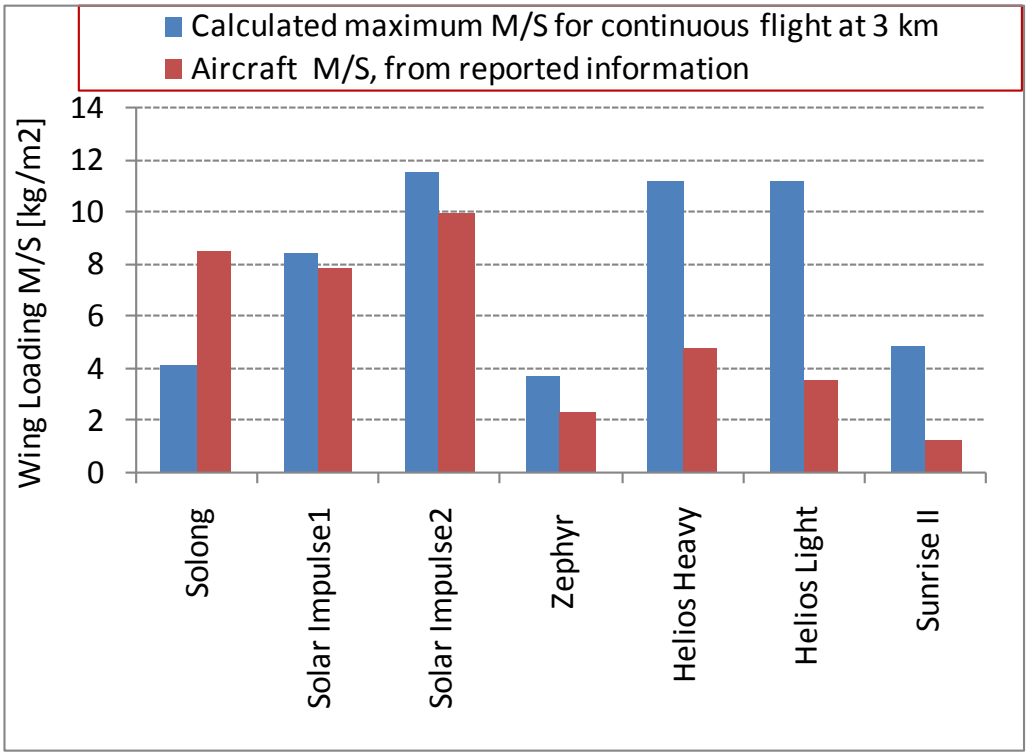

Figure 5.5: Calculated Maximum wing loadings for continuous flights, at a constant altitude of 3Km, compared with the real wing loadings.

Some important comments about the results presented in figures 5.3 to 5.5 are:

- In terms of figure 5.3, one can see that the calculated values in general are close to and higher than the values reported as intended ones; which gives confidence to the equation 4.23 and furnishes guidelines for a better understanding of these aircraft. The differences on Pathfinder+, Solar impulse 1 and Sunrise II can be explained by different reasons. Pathfinder+ possibly has not achieved this level due to systems limitations, improved in Helios; Solar Impulse has no pressurized cockpit; Sunrise II data used are probably overoptimistic.
- In terms of figure 5.4, it is possible to note that the values of altitude obtained for continuous flights are lower than the ones for maximum level altitudes, which is consistent in terms of model, and theoretically confirms the potential of these aircraft – except by Solong - to perform a flights of more than 24h. The representation of the negative altitude related to well-succeeded Solong, means that, in the conditions of the analysis, it should not capable of perform a 24h flight. And in fact the Solong achieved the record of 48hs of flight in 2005; probably this achievement has been made with the aid of thermals, which certainly required very good strategies and skills from the pilots on ground. Figure 5.4 also confirms that the continuous flight for Solar Impulse 1 and 2 is possibly aimed for low-altitude, which is consistent to the declared values and the unpressurized cabin; and that Zephyr continuous operation altitude is above 40,000, and Helios is above 60,000 feet or above 80,000 feet depending on the installed mass.
- From Figure 5.5 it is possible to have one idea of the margin in terms of M/S each aircraft presents to reach a low-altitude, 3km or 10,000 feet, continuous flight. From this figure it is possible to note that a good small aircraft to present continuous flight in low altitude should one aircraft at the half way from Sunrise to Solong.

5.2) Drag, Propulsion, Performance of 'Already-Flown' Low-Speed Aircraft

5.2.1) List of Main Analysis

The analyses performed for some of the already-flown air vehicles have been from fundamental importance for all the study, since they provided confidence in the tools developed, prior to use them in the new designs, or to check the Sun-powered aircraft whose characteristics are still not

well-known. The aircraft analyzed and the types of analyses performed are presented in the summary table 5.1. Despite all the aerial vehicles presented have in common the aspect of low speed, the configurations, payload, typical missions, means of construction, financial value invested and technological levels differ significantly among them. One of the vehicles is an airship, the SD N.9; some present a clean aerodynamic but are stiffened by strings, the Gossamer Condor and the Solar Challenger; some of them are subjected to low-Reynolds number issues, as Zephyr, Sunrise, Solong, Helios, High Flight. The only aircraft not flown yet in the table is the High Flight which is designed throughout this study.

Table 5.1: Summary of the types of Analyses performed for the Low Speed Aircraft

Type of Analysis:[1]		Mass Analysis	Propeller thrust	Glide [2]	T-off	Max Speed	Mission Analysis
Air Vehicle:	Solar?	Study is done?					
Otto Lilienthal Gliders	No	Yes	N.A.	Yes	Yes	N.A.	N.A.
S. Dumont N.9 Airship		Yes	Yes	N.A.	N.A.	Yes	N.A.
S. Dumont N.14 plus 14Bis		Yes	Yes	Yes	Yes	Yes	N.A.
S. Dumont 14Bis Biplane		Yes	Yes	Yes	Yes	Yes	N.A.
S. Dumont Demoiselle		Yes	Yes	Yes	Yes	Yes	N.A.
MacCready Gossamer Condor		Yes	Yes	Yes	Yes	Yes	N.A.
MacCready Solar Challenger	Yes	Yes	Yes	Yes	Yes	Yes	N.A.
R&R Boucher Sunrise		Yes	Yes	Yes	N.A.	Yes	Yes
A. Cocconi Solong		Yes	No	Yes	No	No	Yes
E .Raymond Sunseeker		Yes	No	Yes	No	No	No
Aerovironment Helios1		Yes	Yes	Yes	No	No	Yes
B. Piccard Solar Impulse		Yes	No	Yes	No	No	No
Qinetiq Zephyr		Yes	No	Yes	No	No	No
Author's High Flight		Yes	Yes	Yes	No	No	Yes

Notes: 1: Drag evaluation has been performed for all of the aircraft.

2: Glide evaluation includes required level power at sea level.

N.A.: Not Applicable

5.2.2) Example of Analysis

The aerial vehicle presented in the SD N9 Balladeuse airship, flown in 1903. It used the buoyancy of hydrogen at its hull, instead of wing lift, to balance the weight; despite this, in terms of the analysis of drag, propulsion and performance the procedure is almost the same as the one performed for the airplanes, so it can be used for the purposes of presenting a the example of the procedure.

The starting point is collecting aircraft mass and geometric data. To define a specific reference drawing of the vehicle is important for the consistence of the values. The aircraft geometry drawing elaborated is presented in figure 5.6.

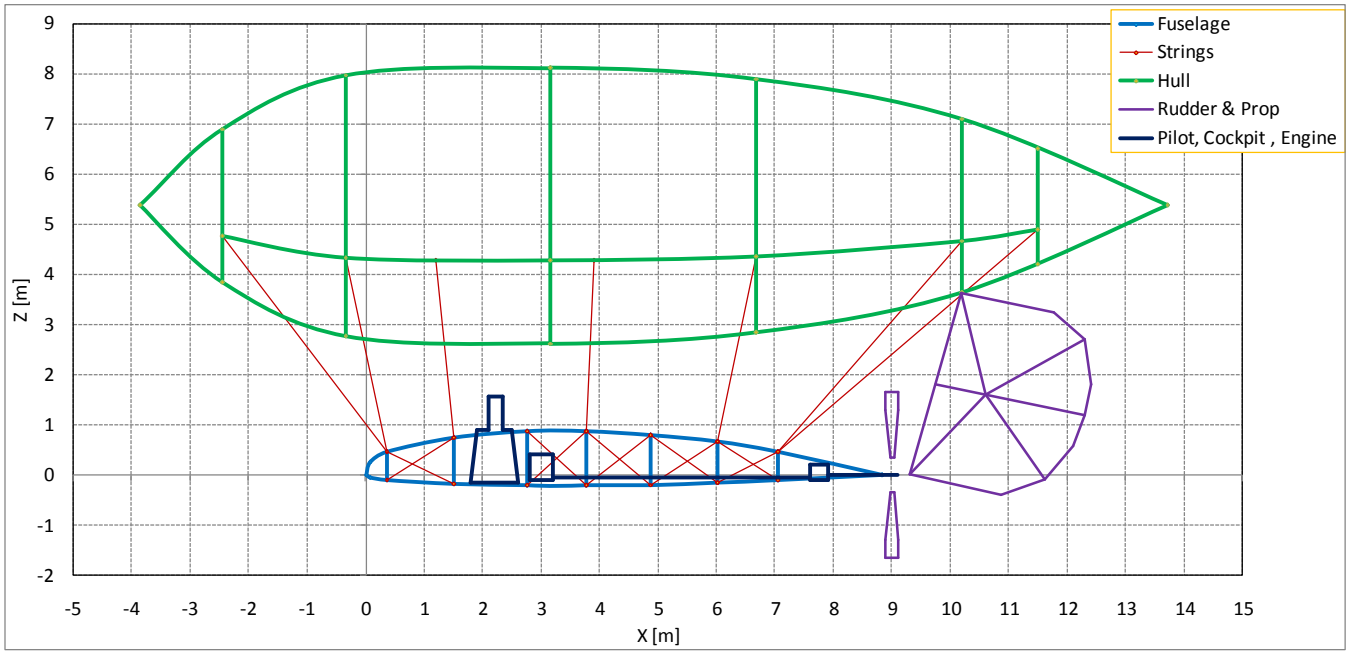

Figure 5.6: Santos-Dumont N.9 ‘Balladeuse’ Airship

With the geometry and the aircraft speed, the CDo of the aircraft components are evaluated. The evaluation of the CDo of some of the items of the vehicle, in function of the thickness ratio t/c and the Reynolds number is exemplified in figure 5.7.

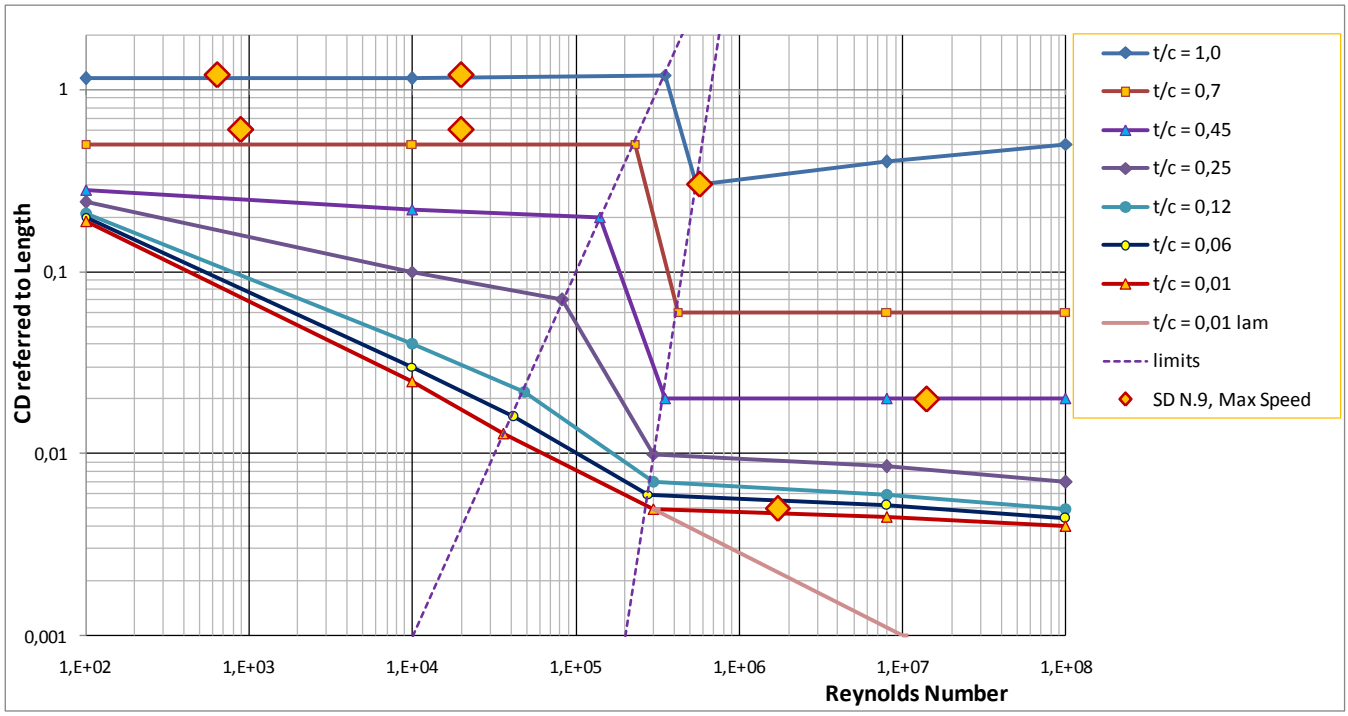

Figure 5.7: Evaluation of CDo of vehicle items, in function thickness ratio t/c and Reynolds number

The total drag area of the vehicle, CDo.S obtained with the contributions of the aircraft items is 4,545 m^2. The reference area is considered as being the hull frontal area, 23.76 m^2. So the aircraft drag coefficient, obtained by division of the total drag area of the vehicle by the reference area is 0.1913. The contributions of the several vehicle items for the drag area are grouped in main components, as presented in figure 5.8.

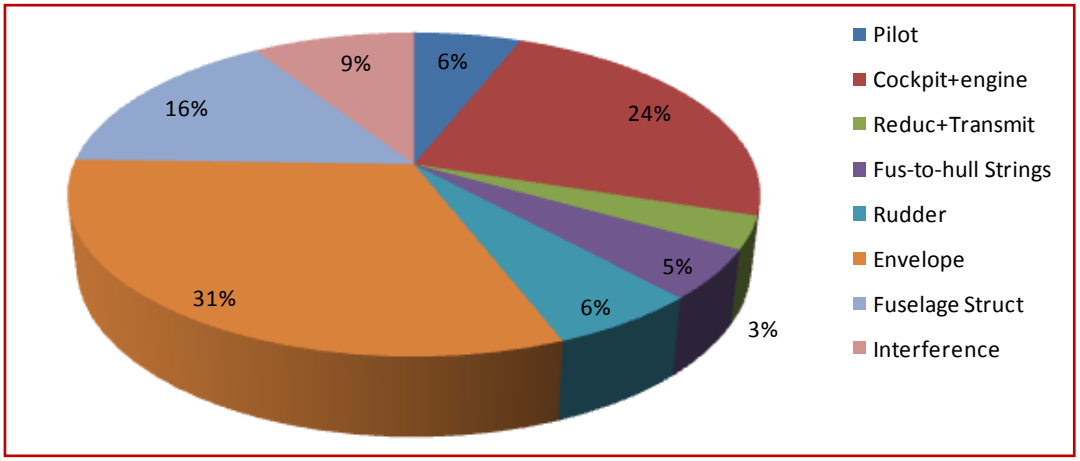

Figure 5.8: Pie-Chart Diagram of the SD N.9 Balladeuse Parasite Drag Breakdown

In terms of propulsion analysis, the propeller geometry is defined from the available sources. The geometry relevant information is the propeller airfoil shape presented in figure 5.9; and the propeller blade planform and the distribution of the pitch angles β, as presented in figure 5.10. In the figure 5.10 it is shown that three linear variations of β are assumed, and they are identified by the value of the pitch angle at 75% of the radius, which is named as beta75.

Besides the geometry, the propeller RPM, the maximum output power from the engine are requested input information.

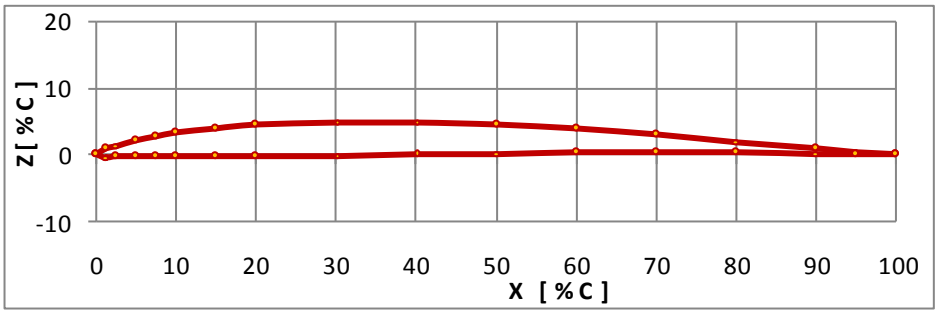

Figure 5.9: Propeller blade airfoil geometry

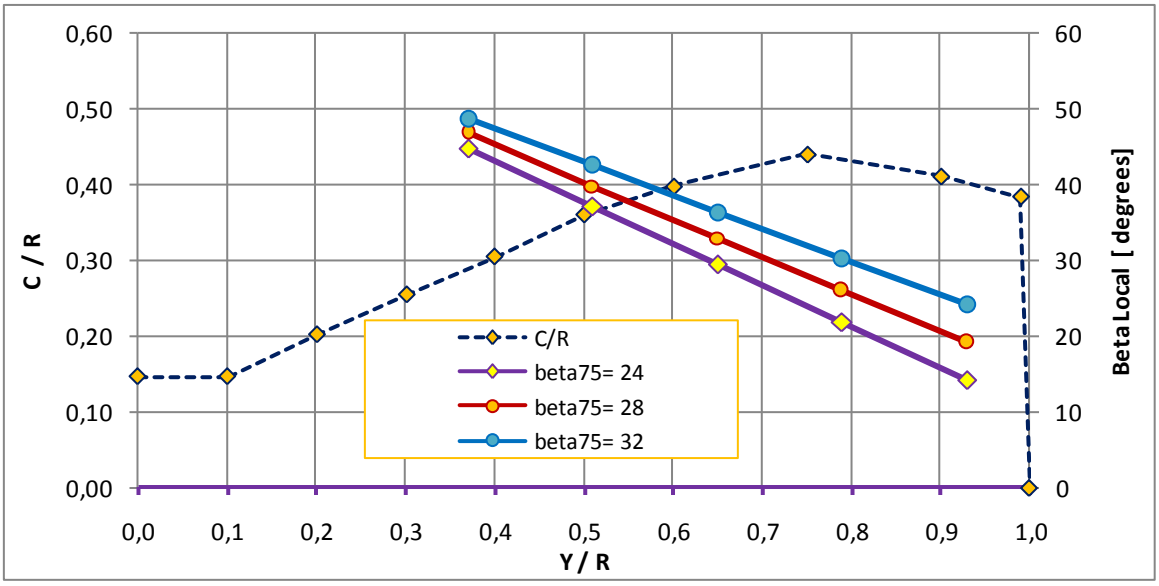

Figure 5.10: Propeller blade planform, and 3 possible pitch angle variations

With the airfoil shape, dimensions and speeds, the Reynolds number in three propeller sections along the radius are evaluated, and one Reynolds number is chosen as the representative, in general in

the vicinity of 75% of the radius. In function of this number, the propeller airfoil, and the blade aspect ratio, the three-dimensional aerodynamic coefficients of the propeller airfoil are determined. Figure 5.11 presents the Reynolds number evaluation at three sections of the propeller, 51, 65 and 79% of the radius; at different inflow speeds being the propeller at maximum RPM. Figure 5.12 presents the three-dimensional aerodynamic coefficients of the propeller airfoil.

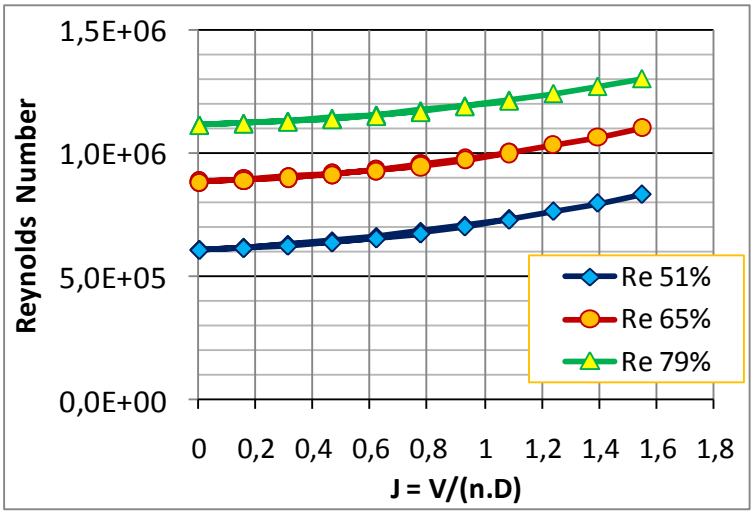

Figure 5.11: Reynolds number evaluation for three propeller sections.

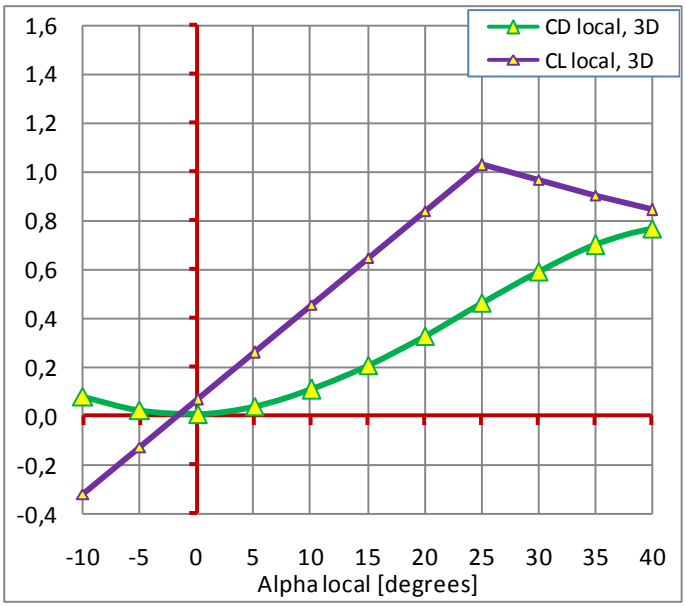

Figure 5.12: Three-dimensional coefficients CL and CD of the propeller airfoil, in function of α local.

With the airfoil determined and the geometry of the propeller, the curves of CT, CP and η_{prop} are determined according to the method presented in section 4.4. The curves of CT, CP and η_{prop} are presented in the figures 5.13 to 5.15, in function of the advance ratio J, for the three distributions of pitch angles. In figures 5.13 and 5.14 the upper curve corresponds to beta75 of 32°, and the lower curve corresponds to beta75 of 24°. In figure 5.15 the curve at right corresponds to beta75 of 32° and the curve at left corresponds to beta75 of 24°.

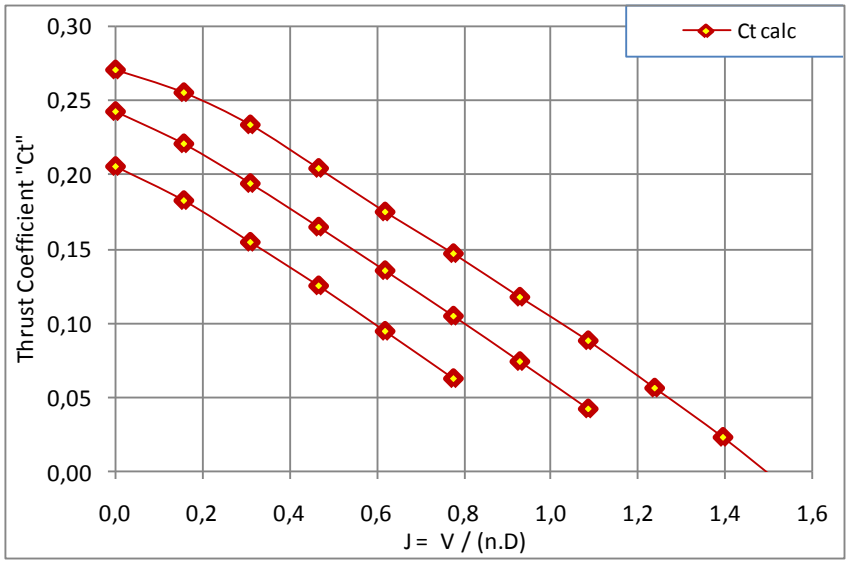

Figure 5.13: Curves of CT versus J for the three pitch angle distributions.

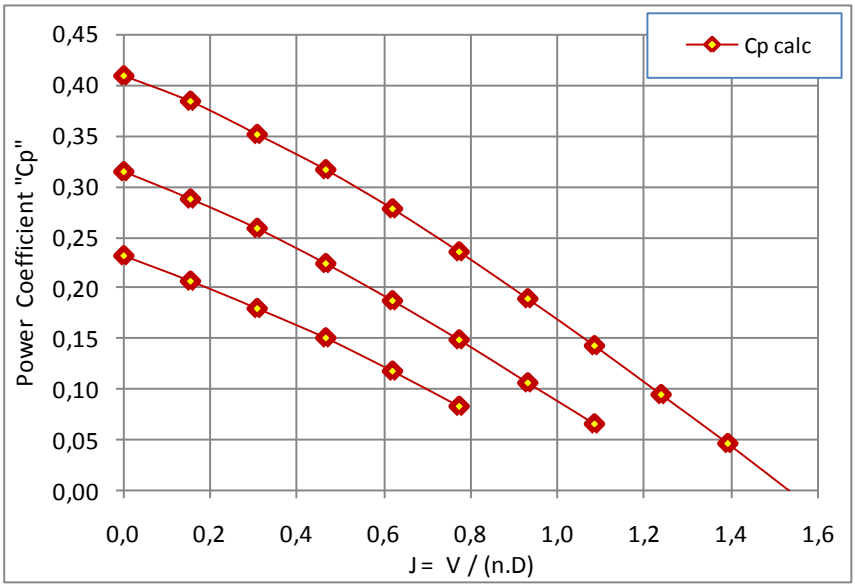

Figure 5.14: Curves of CP versus J for the three pitch angle distributions.

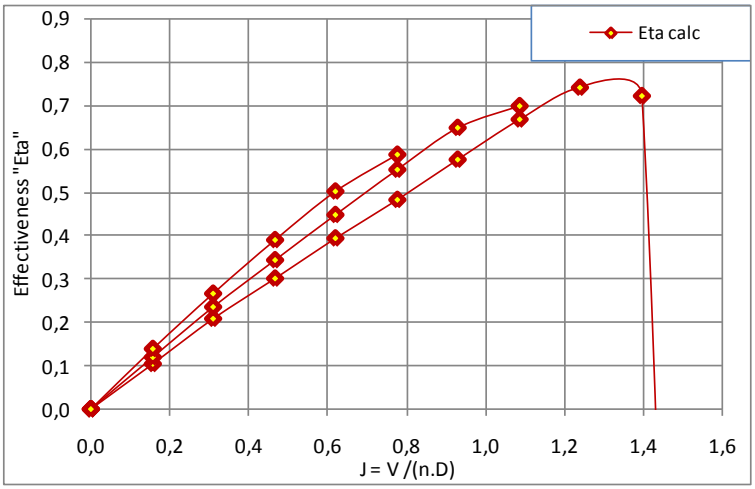

Figure 5.15: Curves of η_{prop} versus J for the three pitch angle distributions.

Once calculated the vehicle drag coefficient it is possible to define the curve of drag for horizontal flight in function of airspeed; and from the maximum engine output power, and the from the curves of figures 5.13 and 5.14, the curve of maximum thrust in function of airspeed can be defined. The two curves, horizontal flight drag and maximum thrust are presented in figure 5.16. These 2 curves are useful for several uses, including the determination of the ratio of climb when applied to airplanes.

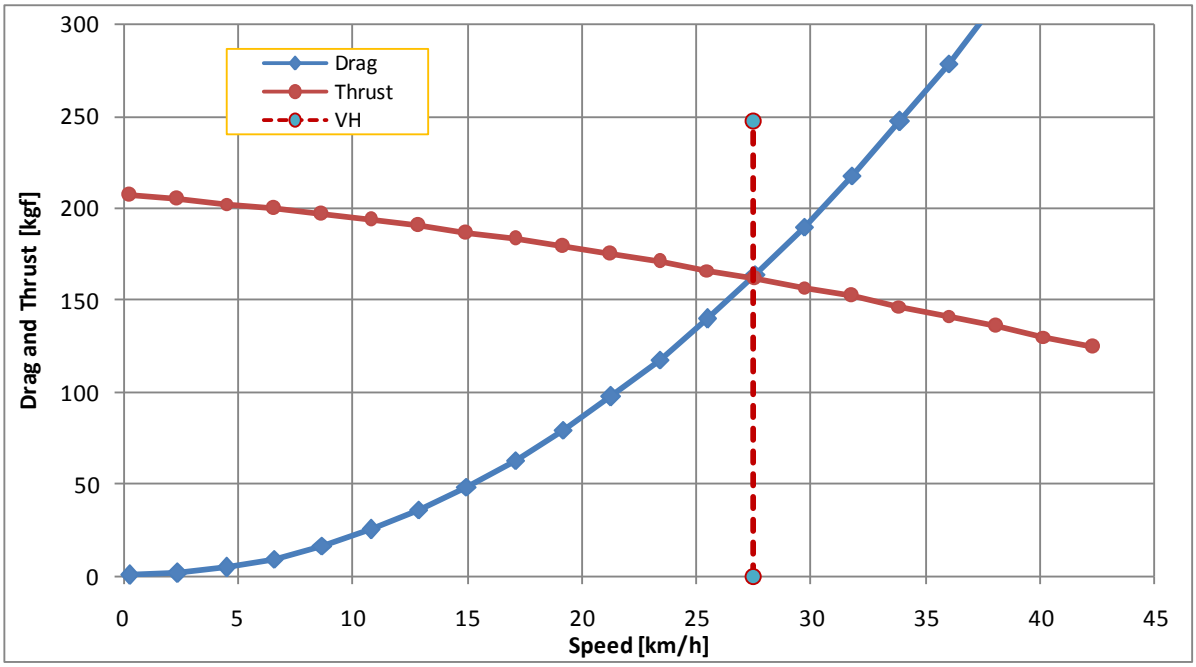

Figure 5.16: Curves of drag and maximum thrust in function of airspeed, and VH determination.

One very important use for the curves of horizontal flight drag and maximum thrust, presented in figure 5.16, is the determination of the maximum horizontal speed, VH. It is obtained by the intersection of the two curves, as also shown in the figure 5.16. In figure 5.16 the value of maximum thrust is for beta75=32^{o}. The curve beta75=28^{o} presented almost the same VH, and the maximum VH is found to correspond to a intermediate value, beta75=30^{o}, with VH slightly higher than the value presented in the figure 5.16 but still below 28 km/h.

5.2.3) Comparison of drag and performance for the analyzed aircraft

In this sub-section, the drag, thrust, speeds and some performance parameters are compared. The values have been calculated according to the methodologies presented in chapter 4 and exemplified in sub-section 5.2.2.

The drag polars calculated for two high-technology aircraft from 1970-80 decades, the Gossamer Condor and the Solar Challenger, are compared with the drag polars calculated for four pioneer aircraft from 1890-1900 decades, in the figure 5.17. All are manned aircraft, all present a low wing-load. Taking into account that these curves are made in the form of equation 3.2, one can note the difference in terms of CDo from the pioneer aircraft to the more modern ones. From the analysis performed using the equation 4.23, the low values of CDo, in the order of magnitude presented by the Solar Challenger or Gossamer Condor, are necessary for the feasibility of solar aircraft.

The values of horizontal flight drag and maximum thrust versus airspeed for seven low speed air vehicles are presented in the figure 5.18. In this figure, the crossing of the Drag and Thrust Curve, as presented in sub-section 5.2.2, figure 5.16, define the maximum level speed VH for each aircraft. At the figure 5.18, two aircraft are gliders so no thrust curve for them is presented. Similarly to figure 5.17, all the aircraft of figure 5.18 are manned. It is possible to note from the figure 5.18 that the Solar Challenger, from 1981, presents a slightly higher speed than the 14 Bis from 1906, but presenting almost one tenth of the 14 Bis thrust. This also can provide one idea of the advancement of the low-speed aerial technology in 75 years. One can also note the efficiency gain in three years, by comparing the speed and thrust characteristic of Demoiselle of 1909 related to the same parameters of the 14 Bis.

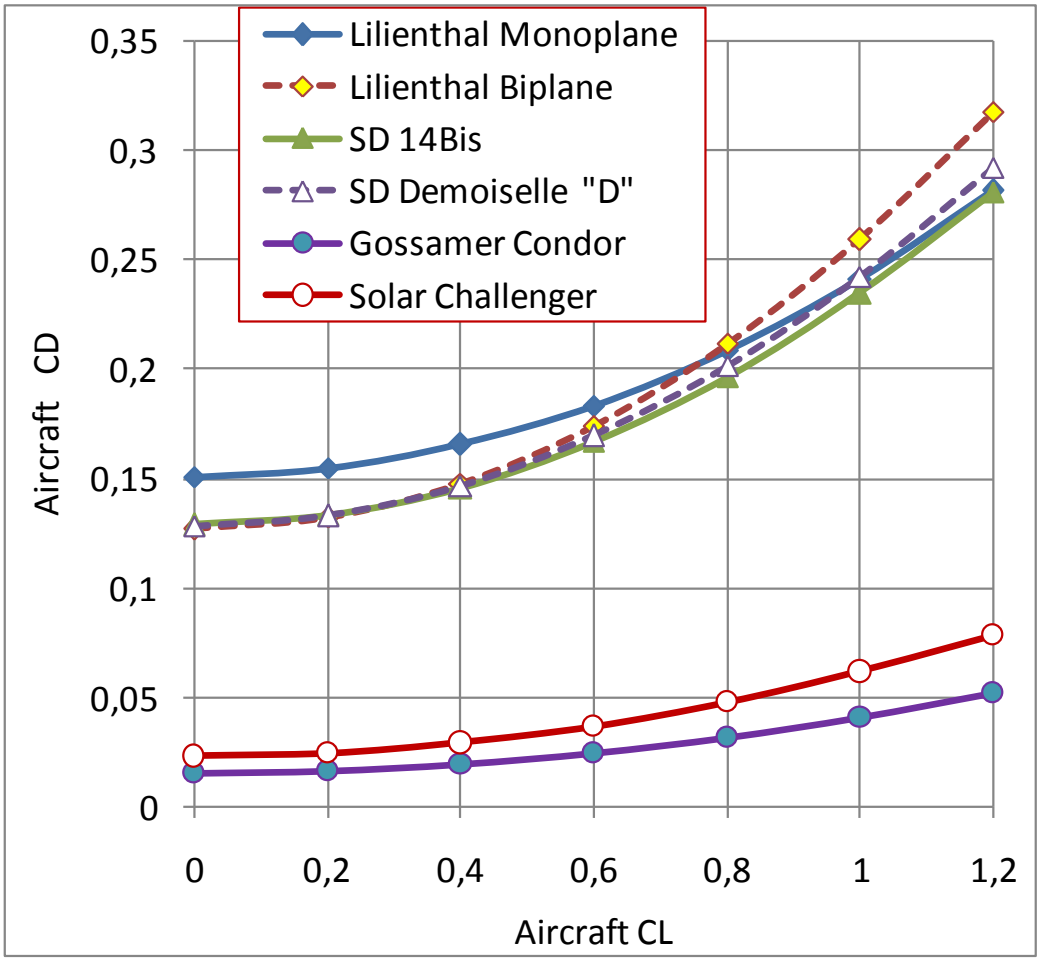

Figure 5.17: Comparison of drag polars of six low-wing load aircraft

Important performance parameters of some of the analyzed aircraft are presented in figure 5.19, compared with available reported parameters.

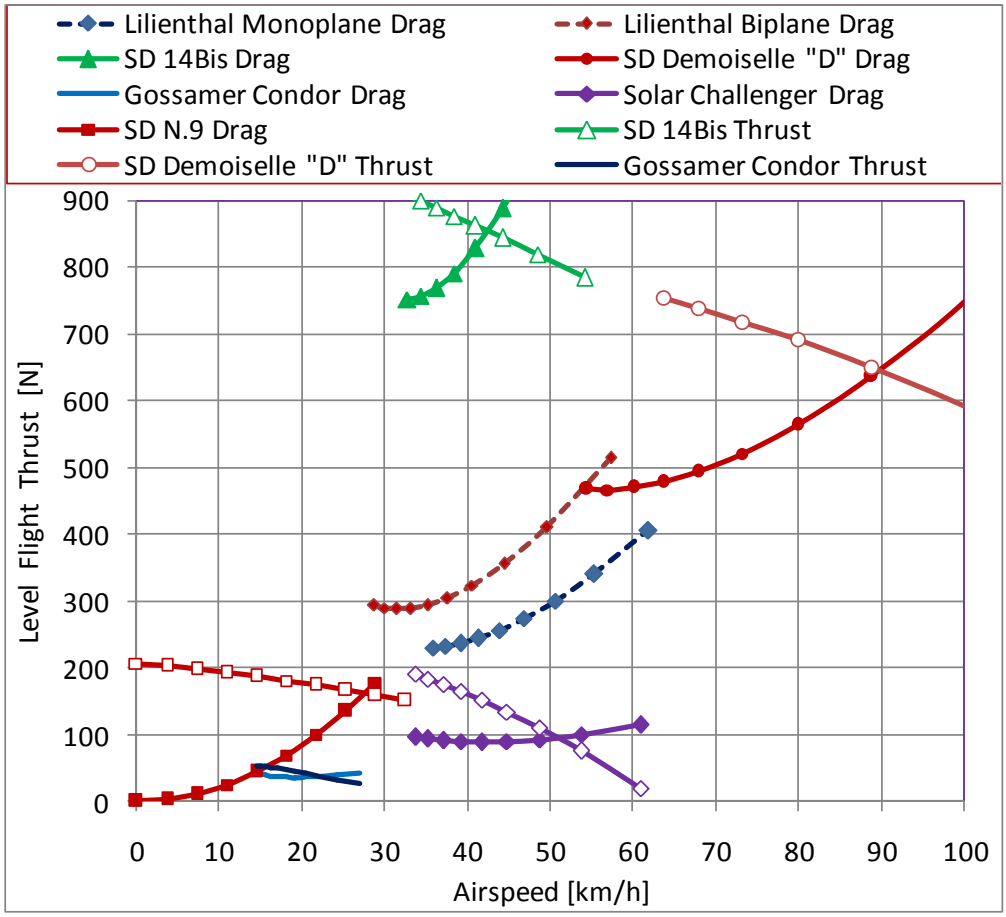

Figure 5.18: Drag and Thrust versus Speed for the analyzed aircraft

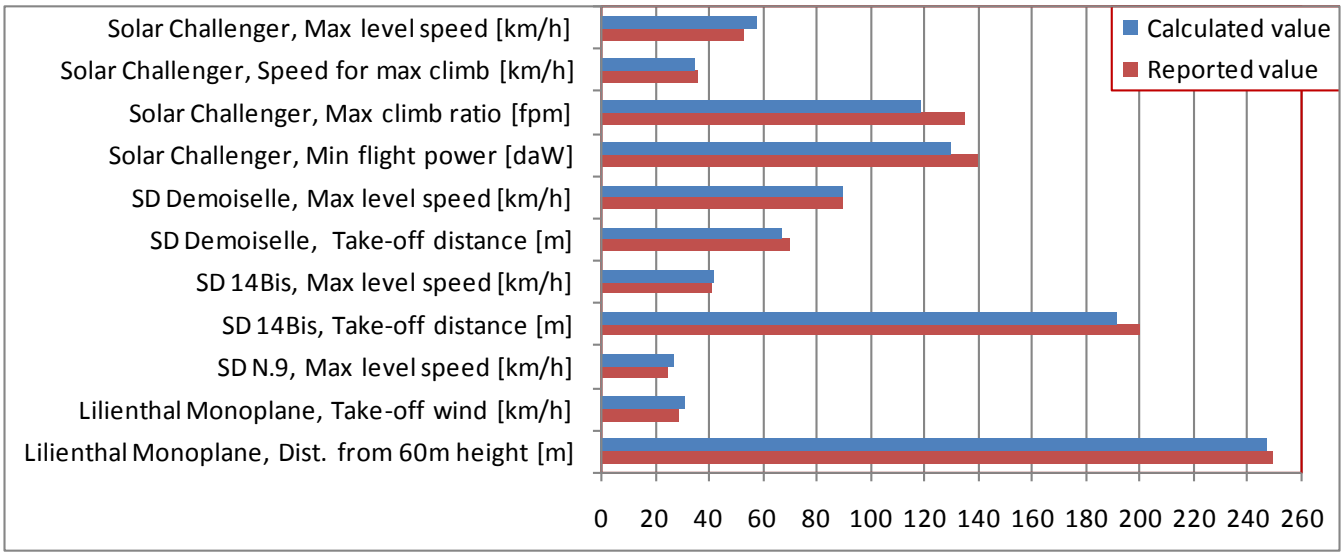

Figure 5.19: Comparison between calculated and reported values of performance parameters for the some of the aircraft studied

5.2.4) Comparison of results for a specific solar aircraft: Sunrise

The published results for Sunrise aircraft are compared to the corresponding calculated values, which have been obtained using the methodology presented in chapter 4. The published results for Sunrise are from flight tests and theoretical evaluations presented in Boucher (1985) and Boucher (2003). The comparisons are presented as follows.

a) Drag Polar curves for 'Sunrise I without Solar Panels':

The theoretical polar curve for Sunrise I at power-off condition is compared with the one reduced from flight trials in the figure 5.20. The aircraft is without solar cells. The curve reduced from flight tests is the dashed one, which is the one presented in figure 3.1. One can see from this figure the proximity between the two curves which can validate the drag evaluation method.

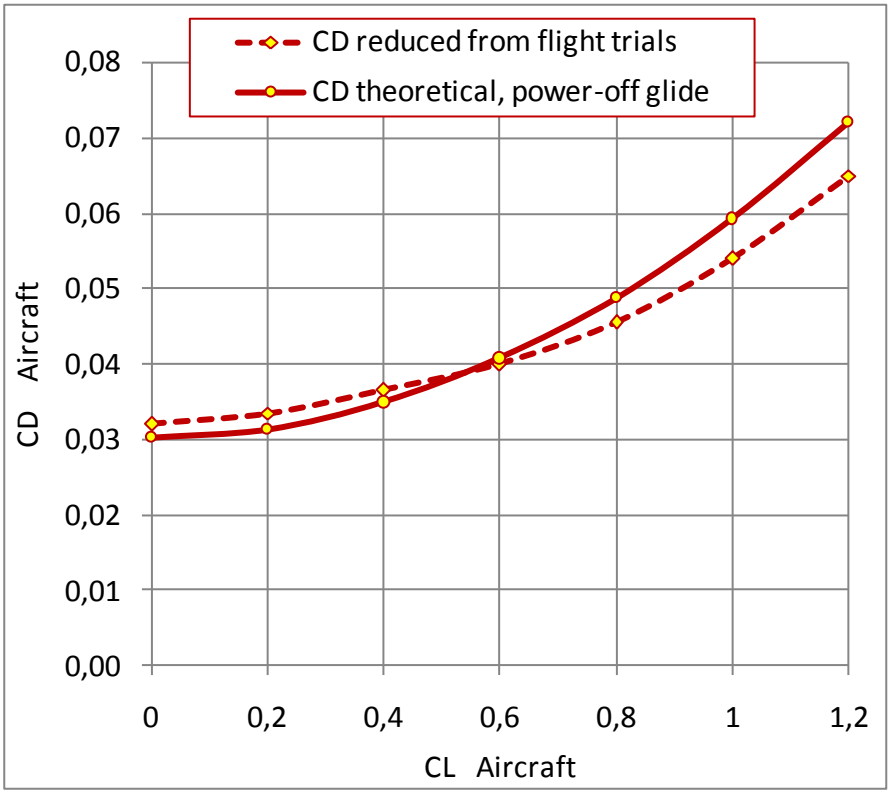

Figure 5.20: **Sunrise I without** solar array, comparison between drag polar curves: theoretical and from tests

b) Definition of the incremental Drag value for Sunrise I Solar Array:

By comparison of the Sunrise I polar curves from flight tests, with and without solar cells, presented in figure 3.1, and using the aircraft theoretical polar, the best match for the drag coefficient of the Solar Array referred to panel area is 0.0252 which is 210% above wing airfoil drag. This represents, with the associated interference, about 61% of increasing in the aircraft glide polar without the panels, and about 38% of the CDo of the aircraft with the solar panels.

The comparison between polar curves for Sunrise II is presented in the figure 5.21. Three curves are presented, the theoretical curves with and without solar panels, and the curve from flight trials with solar panels. Initially the thin curve, theoretical, of the aircraft without solar panels is calculated. By comparison of this curve and the dashed one, from flight tests, the value of ΔCD due to the solar panel is obtained. This value is found as 0,0071. This additional drag due to the solar panels represents an increasing of 24% on the CDo of aircraft without them, and a percentage of 19,4% of the aircraft CDo with them. These values are significantly lower than the ones from Sunrise I, showing the advancement on the lessons learned. But, despite this, these values indicate that strong efforts and attention must be employed in the solar aircraft design in order of not reduce the aerodynamic cleanness of the aircraft with the installation of the solar panels.

In figure 5.21, by adding the ΔCD value in the theoretical curve of without solar panels, it is obtained the third curve, the curve of theoretical CD for aircraft with solar panels, which is the thicker continuous curve. One can note that the polar curves - the dashed curve from flight tests; and the thicker continuous, theoretical curve - coincided along the whole range of CL, indicating that not only the CDo, but also the factor K, fully obtained theoretically, is well established.

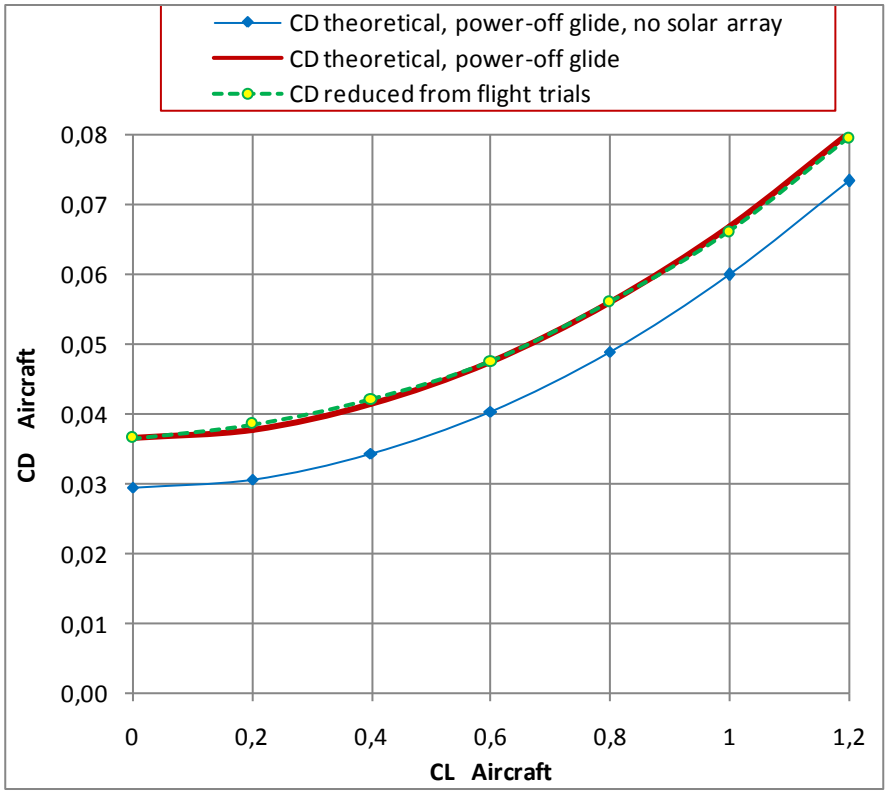

Figure 5.21**: Sunrise II** with solar array, drag polar curves; comparison between the curve reportedly reduced from flight trials, and the theoretical ones obtained through this work.

c) Performance of Sunrise I without solar arrays

Robert Boucher (1984) presents the curves of sink speed and climb speeds vs airspeed, for aircraft mass as 20 lbs, sea level, and 450 W of battery output, from flight tests. So it has been highly valuable to use the methodology to calculate these parameters and compare with the test results.

The engine efficiency is considered as 85%, according to Roland Boucher (2003). The drag considered is the one presented previously, with the following peculiarities:

- For glide flight propeller is stopped so its drag is considered
- For climb flight the drag due to power is considered, and the propeller effectiveness is calculated.

Propeller diameter is 32 inches, the pitch is about 15 inches, and RPM= 2000, according to Roland Boucher (2003). Propeller Blade Reynolds number is about 300 000, slightly above the level in which thick airfoils are loss their advantage over curved plates. So a conventional airfoil is considered for the propeller analysis.

Propeller curves have been calculated by the procedure presented in the chapter 4, and exemplified in sub-section 5.2.2. With the propeller curves, the climb rate can be calculated. The results of the climb rate and glide rate, compared to the flight test values are presented in the figure 5.22.

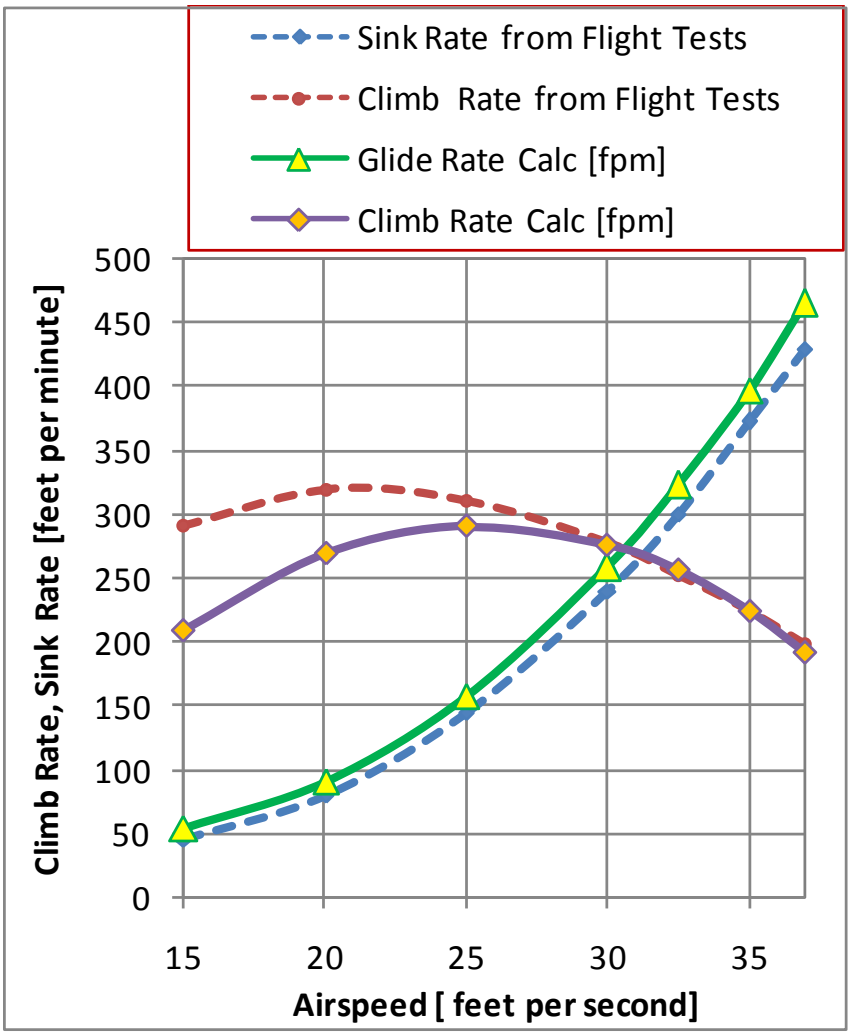

Figure 5.22**:** Comparison between calculated values (continuous lines) and the ones reduced from flight Tests for Sunrise I sink rate and glide rate.

In order to illustrate the importance of the propeller analysis, as performed for the other powered aircraft of this work, and presented in the chapter 4, the figure 5.23 presents the calculated Climb ratio, if the propeller effectiveness η_{prop} was assumed as having a constant value of 0.6, which has been suggested by Roland Boucher (2003). One can note by figure 5.23 that the calculated Climb rate values considering the Propeller Analysis (which leads the values η_{prop} to vary in function of

airspeed) are significantly closer to the values from flight tests, than the Climb values calculated with the constant η_{prop} value of 0.6.

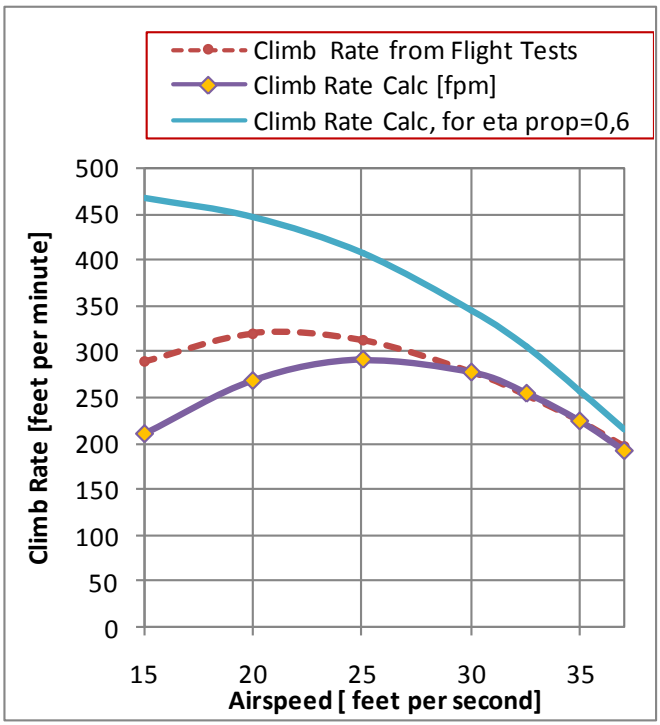

Figure 5.23**:** Sunrise I climb rate curves. Comparison between the one from Flight Tests and two ones calculated, with propeller methodology, and with constant effectiveness.

Three additional important remarks in terms of performance evaluation, to be noted are:

- As per figure 5.22, the order of magnitude of the calculated results for climb rate and glide rate, are close to the test results, and the tendencies of calculated results are similar to the results from flight tests; the calculated values are conservative compared to the test results.
- As presented in figure 5.23, in order to allow realistic comparisons, the propeller analysis shall be performed in order to obtain its effectiveness.
- For high altitude flights, or even for low altitude flights with lower RPM (which can happen at the starting of a purely solar-powered mission, with low sun power) the propeller Blade Reynolds number could easily reach values lower than 100 000, in which the conventional blade airfoil should drastically diminish its L/D values, and the propeller could turn to be significantly less efficient.

d) Mission Analysis of Sunrise I: Nominal Evaluation

The altitude profile considered for the Sunrise I is the one presented in figure 3.2. This is not the really flown profile, but the intended one, according to Boucher (1985). This profile is reproduced again in the figure 5.24, compared with the calculated profile, using the Mission Analysis Methodology presented in chapter 4, and the drag and thrust values considered in the previous paragraphs of this sub-section 5.2.4. The main parameters taken into account for this Mission Analysis are presented in the column corresponding to the Run#8 of table 5.2. It is possible to note at the figure 5.24 that the altitudes obtained are almost the same, and the flight profiles resulted to be very similar; which can increase the confidence in the methods developed. As additional information, two important parameters corresponding to the altitude profile of figure 5.24 are presented in figure 5.25: The local solar intensity variation along the day, which is an input; and the ratio of climb RoC, which is an output.

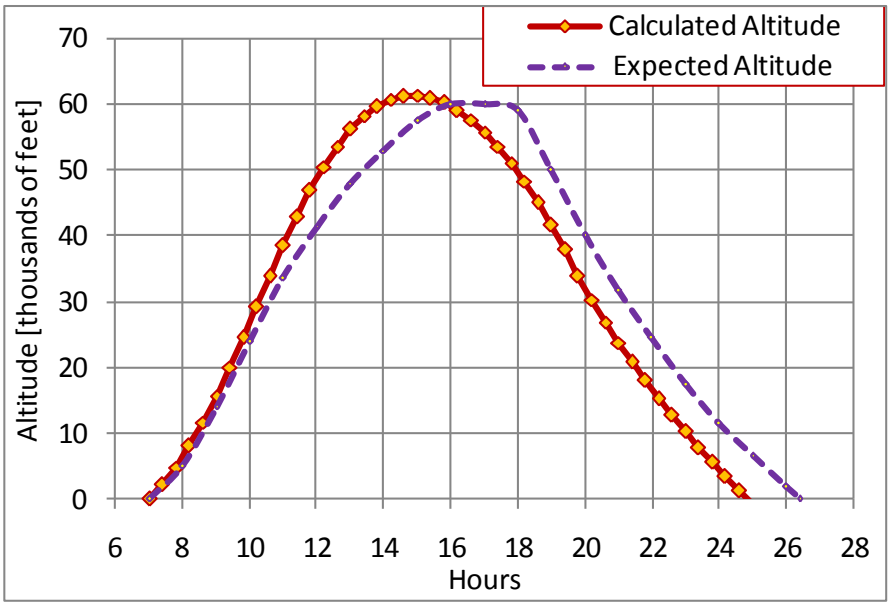

Figure 5.24**:** Sunrise I, comparison of mission altitude profile for 21June, California, USA; calculated values and expected from its designers.

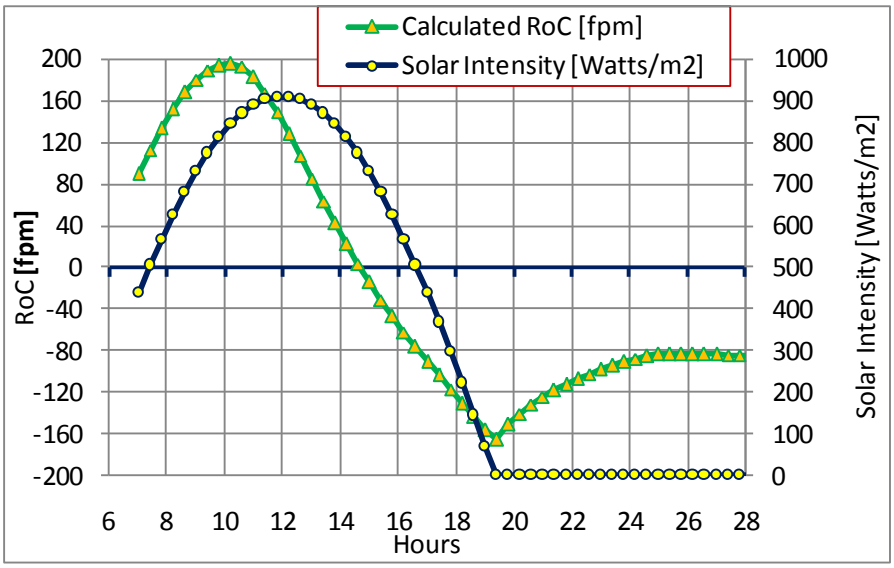

Figure 5.25**:** Sunrise I, mission analysis: Rate of climb (output) and solar intensity at jun21, California (input).

e) Mission Analysis: Sensitiveness Studies

In order to better understand the cause-and-effect relationships in the Sunrise I performance potential, mainly focusing the capabilities of achieving or not high altitudes, parametric – or sensitiveness - studies have been performed in terms of Mission Analysis. These studies are summarized in table 5.2 and the flight profiles obtained are presented in figures 5.27 and 5.28. From the performed runs for the parametric study, the first run, the most optimistic one, corresponds to the profile calculated and presented by Roland Boucher (2003). The run #8 corresponds to the profile presented in figure 5.24, which is taken as the nominal one. From the table 5.2 it is possible to understand the dependency of the maximum altitude and rate-of-climb from the aircraft mass, drag, lift coefficient, and solar array effectiveness. All other data are the same as the nominal profile presented above.

The figures 5.27 and 5.28 present the Mission altitude profiles corresponding to the runs #1 to 10 of table 5.2.

Table 5.2: Parametric studies for Sunrise I Mission Analysis

	Run #:	1	2	3	4	5	6	7	**8**	9	10	11
Input	CD const 0/ variab 1:	0	1	1	1	1	1	1	**1**	1	1	1
	CL :	0,90	0,90	0,90	0,90	0,90	0,90	0,90	**0,90**	0,90	0,60	0,60
	Propeller Effectiven.:	0,62	0,62	0,62	0,62	0,62	0,62	0,62	**0,62**	0,62	0,62	Var
	Array effectiveness:	0,125	0,125	0,095	0,095	0,095	0,095	0,125	**0,113**	0,095	0,095	0,095
	Mass [kg]:	9,68	9,68	9,68	9,68	9,68	11,79	11,79	**11,79**	11,79	11,79	11,79
	CD arrays:	0,000	0,000	0,000	0,000	0,019	0,019	0,019	**0,019**	0,000	0,019	0,019
	Aircraft CDo @SL:	0,022	0,022	0,022	0,0314	0,051	0,0503	0,0503	**0,0503**	0,0309	0,0491	0,0491
Output	Max altitude [kft]:	104,5	86,4	75,9	72,3	65,4	52,9	66,8	**61,4**	62,1	39,0	27,1
	RoC [fpm]:	327,0	320,5	245,4	233,3	209,7	160,1	221,3	**196,3**	184,0	123,0	84,1

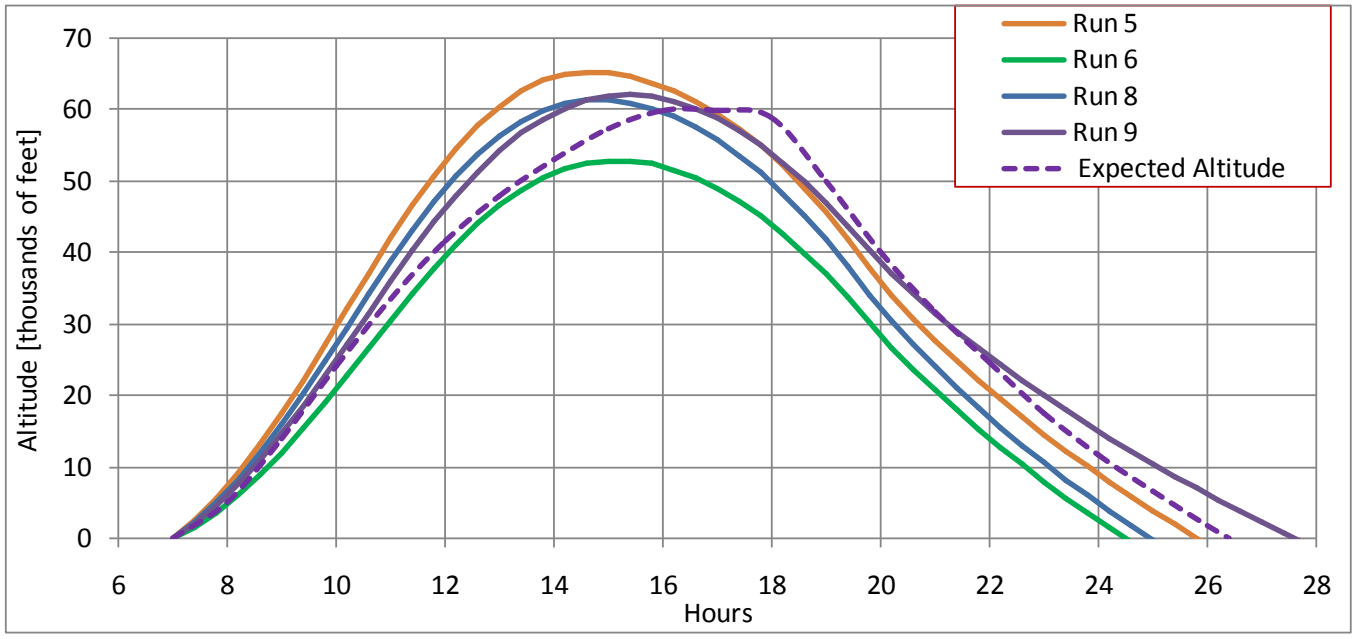

Figure 5.27**:** Sunrise I, mission altitude profile, sensitiveness studies; 21June, California, USA

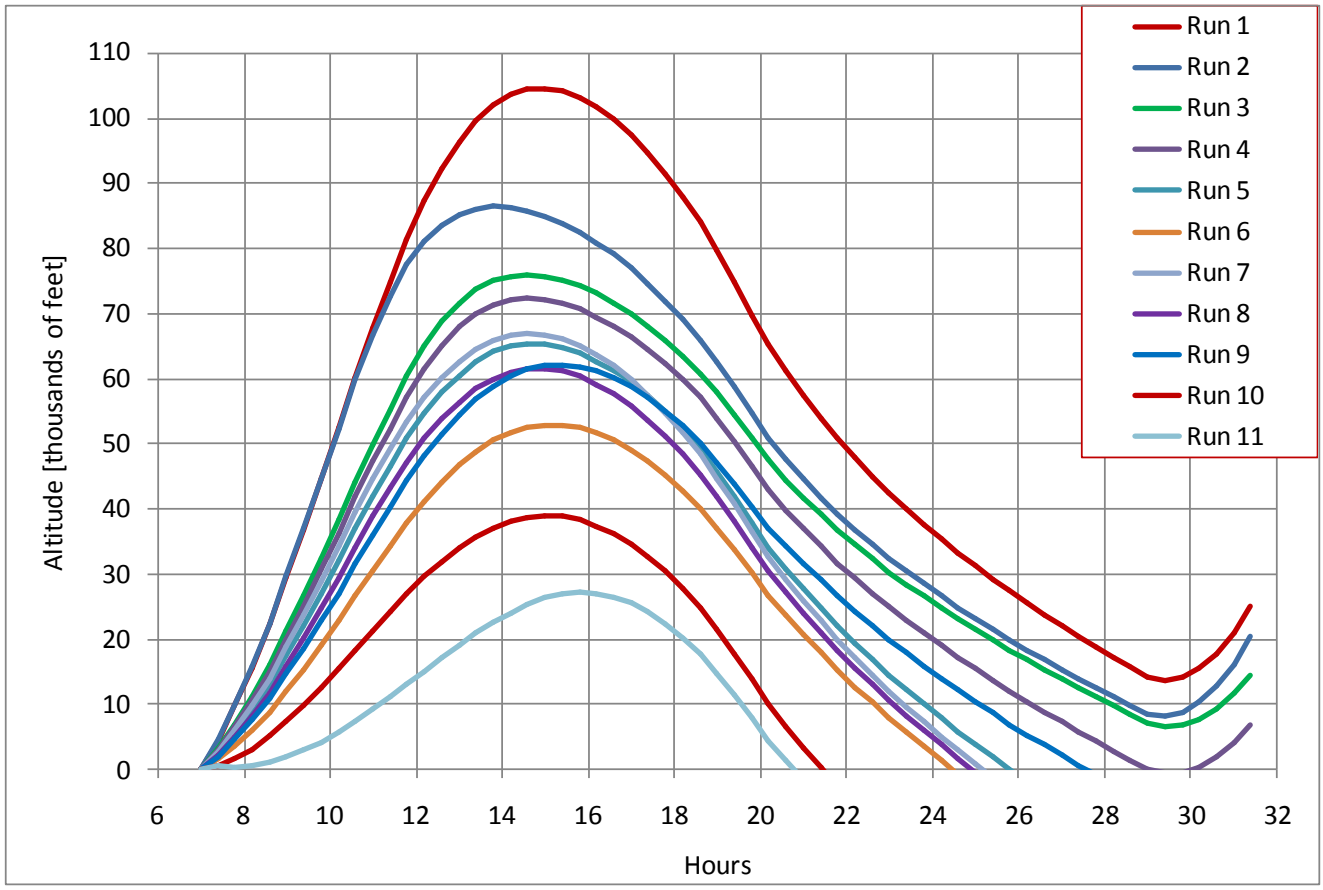

Figure 5.28**:** Sunrise I, mission altitude profile, sensitiveness studies;
21June, California, USA, all runs

The same flight mission analyses presented in figures 5.27 and 5.28 for the Sunrise aircraft have been also performed for Helios, Solong, and High Flight aircraft. The mission analysis results for High Flight aircraft are presented in chapter 6.

6) RESULTS

This chapter presents examples of conceptual design of solar aircraft, based on the tools and metrics developed and presented in chapter 4. The examples are three different aircraft, defined through the tools, from different mission requirements.

These three aircraft have been defined, from the above requirements, mainly from the Method for Solar Aircraft Design, presented in section 4.5. Once these three aircraft are defined, their configurations are presented in section 6.3.

One of these aircraft is destined to high altitude flight. So specifically for this aircraft, the specific tool for checking and adjustment of the aircraft Mission Analysis Method, presented in section 4.11, is used. The main outputs from this method for this specific aircraft are presented in section 6.4.

Both tools, the Method for Solar Aircraft Design and the Mission Analysis, can be run with the contributions from the other tools and metrics as: The Solar Incidence Model presented in section 4.12, the Mass Estimation presented in section 4.13, the Drag Analysis presented in section 4.9, the Propeller Studies presented in section 4.8, the Reynolds Influence on Lift and Drag presented in section 4.6.

6.1) Requirements for the Conceptual Design of the three Solar Aircraft

For each of the three aircraft one a specific mission and requirement has been defined, and due to this, the configuration obtained from each one is significantly different from the other ones. In order to identify each one, the three aircraft received names related to their main functions. The aircraft are identified as the Sport Flight, the Travel Flight and the High Flight.

The main characteristics and requirements for these aircraft are:

- Sport Flight: A manned aircraft for low altitude (one pilot only in an unpressurized cabin), aimed for daylight flights, with additional batteries for 1 hour of horizontal flight. Take-off and landing are allowed by a ‘as-simple and light as possible’ landing gear. Engine, reduction and propeller

should be as light as possible; propulsion for take-off can be marginal, i.e. typical take-off is expected to be from a prepared hilltop. Glide ratio better than a normal hang-glider is expected; not needing to be better than 30 to 1 (normal-class sailplane).

- Travel Flight: A constant, very low altitude, manned aircraft (one pilot only in an unpressurized cabin), aimed for continuous flights of more than 24 hours, with use of batteries for night flight. Payload is the pilot, shelter, and minimum quantity of water and food to allow 3 days of flight, which is in the range of 85 to 120 kg. Pilot should have enough space to change his position during flight.
- High Flight: A variable altitude, unmanned aircraft, aimed for flights of more than 24 hs; batteries shall be kept as a minimum as possible and should be used only for take-off and initial climb; night flight should be accomplished through gliding flight; no atmospheric updrafts should be taken into account. Payload can be in the range of 0.8 to 5 kg.
- Additionally to the specific requirements, a common requirement for all is that the three aircraft shall have propulsion by electrical engines only, and their power supply shall be obtained only through the solar cells installed in the aircraft.

6.2) Example of the Design Parameters Definition Iterative Process

From the requirements presented in the previous section, the Method for Solar Aircraft Design, presented in section 4.5, is used for the definition of the aircraft parameters.

In the process of using the Method for Solar Aircraft Design is a iterative procedure, in which initial values are given as inputs, defining the starting point for the analysis. And from this initial point, through the Method, the aircraft characteristics are recalculated internally, up to a convergence is obtained. Some parameters, associated to physical constraints, physical laws, design requirements and assumptions, are kept constants during the iterative process.

The main input data in terms of the constant parameters for the iterative process is presented in table 6.1; and the final values obtained after the iterative process are presented in the table 6.2. Both tables are for the three aircraft.

Between these tables, the variation of the values of Wing Area and Total Mass, for the Travel Flight aircraft, along the calculation iterations is shown in figure 6.1; in this figure one can note the convergence of these values along the calculation iterations.

Table 6.1: Data and Constraints Pre-Defined for the Conceptual Design of Three Different Types of Solar Aircraft

Aircraft :	High Flight	Travel Flight	Sport Flight
Local of flight :	Lat -30°		
Date of flight :	23 Dec		
Daily Solar Intensity [kW.h/m^2] :	8,55		
1/24 of solar cells daily output [W.h/m^2] :	53,4		
Morning time limit of available direct solar power for flight [hs] :	6,0	7,5	
Afternoon time limit of available direct solar power for flight [hs] :	18,0	16,5	
Duration of flight powered directly with solar cells [hs per day] :	12,0	9	
Duration of flight powered with support of batteries [hs per day] :	0	15	1
Initial Payload [kg] :	5	120	80
Wing Oswald Efficiency Factor at Cruise Reynolds Number :	0,95	0,95	
Wing CDo Coefficient at Cruise Reynolds Number :	0,011	0,009	
Empennage Equivalent Drag Area 'Cd*S' [m^2] :	0,022	0,044	
Fuselage Equivalent Drag Area 'Cd*S' [m^2] :	0,001	0,49	

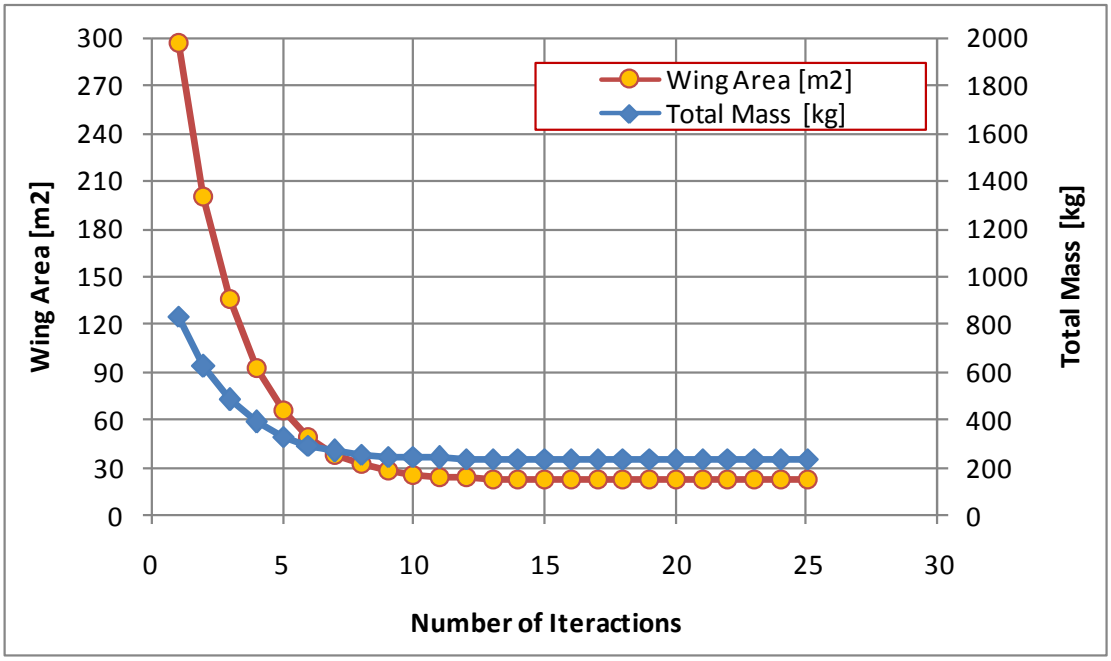

Figure 6.1: Visualization of the parameter values variation throughout the iterative design process of the Method of Solar Aircraft for the Travel Flight aircraft.

Table 6.2: Parameters Obtained from Conceptual Design of Three Types of Solar Aircraft

Aircraft:	High Flight	Travel Flight	Sport Flight
Parameter	Value		
Cruise Speed EAS [km/h] :	25	27	43
Cruise Speed EAS [m/s] :	6,9	7,5	11,9
Volume of Buoyancy Gas Envelope [m^3] :	0	220	0
Lift Coefficient at Cruise :	1,00	0,62	0,83
Wing Aspect Ratio:	15	10	6
Mass of Batteries:	0	65	11
Mass Engine + Cells + Controls + Harness :	7,9	25	32
Buoyancy Envelope Mass :	0	13	0
Structural Mass :	6,8	12	32
Total Mass :	20	234	154
Buoyancy Envelope Area [m^2] :	0	206	0
Wing + Fuselage wetted Area [m^2] :	14,6	263	55
Buoyancy force [kg] :	0	186	0
Weight minus Buoyancy [kg] :	20	48	154
Wing Area [m^2] :	6,7	22	21
Wing Span [m] :	10,0	15,0	11,0
Wing Mean Geometric Chord [m] :	0,67	1,5	1,9
Input power at Engine for Cruise [hp] :	0,07 to 0,66	0,86	2,12
Distance Flown in 1 Day [km] :	2260	648	430
Flight Time per Day [h] :	24	24	10
Buoyancy Envelope Length [m] :	0	17	0
Buoyancy Envelope Diameter [m] :	0	5,2	0,0
Buoyancy Envelope Frontal Area [m^2] :	0	21	0
CD * S Buoyancy Envelope [m^2] :	0	1,5	0,0
Total CD * S [m^2] :	0,100	2,2	0,7
$S*k*CL^2$ [m^2] :	0,149	0,3	0,8
Cruise Power Delivered to the Air, DV [watts] :	51 to 416	647	1588
Engine Shaft Power at Cruise, DV / η_{PROP} [watts] :	84 to 693	863	2117
Engine Maximum Power [hp] :	0,79	4,6	11,4
Solar Area needed [m^2] :	6,0	16,1	16,5
Solar Area [m^2]:	6,0	17,6	16,6
Solar Area at Fuselage [m^2]:	0,0	0,0	0,0
Solar Panel Length at Fus /Fuselage Length :	0,00	0,00	0,00
Wing Structural Mass [kg] :	4,1	8,6	23,7
Wing Structural Mass/Area[kg/m^2] :	0,61	0,39	1,14

6.3) Definitions for the New designs

The three examples of different applications of Solar Aircraft are presented as follows; each one defined to comply with the different Mission Requirements presented in section 6.1. The aircraft names are provisory and are intended to provide easy identification of the aircraft according to the required mission. The configurations obtained for the three aircraft, the Sport Flight, the Travel Flight and the High Flight, are sketched in figures 6.2, 6.3 and 6.4 respectively.

6.3.1) The Sport Flight, Solar Aircraft Proposal:

Configuration characteristics of speed, mass, dimensions, power obtained:

- Cruise EAS=43 km/h @ CL=0.83, 10hs (430km) of flight per Day;
- MTOW=154 kg, EEW=80 kg;
- Span=11m, Total Area=21m^2, Solar Area= 16.6 m^2, max engine power=10 hp.

Mass breakdown:

- Batteries: 11 kg, allowing 1 hour of flight; engine + cells + electrical systems: 32 kg;
- Structure: 30 kg; payload (pilot): 74 kg.

Other relevant characteristics:

- Retractable nose landing gears, foldable propeller, low-cost solar cells;
- Straight surfaces behind leading edge; a la Facetmobile, as presented by Wainfan (2008);
- Can be disassembled in 3 parts;
- Can be launched in hang-glider mountain sites, and landed in small fields.

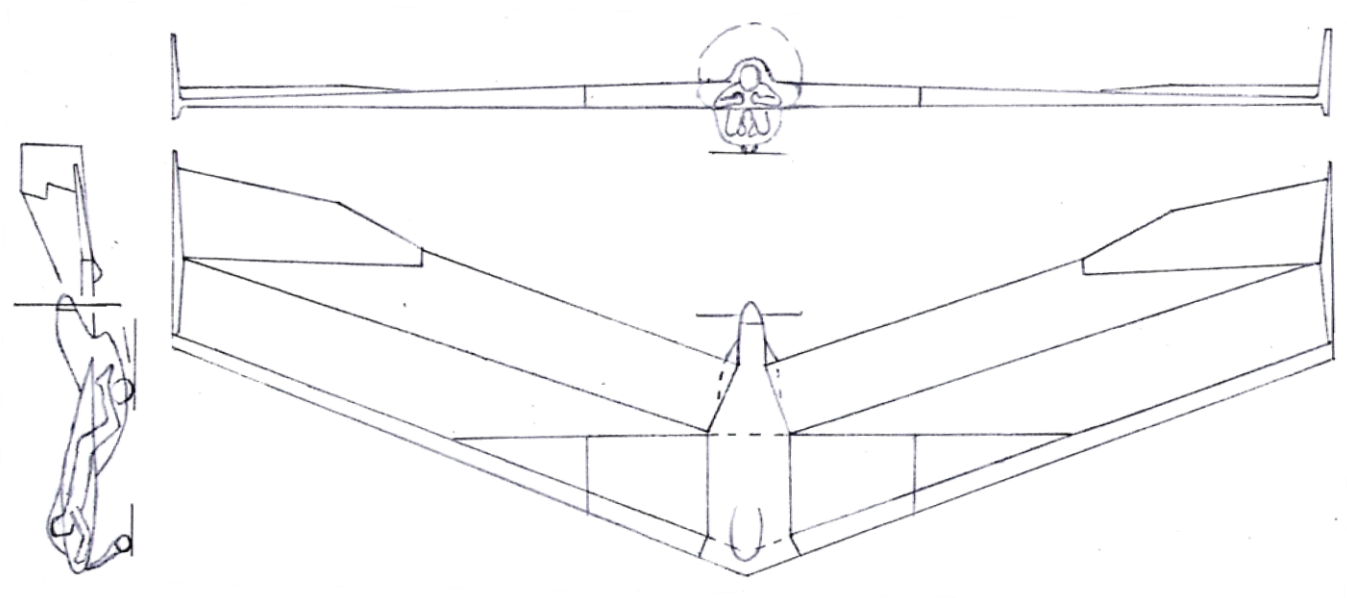

Figure 6.2: “Sport Flight” Solar Aircraft Proposal

6.3.2) The “Travel Flight” Solar Aircraft Proposal:

Configuration characteristics of speed, mass, dimensions, power obtained:

- Cruise EAS=27 km/h @ CL=0.62, 24hs (650km) of flight per day;
- MTOW=235 kg, EEW=150 kg, Buoyancy force=185 kgf;
- Span=15m, Length =17m Wing Area=22m^2, Solar Area= 17.5 m^2,
- Gas Volume = 220 m^3 max engine power=5 hp.

Mass breakdown:

- Batteries: 65 kg, engine + cells + electrical systems: 25 kg;
- Navigation, communication, emergency and additional systems: 12 kg;
- Structure: 35 kg; payload (pilot+water): 85 kg; gas envelope (or ‘hull’): 13 kg.

Other relevant characteristics:

- Solar Panels above the envelope and in the outboard part of wings.
- Internal space for pilot to stay in different positions:
    - Standing, using part of the ballonet volume; sitting; lying; or prone.
- Normal controls in prone or sitting position.

- Autopilot, GPS and altimeter for autonomous flight during pilot sleeping periods.
- Besides the solar features, the general flying machine concept and dimensions are based on Santos-Dumont airships N.9, presented in sub-section 5.2.2, and N.16.

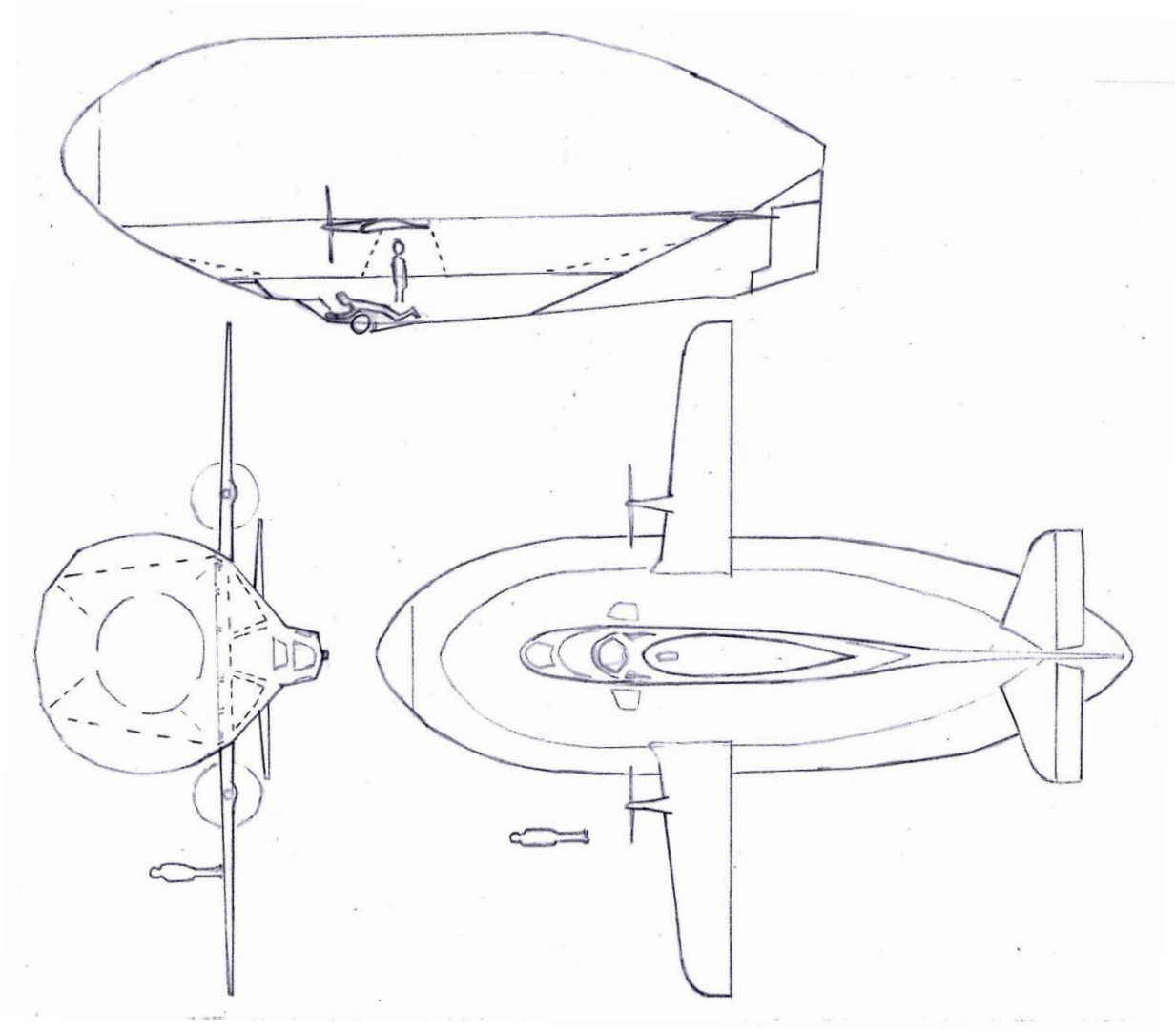

Figure 6.3: “Travel Flight” Solar Aircraft Proposal

6.3.3) The “High Flight” Solar Aircraft Proposal:

Configuration characteristics of speed, mass, dimensions, power obtained:

- Cruise TAS=17 to 138 km/h @ CL=1,0
- From December and January, Lat 30: altitude: 103 to 9 kft, 24hs (1450km) of flight per day;

- MTOW=30 kg, M/S=1.4 kg/m^2
- Span=18.5m, Wing Area=21m^2, Solar Area= 19m^2, A=16,
- Level power: 0.1 to 2.2 hp, max engine power=3.7 hp.

Mass Breakdown:

- Batteries: 0.8 kg, structure: 9.5 kg, solar cells: 13.5 kg, payload (sensors) 0.8 kg.

Other relevant characteristics:

- Launched by very-low speed trolley, or by assistance of team members, running together;
- Four to five engine-propeller assemblies; propellers are fold automatically, a la 'Solong', during the glide segments of the flight;
- Wing is divided in three segments to allow easier transportation;
- Will need ground station support to check atmosphere (avoid bad meteorological conditions, or cloudy sky regions, during low-altitude flight phases);
- Systems and structure shall be qualified for 'under zero' temperatures, down to -60^o Celsius.

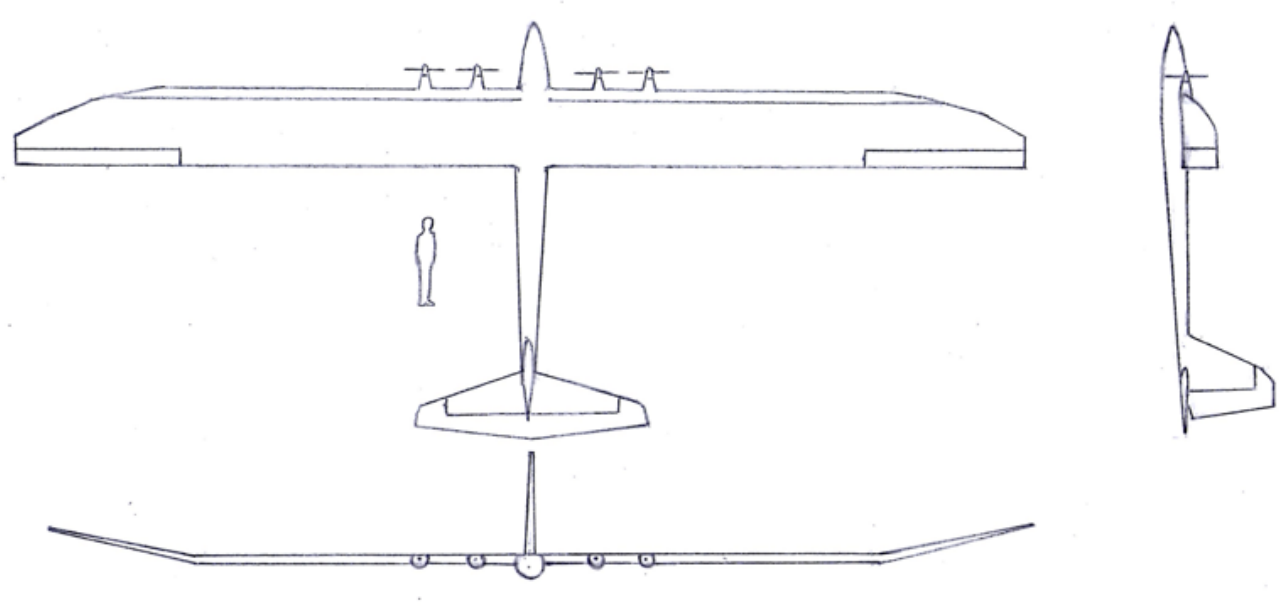

Figure 6.4: "High Flight" Solar Aircraft Proposal

6.4) Example of Mission Analysis

The Mission analysis is a tool developed for fine adjustment of the aircraft parameter values and for validation of the aircraft characteristics through simulation of the intended mission. This tool is more applicable, in terms of solar aircraft, for missions in which large variations of altitude occur. These large variations of altitude can occur for missions of some solar aircraft aimed for long endurance; and are destined to store part of energy collected from the sun, as mechanical energy, to be used during the night parts of the flight. The method developed for Mission Analysis is presented in chapter 4.

In these flights with large variation of altitude, there are large variation of air specific mass, the aircraft needs to accelerate as it climbs, in order to keep the same equivalent airspeed, the needed power increases due to the increasing of true airspeed, and the aerodynamic characteristics of the wing and propeller airfoils can change drastically, as also presented in chapters 3 and 4.

Due to this, in order to validate and adjust the values obtained from Method for Solar Aircraft Design, whose results are presented in the section 6.2, the Mission Analysis shall be performed. This is applicable for aircraft aimed to missions of large altitude variation. Among the three aircraft defined with the Method for Solar Aircraft Design, and described in the section 6.3, this is the case, of the High Flight aircraft. The following subsections present, as example of use of the method, the main inputs and outputs.

6.4.1) Initial and Intermediate Data

The initial data for the analysis is presented in the table 6.3. The intermediate data, which do not need to be specifically defined for each case, i.e. which are a consequence of the main data, are presented in Table 6.4.

Table 6.3: Example of main data for mission analysis

Data Parameter and Unit	Value
Aircraft Name:	High Flight
Battery/(Battery + Payload) Mass Ratio:	0,500
Mission Simulation Time Interval [minutes] =	10,0
Daily Mean Equivalent Value for Wind Updraft Speed [m/s] =	0,00
Aircraft Total Mass, M [kg] =	30,0
CL cruise =	1,00
Code for Irradiance Profile Chosen:	10,0
M/S [kg/m^2] =	1,4
Solar Panel Area/Wing Area Ratio, SAR =	0,90
Mean Solar Panel Effectiveness, ηcell =	0,15
delta Cdo=	0,002
A =	16,0
e =	0,95
Propeller + Reduction+ Engine Effectiveness, ηengprop =	0,60
Clmax =	1,50
Initial Day Hour of Flight:	7,0
Coef#1 for Structural Wing Mass Trend:	0,0543
Coef#2 for Structural Wing Mass Trend:	1,1111
Wing Structural Mass/ Aircraft Structural Mass, WSM/Mst =	0,7
Engine Mass/Power Ratio [kg/kW] =	1,2
Solar Cells Mass/Area Ratio [Kg/m^2] =	0,7
Eng Max Power/ Max level Power =	1,0
Control &Cable mass [kg] =	2,0
'bat power at engine' / 'additional req. to achieve horizontal flight' Ratio =	0,80
Part from Power from solar cells to feed battery =	0,016
Effectiveness on transmission Cells to Battery =	0,90
Battery Mass/Energy Ratio [kg/kWh] =	5,0
Lower Limit altitude for feeding Engine with Battery [kft] =	10,0
Upper Limit altitude for stop feeding Engine with Battery [kft] =	10,0

Table 6.4: Example of intermediate data during Mission Analysis

instants in 24hs:	144
S [m^2] =	21,4
Ssol [m^2] =	19,3
M to acelerate [kg] =	30,0
Cdomin =	0,0521
Cdomax =	0,0112
E cruz =	43,6
k =	0,0209
Span [m] =	18,52
Chord [m] =	1,16
M .$A^{1/2}$/100 =	1,20
Vs [m/s] =	3,9
Vs [km/h] =	13,9
M str [kg] =	9,5
M cells [kg] =	13,5
EEW [kg] =	28,3
Payload+Bat [kg] =	1,7
Bat [kg] =	0,8
Payload [kg] =	0,8
M struct wing [kg] =	6,65
M struct wing/S [kg/m^2] =	0,31
M eng+Cells +Controls+Harness =	18,8
CD*S tail [m^2] =	0,073
CD*S fus [m^2] =	0,0004
Cd*S wing [m^2] =	0,229
interference =	0,018
CD*S total [m^2]=	0,3211
CDo =	0,015
CDtot/CDwing =	1,400
S wet fus=	0,9721
S wet wing =	45,00
S wet wing+fus=	45,972
S*K*CL^2=	0,449

6.4.2) Example of Results from a Mission Analysis

The Plots below present the most important flight mission parameters, for the proposed High Flight solar aircraft. These parameters are the output from the mission simulation routine, developed in this work, and described in the chapter 4, Methodology. The Aircraft propeller is also defined and analyzed by the author through the methodologies related to propeller, airfoil and Reynolds Number, also presented in the chapter 4.

The main important simulation outputs are presented in the figures 6.5 to 6.22. The figures are grouped in two types, explained as follows. In Figure 6.5 up to Figure 6.17, the time histories of the main parameters are presented. From these figures the aircraft movement and the main relation between the parameters can be checked. The second group of results, from figure 6.18 up to figure 6.22, is the selection of important relationships between some of the parameters.

From this second group of results, the most important figure is the 6.19, in which the Propeller effectiveness is plotted in function of advance ratio 'J'. It is possible to observe in this curve the transition of the propeller effectiveness between two curves, one for low altitude, with higher effectiveness, and one for high altitude, with lower effectiveness. The difference between the effectiveness of both curves is due to the difference of Reynolds numbers. One can note that the propeller is operating between the two curves, and the variation of the propeller effectiveness is a function of the Reynolds number at the time interval. One can also note that, despite the propeller is specifically designed for the low Reynolds number characteristic of the high altitudes of the mission; the effectiveness is low if compared with conventional, low altitude propellers. This is an expected feature, from information collected related to the existing high-altitude solar aircraft. The important aspect in this case, is that it has been possible to quantify the effect of the low Reynolds number not only in the wings, but also on the propeller, it has been possible to design a propeller accordingly, and it has also been possible to check that, despite the expected low effectiveness compared to a low-altitude propeller, the continuous flight of the aircraft can be feasible.

a) Mission Simulation Time Histories:

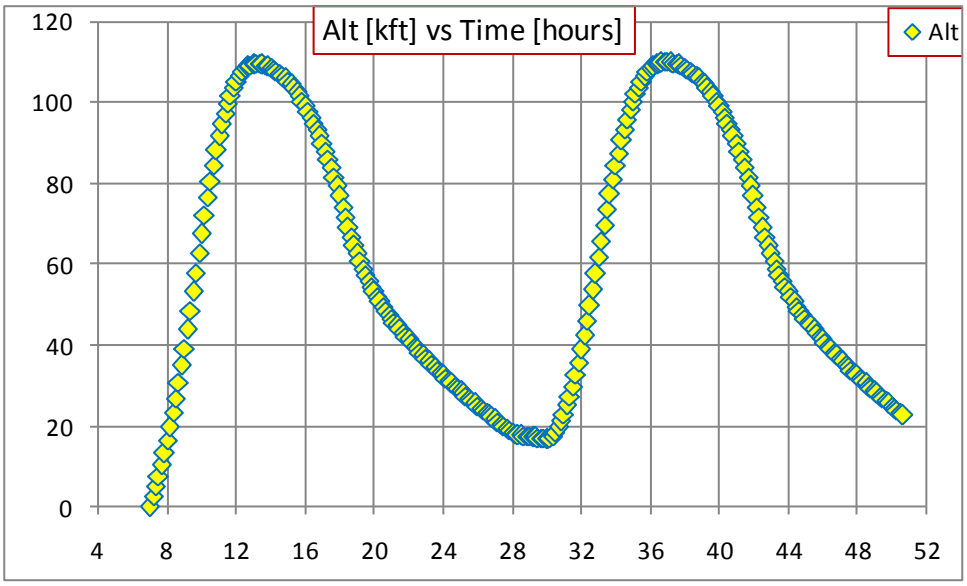

Figure 6.5: "High Flight" mission time history: Altitude [kft] vs time [hs]

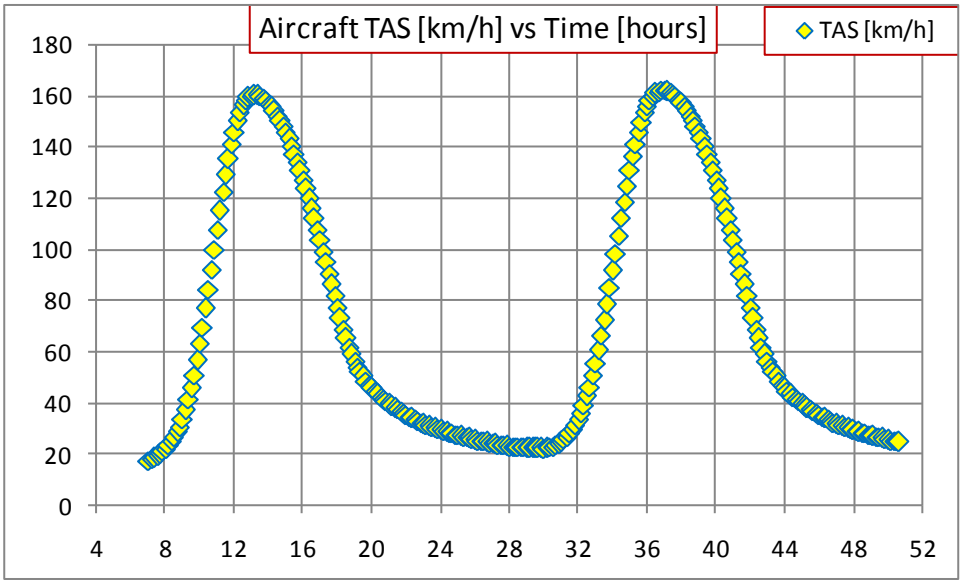

Figure 6.6: "High Flight" mission time history: TAS [km/h] vs time [hs]

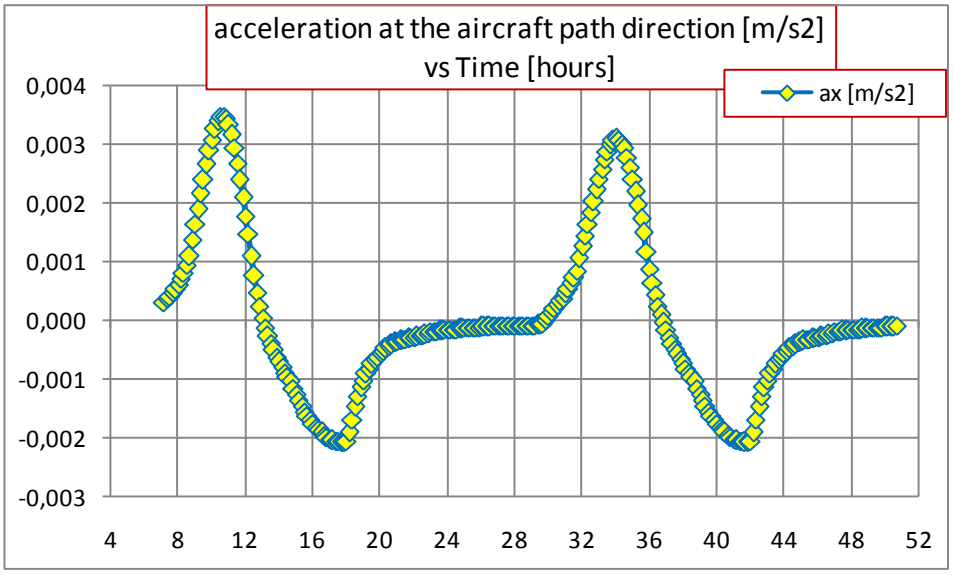

Figure 6.7: "High Flight" mission time history: acceleration in path direction [m/s^2] vs time [hs]

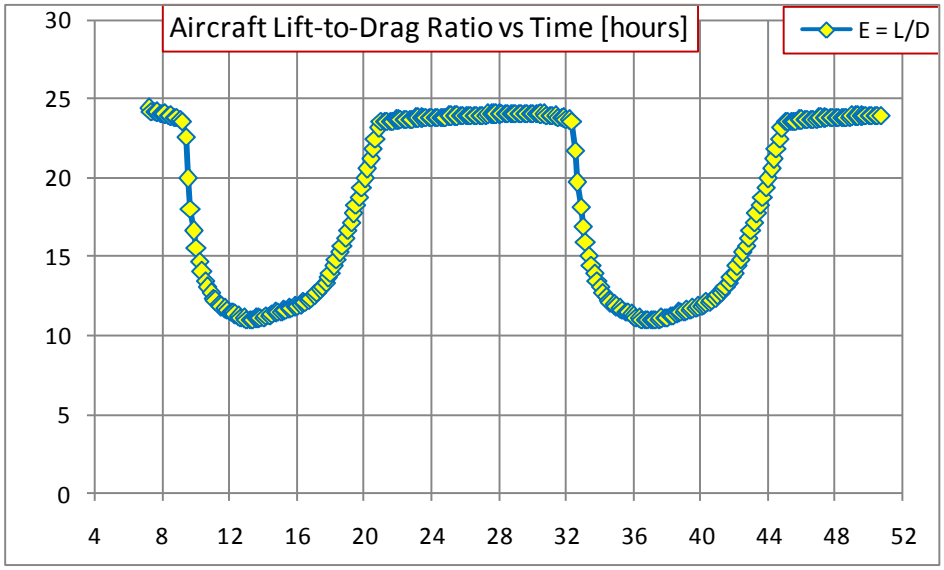

Figure 6.8: "High Flight" mission time history: Lift-to Drag ratio vs time [hs]

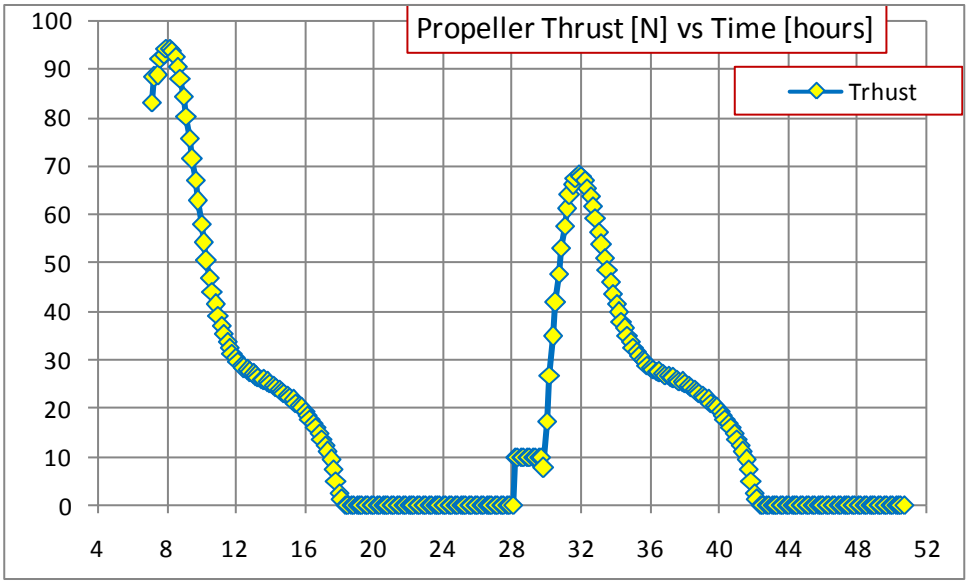

Figure 6.9: "High Flight" mission time history: Propeller thrust [N] vs time [hs]

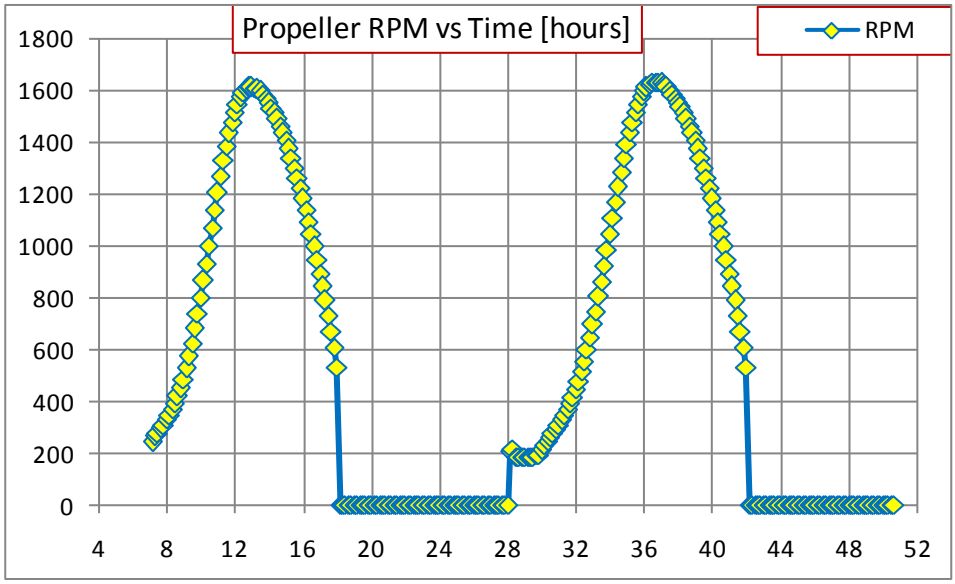

Figure 6.10: "High Flight" mission time history: Propeller RPM vs time [hs]

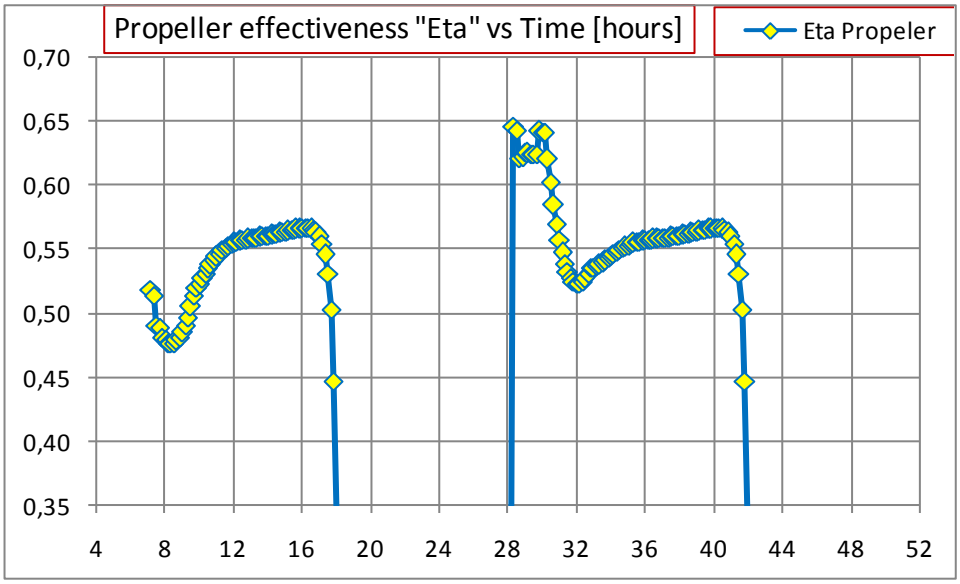

Figure 6.11: "High Flight" mission time history: Propeller effectiveness vs time [hs]

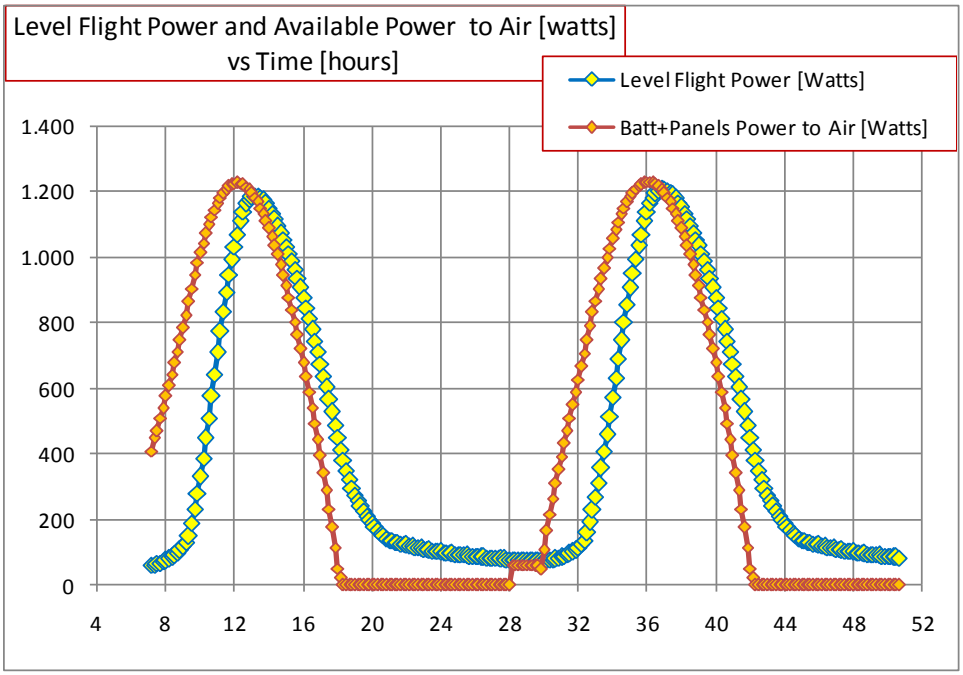

Figure 6.12: "High Flight" mission time history:
Available power and horizontal flight power, vs time [hs]

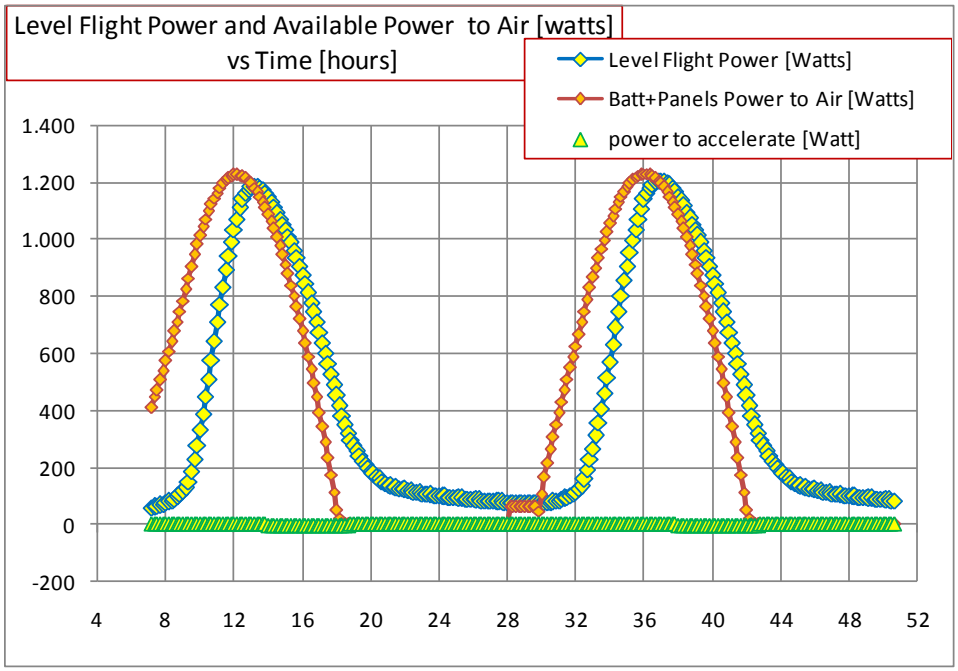

Figure 6.13: "High Flight" mission time history:

Same figure as 6.12, but adding the necessary power to accelerate vs time [hs]

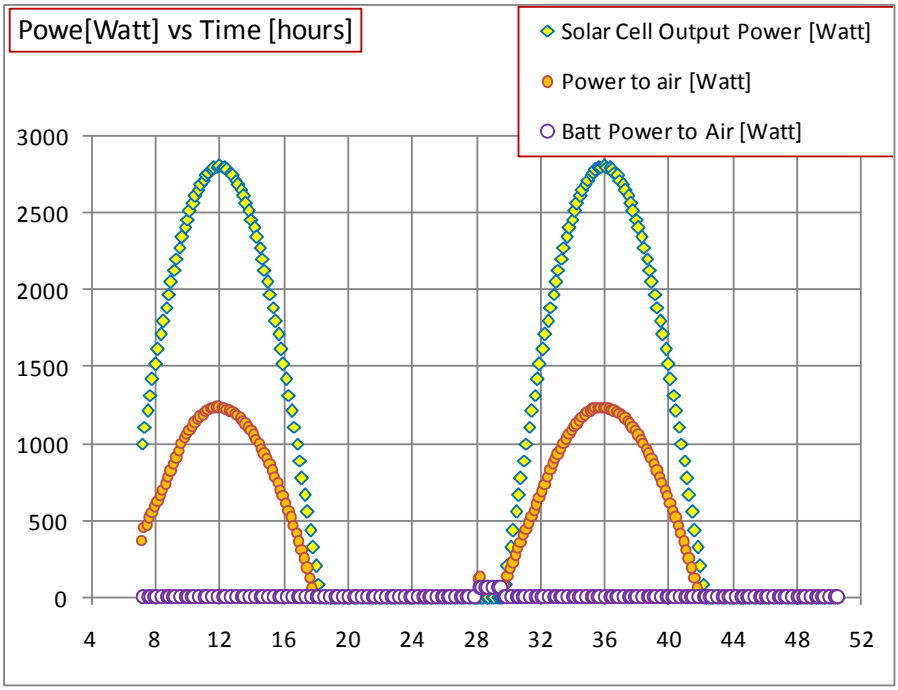

Figure 6.14: "High Flight" mission time history:

Cells output power, power delivered to air, power from batteries to air, vs time [hs]

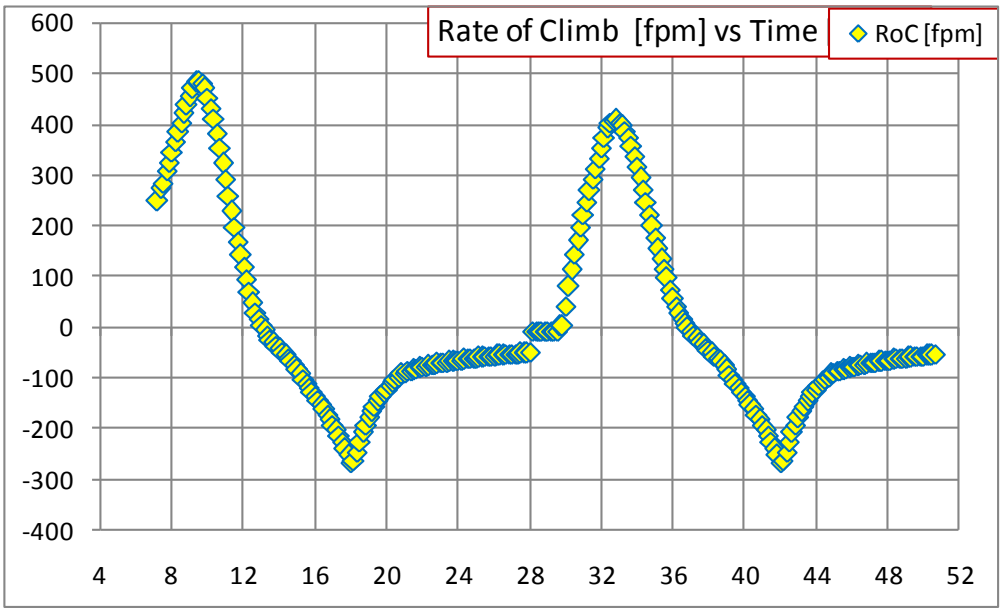

Figure 6.15: "High Flight" mission time history: Rate-of-climb [fpm] vs time [hs]

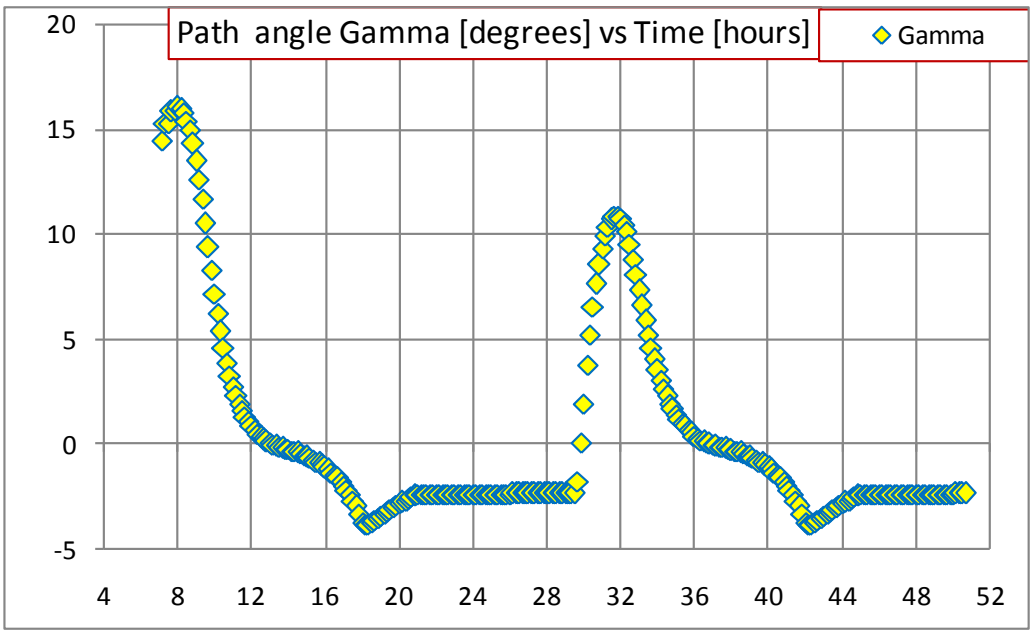

Figure 6.16: "High Flight" mission time history: Gamma, γ, [degrees] vs time [hs]

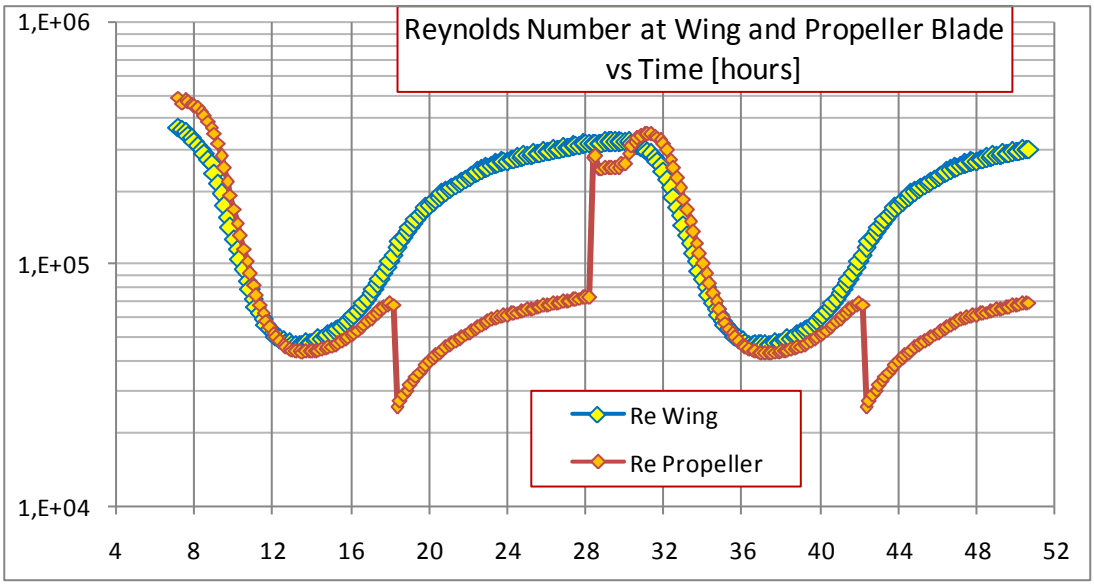

Figure 6.17: "High Flight" mission time history: Re at wing and propeller vs time [hs]

From figure 6.17 an important observation can be made: the drops in the curve of the Reynolds number of the propeller refer to the points where the propeller stops spinning.

b) Visualization of Relationships between Parameters:

Altitude and True Airspeed: The variation of TAS with airspeed in a continuous flight of more than 24 hs; is presented in Figure 6.18. The part below 18 thousand feet corresponds to take-off and initial climb; the part above 18 thousand feet corresponds to the continuous daily flight cycles. All the flight is considered to be performed at the same EAS. One can note the huge difference between the TAS at about 100 thousands of feet and the one at about 20 thousands of feet; which requires the aerodynamic design of the aircraft and propeller to be very versatile in terms of power requirement and Reynolds Number.

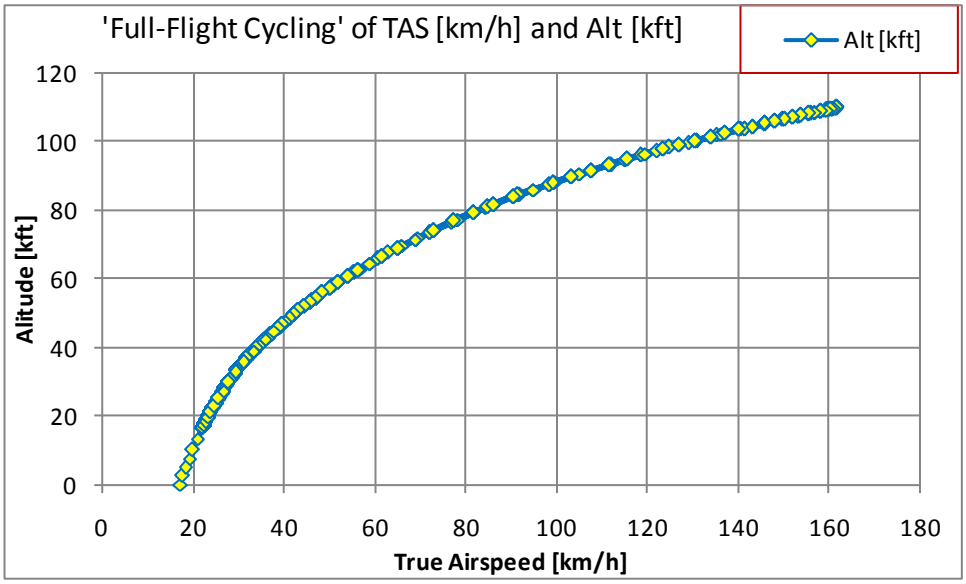

Figure 6.18: "High Flight" mission: Altitude [kft] vs TAS [km/h]

Propeller effectiveness versus Advance Ratio J: The variation of propeller effectiveness during the whole 24 hours flight cycle is presented in figure 6.19. The following comments are presented in order to provide some description of the figure 6.19. The curve of Eta propeller at each mission instant, as presented in the figure 6.19, is limited for the two effectiveness curves:

- For very high altitude flight; very low Reynolds number, 20 000, and
- For low altitude flight; normally conceived Reynolds number, 1000 000.

The propeller has been designed for the Reynolds number corresponding to high altitude flight conditions.

One can note the high density of points of the Eta Propeller curve, about J=0.6 in the figure 6.19. This is the indication that, in most part of the powered flight, the aircraft is flying close to the curve of High Altitude Flight, and also close to the maximum effectiveness region of the propeller at high altitude, which confirms the both aspects, the selected propeller design point, and the propeller design.

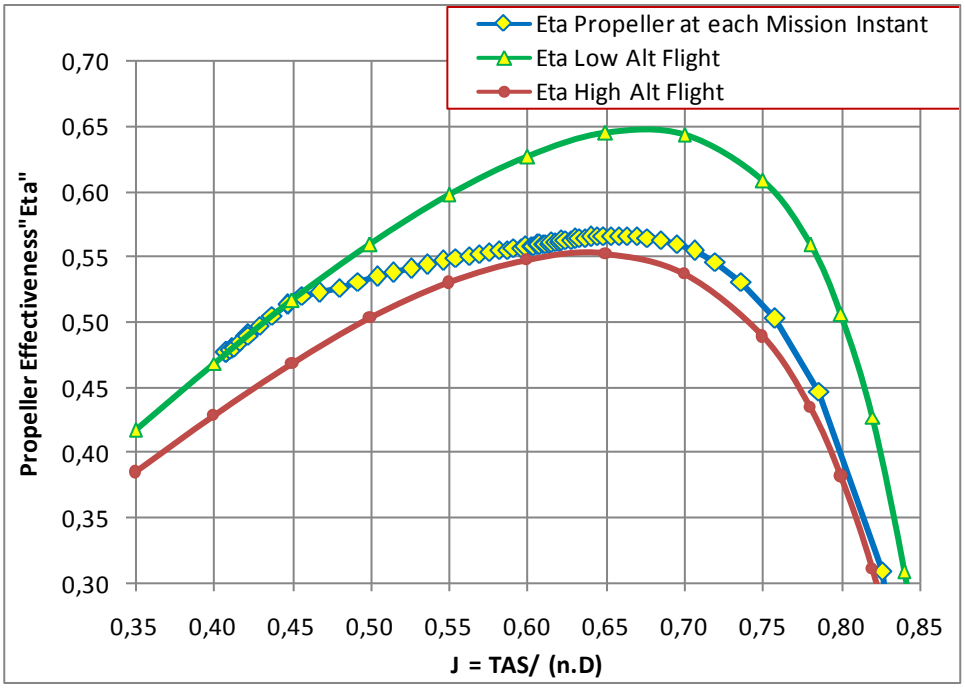

Figure 6.19: "High Flight" mission: Propeller effectiveness vs advance ratio 'J'

Propeller RPM versus Power Delivered from Aircraft to Air: The curve of propeller RPM versus Power Delivered from Aircraft to Air is presented in figure 6.20 and is aimed to be used also as check for propeller analysis; one can compare this figure with figure 6.21 to be check the reduction of power due to propeller effectiveness.

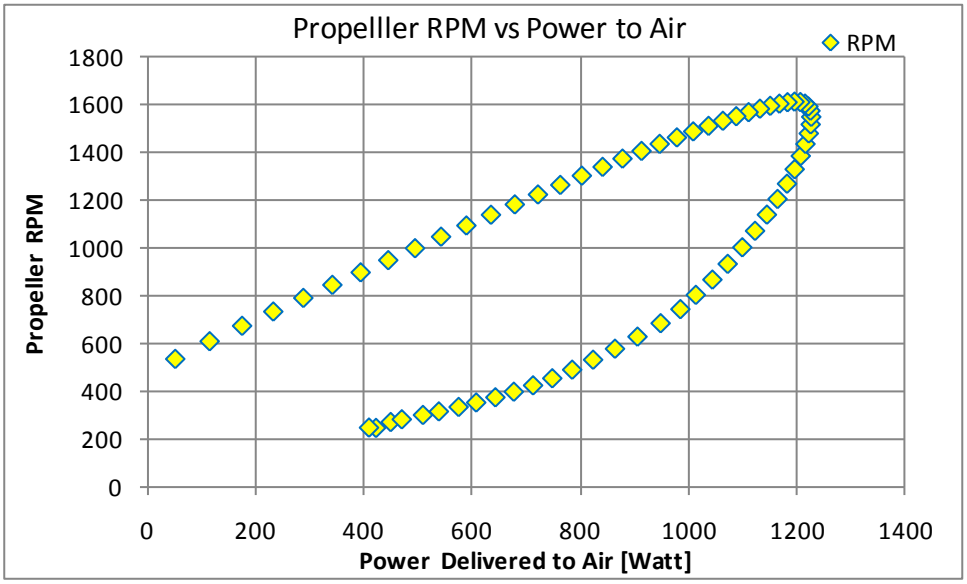

Figure 6.20: "High Flight" mission analysis: Propeller RPM vs power delivered to air [Watt]

Propeller RPM versus Engine Output Power, and Outside Air Temperature: The two figures 6.21 and 6.22 present the relationship between atmosphere temperatures, engine power and engine RPM from the Mission Analysis; it is important to point out that these two figures shall be used as part of the requirements for acquisition or design of the arrangement engine plus reduction.

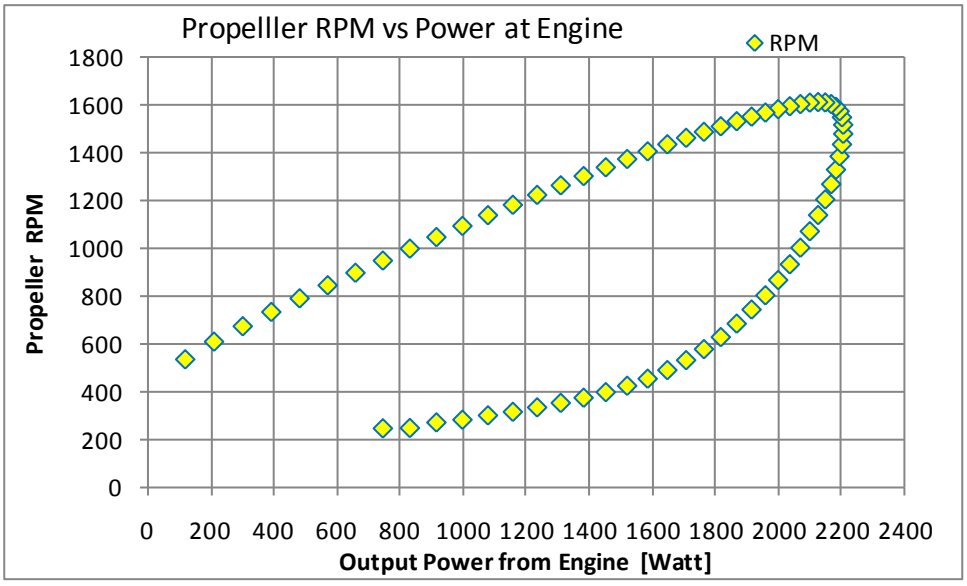

Figure 6.21: "High Flight" mission analysis: Propeller RPM vs engine output power [Watt]

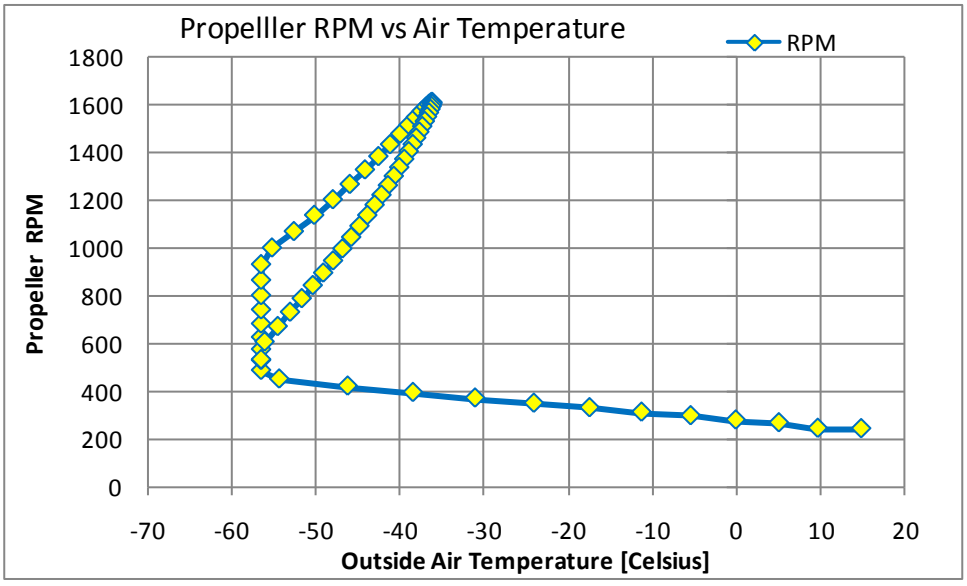

Figure 6.22: "High Flight" mission analysis: Propeller RPM vs air temperature [Celsius]

6.5) Diagrams of Flyable Region and Long Endurance Region

The figures 6.23 and 6.24 present the daily maximum and minimum altitudes achieved for the High Flight aircraft, during a several days uninterrupted sun-powered flight mission. These values are several different months of year, and several latitudes on the southern hemisphere. These plots are obtained through the Mission Analysis tool, with the aircraft being analyzed for different months and locations. As other main output of this mission study, the figure 6.25 present the flown distance per day for the "High Flight" aircraft, in the same time and position references from figures 6.23 and 6.24.

The region at the diagrams of figure 6.23 in which the values are above zero corresponds to the time and location in which flights are possible. This diagram is so named as Flyable Region Diagram.

The region at the diagrams of figures 6.24 and 6.25 in which the values are above zero corresponds to the time and location in which long endurance flights – of a week or more - of High Flight aircraft are theoretically possible; so these regions can be defined as the Long Endurance Region Diagram.

Inside the Long Endurance Region Diagram, and considering other necessary conditions such as a clear sky, the reliability of the aircraft systems and low level of turbulence, the perpetual flight is theoretically possible for the High Flight aircraft.

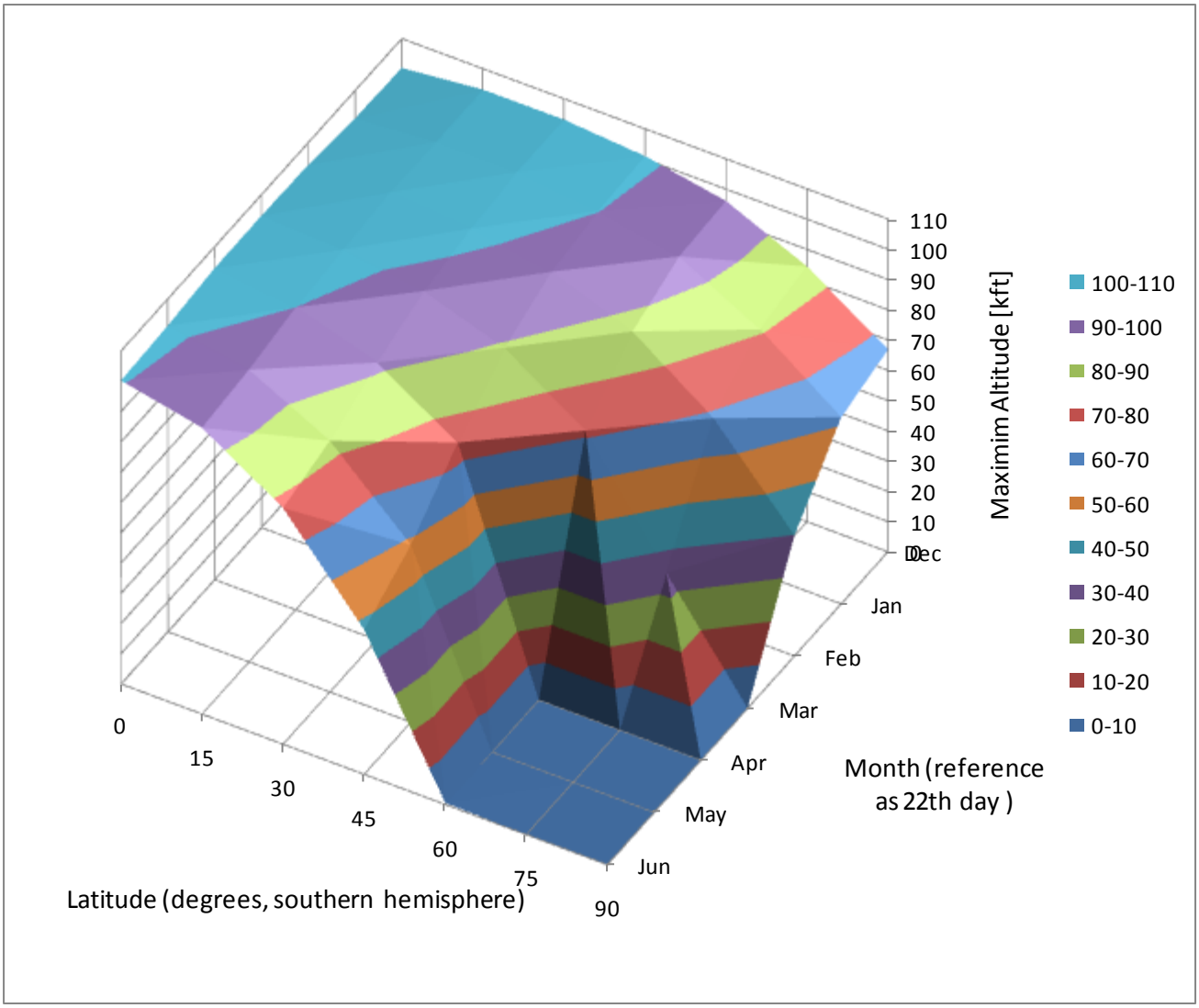

Figure 6.23: Maximum altitude in function of latitude and month for the High Flight aircraft; southern hemisphere.

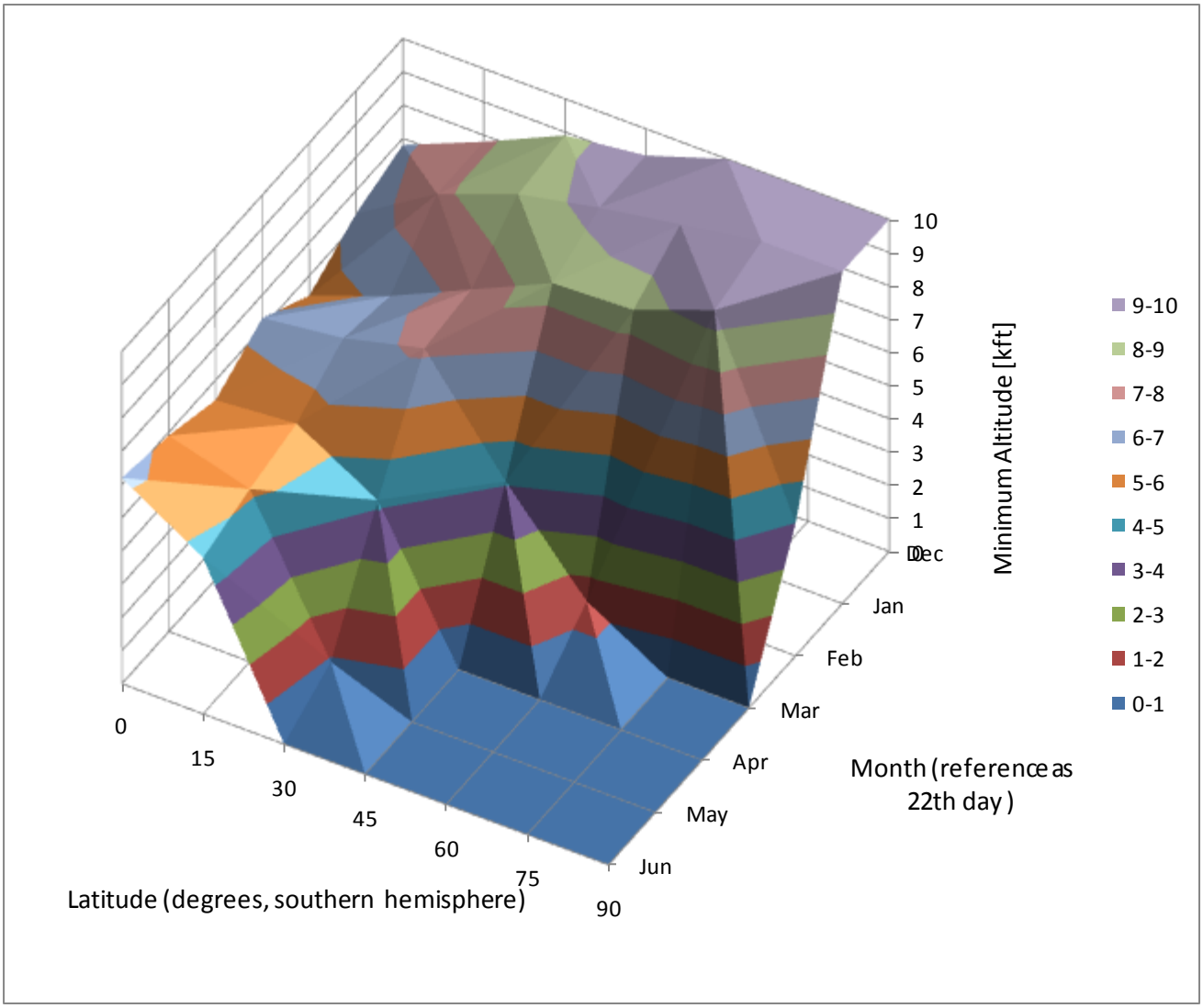

Figure 6.24: Minimum altitude in function of south latitude and month for the High Flight aircraft.

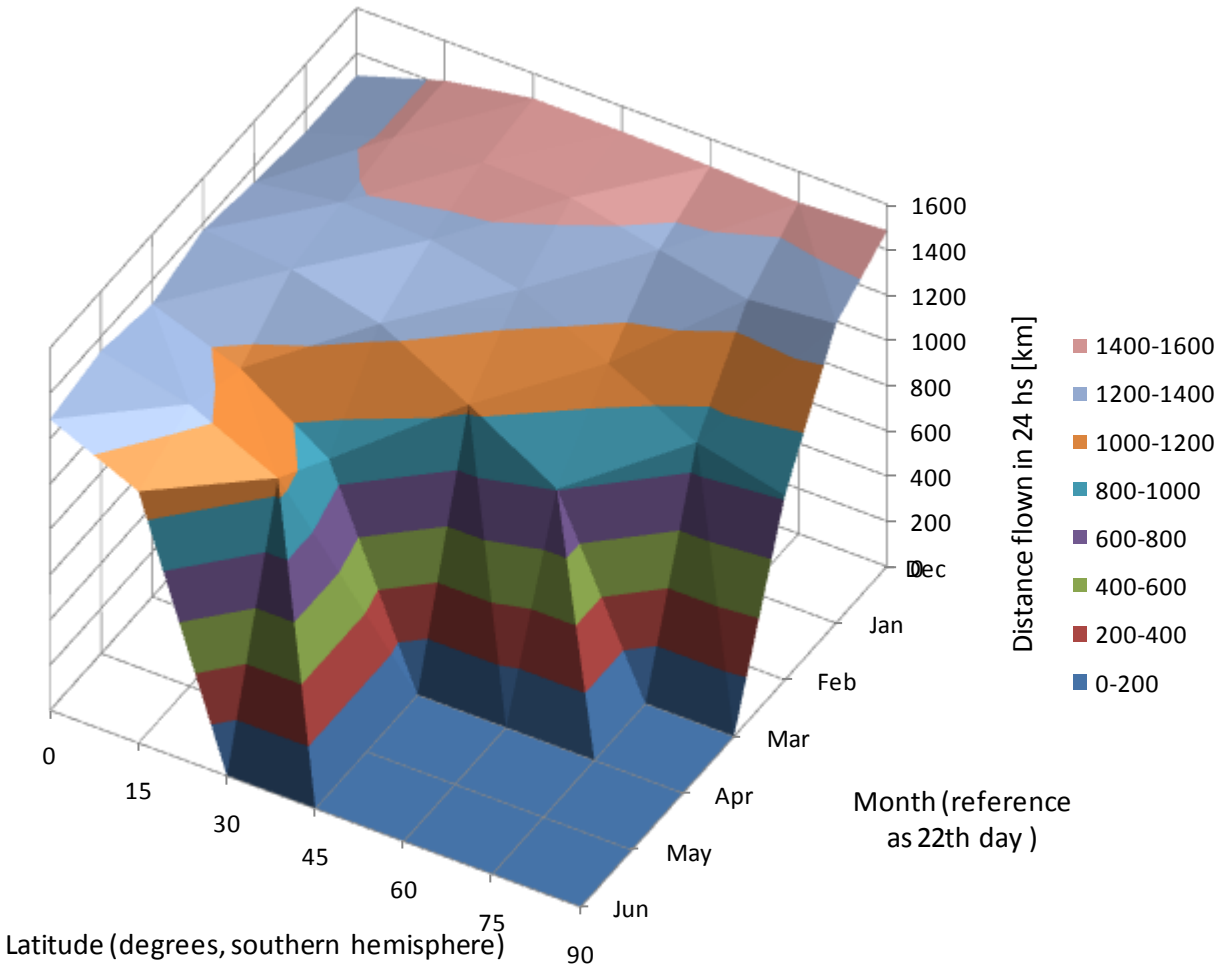

Figure 6.25: Daily distance flown in function of south latitude and month for the High Flight aircraft;

Considering the average daily speeds at figure 6.25, and non-considering the atmosphere wind speeds, it would be possible to think in a round-the World theoretical flight mission; in a average speed of 1300 km a day by the Earth's equatorial perimeter of about 40000 km the resultant round-the-World time for this mission should be 30.8 days. By the diagram of figure 6.5-3, this theoretical mission could be performed at any month of the year. Other long range mission could be starting from Equatorial latitude, flying towards the pole, and going ahead up to the Equator in the opposite point, on Earth, related to the starting point. The total distance should be about 20000 km, if flying in the correct month – December for southern hemisphere - for and depending on the month, the speed could also be about 1300 km a day, resulting in a total flight time equator-to equator passing by the pole, of about 15.4 days.

7) CONCLUSIONS

7.1) Overall

In this work some tools and metrics have been developed to analyze low-speed air vehicles. In order to obtain confidence with the tools, some analyzes have been performed for already-flown low-speed aircraft, and the results compared to the reported ones for these aircraft. A dedicated propeller analysis and the special care with Reynolds number have been discovered as of fundamental importance when checking the calculated results with the ones reported in the literature for the existing aircraft. Other relevant points are the consideration of thrust effect on drag, as an effect to allow the matching between calculated performance values and reported ones; and the need to obtain a more reliable structural mass evaluation. In order to correct estimate the Reynolds Number effect, the definition of kinematic viscosity at very high altitude, above 50 thousand feet, was investigated.

Besides the tools for analysis of general low-speed vehicles, the tools specific for solar propulsion have been developed, as the solar incidence model, and the mass studies specific for the sun-powered aircraft.

In terms of tools dedicated to Solar Aircraft, the General Rules for Maximum Wing Load, and the Method for Solar Aircraft Design proved to be very reliable and versatile.

The mission analysis represented a good solution of the challenge of managing the energy flow between batteries, solar panels and engine, besides the changes constantly occurring, the energy source from the sun, and the atmosphere characteristics, as the aircraft climbs and descents continuously. The Mission Analysis tool is one fundamental part of the process towards a feasible sun-powered aircraft aimed to missions involving cyclical climbs and descents.

The link between airfoil characteristics and propeller curves has been also a very useful advancement since, among other benefits, it can provide means of understanding how low-Reynolds propellers, which are vital for certain types of sun-powered aircraft, can be designed. Apparently it is possible to tackle with Reynolds number constraints to design a feasible solar aircraft and its propeller, aimed for high altitude - above 50 thousand feet - flights.

At the end of this work, a group of tools - each one very simplified and primitive, deserving each one to receive large amounts of improvements, but each one already of fundamental importance for the success of low speed aircraft and sun-powered aircraft analyses performed – has been defined.

It has been possible to define, using the developed tools, three different types of solar aircraft, each one with a specific application. One of these designs is an aircraft for continuous flight with a very reduced use of batteries, relying almost completely in the storage of mechanic energy by climbing at altitudes about one hundred thousand feet.

By considering a consistent solar irradiance model, with effects of atmosphere thickness it is possible to define a large extension in Earth planet in which continuous, long endurance, long range flights, can be achieved; and by considering a general solar irradiance model and a general atmosphere model, the sun-powered flight in extraterrestrial atmospheres, such Mars or Venus could also be investigated.

7.2) Next Steps

Some of the relevant lines that should be considered as continuation of this work are:

- To improve the studies of low Reynolds characteristics, and to identify a higher number of airfoils capable of provide good Lift-to-Drag ratios at low and normal Reynolds numbers.
- To improve the metrics of mass analysis, focusing a databank of systems mass and refining the laws for definition of structural wing mass analysis.
- To present the mission analysis of Helios, Pathfinder, Zephyr, Solar Impulse, Sky-Saylor and Sunseeker in a comparative form.
- To develop dedicated cost metrics and tools, to allow cost analysis for solar aircraft of interest.
- To detail the three designs defined in this work.
- To improve knowledge in electronic systems architecture and equipment;
- To check the feasibility of a engine to fit with the parameters shown at section 6.4.
- To define a simplified version from the designs presented, to be built and tested, in order to allow a suitable learning curve towards a feasible construction and test of more complex configuration.
- To improve specific understanding on Earth atmosphere, climate, gusts and air streams.
- To perform the research of Mars and Venus environments, in order to check the feasibility and conceptual definition of flying vehicles destined to Mars and Venus atmospheres.

8) REFERENCES

The most important references consulted related to this work are listed as follows. Due to the diversity of subjects consulted for the present study, the references are grouped in specific sections, according to the type of information obtained from them. The groups are: 1) Pioneer aircraft; 2) Sun-powered and man-powered aircraft; 3) Lift, Drag and Performance analysis; 4) Propeller analysis; 5) Other subjects.

8.1) References Related to Early Aviation Pioneer Aircraft

1. BADEN-POWELL, B.F.S. **Progress with Air Ships**, in: **Illustrated Scientific News.** London, UK, 1903.

2. BARROS, HENRIQUE. L. **Santos Dumont: O Vôo que Mudou a História da Aviação**, in **Parcerias Estratégicas.** No.17, Brasilia, Brazil: CGEE, 2003. Available in <http://www.cgee.org.br/parcerias/> Last access June 2014.

3. COSTA, F. H. **Alberto Santos Dumont**. Brazil: Ministério da Aeronáutica, 1971.

4. FERRIS, R. **How it Flies.** New York, USA: Thomas Nelson and Sons, 1910.

5. KARLSON, P. **A Conquista dos Ares**. Porto Alegre, Brazil: Livraria do Globo, 1940.

6. LILIENTHAL, O. **Der Vogelflug als Grundlage der Fliegekunst (The Flight of Birds as the Basis of Fly Art).** Berlin, Germany: R. Gaertners Publishing House, 1889.

7. MELLO, Marcus **Santos Dumont, uma Homenagem.** Available in <http://www.cabangu.com.br/pai_da_aviacao> 2002, last update 2012; last access June 2014.

8. OTTO LILIENTHAL MUSEUM **Otto Lilienthal - to Fly Like a Bird.** Available in <http://www.lilienthal-museum.de/olma/eotto.htm> Last update 2011; last access May 2013.

9. THEIR FLYING MACHINES **Santos-Dumont Demoiselle.** Available in <http://flyingmachines.ru/Site2/Crafts/Craft28341.htm> 2011, last update 2014; last access 2014.

10. VILLARES, H. D. **Quem Deu Asas ao Homem**. São Paulo, Brazil: Instituto Nacional do Livro, 1957.

8.2) References Related to Solar and Man-Powered Aircraft

1. NOTH, A., SIEGWART R., and ENGEL W. **Design of Solar Powered Airplanes for Continuous Flight**. Zurich, Switzerland: ETH Swiss Federal Institute of Technology, 2007.

2. NOTH, A. **Design of Solar Powered Airplanes for Continuous Flight**, PHD Thesis, Dissertation ETH No. 18010. Zürich, Switzerland: ETH , 2008a.

3. NOTH, A. **History of Solar Flight.** Zurich, Switzerland: ETH, 2008b.

4. NOTH, A. **Sky-Sailor Solar Powered Airplane Proved Continuous Flight.** Zurich, Switzerland: Autonomous Systems Lab, ETH, 23 june2008c.

5. NOTH, A. **Sky-Sailor.** ETH Zurich. Available in <www.sky-sailor.ethz.ch> Last update April 2008d; last access June 2014.

6. ROSS, H. **Fly around the World with a Solar Powered Airplane.** Sevilha, Spain: EWADE Conference, 2009a.

7. ROSS, H. **Solar Powered Aircraft, the True All Electric Aircraft.** Sevilha, Spain: EWADE Conference, 2009b.

8. JABAS, M.; LEUTENEGGER, S. **Extension to a Solar Airplane Conceptual Design Tool.** Zurich, Switzerland: ETH, 2010.

9. MONTGOMERY, S. and MOURTOS, **Design of a 5 Kilogram Solar-Powered Unmanned Airplane for Perpetual Solar Endurance Flight.** USA: AIAA, 2008.

10. BAHTT, M. R. **Solar Power Unmanned Aerial Vehicle: High Altitude Long Durance Applications.** USA: San Jose University, 2012.

11. COCCONI, A., **AC Propulsion's Solar Electric SoLong UAV.** USA: AC Propulsion. USA, June 2005. Available in <www.acpropulsion.com> Last access May 2014.

12. MACCREADY, P. B. et al. **Sun-Powered Aircraft Designs**, Journal of Aircraft, Vol. 20, No.6. USA: AIAA, 1983.

13. BOUCHER, ROLAND, **Project Sunrise .** Available in <http://www.projectsunrise.info/> Last update 2003; last access may 2014.

14. BOUCHER, ROBERT **Sunrise, the Word's First Solar-Powered Airplane.** Journal of Aircraft. USA: AIAA, 1984.

15. NOLL, T. et al. **Investigation of the Helios Prototype Aircraft Mishap.** USA: NASA Langley Research Center, 2004.

16. BURKE, J. **The Gossamer Condor and Albatross: A Case Study in Aircraft Design.** Professional Study Series. USA: AIAA, 1980.

17. RAPINETT, A. **Zephyr: A High Altitude Long Endurance Unmanned Air Vehicle.** UK: University of Surrey, 2009.

18. JEX. H. R.; MITCHELL D. **Stability and Control of the Gossamer Human-Powered Aircraft by Analysis and Flight Test.** C. R. 3627. USA: NASA, 1982.

19. HARDY R. J., **The Optimized Man Powered Aircraft,** Man-Powered Aircraft Group Symposium. UK: Royal Aeronautical Society 1975;

20. LANDIS A. G.; LAMARRE C. M.; COLOZZA, A. **Atmospheric Flight On Venus**, TM-2002-0819. USA: AIAA and NASA, 2002.

21. LISOSKI, D. L.; TISCHLER M. B. **Solar Powered Stratospheric Research Aircraft - Flight Test and System Identification**. Madrid, Spain: RTO SCI Symposium, 1998.

22. MOULTON, R.; COWLEY, M.; LLOYD, P. **The Gossamer Albatross** in Aeromodeller Magazine. USA: September 1979.

23. MATTOS, B.S., SECCO, N. R., SALLES, F. E. **Optimal Design of a High-Altitude Solar-Powered Unmanned Airplane**, JATM, Sao Jose dos Campos, Brazil: 2013.

24. NAJAFI, Y. **Design of a High Altitude Long Endurance Solar Powered UAV.** USA: San Jose State University, 2011

25. VIDALES, H.M.G. **Design, Construction and Test of the Propulsion System of a Solar UAV**. Lisbon, Portugal: IST Universidade Tecnica de Lisboa, 2013.

26. NATIONAL AERONAUTICS and SPACE AGENCY **Armstrong Fact Sheets**. Available in <http://www.nasa.gov/centers/dryden/news/FactSheets/> Last update July 2014.

27. NASA **Dryden Historical Aircraft Photo Collection.** Available in <http://www.dfrc.nasa.gov/Gallery/Photo,> Last update May 2010 .

28. PHILLIPS, W. H. **Some Design Considerations for Solar-Powered Aircraft,** NASA TP-1675. Hampton, USA: NASA Langley Center, 1980.

29. HALL, D. W. et al. **Mission Analysis of Solar Powered Aircraft** NASA C R 172583, Hampton, USA: NASA Langley Center, 1985.

30. HALL, D. W. et al. **A Preliminary Study of Solar-Powered Aircraft and Associated Power Trains** NASA C R 3699, Sunnyvale, USA: Lockheed Missiles and Space Company, 1983.

31. HALL, D. W.; HALL, S. A. **Structural Sizing of a Solar Powered Aircraft.** NASA C R 172313 Sunnyvale, USA: Lockheed Missiles and Space Company, 1984.

32. COLOZZA, J. A. **Effect of Power System Technology and Mission Requirements on High Altitude Long Endurance Aircraft** NASA C R 194455, Cleveland, USA: NASA Lewis Research Center, 1994.

33. COLOZZA, J. A.; SCHEIMAN, D. A. **GaAs/Ge Solar Powered Aircraft** NASA TM 208652. Cleveland, USA: NASA Lewis Research Center, 1998.

34. M.D. BAILEY M. D.; BOWER, M. V. **High Altitude Solar Power Platform** NASA TM 103578. USA: NASA George C Marshall Space Flight Center, 1992

35. PENNER, H. **The Solar Aircraft** NASA TM-77327, Washington, USA: NASA, 1983

36. COLELLA, N. J. ; GORDON S. WENNEKER G. S. **Pathfinder and the Development of Solar Rechargeable Aircraft** in Energy and Technology Review, E&TR, USA: July 1994. available in https://str.llnl.gov/etr/pdfs/07_94.1.pdf

37. COWLEY, M.; LLOYD, P. **Solar Challenger** in Aeromodeller Magazine. USA: June 1981.

38. ELARIO, D.S. et al. **N.A.S.A Advanced Aeronautics Design Solar Powered Remotely Piloted Vehicle** NASA.CR 190007. USA: Worcester Polytechnic Institute, 1991.

39. CHAN, A. et al. **NASA Advanced Design Program Analysis, Design, and Construction** NASA.CR 192040. USA: Worcester Polytechnic Institute, 1992.

40. BENEDEK, L. **Solar Energy and the Aeronautics Industry** NASA TM-77957, Olivos, Argentina, and Pittsburg, USA: The Corporate Word, 1985

8.3) References Related to Drag, Lift, Performance, Atmosphere and Mass Analysis

1. HOERNER, S. **Fluid-Dynamic Drag**. New Jersey, USA: Published by the author, 1958.

2. HOERNER, S.; BORST, H. **Fluid-Dynamic Lift**. 2nd Edition. Vancouver, USA: Published by L. Hoerner. 1985.

3. MCCORMICK, B. **Aerodynamics, Aeronautics and Flight Mechanics**. New York, USA: John Wiley and Sons, 1979.

4. NACA. **Aerodynamic Characteristics of Airfoils-V.** NACA Report 286. USA: 1928.

5. NACA. **Aerodynamic Characteristics of Airfoils-IV.** NACA Report 244. USA: 1927.

6. NACA. **Aerodynamic Characteristics of Airfoils-III.** NACA Report 182. USA, 1924.

7. NACA. **Aerodynamic Characteristics of Airfoils-II.** NACA Report 124. USA, 1923.

8. NACA. **Aerodynamic Characteristics of Airfoils-I.** NACA Report 93. USA, 1921.

9. PINKERTON, R.; GREENBERG, H. **Aerodynamic Characteristics of a Large Number of Airfoils Tested in the Variable-Density Wind Tunnel.** NACA Report 628, USA, 1937.

10. LISSAMAN, P.B.S.; JEX, H.R.; MACCREADY, P.B. **Aerodynamics of Flight at Speeds Under Five m/s.** London, UK: The Royal Aeronautical Society, 1979.

11. PRANDTL, L. et al **Ergebnisse der Aerodynamischen Versuchsanstalt zu Göttingen** Vols. 1 to 4, Germany: 1920, reprinted in 2009.

12. SHMITZ, F.W. **Aerodynamics of the Model Airplane.** Germany: 1942. Reprinted in the USA: 1967.

13. LOUDEN, F.A. **Collection of Wind-Tunnel Data on Commonly used wing Sections**. NACA Report 331. USA: 1929.

14. SELIG, M. S.; GUGLIELMO, J. J.; BROEREN, A. P.; GIGUERE, P. **Summary of Low-Speed Airfoil Data**, Volume 1. Champaign, USA: Department of Aeronautical and Astronautical Engineering, University of Illinois at Urbana-Champaign, 1995.

15. WILLIAMSON, G. A. et al. **Summary of Low-Speed Airfoil Data**, Vol 5, Champaign, USA: Department of Aerospace Engineering, University of Illinois at Urbana-Champaign 2012.

16. SELIG, M. S.; DONOVAN; FRASER. **Airfoils at Low Speeds**. USA: H. A. Stokely publisher, 1989.

17. UIUC **List of airfoils tested, Summary of Low-speed airfoil Data books.** Available in <http://aerospace.illinois.edu/m-selig/uiuc_lsat_airfoilsTested.html> Last update 2014a; last access june 2014.

18. UIUC **Airfoil Tools.** Available in <http://airfoiltools.com> Last update 2014b, last access June 2014.

19. ABBOTT, I. H.; VON DOENHOFF A. E.; STIVERS JR., L. S. **Summary Of Airfoil Data** NACA Report 824. USA: 1945.

20. CHEN, W.; P. BERNAL L. P. **Design and Performance of Low Reynolds Number Airfoils for Solar-Powered Flight**. USA: University of Michigan, 2008.

21. SPEDDING, G. R.et al. **The implications of low-speed fixed-wing aerofoil measurements on the analysis and performance of flapping bird wings** in The Journal of Experimental Biology 211, USA: 2008.

22. CROWLEY J. W. **Investigation of Slipstream Velocity**, NACA Report 194, U.S.A:1925.

23. PINTO, R. U. F.; OLIVEIRA, P. H. I. A., BARROS, C. P. **Um procedimento Alternativo para Cálculo Aerodinâmico de Aeronaves Leves Subsônicas**, Brazil: Congresso Internacional da Engenharia da Mobilidade, 1999.

24. KROO, I.; ALONSO, J., **History of airfoil Development**. U.S.A: Stanford University. Available in <http://adg.stanford.edu/aa241/airfoils/airfoilhistory.html.> 2005, last update 2012, last access June 2014.

25. ENGINEERING SCIENCES DATA UNIT **Equations for Calculation of International Standard Atmosphere and Associated Off-Standard Atmospheres,** ESDU 77022. UK: 1986.

26. NAOAA; NASA; USAF. **US Standard Atmosphere.** USA: 1976.

27. NACA; ICAO, **Manual of the ICAO Standard Atmosphere, Calculations by the NACA**. NACA TN 3182. USA: 1954.

8.4) References Related to Propeller Analysis

1. STACK, J. **The NACA High Speed Wind Tunnel and Tests of Six Propeller Sections**, NACA Report 463, USA: NACA, 1933.

2. SILVERSTEIN, A. **Scale Effect on Clark Y Airfoil Chraracteristics from NACA Full-Scale Wind-Tunnel Tests**, NACA Report 502, USA: NACA, 1934.

3. HARTMAN, E. P.; BIERMANN, D. **The aerodynamic characteristics of full scale propellers having 2, 3 and 4 blades of Clark Y and RAF 6 Airfoil Sections**, N.A.C.A. Technical Report No. 640, EUA: NACA, 1937.

4. BIERMANN, D.; HARTMAN, E. P. **Tests of Five Full-Scale Propellers in the Presence of a Radial and Liquid-Cooled Engine Nacelle, Including Tests of Two Spinners**, N.A.C.A. Technical Report No. 642, EUA: NACA, 1937.

5. BIERMANN, D.; HARTMAN, E. P. **Tests of two Full-Scale Propellers with different Pitch distributions, at Blade Angles up to 60^{o}**, N.A.C.A. Technical Report No. 658, EUA: NACA, 1938.

6. HARTMAN, E. P.; BIERMANN, D. **Static Thrust and Power Characteristics of Six Full Scale Propellers**, N.A.C.A. Technical Report No. 684, EUA: NACA, 1939.

7. PROPDESIGNER **Malcom's Human-Powered Aircraft Site.** Available in <http://library.propdesigner.co.uk> Last update 2013; last access June 2014

8. LARRABEE, E. E. **Design of Propellers for Motorsoarers**. USA: MIT, 1979.

9. WEICK, F. E. **Aircraft Propeller Design.** U.S.A.: NACA, 1930.

10. WEICK, F. E. **Full-Scale Wind-Tunnel Tests of a Series of Metal Propellers on a VE-7 Airplane.** NACA Report 306. U.S.A.: NACA, 1929.

8.5) References, other Subjects

1. AIRBUS A380 in WIKIPEDIA. Available in <http://en.wikipedia.org/wiki/Airbus_A380> last access at june 2014

2. AIRBUS A380 in AIRLINERS.NET. available in <http://www.airliners.net/aviation-forums/tech_ops/read.main/202430/t> last access at June 2014.

3. BIRD, R. E; HULSTROM, R. L. **A Simplified Clear Sky Model For Direct And Diffuse Insolation On Horizontal Surfaces.** USA: Solar Energy Research Institute, 1981.

4. BRAU, J. **Astronomy 121.** University of Oregon. Available in <http://pages.uoregon.edu/jimbrau/astr121-2005/Notes/Exam2rev.html> Last update 2005; last access June 2014.

5. EUROPEAN SPACE AGENCY ESA **Space in Images**. Available in <http://www.esa.int/spaceinimages/Images/2007/11/Vertical_profiles_of_pressure_on_Earth_and_Venus> Last update 2007; last access June 2014.

6. FÉDÉRATION AÉRONAUTIQUE INTERNATIONALE, available in <http://www.fai.org> last update 2014, last access2014.

7. FYSON, D., **Design, Install &Commission grid connected photovoltaic power systems**, available in http://renewableenergystudentresource.weebly.com/, last access June 2014

8. GANE, C., SARSON, T. **Análise Estruturada de Sistemas**. São Paulo, Brazil: Livros Tecnicos e Científicos Editora, 1984.

9. GEOGRAPHIC RESOURCES ANALYSIS SUPPORT SYSTEMS **GRASS GIS.** Available in <http://grass.osgeo.org> 1998, last update 2014, last access May 2014.

10. JOINT RESEARCH CENTRE INSTITUTE for ENERGY and TRANSPORT (IET) **Solar Radiaton and GIS**, available in <http://re.jrc.ec.europa.eu/pvgis/> Last update 10 February 2012, last access May 2014.

11. NASA **The Mars Orbiter Laser Altimeter.** Available in <http://mola.gsfc.nasa.gov/> Last update 2007; last access June 2014.

12. NASA GODDARD SFC **Planetary Laser Altimeter.** Available in <http://tharsis.gsfc.nasa.gov/ > Last update 2006; last access June 2014.

13. NEWPORT CORPORATION **Sunlight Simulators** Available in <http://www.newport.com/Introduction-to-Solar-Radiation/411919/1033/content.aspx> 1996-2014; last access June 2014.

14. PACIFIC POWER ASSOCIATION; E7 NETWORK OF EXPERTISE FOR THE GLOBAL ENVIRONMENT, **Photovoltaic Systems**, Majuro, Republic of the Marshall Islands: Joint PPA/e7 Workshop on Renewable Energies, March 2005. Available in <http://www.globalelectricity.org/Projects/Majuro> Last update March 2005, last access June 2014.

15. RIGOLLIER, C.; BAUER, O.; WALD, L. **On the Clear Sky Model of the ESRA - 4th European Solar Radiation Atlas with respect to the Heliosat Method**. Published in 'Solar Energy', 68(1). Paris, France: Ecole des Mines de Paris, 2000.

16. RENO, M. J.; HANSEN, C. W.; STEIN, J. S. **Global Horizontal Irradiance Clear Sky Models: Implementation and Analysis.** Sandia Report SAND2012-2389. USA: Sandia Laboratories, 2012.

17. STINE, W.; GEYER, M.; HARRIGAN, R. W. **The Power from the Sun**. Available in <http://www.powerfromthesun.net/Book/chapter02/chapter02.html> Last update 2001; last access June 2014.

18. WAINFAN, B. **Facetmobile.** Available in <http://www.facetmobile.com/> Last update 2008; last access June 2014.

19. SOLAR MADE CORP. **Power Film Ultra Flixeble Solar Module**. Available in <http://www.solarmade.com/PowerFilm.htm> Last update Jan. 2013; last access June 2014.

20. SION POWER CORP. **Sion Power's Lithium-Sulfur Batteries Power World Record Flight**. Press Release available in <http://www.sionpower.com/pdf/articles/Sion Power Zephyr Press Release 29-07-2010.pdf> Last update 29 July 2010; last access June 2014.

21. SUN POWER CORP. **A-300 Solar Cell Data Sheet**. Available in <http://www.10suns.com.au/Sunpower300.pdf> Last update March 2009; last access June 2014.

22. SUN POWER CORP. **Sun Power Joins Solar Impulse Project as Official Supplier.** Press Release cited in http://www.prnewswire.com/news-releases/sunpower-joins-solar-impulse-project-as-official-supplier-135153163.html 7dec2011; last access June 2014

23. NATIONAL AERONAUTICS and SPACE AGENCY **Planetary Fact Sheet.** Available in <http://nssdc.gsfc.nasa.gov/planetary/factsheet/index.html> Last update: 25 April 2014; last access June 2014.

24. DARLING, D. **Atmosphere of Venus.** Available in <http://www.daviddarling.info/encyclopedia/V/Venusatmos.html> Last update 2012; last access June 2014.

25. SQUYRES, S W. **Venus**. Encyclopedia Britannica Online. Available in <http://www.britannica.com/EBchecked/topic/625665/Venus/54178/The-atmosphere> Last update 5 May 2014; last access June 2014.